EFFECTIVE STRESS-STRENGTH BEHAVIOR OF CEMENTED SOILS

by

ANWAR ERNEST ZAKI WISSA

B.A. (Hons.), Oxford University, 1957
S.M., M.I.T., 1961
M.A., Oxford University, 1962

Submitted in partial fulfillment of the
requirements for the degree of
DOCTOR OF SCIENCE
at the
MASSACHUSETTS INSTITUTE OF TECHNOLOGY
June 1965

Signature of Author.....
February 1, 1965, Department of Civil Engineering

Certified by.....

.....
Thesis Supervisors

Accepted by.....
Chairman, Departmental Committee
on Graduate Students

Abstract

EFFECTIVE STRESS-STRENGTH BEHAVIOR OF CEMENTED SOILS

by

ANWAR ERNEST ZAKI WISSA

Submitted to the Department of Civil Engineering on February 1, 1965, in partial fulfillment of the requirements for the degree of Doctor of Science.

The objective of this thesis was to determine the influence of cementation on the stress-strain and strength behavior of soils and to develop a mechanistic picture which would help predict field performance.

The following conclusions are based on the results of triaxial compression tests on three untreated and artificially cemented (stabilized) soils: a sand, a clayey silt, and a plastic clay cemented with hydrated lime and/or portland cement. The samples were compacted, saturated, and tested in drained shear with volume change measurements and/or in undrained shear with pore water pressure measurements over a wide range of consolidation pressures (0 to over 50 kg/cm^2).

The major conclusions are:

(1) The effective stress principle applies to the strength behavior of saturated stabilized soils, i.e., the Mohr-Coulomb envelope in terms of effective stresses is essentially independent of drainage conditions whereas the total stress envelope is dependent on the drainage conditions during shear.

(2) The addition of a cementing material such as hydrated lime or portland cement can substantially increase the Mohr-Coulomb effective cohesion intercept, c, of both coarse-grained and fine-grained soils. c increases with increasing cement content and increasing curing time (strength of the cement). The development of shrinkage cracks due to volume changes which occur during curing or weathering (cycles of wet-dry) will cause a decrease in c, and may induce premature fracture at low consolidation pressures (while the cracks remain open) which exhibits itself as an apparent further decrease in c and an apparent increase in $\bar{\phi}$.

(3) Cementation has essentially no effect on the effective Mohr-Coulomb angle of internal friction, $\bar{\phi}$, of a coarse-grained soil provided the density of the sand

excluding the cement is kept constant. Cementation can increase $\bar{\phi}$ of a fine-grained soil by as much as 10°. The more plastic the soil and more cement added the larger is the increase. Curing time (strength of the cementation) and weathering have no effect on $\bar{\phi}$.

(4) For stabilized soils the Mohr-Coulomb criterion of failure in terms of effective stresses represents conditions when the sum of the cohesive resistance due to cementation and the frictional resistance due to particle-particle contact, geometric interference (interlocking of particles), and dilatancy in the case of drained shear, is a maximum.

(5) At any given axial strain the total shearing resistance of a soil cemented with hydrated lime or portland cement can be considered to have two components: a cohesive resistance which is effective stress independent and a frictional resistance which is effective stress dependent and therefore a function of the pore pressures developed during shear.

(6) The maximum cohesive resistance of a soil cemented with a nonductile material, such as lime or cement, occurs at smaller strains than the effective Mohr-Coulomb envelope. $\bar{c}$ is lower than the maximum cohesive resistance because partial breakdown of the cementation has occurred by the time the envelope is reached and it can be as little as 30% of the maximum value. By the time ultimate conditions are reached the cohesive resistance in the zone of shearing is completely destroyed and the shearing resistance is purely frictional.

(7) The maximum frictional resistance occurs at larger strains than the Mohr-Coulomb envelope and it is fully mobilized at ultimate conditions when the effective stress and shear stress remain constant with further straining. It can be 5° to 10° higher than the Mohr-Coulomb $\bar{\phi}$.

(8) The large increase in the frictional resistance of a fine-grained soil when a stabilizer such as lime or cement is added is believed to be due to the formation of strongly cemented large aggregates of fine-grained particles which are held together by a weaker continuous cementation. The aggregation forms during mixing and compaction and remains essentially constant during curing which account for $\bar{\phi}$ being independent of length of cure. In the case of sands aggregation does not occur during mixing because of the large size of the grains and therefore $\bar{\phi}$ is independent of the cementation per se.

Abstract (continued)
ANWAR ERNEST ZAKI WISSA

(9) The addition of lime or cement to fine-grained soils causes its undrained shear strength to increase due to an increase in $\bar{c}$ and in some cases $\bar{\phi}$. The excess pore pressures which develop during undrained shear are not significantly influenced by the cementation.

(10) The shear strength of a stabilized soil increases with increasing consolidation pressure. The rate of increase in strength with increasing consolidation pressure is greater in drained shear than in undrained shear.

(11) The addition of lime or cement to a soil causes an increase in its initial tangent modulus and reduces the strain required to reach the maximum principal stress difference.

Thesis Supervisors:	Titles:
T. William Lambe	Professor of Civil Engineering
Charles C. Ladd	Associate Professor of Civil Engineering

ACKNOWLEDGEMENTS

The author is indebted to numerous members of the Faculty and Staff of the Soil Mechanics Division for their assistance in making this work possible. In particular the author wishes to express his sincere thanks to:

His thesis supervisors, Dr. T. William Lambe and Dr. Charles C. Ladd. Dr. Lambe introduced the author to the general topic and provided encouragement throughout the work. Dr. Ladd spent long hours with the author reviewing and discussing the work and he made invaluable suggestions and constructive criticisms which were extremely helpful.

His student, Mr. Jin H. Kim, who as a Research Assistant in Soils, helped the author with most of the experimental work and prepared the Computer Program used to analyze the data.

Mr. Rodger Roseman, an undergraduate in Civil Engineering, who assisted in the computations; and Mr. Richard S. Ladd, Research Engineer in Soils, who helped assemble and improve the high pressure triaxial equipment.

Mr. Carl M. Stahle, Senior Technician, who saved the author considerable effort and time by being able to skillfully construct special testing equipment from rough engineering drawing. He also was very helpful in maintaining the equipment in operating condition.

Mrs. Gladys Nichols who edited and typed this thesis from an illegible handwritten manuscript which a less patient person would not have attempted to decipher.

The author's wife, Enid, without whose patience, understanding, and moral support this thesis would have never been completed.

Finally, the author wishes to express his gratitude to the Waterways Experiment Station, Corps of Engineers, U. S. Army, whose sponsorship of the work made this thesis possible.

TABLE OF CONTENTS

TABLE OF CONTENTS (Continued)

TABLE OF CONTENTS (Continued)

LIST OF TABLES

LIST OF FIGURES

Note: Figures are placed at the end of each Chapter.

LIST OF FIGURES (Continued)

LIST OF FIGURES (Continued)

LIST OF FIGURES (Continued)

LIST OF FIGURES (Continued)

LIST OF FIGURES (Continued)

LIST OF FIGURES (Continued)

LIST OF FIGURES (Continued)

LIST OF FIGURES (Continued)

LIST OF FIGURES (Continued)

LIST OF FIGURES (Continued)

LIST OF FIGURES (Continued)

LIST OF FIGURES (Continued)

LIST OF FIGURES (Continued)

DEFINITIONS OF SYMBOLS

Symbol	Definition
A	Skempton A Factor or pore pressure coefficient A
$\bar{A}$	Skempton $\bar{A}$ Factor or pore pressure coefficient $\bar{A}$, $\bar{A} = AB$
A_o	Initial area of test specimen, cm^2
A_ϵ	Area of test specimen during shear, cm^2
$\bar{a}$	Effective cohesion intercept on $\bar{p}$ versus plot, $kg/cm^2 \cdot \bar{a} = \bar{c} \cos \bar{\phi}$. Also, effective cohesive resistance from strain contours on $\bar{p}$ versus q plot, kg/cm^2
B	Skempton B Factor or pore pressure coefficient B. Also called pore pressure response when given as a percentage.
CBR	California Bearing Ratio
C_c	Compressibility of the soil skeleton, cm^2/kg
C_w	Compressibility of water, cm^2/kg
c	Cohesion intercept in terms of total stresses, kg/cm^2
$\bar{c}$	Effective cohesion intercept of Mohr-Coulomb effective stress envelope, kg/cm^2
CD	Consolidated-drained triaxial compression test
CU	Consolidated-undrained triaxial compression test.
$\overline{CU}$	Consolidated-undrained triaxial compression test with pore pressure measurements
$Ca(OH)_2$	Calcium hydroxide, hydrated lime
E	Initial tangent modulus or Young's modulus, kg/cm^2
e	Void ratio

DEFINITIONS OF SYMBOLS (Continued)

Symbol	Definition
Fe_2O_3	Ferric Oxide
G	Specific gravity of solids
K	Bulk modulus of soil skeleton, kg/cm^2
L.L.	Liquid limit, %
M-21	Massachusetts clayey silt
$Subscript_M$	At maximum stress difference
n	Porosity
NaCH	Sodium Hydroxide
P	Maximum Axial Load in Unconfined Test, kg/cm^2
P.I.	Plasticity index, %
P.L.	Plastic limit, %
p	Total normal stress on 45° plane, kg/cm^2 x $p = 1/2\ (\sigma_1 + \sigma_3)$
$\bar{p}$	Effective normal stress on 45° plane, kg/cm^2 x $\bar{p} = 1/2\ (\bar{\sigma}_1 + \bar{\sigma}_3)$
q	Shear stress on 45° plane or half principal stress difference, kg/cm^2 · $q = 1/2\ (\sigma_1 - \sigma_3)$
Δq	Change in shear stress on 45° plane, kg/cm^2
S	Degree of saturation, %
s	Shear strength, kg/cm^2
s_d	Drained shear strength, kg/cm^2
s_u	Undrained shear strength, kg/cm^2
S.L.	Shrinkage limit, %
t	Curing time, days

DEFINITIONS OF SYMBOLS (Continued)

Symbol	Definition
Subscript$_T$	At point of first tangency with the effective stress envelope
u	Pore pressure, kg/cm^2
u_B	Back pressure, kg/cm^2
Δu	Change in pore pressure, kg/cm^2
V	Volume of sample prior to shear, cc
ΔV	Change in volume, cc
$\dot{v}$	Volumetric Strain = dv/v
VBC	Vicksburg Buckshot Clay
w	Water Content, %
w_o	Water Content after Consolidation and Saturation, %
w_M	Water Content at maximum stress difference in drained shear, %
w_F	Water Content at End of Drained Test, %
$\tan\alpha$	Slope of total stress envelope on p versus q plot. $\tan\alpha = \sin\phi$
$\tan\bar{\alpha}$	Slope of effective stress envelope on p versus q plot. $\tan\bar{\alpha} = \sin\bar{\phi}$. Also slope of axial strain contours on p versus q plot.
$\tan\bar{\alpha}_{ult}$	Slope of effective stress versus strength relation at ultimate conditions on p versus q plot
γ_d	Dry Density, lb/cu ft
γ_w	Density of water, lb/cu ft
γ_{max}	Maximum Dry Density of Sand, lg/cu ft
γ_{min}	Minimum Dry Density of Sand, lg/cu ft

DEFINITIONS OF SYMBOLS (Continued)

Symbol	Definition
$\frac{1-\gamma_{min}/\gamma}{1-\gamma_{min}/\gamma_{max}}$	Relative Density, %
ε	Axial strain, %
ε_M	Axial strain at maximum principal stress difference, %
θ	Orientation of total stress failure plane with respect to major principal plane, degrees
$\bar{\theta}$	Orientation of effective stress failure plane with respect to major principal plane, degrees
ν	Poisson ratio
σ	Total normal stress, kg/cm^2
$\bar{\sigma}$	Normal effective stress, kg/cm^2
σ_o	Cell pressure, kg/cm^2
$\Delta\sigma_o$	Increment of cell pressure, kg/cm^2
$\bar{\sigma}_o$	Consolidation pressure, kg/cm^2
σ_f	Total normal stress on total stress failure plane at failure, kg/cm^2
σ_{ff}	Total normal stress on effective stress failure plane at failure, kg/cm^2
$\bar{\sigma}_{ff}$	Effective normal stress on failure plane at failure, kg/cm^2
$\bar{\sigma}_{cm}$	Maximum past pressure, kg/cm^2
$\Delta\bar{\sigma}_o$	Change in consolidation pressure, kg/cm^2
$\bar{\sigma}_M$	Effective normal stress on maximum stress difference failure plane at maximum stress difference, kg/cm^2
$\bar{\sigma}_{ult}$	Effective normal stress on ultimate failure plane at ultimate conditions, kg/cm^2

DEFINITIONS OF SYMBOLS (Continued)

Symbol	Definition
σ_1	Total major principal stress, kg/cm^2
$\bar{\sigma}_1$	Effective major principal stress, kg/cm^2
σ_3	Total minor principal stress, kg/cm^2
$\bar{\sigma}_3$	Effective minor principal stress, kg/cm^2
$\bar{\sigma}_1 / \bar{\sigma}_3$	Effective principal stress ratio (obliquity)
τ	Shear stress, kg/cm^2
τ_f	Shear stress on total stress failure plane at failure, kg/cm^2
τ_{ff}	Shear stress on effective stress failure plane at failure, kg/cm^2
τ_M	Shear stress on maximum stress difference failure plane at maximum stress difference, kg/cm^2
τ_{ult}	Shear stress on ultimate failure plane at ultimate conditions, kg/cm^2
ϕ	Angle of shearing resistance in terms of total stresses, degrees
$\bar{\phi}$	Angle of shearing resistance in terms of effective stresses, degrees
$\tan \bar{\phi}_M$	Slope of effective normal stress versus shear stress relation at maximum stress difference
$\tan \bar{\phi}_{ult}$	Slope of effective normal stress versus shear stress relation at ultimate conditions

Chapter 1

INTRODUCTION

The addition of a small amount of a cementing material, such as portland cement or hydrated lime, to a soil prior to mixing and compaction may substantially improve its engineering properties. This process of improving the engineering properties of a soil by artificial cementation is called soil stabilization and the resulting product is known as a stabilized soil.

Stabilized soils are commonly used in the construction of highway and airfield pavements when suitable natural soils are not readily available. They have been used as linings for canals and in place of riprap to protect earth embankments from erosion.

The two tests most commonly used for evaluating stabilized soils are the California Bearing Ratio (CBR) and the unconfined compression test. Unfortunately both tests have severe limitations. The CBR is an empirical test which can be justified only by its extensive correlation with field performance of pavements. The unconfined compression test is of limited use because it is a measure of the strength of a stabilized soil under only one specific set of testing conditions.* If field conditions differ substantially from those represented by the test, then the

*The unconfined compression test measures the strength of a sample in undrained shear (constant water content) when the confining pressure is zero.

strength in the field may be considerably different from the unconfined strength.

In order to predict the strength behavior of stabilized soils under various field conditions it is necessary to know the influence of drainage conditions and confining pressure on the strength. This can be achieved by determining the effective stress-strength parameters in the laboratory.

Two soil-stabilizer systems having the same unconfined compressive strength in the laboratory could have considerably different field performances since the unconfined compressive strength is dependent on the magnitude of the pore pressures which develop during shear as well as the effective cohesion intercept, $\bar{c}$, and the effective angle of internal friction, $\bar{\phi}$, of the Mohr-Coulomb envelope. It is therefore desirable to know how various cementing agents (stabilizers) influence the effective stress parameters, $\bar{c}$ and $\bar{\phi}$, and the pore pressure behavior of soils. This knowledge would make it possible to more rationally select a stabilizer for a specific field application. For example, if large confining pressures will occur in the field then an increase in $\bar{\phi}$ due to cementation may be more desirable than an increase in $\bar{c}$ and vice versa. Similarly if a stabilized soil is to be used in the construction of a pavement it will be subjected mainly

to transient loads due to moving vehicles in which case the magnitudes of the pore pressures during undrained shear may be of prime importance. On the other hand if the stabilized soil will be used as a raft foundation for a building then the drained strength may be the controlling factor.

One of the limiting factors in the use of stabilized soils is their durability or resistance to weathering (cycles of wet-dry and/or freeze-thaw). At the present time there is no rational way to determine the influence of weathering on the performance of stabilized soils. In England the criterion used to measure durability is the loss in unconfined strength with cycles of weathering whereas in the United States the abrasion resistance to a wire scratch brush following cycles of weathering is used.* Both methods are time-consuming and do not give any information about the changes in properties which may occur due to weathering. Further both methods have been only empirically related to field performance. Before a rational testing procedure can be developed to evaluate the durability of stabilized soils it is necessary to determine which fundamental properties of a stabilized soil are altered by weathering.

Based on the above thoughts the aim of this thesis was to determine the influence of stabilizers on the

*See ASTM Testing procedures D559-57 and D560-57 or AASHO procedures T135-37 and T136-57.

effective stress-strength behavior of various soils and to obtain an understanding about strength generation in artificially cemented soils.

To simplify this investigation only completely saturated systems were studied. The strength behavior was determined from triaxial compression tests over a wide range of consolidation pressures (0 to over 50 kg/cm^2). The influence of drainage conditions during shear was obtained by running both drained and undrained tests. In addition the influence of curing time and cycles of wet-dry was obtained for some of the systems investigated.

It is to be hoped that the results presented in this thesis will help set the groundwork for the development of more rational methods for evaluating and predicting the behavior of stabilized soils. The results of this investigation should also shed some light on the behavior of naturally cemented soils.

Chapter 2

DESCRIPTION OF MATERIALS AND TESTING PROCEDURES*

2.1 Soil Types

The two fine-grained soils used in this investigation were a glacial till called Massachusetts Clayey Silt (M-21) and Vicksburg Buckshot Clay (VBC). M-21 is actually a CL-ML soil having a liquid limit of 20.5% and a plasticity index of 5.8%. VBC is a highly plastic clay with a liquid limit of 64.5% and a plasticity index of 36.0%. The textural composition, physical properties, and mineralogical composition of the soils are given in Table 2-1. The particle size distributions are shown in Figure 2-1. M-21 has essentially zero organic matter, about 3% Fe_2O_3 and illitic clay minerals: VBC contains 1.1% organic matter, 1% Fe_2O_3 and illite-montmorillonite clay minerals. The natural fine-grained soils were first air-dried and passed through a No. 4 sieve. The material passing that sieve was then mechanically ground to break up any large soil aggregates. Only the material passing the No. 40 sieve was used in this investigation.

The coarse-grained soil was Ottawa sand which is essentially pure quartz. Two sizes of the sand were used. The coarse Ottawa sand consisted of a uniform sand having

*A detailed description of the testing equipment is given in Appendix A.

100% passing the No. 20 sieve and 95% retained on the No. 30 sieve. The medium Ottawa sand was obtained by sieving a well graded Ottawa sand through No. 40 and No. 60 sieves. The material passing the No. 40 sieve but retained on the No. 60 sieve was used in this investigation. The coarse sand was better rounded than the medium sand as determined from examination under a microscope. For the coarse sand the maximum obtainable dry density was 112.3 lb/cu ft and the minimum obtainable dry density was 96.9 lb/cu ft. The maximum for the medium sand was 107.9 lb/cu ft and the minimum 90.5 lb/cu ft.

2.2 Type and Amount of Stabilizer

The two chemical stabilizers used were reagent grade calcium hydroxide (hydrated lime) and portland cement Type I (commercial grade).

The following soil and soil-stabilizer systems were investigated:

(1) Untreated M-21

(2) M-21 + 3% cement*

(3) M-21 + 5% cement*

(4) M-21 + 5% lime*

(5) Untreated VBC

(6) VBC + 5% lime

*The per cent stabilizer was based on the air-dry weight of soil instead of the oven-dry weight. The error involved is insignificant since the air-dry water content of the soils was about 1%.

(7) VBC + 10% cement + 0.5 N. NaOH

(8) Untreated coarse Ottawa sand

(9) Coarse Ottawa sand + 5% cement

(10) Untreated medium Ottawa sand

(11) Medium Ottawa sand + 5% cement

(12) Medium Ottawa sand + 10% cement

The Atterberg Limits of the fine-grained, soil-stabilizer systems are given in Table 2-2.

2.3 Mixing Procedures

The stabilizers were mixed with the air-dry soils until homogeneous mixtures were obtained. About 1% extra water above the desired amount was added to all the mixes to compensate for evaporation losses which occurred during mixing. The water was mixed in by hand for about five minutes.

2.3.1 Untreated Fine-Grained Soils

After addition of the desired amount of water and mixing the mixes were allowed to equilibrate for three days in sealed glass containers prior to compaction.

2.3.2 Fine-Grained Soil-Lime Mixes

A batch of soil-lime for 4 or 5 compacted samples was prepared at a time. While each sample was being compacted the remaining soil was kept covered with a moist towel and intermittently remixed. All samples from a

batch were compacted within four hours after addition of the mixing water. A water content of the mix was taken before compacting each sample.

2.3.3 Fine-Grained Soil-Cement Mixes

The soil for each compacted sample was mixed separately and compacted immediately after mixing. Two water contents of the mix were taken for each sample, one before and one after compaction. The time between first mixing in of the water and final compaction was not allowed to exceed fifteen minutes.

2.3.4 Sands

The exact weight of dry sand for one sample was hand-blended with the desired amount of cement. The molding water was then added and mixed in thoroughly by hand. One per cent extra water was added to compensate for the moisture lost during mixing.

2.4 Preparation of Test Specimens

2.4.1 Fine-Grained Soils

Two-end static compaction was used to prepare all the fine-grained test specimens. The mold was teflon-lined to minimize wall friction during compaction and it had guided top and bottom plungers.

Mold size:

Length = 3.150 in.

Diameter = 1.405 in.

Volume = 80 cc.

Compactive effort:

A compactive effort of 400 psi was gradually applied to the two rams by means of a hydraulic press. The full pressure was maintained on the samples for approximately one minute before releasing the load off the rams. Sufficient mix was placed in the mold such that neither ram reached the end of its travel when the full compactive effort was applied. Precautions were taken to prevent the top and bottom rams from moving together at different rates so that neither ram reached the end of its travel under the full load.

To investigate the effect of molding dry density a few samples were prepared using a compactive effort of 800 psi instead of 400 psi.

Trimming:

Approximately 15 gm. of excess soil was added to the mold prior to compaction so that both ends of the samples could be carefully trimmed after compaction but prior to extrusion. A sharp straightedge was used to trim the ends of the samples and great pains were taken during trimming to minimize seating imperfections.

2.4.2 Sands

The untreated sand samples were prepared in the triaxial cells using a three-part split sand former. The samples were 3.15 in. long and 1.405 in. in diameter. The sand former supporting the rubber membrane was filled with water and sand poured into the water. The desired density was achieved by rodding the sand with a fine hypodermic needle. The sand former was removed after sealing the sample and applying a small negative pressure to the pore water.

The stabilized samples were prepared in two-part split lucite molds. The samples were compacted in 10 to 15 layers using ten soft tamps per layer applied with a 0.5-in. diameter tamper.

2.5 Curing Conditions

2.5.1 Fine-Grained Soils*

The samples were humid cured by placing them in a desiccator jar which had water in its base. After the desired time of humid cure the stabilized samples were completely immersed in water for at least 24 hours before being placed in the triaxial cells.

In the case of the unstabilized soil samples no humid curing or immersion was used after compaction.

*See Kim (1964)** for details on the cycles of wetting and drying. A mild cycle consisted of 3 days' drying at 30% R.H. followed by 1 day at 100% R.H. and 2 days' gradual soaking by surrounding the sample with a wet sponge. A severe cycle consisted of 2 days' air drying at room temperature followed by 1 day complete immersion in water.

**Items indicated thus, Kim (1964), refer to corresponding entries arranged alphabetically in the List of References.

2.5.2 Sands

The sand-cement samples were cured in a similar manner to the stabilized fine-grained samples except that the lucite molds were stripped after three days of humid curing.

2.6 Consolidation and Saturation of Fine-Grained Triaxial Samples

2.6.1 For Low Consolidation Pressures Only

The triaxial cells were deaired and placed in a deep trough of water. The stabilized samples which had been soaked were then placed on saturated coarse porous stones and mounted under water onto the cell pedestals. In the case of the untreated soil samples it was not possible to assemble them under water since they would have disintegrated during assembly. The stabilized samples were mounted under water so as to avoid trapping air during assembly. Eight 1/4-in. wide saturated filter strips were equally spaced down the sides of the samples. The function of the filter strips was to accelerate consolidation. Each sample was enclosed by rolling up from the base two thin rubber membranes with a film of silicon grease between them. The membranes were sealed to the base and top cap by means of neoprene O-rings.

After assembly the triaxial cell chambers were filled with deaired water to approximately a quarter inch

from the top of the cell; the remainder quarter inch was filled with a lightweight lubrication oil.

The samples were then consolidated under a back pressure of 3 to 10 kg/cm^2 to effective stresses varying from 0 to a little over 6 kg/cm^2. Both the cell pressure and back pressure were applied by means of self-compensating mercury columns.

The samples were allowed to consolidate and saturate for one to two days after which the pore pressure response (i.e., Skempton B factor) to a cell pressure increment of 10 psi was measured by means of a mercury null system to check the degree of saturation. If by that time the pore pressure response was less than 90% in one minute the cell pressure and back pressure were increased simultaneously by equal amounts and the samples allowed to saturate for a further 24 hours after which the pore pressure response was checked. In most cases this increase in back pressure was sufficient to saturate the samples. No sample was tested unless at least 90% response was obtained in one minute.

2.6.2 For High Consolidation Pressures Only*

A similar procedure to that used for low consolidation pressures was used for the high consolidation pressure tests except for the following differences:

*A general layout and detailed description of the high pressure equipment can be found in M.I.T. (1963).

i. One hundredth-inch thick rubber membranes were used instead of the two thinner rubber membranes for enclosing the samples since the latter did not have the necessary strength under these high cell pressures.

ii. The pore pressure responses were measured by means of a differential pressure transducer or an absolute transducer.

iii. In the high pressure tests it was not possible to obtain 90% pore pressure response. This was due to the rigid nature of the soil skeleton which had a bulk modulus of the same order of magnitude as that of water. Saturation was therefore determined by increasing the cell pressure in five 20-psi increments and computing the corresponding pore pressure response per increment. If the pore pressure response remained constant for each of the five increments of cell pressure the samples were assumed saturated and ready for test. Further, to insure saturation at the high pressures the samples were always backpressured to at least 10 atmospheres by means of self-compensating mercury columns.

2.6.3 Unconfined Compression

The samples which were to be used for unconfined compression tests were kept completely immersed in water until the corresponding triaxial samples had been saturated

and consolidated and then they were tested at constant water content without further saturating.

2.7 Consolidation and Saturation of Coarse-Grained Triaxial Samples

The cemented sand samples were set up in a similar manner to the fine-grained samples except that no filter strips were used and the samples were consolidated and saturated under a back pressure of 10 kg/cm^2* for two hours prior to shearing.

The untreated sand specimens which were prepared under water in the triaxial cells were consolidated and saturated under a back pressure of 10 kg/cm^2* for two hours prior to shearing. No filter strips were used.

2.8 Triaxial Testing Procedures

2.8.1 Consolidated-Undrained Tests

Having obtained a satisfactory pore pressure response the triaxial samples were tested in undrained shear with pore pressure measurements.

For most of the low consolidation pressure tests the cell pressure was kept constant during shear by means of self-compensating mercury columns and the pore pressures measured with a mercury null system.** However in

*In the case of the undrained tests on the sand systems back pressures of up to 70 kg/cm^2 were used to prevent the pore water from cavitating during shear.

**This equipment is described by Bishop and Henkel (1962).

a few of the tests on the fine-grained samples at consolidation approaching zero large negative pore pressures developed during shear and it was found necessary to vary the cell pressure and maintain the pore pressure constant so as to keep the samples saturated during shear.

At high consolidation pressures (above 6 kg/cm^2) the cell pressure was kept constant by means of nitrogen tank pressure regulators and the pore pressures during shear were measured with a Dynisco differential pressure transducer which towards the end of this investigation was replaced by an absolute transducer.

All tests were strain controlled. A rate of strain of about 6% axial strain per hour was used with the sand samples. One per cent axial strain per hour was used with the M-21 samples and 0.5% per hour with the VBC samples.

The axial loads were measured with proving rings. Since the samples tested had a wide range of strengths, a number of proving rings having capacities ranging from 300 lb to 3000 lb and sensitivities ranging from 1/8 lb/div. to 2.0 lb/div. had to be used to maintain reasonable accuracy. In the case of the undrained tests on the sands it was necessary to use a 10,000-lb proving ring with a sensitivity of 9 lb/div.

Final water contents of the samples were determined at the end of the tests but no rate of consolidation data was obtained.

2.8.2 Consolidated-Drained Tests

The consolidated-drained tests were strain controlled. The sand samples were sheared at 6% axial strain per hour and the VBC samples at 0.045% axial strain per hour. Volume changes during shear were measured under the back pressure of 10 kg/cm^2 to the nearest 0.01%.

2.8.3 Unconfined Compression Tests

The samples tested in unconfined compression were sealed in thin rubber membranes during the test to prevent evaporation. They were sheared at a strain rate of about 0.5% axial strain per minute.

2.9 Miscellaneous Tests

2.9.1 Atterbert Limits

Liquid and plastic limits were obtained for both untreated and the stabilized fine-grained soils according to ASTM specifications. For the stabilized soils the limits were run immediately after adding the stabilizers to the dry soils and mixing in the water.

2.9.2 Specific Gravities

The specific gravities for the untreated fine-grained soils were determined using the procedure described by Lambe (1951). The specific gravities of the fine-

grained soils stabilized with 5% lime were determined in a similar manner after the mixtures had cured for various periods in sealed containers at water contents slightly wet of optimum.

2.9.3 Particle Size Distributions

Particle size distributions of the untreated fine-grained soils passing a No. 40 sieve (after grinding) were obtained using wet sieving and the hydrometry method described by Lambe (1951). A pinch of sodium tetraphosphate (Quadrafos) was used as the dispersant in the hydrometry tests.

Grain-size distributions of the fine-grained stabilized samples were obtained on the triaxial test specimens, after their water contents had been determined by drying at 105°C, by cutting the samples into three equal parts and using a third of the sample for each determination. Each third was further broken up into three parts and each part crushed by using 30 blows of a Harvard Miniature Compaction Tamper spring loading at 40 lb. After crushing the material was sieved through a No. 10 sieve and the material retained on the sieve collected. All the plus No. 10 sieve material from the three parts was then crushed again using the same procedure. The crushed samples were then soaked in water for at least 48 hours before determining their particle size distribution using wet sieving and

hydrometry. The wet sieving was achieved by washing the material through the sieves with a jet of water such that about 30 litres of water went through the sieves in 30 minutes.* The water passing the finest sieve (No. 325) was collected and soil in it allowed to settle out. This soil was then used for the hydrometry analysis.

2.9.4 Moisture-Density Relations

Moisture-density relations were obtained for both the untreated and the stabilized fine-grained soils from samples compacted by static compaction using 400 psi compactive effort. The untreated samples were prepared from mixtures which were equilibrated in sealed glass containers for three days after adding various amounts of molding water to the dry soil and mixing by hand. The stabilized samples were compacted immediately after mixing with various amounts of water.

2.9.5 Maximum and Minimum Density of the Sands

The maximum density of the sands was obtained by spraying the dry sand into a Proctor mold using a glass funnel. The bottom of the funnel was kept 6 in. above the surface of the sand. The funnel was continuously moved

*For comparison purposes this method was also used with the untreated soils. The results using this method showed less fines than the wet sieving method used with the untreated soils which included hand rubbing of the material on the sieves during washing.

during spraying in of the sand such that the surface of the sand remained essentially flat during filling of the mold.

The minimum density of the sands was also obtained using a funnel but the bottom of the funnel was now kept nearly in contact with the apex of the sand pile which developed in the center of the mold because the position of the funnel was kept constant during filling of the mold.

2.9.6 Variations in As-Molded Dry Density and Shrinkage Limit

To determine the variation in dry density and shrinkage limit within statically compacted samples, untreated samples after compaction and stabilized samples after compaction and curing were cut into six discs of approximately equal thickness. The volume of each disc was accurately determined by the mercury displacement method. The water content of each disc was then obtained in the usual manner except that the samples were allowed to dry slowly in the air at room temperature before placing in a 110°C oven to prevent the development of cracks. The oven-dry samples were then used for shrinkage limit determinations according to Lambe (1951).

Table 2-1

PROPERTIES OF UNTREATED FINE-GRAINED SOILS

	M-21	VBC
Textural Composition, % by wt.		
Sand 2 mm to 0.06 mm	42	5
Silt 0.06 mm to 0.002 mm	43	65
Clay 0.002 mm	15	30
Physical Properties		
Liquid Limit, %	20.5	64.5
Plastic Limit, %	14.7	28.0
Plasticity Index, %	5.8	36.5
Specific Gravity	2.75	2.66
Max. Dry Density(1), lb/cu ft	123.0	106.0
Optimum Water Content(1), %	13.2	18.8
Classification		
Unified	CL-ML	CH
AASHO	A-4(0)	A-7-7(20)
Chemical Properties(2)		
Organic Matter, % by wt.	0.2	1.1
Cation Exchange Capacity meq./100 gm	10	30
Glycol Retention mg/gm	22	65
Mineralogical Composition(2)		
Clay Composition, % by wt.	30	50
Illite: Montmorillonoid	1:0	1:1(3)
Free Iron Oxide, % Fe_2O_3	2.9	1.0

(1) Static compaction, 400 psi effort.

(2) For minus 0.074 mm fractions obtained from a different batch of soil.

(3) Most montmorillonoid mineral is montmorillonite.

Table 2-2

ATTERBERG LIMITS OF SOIL STABILIZER

Soil	Stabilizer	Liquid limit $w_{\ell\ell}$ %	Plastic limit $w_{p\ell}$ %	Plasticity index P.I. %
M-21	None	20.5	14.7	5.8
M-21	5% lime*	22.5	19.4	3.1
M-21	3% cement*	21.3	17.7	3.6
M-21	5% cement*	21.2	17.6	3.6
VBC	None	64.5	27.9	35.6
VBC	5% lime*	61.4	47.3	15.1
VBC	10% cement + 0.5N NaOH*	54.6	40.6	14.0

*Determined immediately after mixing in of the water.

FIGURE 2-1 GRAIN SIZE DISTRIBUTION OF THE UNTREATED FINE-GRAINED SOILS

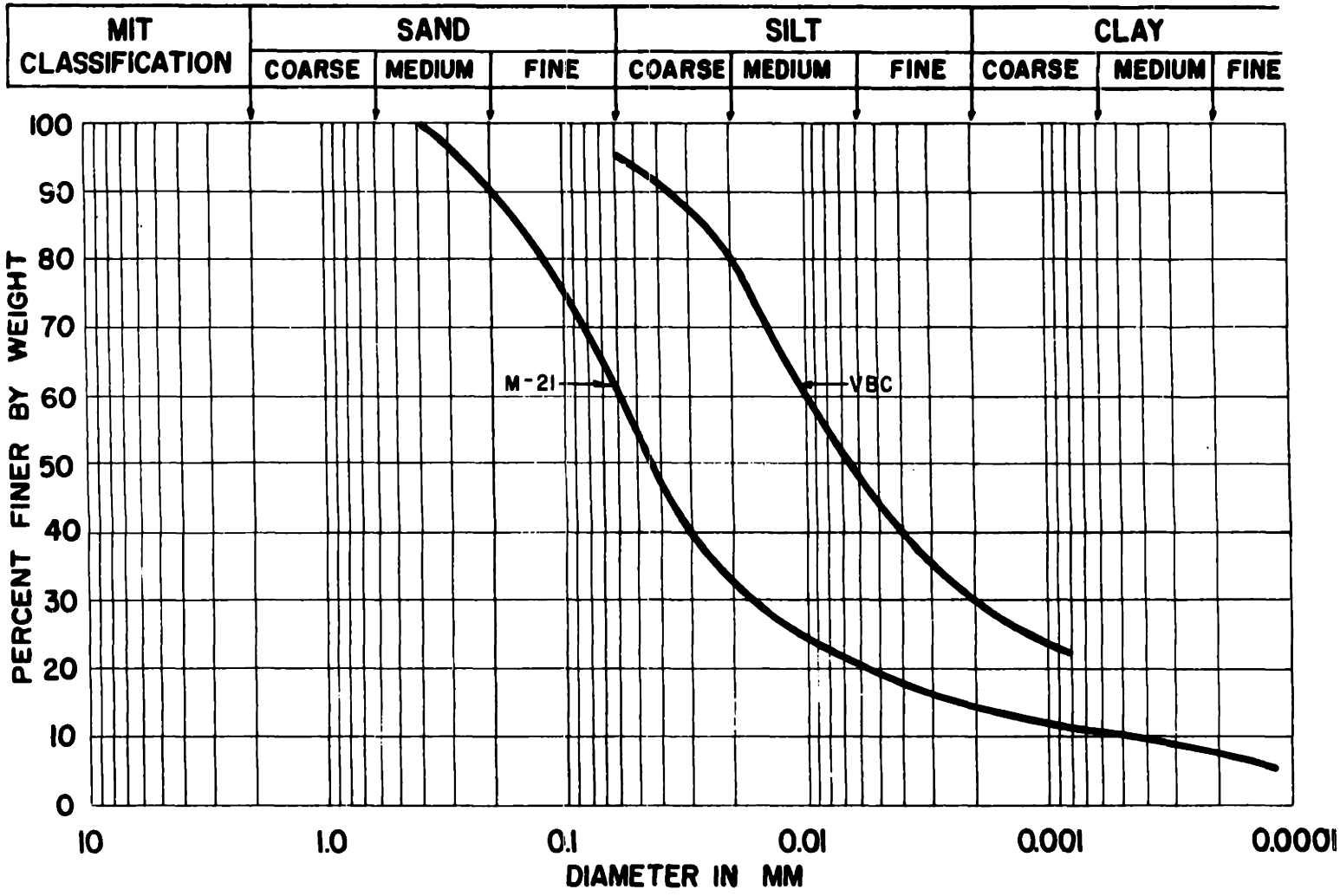

Chapter 3

DISCUSSION OF TESTING PROCEDURES AND COMPUTATIONS

3.1 Uniformity of the Fine-Grained Soil-Stabilizer Mixtures

The desired percentage of chemical stabilizer based on the dry weight of soil was added to the air-dry soil and mixed until streaks of the stabilizer were no longer visible in the mixture. The streaks disappeared only when the mixtures were completely homogeneous.

3.2 Addition of Water to the Dry Mixture

3.2.1 Untreated Fine-Grained Soils

After thoroughly mixing in the desired amount of water the untreated soil mixtures were sealed in glass containers for three days to allow them to equilibrate prior to compaction. This eliminated the possibility of any dry soil aggregates remaining in the mixture.

3.2.2 Soil-Lime Mixtures

A large batch of soil-lime mixture was mixed with the desired amount of water for about five minutes. Each batch contained sufficient material to compact four or five samples, which took about three hours. During this time a damp cloth was kept over the mixture to prevent drying out and the mixture was intermittently remixed to retard the initial set. In the case of hydrated lime stabilization a

few hours' delay between first mixing of the water and final compaction is permissible because the reaction is relatively slow. Consequently the delay has no effect on the as-molded dry density and strength of the stabilized soil.

3.2.3 Soil-Cement Mixtures

The time between first adding the water and final compaction of the fine-grained mixtures was not permitted to exceed 15 minutes. Therefore it was possible only to mix in the water for one sample at a time. This time limitation was imposed because portland cement sets up very rapidly with M-21. Fig. 3-1, which has been plotted from data obtained by Serani (1961), shows that a delay of a few hours between first adding the water and final compaction causes a substantial loss in the as-molded dry density and unconfined compressive strength of M-21 + 5% cement.

3.3 Compaction

Two-end static compaction was used in the preparation of all specimens, a full description of which was given in Chapter 2. Static compaction was chosen in preference to kneading compaction because it eliminates the laminations between layers which occur with kneading compaction. However static compaction produces specimens

which are not uniform in density, as can be seen from Fig. 3-2 and Table 3-1. The lower dry density at the center of the specimens is due to wall friction during compaction. Provided the two compaction rams move together simultaneously, the distribution of density is symmetrical about the middle of the specimen even though the density in the middle may be 4 to 5 lb/cu ft lower than the density at the ends (Fig. 3-2). Specimens having the same overall dry density may then be assumed to have the same distribution of density along their length. This is satisfactory for investigating all of the variables considered herein, as long as it is remembered that the densities reported are average densities and not the actual densities in the failure zones.

Even though the ends of the samples were made as smooth as possible, seating imperfections were not always eliminated, especially with the stronger samples.

3.4 Curing

3.4.1 Humid Cure

The stabilized soil samples were humid cured in desiccator jars above a free water surface. It was observed that samples compacted wet of optimum lost water during the period of humid cure. It is now believed that the loss of moisture was caused by having too many samples

in each disiccator which caused the relative humidity in the desiccators to drop below 100%.

Furthermore, when samples compacted wet and dry of optimum were placed in the same desiccator, the samples dry of optimum picked up moisture and samples wet of optimum lost moisture.

One should therefore cure samples dry and wet of optimum in separate containers and keep the number of samples per container to a minimum.

3.4.2 Soaking

The stabilized soil samples were first subjected to unconfined soaking by completely immersing them in water. Some of the samples were then set up in triaxial cells, consolidated, and saturated. The time required for saturation depended on the amount of air entrapped during setting up as well as the initial degree of saturation of the samples and magnitude of back pressure applied. Since the time required for saturation varied considerably from sample to sample it was not feasible to keep the time of confined soaking prior to shear the same for all the tests; rather each set of triaxial tests was run when saturation was reached. The samples to be tested in unconfined compression were left immersed in water until their triaxial counterparts had been tested. They were then tested in unconfined compression.

3.5 Saturation of Triaxial Samples

The triaxial samples were saturated by means of back pressuring the pore fluid during consolidation.

Self-compensating mercury control systems were used to apply the back pressure, a full description of which is given by Bishop and Henkel (1962). These systems have a working pressure range of 0 to 160 psi. Deaired water was used in the mercury control systems to increase the solubility of the air from the samples. Since the water in these systems is not in contact with the atmosphere, only the air from the samples will dissolve in it.

Mercury control systems were also used to apply the cell pressure for the low consolidation pressure samples (0 to 6 kg/cm^2) in order to eliminate the possibility of air diffusing into the samples from the water in the triaxial chambers.

The cell pressure was applied by nitrogen tanks for the high consolidation pressure samples, but special precautions were taken to prevent nitrogen from diffusing into the samples.*

3.6 Testing of Triaxial Samples

The effective stress-strength behavior of a soil can be obtained either from consolidated-drained tests

*For further details see Phase Report No. 2, M.I.T. (1963).

(CD) or from consolidated-undrained tests ($\overline{CU}$) with pore pressure measurements.

In the CD test, drainage is permitted such that no excess pore pressures are set up during shear. This requires a sufficiently slow shear rate to allow the excess pore pressure to dissipate. Further, since the sample volume is changing in CD tests an energy correction must be applied if these results are to be compared to those obtained from $\overline{CU}$ tests. CD tests were usually used with the sand systems for reasons mentioned later.

In the $\overline{CU}$ test no drainage is permitted during shear and the test is a constant volume test provided the sample remains saturated. Another advantage is that $\overline{CU}$ tests may be run at a faster rate of strain than CD tests since the amount and length of flow required for pore pressure redistribution due to nonuniform stress conditions are lower than for complete drainage. $\overline{CU}$ tests were usually used with the fine-grained systems. A discussion of the pore pressure measuring equipment is given in Appendix A.

3.7 Computation of Degree of Saturation for Unconfined Compression Test Samples

In computing the degree of saturation of the unconfined compression test samples the following assumptions were made:

1. The triaxial samples were 100% saturated.
2. The volume change of the stabilized soil triaxial samples due to small consolidation pressures was negligible.
3. The specific gravity of the stabilized soils was independent of curing time. (This is a reasonable assumption as can be seen from Fig. 3-3.)
4. The ratio of the final void ratios of the triaxial samples at the lowest consolidation pressures to the void ratios of their corresponding unconfined compression test samples after soaks is the same as the ratio of their as-molded void ratios.

Using the above assumptions the degree of saturation of the unconfined compression samples can be obtained from the following equation:

$$S = \frac{G\gamma_w - \gamma_{d_1}}{G\gamma_w - \gamma_{d_2}} \cdot \frac{\gamma_{d_1}}{\gamma_{d_2}} \cdot \frac{w_2}{w_1} \cdot 100$$

where S = Degree of saturation of the unconfined sample, %

G = Specific gravity of the stabilized soil

γ_{d_1} = As-molded dry density of the triaxial sample

w_1 = Final water content of the triaxial sample after saturation and consolidation to a small pressure (less than 0.5 kg/cm^2)

γ_{d_2} = As-molded dry density of the corresponding unconfined compression sample

w_z = Final water content of the unconfined compression sample

γ_w = Density of water

3.8 Calibrations

All pressure gauges and proving rings used in this investigation were calibrated every three months. The differential pressure producers used with the high pressure tests were calibrated after each test because their zero point did not remain constant for long periods of time. The absolute transducers did not need such frequent calibrations.

3.9 Area Corrections

As a result of the lower density in the middle of the triaxial specimens and the end restraints, excessive bulging often took place in the middle half of the samples during shear. The conventional assumption, i.e., that the sample remains cylindrical with strain, used to calculate the cross-sectional area as a function of axial strain, ε, considerably underestimated the actual cross-sectional area when excessive bulging occurred. The conventional equation $A = A_o/(1 - \varepsilon)$ was in these cases replaced by $A = A_o/(1 - 2\varepsilon)$ to account for the excess bulging. This modified area equation gave results which were in better agreement with the cross-sectional areas measured at the

end of the tests. When a brittle failure occurred or when only slight bulging was observed, the conventional equation was used to calculate the area. To obtain the effective stress-strength relations at ultimate conditions the actual final cross-sectional areas of the samples were used to compute the stresses.

3.10 Triaxial Test Computations

An IBM 1620 computer program was used to compute and plot the triaxial test results. All necessary calibrations were included in the program. Complete details of the program have been given in Soil Stabilization Phase Report No. 2, M.I.T. (1963).

Table 3-1

DRY DENSITY AND SHRINKAGE LIMIT VARIATIONS WITHIN STATICALLY COMPACTED SAMPLES

Sample No.	Disc No.	γ_d of whole sample lb/cu ft	γ_d of disc lb/cu ft	Variation* in γ_d %	Shrinkage* limits of discs %	Change* in S.L. %
(M-21 Untreated)						
	1		125.2	4.2	15.3	0
	2		122.4	1.8	16.8	1.5
I	3	122.4	120.4	0.2	19.6	4.3
	4		120.2	0	19.9	4.6
	5		121.9	1.4	17.2	1.9
	6		124.4	3.5	15.6	0.3
(M-21 Untreated)						
	1		124.8	4.2	15.6	0.8
	2		122.0	1.8	17.1	2.3
II	3	122.2	119.8	0	19.6	4.8
	4		120.2	0.3	19.4	4.6
	5		121.7	1.6	16.5	1.7
	6		125.2	4.5	14.8	0
(M-21 + 5% lime)						
	1		115.2	2.4	14.6	0.2
	2		113.0	0.4	15.0	0.6
III	3	113.9	112.5	0	16.7	2.3
	4		112.6	0.1	16.3	1.9
	5		114.0	1.3	15.1	0.7
	6		116.0	3.1	14.4	0
(M-21 + 5% lime)						
	1		115.7	2.9	14.5	0
	2		113.2	0.7	15.3	0.8
IV	3	113.8	112.5	0.1	16.4	1.9
	4		112.4	0	16.6	2.1
	5		113.7	1.1	15.4	0.9
	6		115.2	2.5	14.9	0.4

*Based on the lowest value among the discs of each sample.

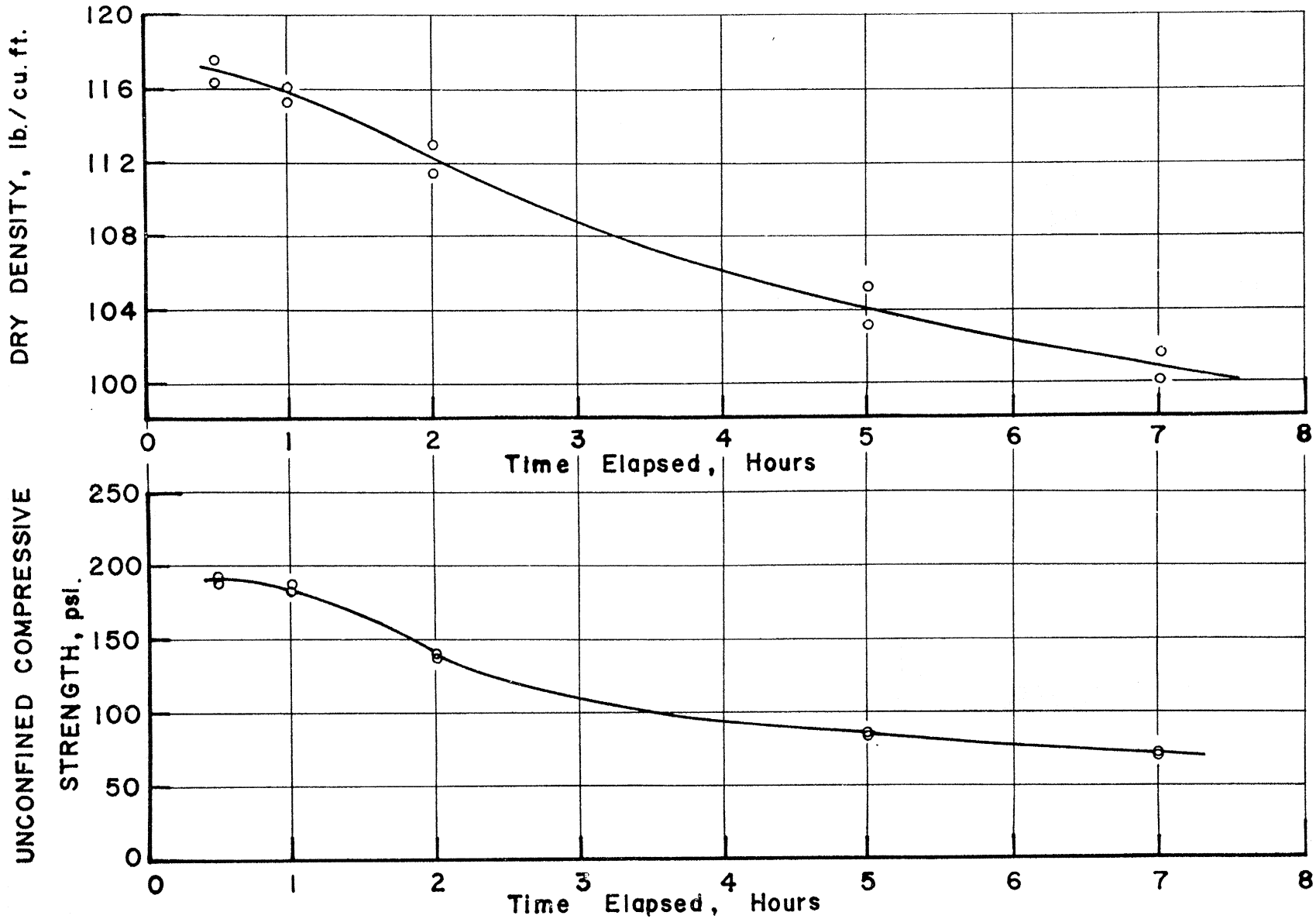

FIGURE 3-1. EFFECT OF DELAYED TIME BETWEEN MIXING AND COMPACTION ON DRY DENSITY AND COMPRESSIVE STRENGTH OF MASSACHUSETTS CLAYEY SILT PLUS 5% CEMENT

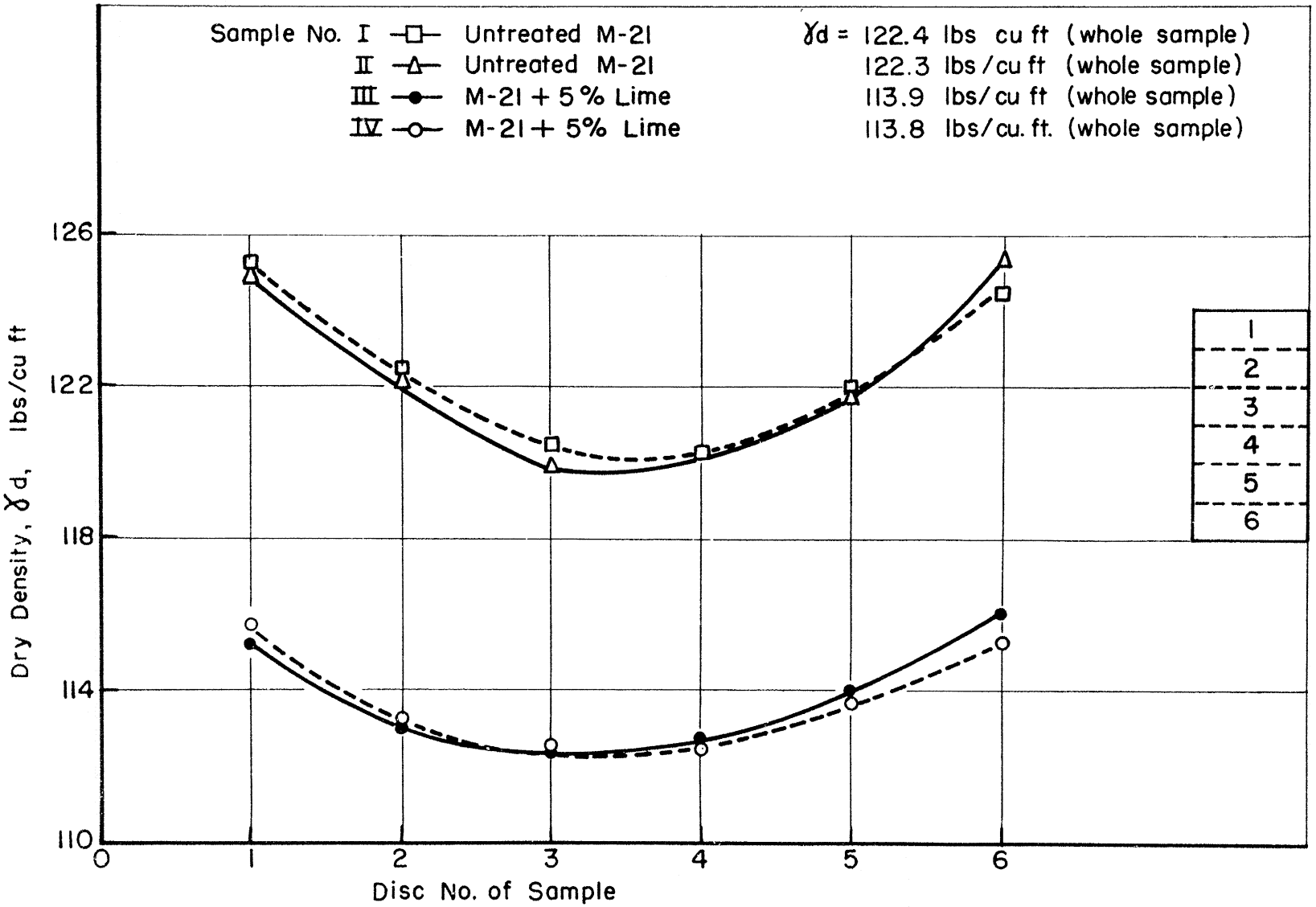

FIGURE 3-2. VARIATION IN DRY DENSITY WITHIN A SAMPLE PREPARED BY TWO-END STATIC COMPACTION

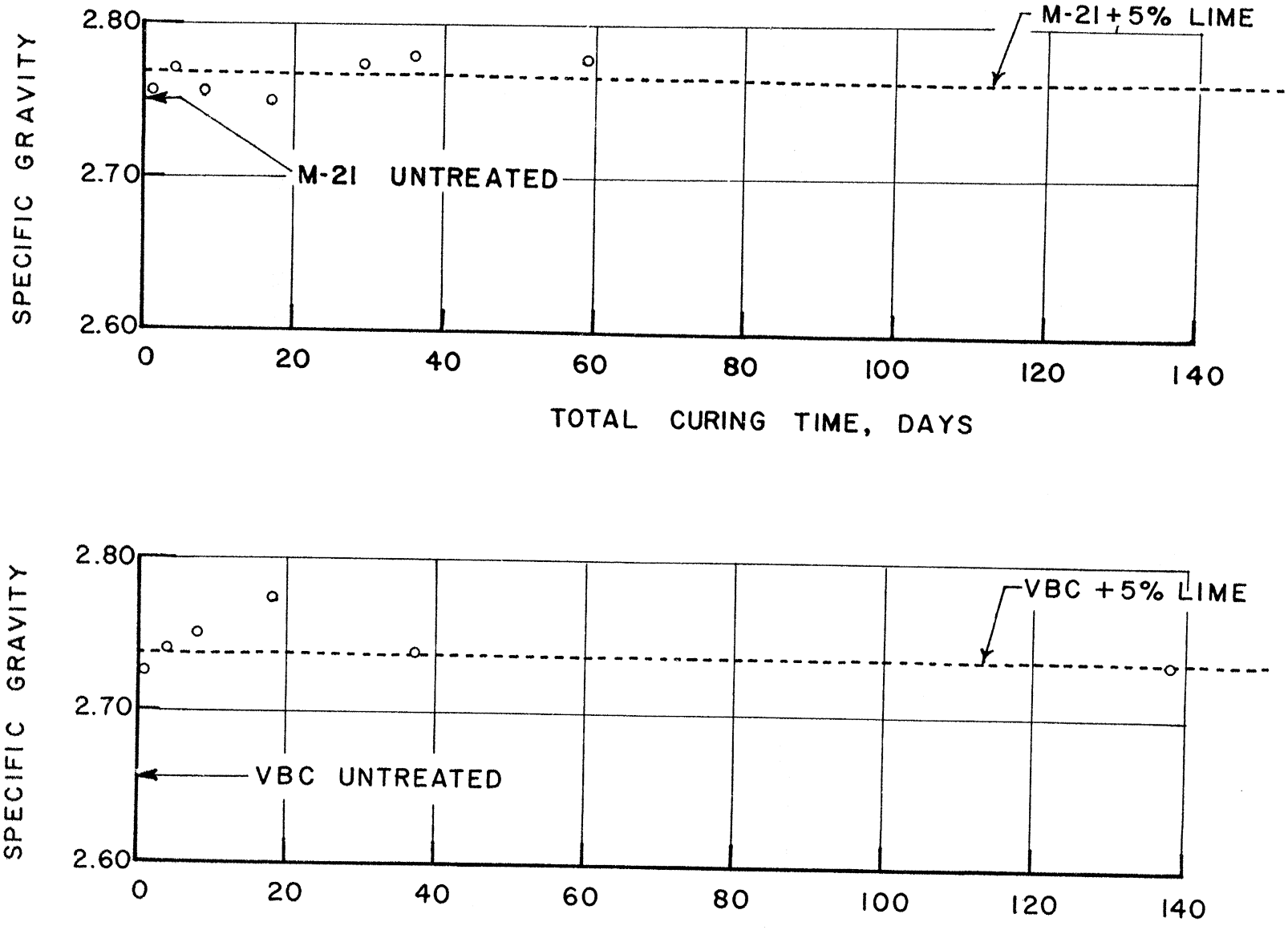

FIGURE 3-3. EFFECT OF CURING TIME ON SPECIFIC GRAVITY OF LIME STABILIZED SOILS

Chapter 4

PRESENTATION OF TEST RESULTS

4.1 Preshear Data

The preshear data for all the triaxial test samples and their unconfined compression test counterparts are given in Tables 4-1 through 4-3. Molding conditions, curing times, consolidation pressures, final water contents, pore pressure responses, and degrees of saturation are included in these tables.

The preshear data for the moisture-density relations have been plotted in Figs. 4-1 through 4-3.

4.2 Stress-Strain Data

Stress-strain curves for all the triaxial tests are given in Appendix B. Since an average of sixty sets of reading were taken per test, an IBM 1620 computer* was used to analyze and plot the data. The curves in Appendix B were drawn through all the points plotted by the computer but only a few points have been shown in these figures. Each figure for the undrained tests gives plots of stress difference, $(\sigma_1 - \sigma_3)$, excess pore pressure, (Δu), $\bar{A}$ factor and principal effective stress ratio, $\bar{\sigma}_1 / \bar{\sigma}_3$, versus axial strain for a single triaxial test.

---

*See Soil Stabilization Phase Report No. 2, M.I.T. (1963).

For the drained tests $(\sigma_1 - \sigma_3)$ and $\Delta V/V$ were plotted against axial strain.

The stress-strain curves for the unconfined compression tests have not been included in this thesis.

A summary of the stress-strain characteristics of all the tests are given in Tables 4-4 through 4-6. These tables include initial tangent moduli and the stress-strain characteristics at both $(\sigma_1 - \sigma_3)_T$ and $(\sigma_1 - \sigma_3)_M$* for the undrained tests and at $(\sigma_1 - \sigma_3)_M$ and ultimate for the drained tests.

4.3 Effective Stress Paths and Effective Stress-Strength Envelopes

The effective stress paths and effective stress-strength envelopes have been drawn on $\bar{p}$ versus q plots where $\bar{p} = 1/2\ (\bar{\sigma}_1 + \bar{\sigma}_3)$ and $q = 1/2\ (\sigma_1 - \sigma_3)$. A Mohr circle of stresses can easily be obtained for any point, $(\bar{p}, q)$, on such a plot by simply drawing through the point a circle whose radius is equal to the ordinate, q, and whose center lies on the $\bar{p}$-axis at a distance $\bar{p}$ from the origin.

The effective stress path which usually defines the stress history during shear on the plane at $45 + \bar{\phi}/2$

*Suffix T represents conditions at point of first tangency with the effective stress-strength envelope and suffix M represents conditions at maximum stress difference.

to the major principal plane is now the locus of stresses on the maximum shear plane which is still a fixed plane with respect to the principal planes and is at an angle of 45° to them.

The trigonometric relations between the Mohr-Coulomb effective stress parameters, $\bar{c}$ and $\bar{\phi}$, and the q-intercept, $\bar{a}$, and angle $\bar{\alpha}$ of the $\bar{p}$ - q envelope are:

$$\tan \bar{\alpha} = \sin \bar{\phi}$$

$$\bar{c} = \bar{a} \frac{\tan \bar{\phi}}{\tan \bar{\alpha}} = \frac{\bar{a}}{\cos \bar{\phi}}$$

The angle and intercept of the envelopes as obtained on the $\bar{p}$ - q plots have been converted using the above relations and only the values of the effective stress parameters $\bar{c}$ and $\bar{\phi}$ are referred to in this report.

The effective stress paths, like the stress-strain characteristics, were initially plotted by the computer but only a few points have been shown on the figures.

The axial strain contours drawn on the $\bar{p}$ versus q plots have been corrected for seating imperfections when such imperfections were observed in the stress-strain plots.

TABLE 4-I

SUMMARY OF PRE-SHEAR DATA FOR SAND SAMPLES

SAMPLE NO.	SAND TYPE	CEMENT CONTENT %	WATER-CEMENT RATIO	CURING TIME* DAYS	MOLD. DRY DENS. OF SAND ONLY lb/cu.ft.	MOLD. DRY DENS. OF SAND +CEMENT lb/cu.ft.	RELAT. DENSITY OF SAND ONLY-%	CONSOLIDATION PRESS. $\bar{\sigma}_o$ kg/cm^2	CONSOLIDATION WATER CONTENT ω_o - %	TYPE OF TRIAXIAL COMPRESSION
205	COARSE	NONE	—	—	102.9	—	42	10.1	20.6	DRAINED SHEAR
208	COARSE	NONE	—	—	102.9	—	42	25.0	19.6	
207	COARSE	NONE	—	—	102.9	—	42	50.0	19.5	
408	COARSE	5	2:1	28	102.9	109.0	42	0.07	?	
409	COARSE	5	2:1	28	102.9	109.0	42	10.0	?	
404	COARSE	5	2:1	28	102.9	109.0	42	25.0	16.7	
401	COARSE	5	2:1	28	102.9	109.0	42	50.4	17.4	
601	MEDIUM	NONE	—	—	102.9	—	75	10.1	20.0	DRAINED SHEAR
602	MEDIUM	NONE	—	—	102.9	—	76	25.0	20.0	
603	MEDIUM	NONE	—	—	102.9	—	75	50.0	20.0	
606	MEDIUM	NONE	—	—	100.5	—	62	5.0	20.6 ?	
607	MEDIUM	NONE	—	—	100.5	—	62	10.0	?	
604	MEDIUM	NONE	—	—	100.5	—	62	25.0	22.1	
605	MEDIUM	NONE	—	—	100.5	—	62	50.0	21.2	
801	MEDIUM	5	1:1	32	100.8	105.7	63	0.07	?	
802	MEDIUM	5	1:1	33	100.8	105.7	63	10.0	20.1	
803	MEDIUM	5	1:1	32	100.8	105.7	63	25.0	19.7	
804	MEDIUM	5	1:1	33	100.3	105.0	61	50.0	19.5	
1001	MEDIUM	10	1:1	22	101.0	110.1	64	0.07	16.4	
1002	MEDIUM	10	1:1	21	100.9	110.0	64	10.0	16.7	
1003	MEDIUM	10	1:1	21	101.0	110.1	64	25.0	15.8	
1004	MEDIUM	10	1:1	21	101.0	110.1	64	50.0	14.7	
213	COARSE	NONE	—	—	104.8	—	54	6.59	19.4	UNDRAINED SHEAR
214	COARSE	NONE	—	—	102.9	—	42	5.95	21.0	
410	COARSE	5	2:1	25	102.9	109.0	42	8.05	18.4	UNDRAINED SHEAR
501	MEDIUM	NONE	—	—	100.5	—	62	1.90	24.6	UNDRAINED SHEAR
502	MEDIUM	NONE	—	—	100.5	—	62	32.3	20.3	

* INCLUDES 1 DAY SOAKING IN WATER.

TABLE 4-2

PRE - SHEAR DATA FOR THE MASSACHUSETTS CLAYEY SILT SYSTEMS

SAMPLE NO.	SOIL	STABILIZER %	COMPACTIVE EFFORT p.s.i.	AS MOLDED		CURING TIME			Consolidation PRESSURE kg/cm2	FINAL WATER CONTENT %	PORE PRESSURE RESPONSE %	DEGREE OF SATURATION %
				WATER CONTENT %	DRY DENSITY lb/cu.ft.	HUMID CURE DAYS	SOAKING DAYS	TOTAL CURE DAYS				
1	M-21	NONE	400	11.0	117.5	—	6	6	0.08	15.6	95	~100
2	M-21	NONE	400	10.9	117.5	—	6	6	5.34	14.3	98	~100
3	M-21	NONE	400	15.6	118.0	—	6	6	3.22	13.8	98	~100
4	M-21	NONE	400	15.8	117.5	—	6	6	5.18	13.1	93	~100
5	M-21	NONE	800	16.0	119.3	—	6	6	0.02	15.6	98	~100
6	M-21	NONE	800	16.2	119.1	—	6	6	5.34	13.1	97	~100
U	M-21	5% LIME	400	17.3	112.9	8	6	14	0	16.1	—	93.8
7	M-21	5% LIME	400	17.3	112.4	8	6	14	0	17.4	99	~100
8	M-21	5% LIME	400	17.2	112.6	8	6	14	4.42	17.1	98	~100
U	M-21	5% LIME	800	17.9	116.1	8	6	14	0	16.4	—	94.5
9	M-21	5% LIME	800	17.7	116.6	8	6	14	0	17.1	97.5	~100
10	M-21	5% LIME	800	17.6	116.4	8	6	14	4.53	16.9	93.5	~100
U	M-21	5% LIME	400	13.4	111.6	8	6	14	0	17.8	—	90.8
11	M-21	5% LIME	400	13.6	111.3	8	6	14	0	20.1	95	~100
12	M-21	5% LIME	400	13.8	111.3	8	6	14	4.33	19.8	93	~100
13	M-21	NONE	400	13.2	123.7	—	5	5	0.50	13.6	99	~100
14	M-21	NONE	400	13.8	122.4	—	4	4	4.57	12.4	98	~100
15	M-21	NONE	400	12.7	124.4	—	5	5	4.95	12.5	95	~100
16	M-21	NONE	400	13.9	122.6	—	4	4	20.4	11.4	80	~100
17	M-21	NONE	400	13.8	122.6	—	4	4	50.1	10.4	75	~100
U	M-21	5% LIME	400	16.2	111.1	3	1	4	0	18.4	—	92.8
18	M-21	5% LIME	400	15.7	111.6	0	4	4	0.50	19.6	94	~100
19	M-21	5% LIME	400	15.1	111.5	0	4	4	4.93	18.7	93	~100
U	M-21	5% LIME	400	16.3	111.0	6	2	8	0	18.4	—	96.4
20	M-21	5% LIME	400	15.1	112.9	6	2	8	0.44	18.5	98	~100
21	M-21	5% LIME	400	15.1	113.0	6	2	8	4.82	18.2	97	~100
U	M-21	5% LIME	400	16.2	111.9	12	5	17	0	18.1	—	97.8
22	M-21	5% LIME	400	15.8	112.4	12	5	17	0.06	18.5	92	~100
23	M-21	5% LIME	400	15.8	112.4	12	5	17	4.91	18.3	97	~100
U	M-21	5% LIME	400	15.4	111.8	9	11	20	0	16.7	—	—
68	M-21	5% LIME	400	15.4	112.1	9	11	20	0.35	19.0	98	~100
69	M-21	5% LIME	400	15.5	112.3	9	11	20	4.95	18.3	97	~100
70	M-21	5% LIME	400	15.6	112.1	9	11	20	19.4	17.1	79	~100
71	M-21	5% LIME	400	15.6	112.1	9	11	20	54.5	14.0	70	~100
U	M-21	5% LIME	400	16.1	111.9	30	5	35	0	16.0	—	96.1
24	M-21	5% LIME	400	15.7	112.7	30	5	35	0.65	18.5	95	~100
25	M-21	5% LIME	400	15.9	112.6	30	5	35	5.53	17.4	93	~100
26	M-21	5% LIME	400	16.0	112.7	30	5	35	21.2	16.4	90	~100
27	M-21	5% LIME	400	15.9	112.5	30	5	35	44.1	16.1	89	~100

TABLE 4-2

(continued)

PRE - SHEAR DATA FOR THE MASSACHUSETTS CLAYEY SILT SYSTEMS

SAMPLE NO.	SOIL	STABILIZER %	COMPACTIVE EFFORT p.s.i.	AS MOLDED		CURING TIME			Consolidation PRESSURE kg/cm^2	FINAL WATER CONTENT %	PORE PRESSURE RESPONSE %	DEGREE OF SATURATION %
				WATER CONTENT %	DRY DENSITY lb/cu.ft.	HUMID CURE DAYS	SOAKING DAYS	TOTAL CURE DAYS				
U	M-21	5% LIME	400	15.9	112.6	55	4	59	0	17.9	—	96.4
28	M-21	5% LIME	400	14.4	112.3	55	4	59	0.58	18.4	95	≤100
29	M-21	5% LIME	400	14.5	111.7	55	4	59	4.76	19.0	90	≤100
U	M-21	5% LIME	400	15.0	113.4	133	5	138	0	15.1	—	91.5
30	M-21	5% LIME	400	15.0	112.9	133	5	138	0.35	16.9	92	≤100
31	M-21	5% LIME	400	14.9	112.4	133	5	138	4.93	17.0	91	≤100
32	M-21	5% LIME	400	14.9	112.4	133	5	138	19.2	15.9	?	≤100
33	M-21	5% LIME	400	14.8	112.3	133	5	138	53.8	16.0	?	≤100
72	M-21	5% LIME	400	16.1	111.9	?	?	275	4.93	19.9	90	≤100
73	M-21	5% LIME	400	16.0	112.5	?	?	275	19.4	19.1	75	≤100
74	M-21	5% LIME	400	16.0	112.4	?	?	275	53.7	18.3	66	≤100
U	M-21	3% CEMENT	400	15.3	118.0	13	8	21	0	14.1	—	89
42	M-21	3% CEMENT	400	15.1	118.0	13	8	21	0	16.0	91.0	≤100
43	M-21	3% CEMENT	400	14.9	118.3	13	8	21	4.41	15.8	98.0	≤100
44	M-21	3% CEMENT	400	14.9	118.2	13	8	21	24.2	15.0	90	≤100
45	M-21	3% CEMENT	400	14.8	118.2	13	8	21	55.4	13.3	72	≤100
U	M-21	5% CEMENT	400	15.8	117.5	3	7	10	0	15.0	—	93
46	M-21	5% CEMENT	400	15.8	116.6	3	7	10	0.27	16.2	99.0	≤100
47	M-21	5% CEMENT	400	16.4	116.2	3	7	10	5.14	16.5	99.0	≤100
48	M-21	5% CEMENT	400	16.0	116.4	3	7	10	23.2	15.6	87.0	≤100
49	M-21	5% CEMENT	400	16.0	116.2	3	7	10	53.7	14.3	80.0	≤100
U	M-21	5% CEMENT	400	14.5	118.4	38	12	50	0	15.8	—	?
50	M-21	5% CEMENT	400	14.4	118.1	38	12	50	0.19	?	99	≤100
51	M-21	5% CEMENT	400	14.5	118.2	38	12	50	4.98	?	92	≤100
52	M-21	5% CEMENT	400	14.5	118.2	38	12	50	24.0	?	58	≤100
53	M-21	5% CEMENT	400	14.4	118.3	38	12	50	47.2	?	55	≤100
U	M-21	5% CEMENT	400	14.3	117.0	89	9	98	0	14.7	—	86
54	M-21	5% CEMENT	400	14.2	119.0	89	9	98	0.35	16.2	95.0	≤100
55	M-21	5% CEMENT	400	14.2	119.1	89	9	98	5.43	15.6	92.0	≤100
56	M-21	5% CEMENT	400	14.5	118.8	89	9	98	25.2	16.6	58	≤100
57	M-21	5% CEMENT	400	14.2	118.6	89	9	98	48.4	16.4	?	≤100

TABLE 4-3

PRE-SHEAR DATA FOR THE VICKSBURG BUCKSHOT CLAY SYSTEMS

PRE-SHEAR DATA FOR THE UNTREATED AND STABILIZED VICKSBURG BUCKSHOT CLAY SPECIMENS TESTED IN UNDRAINED SHEAR

SAMPLE NO	STABILIZER	AS-MOLDED WATER CONTENT %	AS-MOLDED DRY DENSITY lb/cuft	CURING TIME HUMID CURE DAYS	CURING TIME SOAKING DAYS	CURING TIME TOTAL* CURE DAYS	CYCLES OF WET / DRY	CONSOLIDATION PRESS. kg/cm²	FINAL WATER CONTENT %	PORE PRESS. RESPONSE - %	DEGREE OF SATURATION - %
90	NONE	30.6	91.3	—	—	—	—	0.53	32.8	100	≃100.0
91		31.3	90.7	—	—	—	—	5.0	27.2	97	≃100.0
92		31.1	91.0	—	—	—	—	25.0	20.2	85	≃100.0
93		31.2	91.1	—	—	—	—	50.0	17.8	81	≃100.0
901	5% LIME	27.6	91.0	368	30	398	NONE	0.10	31.9	100	≃100.0
902		28.4	90.7	378	20	398		5.25	29.7	92.5	≃100.0
903		28.2	91.0	362	30	392		24.8	29.0	87	≃ 87
904		29.3	90.7	374	18	392		50.1	27.0	81	≃ 81
UNCONFINED 1109	10% CEMENT + 0.5N.NaOH	21.2	98.2	39	4	43	NONE	0	22.6	—	87
1110		21.2	99.9	30	13	43		0.10	25.8	97	≃100.0
1110		21.2	99.9	30	13	43		5.0	25.6	94	≃100.0
1110		21.5	100.3	30	13	43		25.0	25.7	78	≃100.0
1112		21.4	99.7	30	13	43		50.0	26.3	71	≃100.0
UNCONFINED 1117	10% CEMENT + 0.5N.NaOH	?	?	52	3	55	NONE	0	?	—	?
1118		21.8	99.7	52	3	55		0.10	26.6	96	≃100.0
1119		21.6	99.7	52	3	55		5.0	26.0	93	≃100.0
1120		21.6	100.3	52	3	55		25.0	25.2	75	≃100.0
		21.4	100.1	52	3	55		50.0	24.2	71	≃100.0
UNCONFINED 1121	10% CEMENT + 0.5N.NaOH	21.5	99.8	34	3	55	TWO MILD CYCLES (18 DAYS)	0	23.8	—	92
1122		20.9	99.7	34	3	55		0.10	25.9	97	≃100.0
1123		21.2	100.0	34	3	55		5.0	25.5	95	≃100.0
1124		21.8	100.0	34	3	55		25.0	24.4	80	≃100.0
		21.4	100.1	34	3	55		50.0	23.8	75	≃100.0
UNCONFINED 1125	10% CEMENT + 0.5 N.NaOH	21.2	100.5	77	6	90	TWO SEVERE CYCLES (7 DAYS)	0	23.2	—	92
1126		21.4	100.0	77	6	90		0.10	25.1	94	≃100.0
1127		21.7	99.5	77	6	90		5.0	24.9	91	≃100.0
1128		21.3	99.8	77	6	90		25.0	24.6	77	≃100.0
		21.5	99.7	77	6	90		50.0	25.4	72	≃100.0

PRE-SHEAR DATA FOR THE STABILIZED VICKSBURG BUCKSHOT CLAY SPECIMENS TESTED IN DRAINED SHEAR

SAMPLE NO	STABILIZER	AS-MOLDED WATER CONTENT %	AS-MOLDED DRY DENSITY lb/cuft	CURING TIME HUMID CURE DAYS	CURING TIME SOAKING DAYS	CURING TIME TOTAL* CURE DAYS	CONSOLIDATION PRESS. kg/cm²	WATER CONTENT AFTER CONSOLIDATION %	DEGREE OF SATURATION - %
905	5% LIME	27.4	91.2	368	18	386	0.09	32.4	≃100.0
906		28.1	91.0	367	18	385	5.24	30.7	≃100.0
907		28.7	91.0	362	18	380	24.7	29.8	≃100.0
908		29.1	91.5	362	18	380	50.1	29.4	≃100.0

* INCLUDES PERIOD OF CYCLING WHEN APPLICABLE

TABLE 4-4 SUMMARY OF THE STRESS-STRAIN CHARACTERISTICS OF THE OTTAWA SAND SYSTEMS.

SUMMARY OF STRESS-STRAIN CHARACTERISTICS OF UNTREATED AND STABILIZED SAND SPECIMENS IN DRAINED SHEAR.

SAMPLE NO.	SAND-STABILIZER SYSTEM	TOTAL CURING TIME DAYS	CONSOLIDATION PRESS. $\bar{\sigma}_3$ kg/cm²	INITIAL TANGENT MODULUS E kg/cm²	AT MAXIMUM STRESS DIFFERENCE: AXIAL STRAIN ε %	MINOR PRINCIP. EFFECT. STRESS $\bar{\sigma}_3$ kg/cm²	PRINCIP. STRESS DIFFER. $(\sigma_1-\sigma_3)$ kg/cm²	PRINCIP. EFFECT. STRESS RATIO $\bar{\sigma}_1/\bar{\sigma}_3$	HALF PRINCIP. STRESS DIFFER. $\frac{1}{2}(\sigma_1-\sigma_3)$ kg/cm²	AVERAGE PRINCIP. EFFECT. STRESS $\frac{1}{2}(\bar{\sigma}_1+\bar{\sigma}_3)$ kg/cm²	VOLUME CHANGE $\Delta V/V$ %	WATER CONTENT %	AT ULTIMATE: AXIAL STRAIN ε %	MINOR PRINCIP. EFFECT. STRESS $\bar{\sigma}_3$ kg/cm²	PRINCIP. STRESS DIFFER. $(\sigma_1-\sigma_3)$ kg/cm²	PRINCIP. EFFECT. STRESS RATIO $\bar{\sigma}_1/\bar{\sigma}_3$	HALF PRINCIP. STRESS DIFFER. $\frac{1}{2}(\sigma_1-\sigma_3)$ kg/cm²	AVERAGE PRINCIP. EFFECT. STRESS $\frac{1}{2}(\bar{\sigma}_1+\bar{\sigma}_3)$ kg/cm²	VOLUME CHANGE $\Delta V/V$ %	WATER CONTENT %	REMARKS
205	UNTREATED COARSE	NONE	10.1	3300	4.3	10.1	24.0	3.38	12.0	22.1	0.99	21.3	16.0	10.1	20.2	3.00	10.1	20.2	3.96	23.1	
208		NONE	25.0	5800	5.3	25.0	59.6	3.38	29.8	54.8	1.03	20.1	15.6	25.0	51.4	3.06	25.7	50.7	3.19	21.5	
207		NONE	50.0	8350	5.4	50.0	108.1	3.16	54.0	104.0	0.06	19.6	16.5	50.0	96.9	2.94	48.4	93.4	0.49	19.9	
408	COARSE + 5% CEMENT	28	0.07	3400	0.25	0.07	6.7	9.?	3.35	3.42	−0.04	?	7.3	0.07	0.81	12.57	6.41	0.48	7.76	?	
409		28	10.0	7000	3.7	10.0	30.0	4.0	15.0	25.0	0.35	?	15.5	10.0	23.7	3.37	11.9	21.9	3.11	?	
404		28	25.0	9700	5.5	25.0	60.6	3.42	30.3	55.3	0.30	16.9	17.5	25.0	49.7	2.99	24.9	49.9	2.61	18.3	
401		28	50.4	9400	8.8	50.4	102.2	3.03	51.1	101.5	−0.73	16.8	22.5	50.4	93.5	2.85	46.7	97.1	−0.13	17.3	
601	UNTREATED R.D. = 76 %	NONE	10.1	2850	5.4	10.1	32.1	4.18	16.0	26.1	2.32	21.6	20.5	10.1	21.5	3.13	10.7	20.8	7.45	24.5	
602		NONE	25.0	4900	5.9	25.0	70.2	3.81	35.1	60.1	1.29	20.8	23.4	25.0	51.5	3.06	25.8	50.8	5.60	23.4	
603		NONE	50.0	5800	5.7	50.0	125.7	3.51	62.8	112.8	0.29	20.3	19.8	50.0	106.6	3.13	53.3	103.3	2.29	21.5	SEATING CORRECTION
606	UNTREATED R.D. = 62 %	NONE	5.0	1100	4.1	5.0	15.8	4.16	7.9	12.9	∝1.63	21.6?	13.2	5.0	10.7	3.14	5.4	10.4	∝4.33	23.3?	SEATING CORRECTION
607		NONE	16.0	2400	6.4	10.0	27.3	3.73	13.6	23.6	∝1.60	?	22.7	10.0	20.2	3.02	10.1	20.1	∝5.41	?	
604		NONE	25.0	5200	6.3	25.0	64.0	3.56	32.0	57.0	0.79	22.6	19.0	25.0	55.4	3.21	27.7	52.7	3.40	24.2	
605		NONE	50.0	7000	6.0	50.0	116.5	3.33	58.2	108.2	0.13	21.3	16.8	50.0	106.5	3.13	53.3	103.3	0.95	21.8	
801	MEDIUM + 5% CEMENT	32	0.07	5200	0.62	0.07	23.0	328	11.50	11.57	−0.01	?	8.2	0.07	1.32	19.8	0.66	0.73	7.65	?	
802		33	10.0	12000	0.85	10.0	60.8	7.08	30.4	40.4	−0.03	20.0	14.5	10.0	31.3	4.13	15.7	25.7	5.13	23.0	
803		32	25.0	12600	2.3	25.0	90.9	4.64	45.5	70.5	−0.52	19.4	20.7	25.0	61.1	3.22	30.6	55.6	3.22	21.6	
804		33	50.0	12500	3.6	50.0	143.3	3.87	71.6	121.6	−0.91	18.9	20.0	50.0	111.2	3.22	155.6	105.6	0.58	19.8	
1001	MEDIUM + 5% CEMENT	22	0.07	19500	0.30	0.07	47.5	676	23.7	23.8	−0.26	16.3	3.3	0.07	1.70	25.3	0.85	0.92	4.7	19.0	
1002		21	10.0	19200	0.84	10.0	89.9	9.99	44.9	54.9	−0.11	16.7	12.0	10.0	37.0	4.70	18.5	28.5	5.4	19.7	
1003		21	25.0	19800	1.66	25.0	137.9	6.52	69.0	94.0	−0.21	15.6	15.4	25.0	82.2	4.29	41.1	66.1	3.52	17.6	
1004		21	50.0	19600	2.7	50.0	201.5	5.03	100.8	150.8	−0.54	14.4	18.2	50.0	131.6	3.63	65.8	115.8	2.23	15.9	

SUMMARY OF STRESS-STRAIN CHARACTERISTICS OF UNTREATED AND STABILIZED SAND SPECIMENS IN UNDRAINED SHEAR.

SAMPLE NO.	SAND-STABILIZER SYSTEM	TOTAL CURING TIME DAYS	CONSOLIDATION PRESS. $\bar{\sigma}_3$ kg/cm²	INITIAL TANGENT MODULUS E kg/cm²	AT MAXIMUM STRESS DIFFERENCE: AXIAL STRAIN ε %	MINOR PRINCIP. EFFECT. STRESS $\bar{\sigma}_3$ kg/cm²	PRINCIP. STRESS DIFFER. $(\sigma_1-\sigma_3)$ kg/cm²	EXCESS PORE PRESS. ΔU kg/cm²	A FACTOR $\frac{\Delta U}{\sigma_1-\sigma_3}$	PRINCIP. EFFECT. STRESS RATIO $\bar{\sigma}_1/\bar{\sigma}_3$	HALF PRINCIP. STRESS DIFFER. $\frac{1}{2}(\sigma_1-\sigma_3)$ kg/cm²	AVERAGE PRINCIP. EFFECT. STRESS $\frac{1}{2}(\bar{\sigma}_1+\bar{\sigma}_3)$ kg/cm²	AT POINT OF FIRST TANGENCY WITH ENVELOPE: AXIAL STRAIN ε %	MINOR PRINCIP. EFFECT. STRESS $\bar{\sigma}_3$ kg/cm²	PRINCIP. STRESS DIFFER. $(\sigma_1-\sigma_3)$ kg/cm²	EXCESS PORE PRESS. ΔU kg/cm²	A FACTOR $\frac{\Delta U}{\sigma_1-\sigma_3}$	PRINCIP. EFFECT. STRESS RATIO $\bar{\sigma}_1/\bar{\sigma}_3$	HALF PRINCIP. STRESS DIFFER. $\frac{1}{2}(\sigma_1-\sigma_3)$ kg/cm²	AVERAGE PRINCIP. EFFECT. STRESS $\frac{1}{2}(\bar{\sigma}_1+\bar{\sigma}_3)$ kg/cm²	REMARKS
213	UNTREATED COARSE	NONE	6.59	3000	10.3	58.6	129.1	−52.0	−0.42	3.10	61.6	120.2	3.3	16.5	42.1	−9.9	−0.23	3.56	21.0	37.5	
214		NONE	5.95	2300	12.4	43.3	88.1	−37.3	−0.42	3.04	44.0	87.2	3.8	15.9	37.1	−9.9	−0.27	3.34	18.5	34.5	SEATING CORRECTION
410	COARSE + 5% CEM.	25	8.05	9000	15.2	50.1	95.0	−42.1	−0.44	2.90	47.5	97.6	1.35	8.9	26.5	−0.87	−0.03	3.97	13.2	22.2	
501	UNTREATED MEDIUM	NONE	1.90	150 ?	16.2	49.4	104.1	−47.5	0.46	3.11	52.0	101.5	5.6	14.0	33.5	−12.1	−0.36	3.40	16.8	30.8	SEATING CORRECTION
502		NONE	32.3	6000	9.2	63.2	146.5	−30.9	−0.21	3.32	73.2	136.4	2.7	30.9	79.3	1.4	0.02	3.57	39.6	70.5	

TABLE 4-5

SUMMARY OF THE STRESS - STRAIN CHARACTERISTICS FOR THE MASSACHUSETTS CLAYEY SILT SYSTEMS

SAMPLE NO.	TOTAL CURING TIME DAYS	Consolidation PRESSURE $\bar{\sigma}_c$ kg/cm²	INITIAL TANGENT MODULUS E kg/cm²	AT MAXIMUM STRESS DIFFERENCE $(\sigma_1-\sigma_3)_{max}$ AXIAL STRAIN ε %	MINOR EFFECTIVE PRINCIPAL STRESS $\bar{\sigma}_3$ kg/cm²	PRINCIPAL STRESS DIFFERENCE $(\sigma_1-\sigma_3)$ kg/cm²	EXCESS PORE PRESSURE Δu kg/cm²	$\bar{A}$-FACTOR $\frac{\Delta u}{\Delta\sigma_1-\Delta\sigma_3}$	EFFECTIVE PRINCIPAL STRESS RATIO $\bar{\sigma}_1/\bar{\sigma}_3$	HALF PRINCIPAL STRESS DIFFERENCE $\frac{1}{2}(\sigma_1-\sigma_3)$ kg/cm²	AVERAGE EFFECTIVE PRINCIPAL STRESS $\frac{1}{2}(\bar{\sigma}_1+\bar{\sigma}_3)$ kg/cm²	AT POINT OF FIRST TANGENCY WITH EFFECTIVE STRESS ENVELOPE AXIAL STRAIN ε %	MINOR EFFECTIVE PRINCIPAL STRESS $\bar{\sigma}_3$ kg/cm²	PRINCIPAL STRESS DIFFERENCE $(\sigma_1-\sigma_3)$ kg/cm²	EXCESS PORE PRESSURE Δu kg/cm²	$\bar{A}$-FACTOR $\frac{\Delta u}{\Delta\sigma_1-\Delta\sigma_3}$	EFFECTIVE PRINCIPAL STRESS RATIO $\bar{\sigma}_1/\bar{\sigma}_3$	HALF PRINCIPAL STRESS DIFFERENCE $\frac{1}{2}(\sigma_1-\sigma_3)$ kg/cm²	AVERAGE EFFECTIVE PRINCIPAL STRESS $\frac{1}{2}(\bar{\sigma}_1+\bar{\sigma}_3)$ kg/cm²	REMARKS
1	6	0.08	330	11.4	0.34	0.98	−0.26	−0.26	3.9	0.49	0.83	0.68	0.11	0.60	−0.03	−0.05	6.4	0.30	0.41	
2	6	5.34	800	1.9	2.27	4.39	3.07	0.70	2.9	2.19	4.46	6.9	1.84	3.97	3.50	0.88	3.23	1.99	3.83	
3	6	3.22	1000	12.4	1.61	3.38	1.61	0.48	3.1	1.69	3.30	4.4	1.25	2.90	1.97	0.68	3.3	1.45	2.70	
4	6	5.18	1400	11.7	2.53	5.26	2.65	0.50	3.1	2.63	5.16	3.8	2.06	4.58	3.12	0.68	3.2	2.29	4.35	
5	6	0.02	100	12.1	0.25	0.79	−0.23	−0.29	4.2	0.40	0.65	1.9	0.10	0.52	−0.08	−0.15	6.2	0.26	0.36	
6	6	5.34	1700	9.4	2.81	5.65	2.53	0.45	3.0	2.83	5.64	2.1	2.19	4.77	3.15	0.66	3.2	2.38	4.57	
U	14	0	270	3.8	—	3.08	—	—	—	1.54	—	—	—	—	—	—	—	—	—	
7	14	0	350	13.3	2.25	6.35	−2.25	−0.35	3.8	3.18	5.43	3.3	0.40	4.00	−0.40	−0.10	10.0	2.00	2.40	
8	14	4.42	1000	11.8	4.49	11.12	−0.07	−0.01	3.5	5.56	10.05	2.50	2.41	8.40	2.01	0.24	4.5	4.20	6.61	
U	14	0	290	3.5	—	4.45	—	—	—	2.23	—	—	—	—	—	—	—	—	—	
9	14	0	400	13.4	4.81	12.21	−4.81	−0.39	3.5	6.10	10.91	2.8	1.47	8.04	−1.47	−0.18	6.5	4.02	5.49	
10	14	4.53	1500	12.2	6.49	16.90	−1.96	−0.12	3.6	8.45	14.94	2.0	2.65	10.72	1.88	0.18	5.0	5.36	8.01	
U	14	0	260	3.8	—	3.80	—	—	—	1.90	—	—	—	—	—	—	—	—	—	
11	14	0	650	5.0	1.03	4.28	−1.03	−0.24	5.2	2.14	3.17	0.7	0.03	2.82	−0.03	−0.01	95.0	1.41	1.44	
12	14	4.33	1500	1.2	2.53	8.28	1.80	0.22	4.3	4.14	6.67	0.8	2.41	7.94	1.92	0.24	4.3	3.97	6.38	
13	5	0.50	400	14.2	1.32	2.73	−0.82	−0.30	3.1	1.36	2.68	1.3	0.70	1.81	−0.20	−0.11	3.6	0.91	1.60	
14	4	4.57	800	15.2	2.53	4.98	2.04	0.41	3.0	2.49	5.02	3.8	1.91	4.23	2.66	0.63	3.2	2.11	4.20	
15	5	4.95	840	12.8	2.81	6.08	2.14	0.35	3.2	3.04	5.85	5.8	2.46	5.65	2.49	0.44	3.3	2.83	5.29	
16	4	20.4	6400	9.9	8.2	18.2	12.3	0.67	3.2	9.1	17.2	4.7	7.3	17.0	13.1	0.77	3.3	8.5	15.8	
17	4	50.1	7600	10.6	19.2	41.2	30.9	0.75	3.2	20.6	39.8	6.3	17.9	40.1	32.1	0.80	3.2	20.1	38.0	
U	4	0	500	1.0	—	3.88	—	—	—	1.94	—	—	—	—	—	—	—	—	—	
18	4	0.50	1000	3.9	1.36	4.70	−0.86	−0.19	4.5	2.35	3.71	1.0	0.87	4.00	−0.37	−0.09	5.6	2.00	2.86	
19	4	4.93	2000	1.5	2.88	7.88	2.05	0.26	3.7	3.94	6.82	2.8	2.56	7.61	2.37	0.31	4.0	3.80	6.36	SEATING CORRECTION
U	8	0	900	1.0	—	4.04	—	—	—	2.02	—	—	—	—	—	—	—	—	—	
20	8	0.44	1000	>8.6	>1.8	>6.20	<−1.40	(−0.22	<4.3	>3.10	>4.00	0.9	0.57	3.69	−0.13	−0.04	7.5	1.84	2.41	SEATING CORRECTION
21	8	4.82	1400	2.8	3.11	8.50	1.92	0.23	3.9	4.25	7.15	2.5	3.09	8.45	1.94	0.23	3.9	4.22	7.10	SEATING CORRECTION
U	17	0	1000	1.0	—	6.62	—	—	—	3.31	—	—	—	—	—	—	—	—	—	
22	17	0.08	700	2.8	1.67	7.62	−1.61	−0.21	5.6	3.81	5.48	1.5	0.79	6.04	−0.73	−0.21	8.7	3.02	3.81	SEATING CORRECTION
23	17	4.91	3000	4.0	3.60	11.70	1.31	0.11	4.3	5.85	9.45	1.5	3.19	10.27	2.20	0.21	4.8	5.14	7.85	
U	20	0	800	0.7	—	3.07	—	—	—	1.54	—	—	—	—	—	—	—	—	—	
68	20	0.35	900	2.9	1.74	6.70	−1.39	−0.21	4.8	3.35	5.09	1.1	0.77	5.17	−0.41	−0.08	7.8	2.58	3.35	
69	20	4.95	1500	2.1	3.37	10.64	1.58	0.15	4.2	5.32	8.69	1.0	3.05	9.73	1.91	0.20	4.2	4.86	7.91	SEATING CORRECTION
70	20	19.4	4900	2.1	6.9	18.1	12.5	0.69	3.6	9.1	16.0	2.7	6.7	17.9	12.8	0.71	3.7	9.0	15.6	
71	20	54.3	7500	3.5	17.3	40.1	37.1	0.93	3.3	20.1	37.4	4.8	16.8	40.1	37.7	0.94	3.4	20.1	36.8	
U	35	0	1000	1.8	—	9.50	—	—	—	4.75	—	—	—	—	—	—	—	—	—	
24	35	0.65	2000	10.6	1.97	10.57	−1.32	−0.12	6.4	5.20	7.25	2.8	1.20	9.20	−0.55	−0.06	8.7	4.60	5.80	
25	35	5.53	3000	4.8	3.74	14.31	1.74	0.12	4.7	7.16	10.97	1.5	3.09	12.90	2.46	0.19	5.3	6.60	9.69	
26	35	21.2	4000	2.9	6.0	19.6	15.2	0.77	4.3	9.8	15.8	2.9	6.0	19.6	15.2	0.77	4.3	9.8	15.8	SEATING CORRECTION
27	35	44.1	7000	5.6	12.1	32.9	32.1	0.98	3.7	16.4	28.5	5.6	12.1	32.9	32.1	0.98	3.7	16.4	28.5	

TABLE 4-5

(continued)

SUMMARY OF THE STRESS - STRAIN CHARACTERISTICS FOR THE MASSACHUSETTS CLAYEY SILT SYSTEMS

SAMPLE NO.	TOTAL CURING TIME DAYS	Consolidation PRESSURE $\bar{\sigma}_c$ kg/cm²	INITIAL TANGENT MODULUS E kg/cm²	AT MAXIMUM STRESS DIFFERENCE $(\sigma_1-\sigma_3)_{max}$								AT POINT OF FIRST TANGENCY WITH EFFECTIVE STRESS ENVELOPE								REMARKS
				AXIAL STRAIN ϵ %	MINOR EFFECTIVE PRINCIPAL STRESS $\bar{\sigma}_3$ kg/cm²	PRINCIPAL STRESS DIFFERENCE $(\sigma_1-\sigma_3)$ kg/cm²	EXCESS PORE PRESSURE Δu kg/cm²	$\bar{A}$-FACTOR $\frac{\Delta u}{\Delta\sigma_1-\Delta\sigma_3}$	EFFECTIVE PRINCIPAL STRESS RATIO $\bar{\sigma}_1/\bar{\sigma}_3$	HALF PRINCIPAL STRESS DIFFERENCE $\frac{1}{2}(\sigma_1-\sigma_3)$ kg/cm²	AVERAGE EFFECTIVE PRINCIPAL STRESS $\frac{1}{2}(\bar{\sigma}_1+\bar{\sigma}_3)$ kg/cm²	AXIAL STRAIN ϵ %	MINOR EFFECTIVE PRINCIPAL STRESS $\bar{\sigma}_3$ kg/cm²	PRINCIPAL STRESS DIFFERENCE $(\sigma_1-\sigma_3)$ kg/cm²	EXCESS PORE PRESSURE Δu kg/cm²	$\bar{A}$-FACTOR $\frac{\Delta u}{\Delta\sigma_1-\Delta\sigma_3}$	EFFECTIVE PRINCIPAL STRESS RATIO $\bar{\sigma}_1/\bar{\sigma}_3$	HALF PRINCIPAL STRESS DIFFERENCE $\frac{1}{2}(\sigma_1-\sigma_3)$ kg/cm²	AVERAGE EFFECTIVE PRINCIPAL STRESS $\frac{1}{2}(\bar{\sigma}_1+\bar{\sigma}_3)$ kg/cm²	
U	59	0	1600	0.9	—	11.96	—	—	—	5.98	—	—	—	—	—	—	—	—	—	
28	59	0.58	2400	8.2	5.21	16.68	−4.51	−0.28	4.2	8.34	13.55	1.2	1.78	12.10	−1.20	−0.10	7.8	6.05	7.83	
29	59	4.76	4000	3.9	4.14	15.92	0.62	0.04	4.9	7.96	12.10	1.6	2.93	14.72	1.83	0.12	6.0	7.36	10.29	SEATING CORRECTION
U	138	0	2600	0.7	—	12.90	—	—	—	6.45	—	—	—	—	—	—	—	—	—	
30	138	0.35	2600	3.0	1.40	11.20	−1.05	−0.09	9.0	5.60	7.00	0.9	0.61	10.62	−0.26	−0.03	18.4	5.31	5.9	SEATING CORRECTION
31	138	4.93	3000	3.4	6.82	21.07	−1.89	−0.09	4.1	10.53	17.35	0.7	2.80	15.19	2.13	0.14	6.4	7.59	10.4	SEATING CORRECTION
32	138	19.2	6400	2.9	10.7	30.2	8.4	0.28	3.8	15.1	25.1	4.2	9.8	30.0	9.3	0.31	4.0	15.0	24.9	
33	138	53.8	9000	2.0	18.9	47.9	34.9	0.73	3.5	23.9	42.9	3.4	17.8	47.2	36.0	0.76	3.6	23.6	41.4	SEATING CORRECTION
72	275	4.93	2300	3.2	5.56	29.75	−0.63	−0.02	6.3	14.87	20.44	1.1	0.85	24.75	4.09	0.17	30.3	12.37	13.22	
73	275	19.3	6500	6.7	9.7	37.9	9.6	0.25	4.9	19.0	28.7	0.8	3.5	33.2	15.8	0.47	10.4	16.6	20.1	
74	275	53.7	9400	2.4	15.9	58.0	37.8	0.65	4.7	29.0	44.8	1.9	15.4	57.9	38.3	0.66	4.8	28.9	44.3	
U	21	0	1300	1.4	—	9.42	—	—	—	4.71	—	—	—	—	—	—	—	—	—	
42	21	0	1150	9.1	1.39	11.14	−1.39	−0.12	9.0	5.57	6.96	8.1	1.31	10.82	−1.31	−0.12	9.3	5.41	6.72	
43	21	4.41	2500	5.9	5.07	17.60	−0.66	−0.07	4.5	8.80	13.87	2.7	2.95	14.34	1.46	0.10	5.9	7.17	10.12	
44	21	24.2	4800	11.3	12.0	31.2	12.2	0.39	3.6	15.6	27.6	2.1	7.7	25.9	16.5	0.64	4.4	12.9	20.6	
45	21	55.4	11,500	8.9	20.4	50.2	35.1	0.70	3.5	25.1	45.5	3.8	17.8	48.5	37.6	0.78	3.7	24.3	42.1	
U	10	0	900	1.2	—	13.80	—	—	—	6.90	—	—	—	—	—	—	—	—	—	
46	10	0.27	2800	>4.1	>4.80	>24.25	<−4.53	<−0.19	<6.1	>12.12	>16.92	1.2	0.92	13.41	−0.65	−0.05	15.6	6.70	7.62	
47	10	5.14	1600	6.1	7.35	28.00	−2.21	−0.08	4.8	14.00	21.35	2.7	3.38	20.43	1.76	0.09	7.0	10.22	13.80	
48	10	23.2	9000	>6.7	>13.4	>40.5	<10.1	<0.25	<4.1	>20.2	>33.4	2.0	7.2	32.1	16.0	0.50	5.5	16.0	23.2	
49	10	53.7	12,000	7.7	18.7	64.3	35.0	0.54	4.4	32.1	50.8	2.6	16.0	58.9	37.7	0.64	4.7	29.4	45.4	
U	50	0	2600	1.2	—	11.60	—	—	—	5.80	—	—	—	—	—	—	—	—	—	
50	50	0.19	3850	4.3	7.08	39.87	−6.89	−0.17	6.6	19.93	27.01	1.2	0.19	32.85	0.38	0.01	16.2	16.43	16.24	SEATING CORRECTION
51	50	4.98	3000	2.9	5.79	41.06	−0.81	−0.02	8.1	20.53	26.32	1.9	1.82	37.66	3.16	0.08	21.7	18.83	20.65	SEATING CORRECTION
52	50	24.0	13,000	5.5	16.8	63.4	7.2	0.11	4.8	31.7	48.5	0.8	4.4	45.7	19.6	0.43	11.4	22.9	27.3	
53	50	47.2	13,000	6.5	23.0	82.0	24.2	0.30	4.6	41.0	64.0	1.5	11.8	68.5	35.4	0.52	6.8	34.2	46.1	
U	98	0	2800	1.2	—	27.14	—	—	—	13.57	—	—	—	—	—	—	—	—	—	
54	98	0.35	4000	1.6	1.10	41.18	−0.75	−0.02	37.5	20.09	21.19	1.1	0.04	36.84	0.31	0.01	92.0	18.42	18.46	SEATING CORRECTION
55	98	5.43	5800	>2.4	>8.94	>48.85	(−3.51	(−0.07	<6.5	>24.43	>33.37	0.9	0.24	38.63	5.19	0.13	162.0	19.32	19.56	
56	98	25.2	10,000	6.5	16.9	68.9	8.4	0.12	5.1	34.4	51.3	0.7	4.3	49.9	20.9	0.42	12.5	24.9	29.3	
57	98	48.4	10,000	4.3	20.9	80.7	27.5	0.34	4.9	40.3	61.3	1.0	11.8	72.5	36.6	0.51	7.2	36.2	48.0	

TABLE 4-6

SUMMARY OF STRESS-STRAIN CHARACTERISTICS OF THE VICKSBURG BUCKSHOT CLAY SYSTEMS.

SUMMARY OF STRESS-STRAIN CHARACTERISTICS OF UNTREATED AND STABILIZED VICKSBURG BUCKSHOT CLAY SPECIMENS TESTED IN UNDRAINED SHEAR

SAMPLE NO.	STABILIZER	TOTAL CURING TIME DAYS	CONSOLIDATION PRESS. $\bar{\sigma}_c$ kg/cm²	INITIAL TANGENT MODULUS E kg/cm²	AT MAXIMUM STRESS DIFFERENCE: AXIAL STRAIN ε %	MINOR PRINCIP. EFFECT. STRESS $\bar{\sigma}_3$ kg/cm²	PRINCIP. STRESS DIFFER. $(\sigma_1-\sigma_3)$ kg/cm²	EXCESS PORE PRESS. ΔU kg/cm²	$\bar{A}$ FACTOR $\frac{\Delta U}{(\sigma_1-\sigma_3)}$	PRINCIP. EFFECT. STRESS RATIO $\bar{\sigma}_1/\bar{\sigma}_3$	HALF PRINCIP. STRESS DIFFER. $\frac{1}{2}(\sigma_1-\sigma_3)$ kg/cm²	AVERAGE PRINCIP. EFFECT. STRESS $\frac{1}{2}(\bar{\sigma}_1+\bar{\sigma}_3)$ kg/cm²	AT POINT OF FIRST TANGENCY WITH MOHR-COULOMB EFF. STRESS ENV.: AXIAL STRAIN ε %	MINOR PRINCIP. EFFECT. STRESS $\bar{\sigma}_3$ kg/cm²	PRINCIP. STRESS DIFFER. $(\sigma_1-\sigma_3)$ kg/cm²	EXCESS PORE PRESS. ΔU kg/cm²	$\bar{A}$ FACTOR $\frac{\Delta U}{(\sigma_1-\sigma_3)}$	PRINCIP. EFFECT. STRESS RATIO $\bar{\sigma}_1/\bar{\sigma}_3$	HALF PRINCIP. STRESS DIFFER. $\frac{1}{2}(\sigma_1-\sigma_3)$ kg/cm²	AVERAGE PRINCIP. EFFECT. STRESS $\frac{1}{2}(\bar{\sigma}_1+\bar{\sigma}_3)$ kg/cm²	REMARKS
90	NONE	1	0.53	250	2.3	0.40	1.14	0.13	0.11	3.9	0.57	0.97	0.9	0.30	0.96	0.23	0.24	5.1	0.48	0.78	
91		1	5.0	750	10.7	2.52	3.91	2.48	0.64	2.55	1.95	4.47	5.0	2.52	3.67	2.48	0.67	2.45	1.84	4.36	
92		1	25.0	2800	12.9	17.9	14.3	11.6	0.81	2.06	7.1	20.6	12.9	17.9	14.3	11.6	0.81	2.06	7.1	20.6	
93		1	50.0	4200	11.5	25.4	25.0	24.6	0.99	1.99	12.5	37.9	11.5	25.4	25.0	24.6	0.99	1.99	12.5	37.9	
901	5% LIME	1 YEAR	0.10	3300	1.1	0	27.2	0.10	0.004	∞	13.6	13.6	PREMATURE FAILURE								SEATING CORRECTION
902			5.25	5400	0.9	0.75	29.8	4.5	0.15	41	14.9	15.6	0.9	0.75	29.8	4.5	0.15	41	14.9	15.6	SEATING CORRECTION
903			24.8	8500	1.1	6.6	46.4	18.2	0.45	7.2	20.2	26.7	1.1	6.6	40.4	18.2	0.45	7.2	20.2	26.7	
904			50.1	14000	1.7	15.4	50.5	34.7	0.69	4.27	25.2	40.7	1.7	15.4	50.5	34.7	0.69	4.27	25.2	40.7	
UNCONFINED	10% CEMENT +0.5 N. NaOH	43 DAYS	0	3800	0.7	—	44.5	—	—	—	22.3	—	—	—	—	—	—	—	—	—	
1109			0.10	7500	0.8	0.04	49.7	0.06	0.001	∞	24.8	24.9	PREMATURE FAILURE								SEATING CORRECTION
1110			5.0	13000	0.8	0.90	57.3	4.10	0.07	63	28.6	29.6	0.8	0.90	57.3	4.10	0.07	63	28.6	29.6	
1111			25.0	28000	0.8	6.0	68.2	19.0	0.28	12.3	34.1	40.1	0.8	6.0	68.2	19.0	0.28	12.3	34.1	40.1	
1112			50.0	24000	0.9	12.9	83.8	37.1	0.44	7.5	41.9	54.8	0.9	12.9	83.8	37.1	0.44	7.5	41.9	54.8	
UNCONFINED	10% CEMENT +0.5 N. NaOH	55 DAYS	0	3000	0.9	—	50.2	—	—	—	25.1	—	—	—	—	—	—	—	—	—	
1117			0.10	8000	0.9	0.11	54.9	-0.01	0	482	27.6	27.5	PREMATURE FAILURE								SEATING CORRECTION
1118			5.0	11500	0.9	2.10	61.4	2.90	0.05	30.2	30.7	32.8	0.9	1.05	60.6	3.95	0.07	58.8	30.3	31.3	
1119			25.0	18500	0.7	6.5	70.4	18.5	0.26	11.9	35.2	41.7	0.6	4.8	68.5	20.2	0.30	15.1	34.2	39.0	SEATING CORRECTION
1120			50.0	26000	0.8	13.2	86.9	36.8	0.42	7.57	43.4	56.7	0.8	13.2	86.9	36.8	0.42	7.57	43.4	56.7	
UNCONFINED	10% CEMENT +0.5 N. NaOH	55 DAY CURE (2 CYCLES MILD WET-DRY)	0	3400	0.9	—	41.0	—	—	—	20.5	—	—	—	—	—	—	—	—	—	
1121			0.10	5100	1.0	0	41.3	0.10	0.002	∞	20.6	20.6	PREMATURE FAILURE								SEATING CORRECTION
1122			5.0	6300	1.1	0.5	52.0	4.5	0.09	104	26.0	26.5	1.0	0.4	51.4	4.6	0.09	139	25.7	26.1	SETING CORRECTION
1123			25.0	15000	1.0	8.2	63.8	16.8	0.26	9.8	31.9	40.0	0.7	5.5	59.5	19.5	0.33	11.8	29.8	35.3	
1124			50.0	22000	1.2	14.1	84.7	35.9	0.42	7.0	42.4	56.4	0.9	13.9	83.4	36.1	0.43	7.0	41.7	55.6	
UNCONFINED	10% CEMENT +0.5 N. NaOH	90 DAY CURE (2 CYCLES SEVERE WET-DRY)	0	1300	1.0	—	20.0	—	—	—	40.0	—	—	—	—	—	—	—	—	—	
1125			0.10	2300	3.2	4.4	22.3	-4.3	-0.19	6.06	11.1	15.5	PREMATURE FAILURE								SEATING CORRECTION
1126			5.0	3500	1.5	2.6	36.3	2.4	0.07	14.9	18.1	20.8	PREMATURE FAILURE								SEATING CORRECTION
1127			25.0	17000	0.8	5.9	56.9	19.1	0.33	10.6	28.5	34.4	0.8	5.5	56.3	19.6	0.35	11.1	28.2	33.7	
1128			50.0	18500	1.5	18.1	85.2	31.9	0.37	5.7	42.6	60.7	1.2	17.4	84.5	32.6	0.39	5.88	42.2	59.6	

SUMMARY OF STRESS-STRAIN CHARACTERISTICS OF STABILIZED VICKSBURG BUCKSHOT CLAY IN DRAINED SHEAR

SAMPLE NO.	STABILIZER	TOTAL CURING TIME DAYS	CONSOLIDATION PRESS. $\bar{\sigma}_c$ kg/cm²	INITIAL TANGENT MODULUS E kg/cm²	AT MAXIMUM STRESS DIFFERENCE: AXIAL STRAIN ε %	MINOR PRINCIP. EFFECT. STRESS $\bar{\sigma}_3$ kg/cm²	PRINCIP. STRESS DIFFER. $(\sigma_1-\sigma_3)$ kg/cm²	PRINCIP. EFFECT. STRESS RATIO $\bar{\sigma}_1/\bar{\sigma}_3$	HALF PRINCIP. STRESS DIFFER. $\frac{1}{2}(\sigma_1-\sigma_3)$ kg/cm²	AVERAGE PRINCIP. EFFECT. STRESS $\frac{1}{2}(\bar{\sigma}_1+\bar{\sigma}_3)$ kg/cm²	VOLUME CHANGE Δ V/V %	WATER CONTENT %	REMARKS
905	8 % LIME	386	0.09	4000	0.8	0.09	20.9	234	10.5	10.6	-0.63	32.8	SEATING CORRECTION
906		385	5.24	6000	1.0	5.24	34.1	7.51	17.1	22.3	-1.1	31.4	SEATING CORRECTION
907		380	24.7	12000	5.8	24.7	58.0	3.36	29.0	53.6	-3.8	27.2	
908		380	50.1	12000	7.7	50.1	83.7	2.67	41.9	92.0	-3.3	28.1	

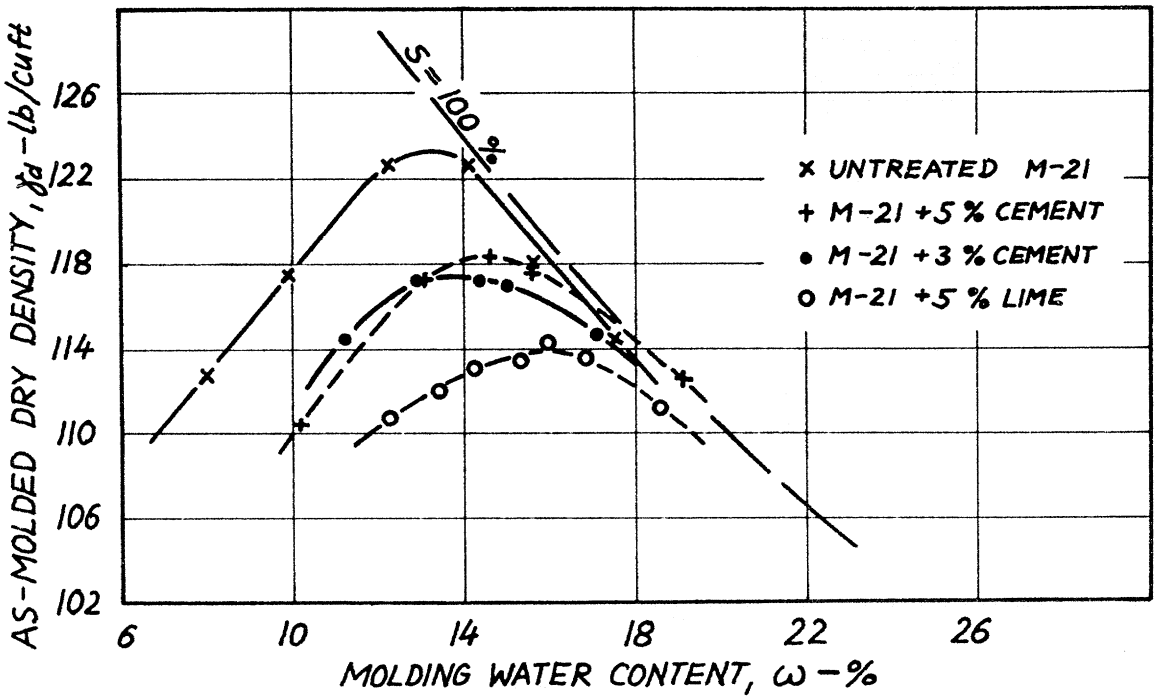

FIG. 4-1. MOISTURE-DENSITY RELATIONS FOR M-21 SYSTEMS

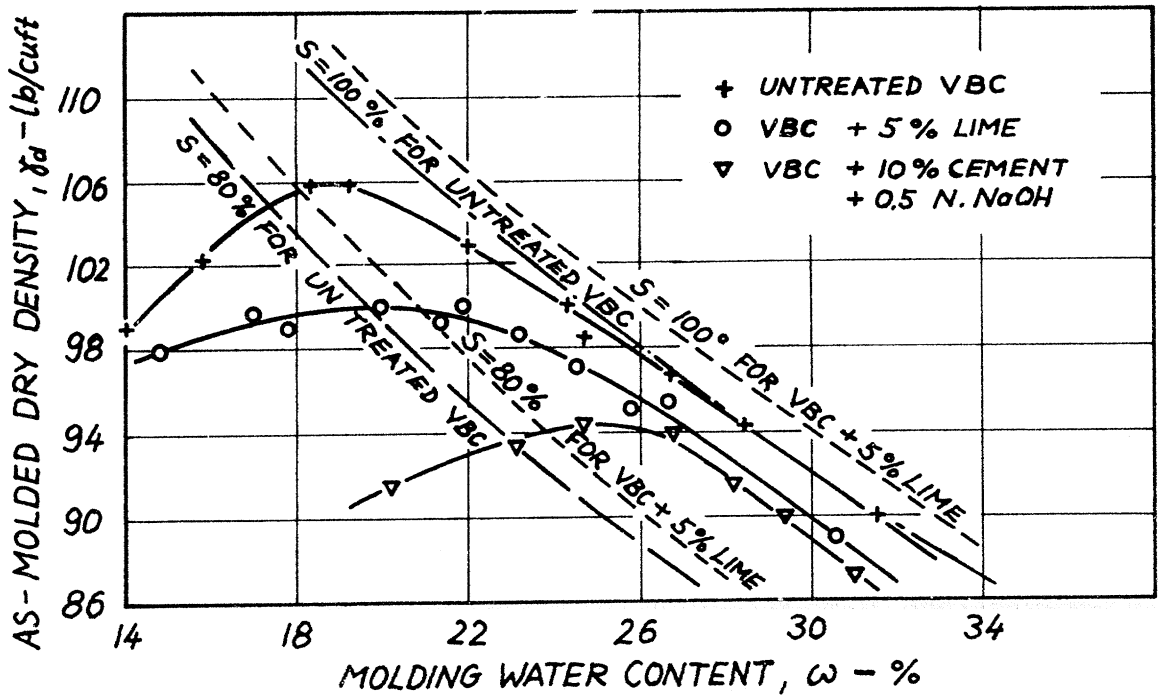

FIG. 4-2. MOISTURE-DENSITY RELATIONS FOR VBC SYSTEMS

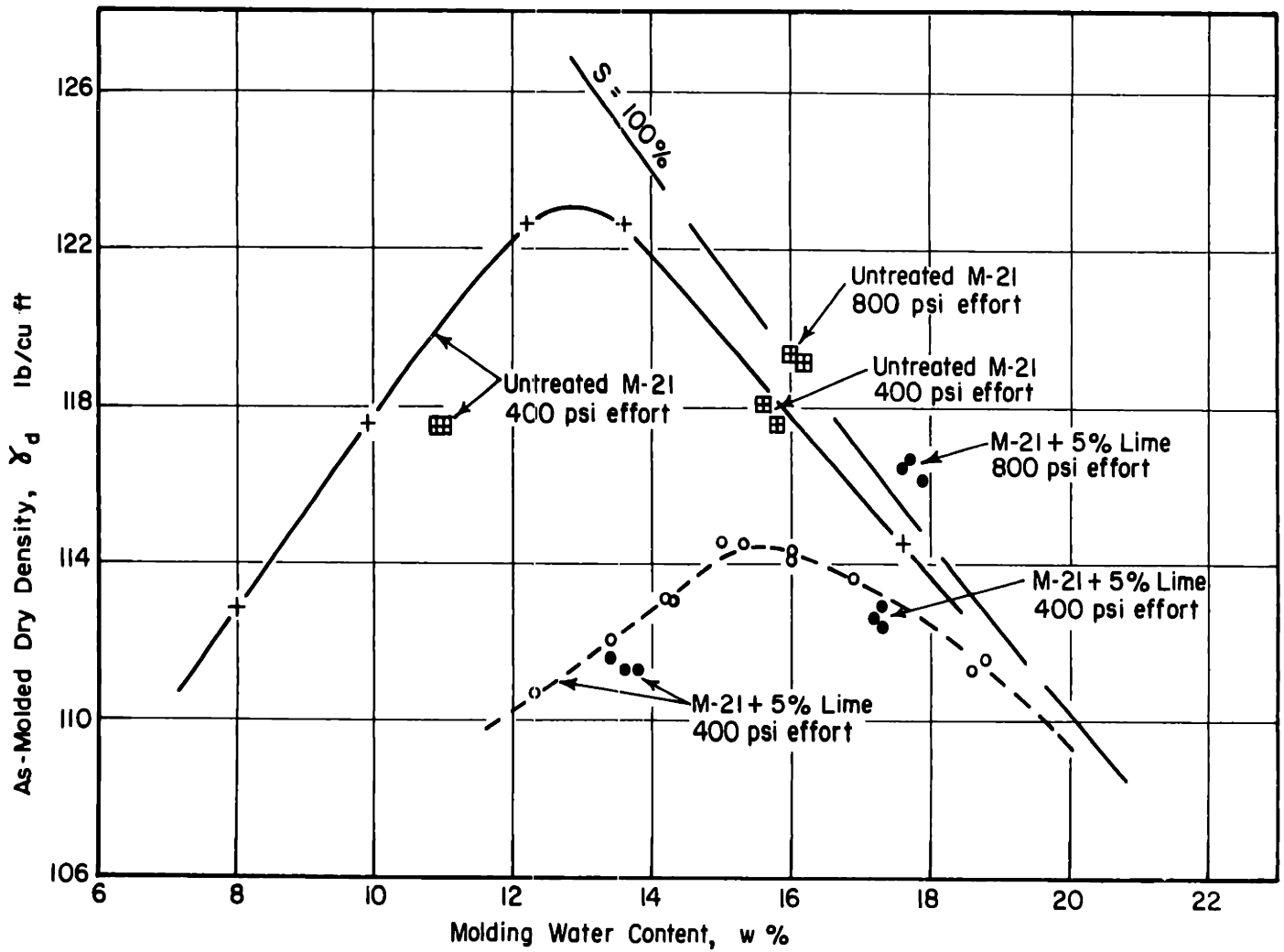

FIGURE 4-3. MOISTURE-DENSITY RELATIONS FOR UNTREATED M-21 AND M-21 PLUS 5% LIME SHOWING INFLUENCE OF COMPACTIVE EFFORT ON DRY DENSITY

Chapter 5

SHEARING RESISTANCE OF ARTIFICIALLY CEMENTED SOILS IN TERMS OF EFFECTIVE STRESSES

5.1 Introduction

Before examining the influence of artificial cementation on the strength behavior of soils it is desirable to review the historical development of some of the more important strength concepts currently used in soil mechanics.*

The strength criterion most widely used today in soil mechanics was first suggested by Coulomb (1776) who used it to investigate the strength behavior of rocks and sands. He showed experimentally that the strength was made up of two physical components which he measured separately. The first component, which he called "cohesion," he assumed was independent of the normal stress on the failure plane and was equal to the tensile strength of the material. The second component he assumed was directly proportional to the normal stress on the failure surface and therefore he called it "friction." He measured friction by determining the resistance to sliding between two surfaces of the material as a function of normal stress. The Coulomb criterion of failure can be given by the following equation:

*Hvorslev (1960) has recently written a comprehensive and thorough review of the current concepts on shear strength of saturated soil, especially clays.

$$s = c + \sigma_f \tan \phi$$

where s = the shear strength of the material

c = the cohesion

σ_f = the normal stress on the failure surface at failure

ϕ = the angle of friction

$\tan \phi$ = the coefficient of friction

He also showed theoretically that the plane of minimum resistance (failure plane) was inclined at an angle of $45^\circ + \phi/2$ to the major principal plane.

Mohr later proposed a more general criterion of failure based on shear stress which assumes that at failure the shear stress on the failure plane, τ_{ff}, and the normal stress on the failure plane, σ_{ff}, are uniquely related, i.e.,

$$\tau_{ff} = f(\sigma_{ff}) \qquad (5.2)$$

and that the functional relation is a characteristic of the material which can be represented on a shear stress versus normal stress diagram by the envelope of <u>all</u> possible Mohr circles of stresses for the material.

When the functional relation of the Mohr criterion of failure is linear it becomes identical to the Coulomb criterion of failure, i.e.,

$$\tau_{ff} = c + \sigma_{ff} \tan \phi \qquad (5.2a)$$

where c = the intercept of the Mohr envelope on the shear stress axis and is known as the cohesion intercept

and $\tan \phi$ = the slope of the Mohr envelope also known as the coefficient of internal friction. ϕ is called the angle of internal friction or the angle of shearing resistance.

The straight line Mohr envelope given by Eq. 5.2a will be referred to as the Mohr-Coulomb envelope. The Mohr envelopes for soils are close to straight lines and therefore can usually be represented by the Mohr-Coulomb equation (Eq. 5.2a). When the envelope is slightly curved an average straight line is used, but in such cases the stress range over which the approximation applies should be stated.

The Mohr criterion of failure assumes that failure is reached at point of first tangency with the Mohr envelope which means that the failure surface is inclined at an angle of $45^{\circ} + \phi/2$ to the major principal plane where ϕ is the angle whose tangent is the slope of the Mohr envelope at the point of first tangency.

In 1923 Terzaghi put forward the effective stress principle which stated that the "effective" stress, $\bar{\sigma}$, controls the deformation behavior of saturated soils and that it is equal to the total stress (external stress),

minus the pore water pressure, u, or stated mathematically:

$$\bar{\sigma} = \sigma - u \qquad (5.3)$$

In a discussion of a paper by Jurgenson (1934), A. Casagrande showed that the effective stress as defined by Eq. 5.3 also controls the strength behavior of soils and that the Mohr-Coulomb envelope in terms of total stresses is not unique but depends on the pore water condition prior to and during shear.

If the Mohr-Coulomb envelope is plotted in terms of effective stresses it is not appreciably influenced by drainage conditions nor the total stress path during triaxial compression. The Mohr-Coulomb criterion of failure for saturated soils can therefore be rendered more unique if it is stated in terms of effective stresses, i.e.,

$$\tau_{ff} = \bar{c} + (\sigma_{ff} - u) \tan \bar{\phi} \qquad (5.4)$$

$$\text{or} \quad \tau_{ff} = \bar{c} + \bar{\sigma}_{ff} \tan \bar{\phi}$$

where τ_{ff} = the shear stress on the failure plane at failure*

σ_{ff} = the total normal stress on the failure plane at failure*

*The orientation of the assumed failure plane with respect to the major principal plane is given by $\theta = 45 + \phi/2$ or $\bar{\theta} = 45 + \bar{\phi}/2$ and since ϕ and $\bar{\phi}$ are not numerically the same the orientation of the assumed failure plane will not be the same in terms of effective stress as in terms of total stress.

u = the pore water pressure at failure

$\bar{\sigma}_{ff}$ = the effective normal stress on the failure plane

$\bar{c}$ = the cohesion intercept in terms of effective stress (effective cohesion intercept)

$\bar{\phi}$ = the angle of shearing resistance in terms of effective stress or angle of internal friction in terms of effective stress (effective angle of internal friction)

For saturated untreated soils the effective stress-strength parameters $\bar{c}$ and $\bar{\phi}$ have been found to be approximately independent of drainage conditions. The Mohr-Coulomb criterion of failure in terms of effective stress is therefore considerably more useful than in terms of total stress in which c and ϕ are completely dependent on testing conditions and may vary over a wide range. Further, the predicted orientation of the failure plane using $\bar{\phi}$ is in closer agreement with the observed failure surface than the orientation using ϕ.

In undrained triaxial tests on soils the point of first tangency with the effective stress envelope* does not always coincide with the point of maximum stress difference and therefore there is some question as to which state of stress constitutes failure. From a practical point of view the choice of which state of stress pertains

*Point of first tangency with the effective stress-strength envelope corresponds to conditions of maximum obliquity, i.e., $\bar{\sigma}_1/\bar{\sigma}_3$ max., only if the cohesion intercept, $\bar{c}$, is zero.

to failure will depend on the particular field application under consideration. From the viewpoint of fundamental research it is desirable to consider both states of stress as well as conditions at ultimate when the shear stress remains constant with further straining.

Considerable disagreement exists concerning the physical significance of the cohesion intercept and angle of shearing resistance as determined by the Mohr-Coulomb envelope. Hvorslev (1937), by modifying the Mohr-Coulomb expression, has shown that for saturated cohesive soils the "effective cohesion" is primarily a function of water content whereas the "effective angle of internal friction" is essentially independent of water content for any given soil.

Lambe (1960) divided the shearing resistance of a soil into three components, cohesion, dilatancy, and friction. He defined cohesion as the shearing resistance which can be mobilized without the necessity of any externally derived normal pressure, and therefore includes artificial cementation. He combined the frictional and dilatancy components together since they are both a direct function of the force acting normal to the shear surface.

In this thesis it will be shown that the shearing resistance of artificially cemented soils can be considered to be composed of two components, one which is

independent of the normal effective stress on the failure plane and the other which increases with increasing normal effective stress on the failure plane. The former will be called the effective cohesive resistance and the latter the effective frictional resistance. It should be noted that in the case of drained tests the dilatancy component is included in the frictional resistance, whereas in undrained tests the dilatancy component is zero since the volume is kept constant during shear.

5.2 Behavior of Untreated Coarse-Grained Soils

The coarse and medium Ottawa sands used in this investigation exhibited curved Mohr effective stress envelopes in drained shear as shown in Figs. 5-1 through 5-3. The slopes of the envelopes decreased with increasing consolidation pressure. For example, Fig. 5-3 shows that for the medium sand at a relative density of 75% the effective angle of internal friction of the Monr envelope decreased from 39° at 0 to 10 kg/cm^2 consolidation pressure to 34.5° at 10 to 25 kg/cm^2 to 31.5° at 25 kg/cm^2 to 50 kg/cm^2. Due to the curvature the Mohr envelopes show an increase in "apparent" effective cohesion intercept with increasing consolidation pressure. The apparent cohesion intercepts given in the figures were obtained because straight-line approximations to the

Mohr envelopes were used over each given consolidation pressure range. They are therefore not intended to have any physical significance.

Most researchers have observed a similar decrease in the slope of drained Mohr envelopes for sands over this range of consolidation pressures. Vesić and Barksdale (1963) have shown that for a dense uniform sand the curvature of the drained Mohr envelope and the apparent cohesion intercept disappeared at slightly higher consolidation pressures than those used in this investigation. They also showed that grain crushing during shear continued to increase with increasing consolidation pressure. This suggests that the curvature cannot be due solely to particle crushing as inferred by Hall and Gordon (1963) who found that the Mohr envelopes of coarse-grained soils were curved whereas the envelopes for fine-grained soils were essentially straight. According to Hirschfeld and Poulos (1963) the curvature of drained Mohr envelopes can be substantially reduced by modifying the principal stress difference to take into account the influence of volume changes on the work done during shear.* They modified the stress difference

*This was first suggested by Taylor (1948). See p. 345 of that text.

using the "stress-dilatancy" equation proposed by Rowe (1962):

$$\text{Modified stress difference} = \frac{\bar{\sigma}_1}{1 + \frac{d\dot{v}}{d\varepsilon}} - \bar{\sigma}_3 \qquad (5.5)$$

where $\dot{v}$ = volumetric strain (volume increase being positive) = dv/v

ε = axial strain (compression being positive)

For the sand they tested the Mohr envelope using the modified stress difference as given by Eq. 5.5 resulted in a straight line.

For the two sands used in this investigation the effective stress-strength relations at ultimate conditions (large strains) were essentially straight lines having zero effective cohesion intercepts (Fig. 5-4). A possible reason for the straight-line relations at ultimate conditions is that at these large strains the rates of volume change with axial strain were tending to zero (as can be seen from Figs. 7-6a, 6b, and 6c) and therefore the stress-dilatancy effect as suggested by Rowe becomes equal to zero since $d\dot{v}/d\varepsilon = 0$ in Eq. 5.5.

In an attempt to determine the influence of dilatancy on the Mohr envelope of cohesionless soils, two samples of medium Ottawa sand at a relative density of 62% were tested at constant volume. The samples were

consolidated to 1.9 kg/cm^2 and 32.3 kg/cm^2 under a back pressure of 68.0 kg/cm^2 and 37.7 kg/cm^2 respectively and the pore pressures measured during undrained shear. The back pressures were sufficiently high to prevent the pore water from cavitating during shear. The effective stress paths reached maximum obliquity conditions at about 6% axial strain and then remained at constant obliquity for a considerable distance before their obliquities decreased slightly as their maximum stress differences were approached. The straight portions of the effective stress paths at maximum obliquity presumably represent the effective Mohr-Coulomb envelopes for this sand at constant volume and the given water contents (see Fig. 5-5). For a water content of 24.6% ($\bar{\sigma}_o$ = 1.9 kg/cm^2) the maximum obliquity in undrained shear was 3.40. ($\bar{\phi}$ = 32°) and for a water content of 20.3% ($\bar{\sigma}_o$ = 32.3 kg/cm^2) the maximum obliquity was 3.57 ($\bar{\phi}$ = 34.5°). The drained envelope for this sand at the same initial relative density (Fig. 5.2) had a maximum obliquity of 3.56. ($\bar{\phi}$ = 34.5°) at ω = 22.6% and 3.33 ($\bar{\phi}$ = 32.5) at ω = 21.3%.*

In the undrained tests $\bar{\phi}$ increased as the void ratio (water content) decreased which is reasonable but in the drained tests $\bar{\phi}$ decreased as the void ratio decreased. If the stress-dilatancy correction given by

*The water contents are those at maximum stress difference and $\bar{\phi}$ was computed using $(\bar{\sigma}_1/\bar{\sigma}_3)_{max} = \tan^2(45 + \bar{\phi}/2)$.

Eq. 5.5 is applied to the drained tests then the curvature of the envelope is considerably reduced and $\bar{\phi}$ ranges from 26° at low consolidation pressures to 28° at high consolidation pressures. These results suggest that the stress-dilatancy correction does not account for the differences in $\bar{\phi}$ between the drained and undrained tests even when the sand is at about the same water content. The stress-dilatancy does however considerably reduce the curvature of the Mohr envelope in drained shear. The stress-dilatancy correction does however make $\bar{\phi}$ increase as the void ratio decreases (as $\bar{\sigma}_o$ increases).

Figs. 5-6 and 5-7 show that both in undrained and drained shear increasing the as-molded relative density of the sands caused an increase in the slopes of the effective Mohr envelopes.

Rowe (1962) has shown that for densely packed particulate cohesionless systems the shearing resistance in drained shear is made up of three components: one due to mineral-mineral friction, one due to geometric interference between particles, and one due to the work done during dilation. The mineral-mineral friction is related to the coefficient of sliding of the grains on a smooth surface of the same material. The shearing resistance due to dilation can be determined from the volume change

versus axial strain curve. The particle interlocking is dependent on the packing and shape of the grains.

In the case of a drained test on a dense sand the maximum particle interlocking or interference occurs at a relatively small axial strain when the volume is a minimum. On further straining the interlocking decreases because the volume is increasing and it reaches a minimum at ultimate conditions when the volume has reached its maximum value. Rowe has shown that throughout dilation the change in packing occurs in such a way that the rate of internal work done by friction is a minimum and therefore the maximum principal stress difference occurs when rate of volume change with axial strain is a maximum, i.e., at the point of inflection of the volume change versus axial strain curve. In all the tests run on the untreated Ottawa sands the maximum principal stress difference occurred at about the same axial strain as the point of inflection which is in agreement with Rowe (see Figs. SC-1, SM-1, and SM-2 of Appendix B).

In undrained shear the volume is kept constant in which case the dilatancy component is zero and then according to Rowe the shearing resistance is made up only of the frictional and interlocking components. The few undrained tests run on the sands suggest that the interlocking, and therefore the packing, remained essentially

constant over a large portion of the tests since the obliquities remained constant. As the maximum principal stress difference was approached the obliquity decreased probably due to a change in packing caused by the crushing of some sand grains at these high effective stresses and local volume changes in the zone of shearing.

Fig. 5-7 shows the influence of initial relative density and grain size on the drained effective stress envelope of Ottawa sand. For medium Ottawa sand the slope of the envelope increased with increasing relative density because the interlocking and dilatancy component increased. At ultimate conditions the effective stress-strength relations were independent of initial relative density (Fig. 5-4) because the final water contents were about the same and therefore the samples had about the same packing even though they started out at different relative densities.

The coarse Ottawa sand at the same density as the medium sand (γ_d = 102.9 lb/cu ft) had a flatter envelope. The coarse sand had better rounded grains than the medium sand and at the same density had a lower relative density. The relative density of the coarse sand was 42% as compared to 75% for the medium sand. When the relative density of the medium sand was reduced to 62% (γ_d = 100.5 lb/cu ft) its envelope was closer to that of the coarse

sand and probably at a relative density of 42% its envelope would have coincided with that of the coarse sand. This suggests that it is the relative density and not the relative packing of the grains which controls the Mohr envelope of this sand. At ultimate conditions the coarse sand had a very slightly lower effective stress-strength relation than the medium sand even though it was at lower void ratios probably due to a lower frictional resistance because rounded grains are able to roll more during shear than angular grains.

Axial strain contours have been drawn on the drained $\bar{p}$ versus q plots for the untreated sands in Figs. 5-1 through 5-3. The slopes started out by increasing with increasing axial strain mainly because the mineral-mineral friction between grains was being mobilized. The mineral-mineral friction is probably fully mobilized at relatively small strains when the volume of the samples reaches a minimum and the interlocking is a maximum. On further straining the samples started to dilate at a gradually increasing rate and therefore the stress-dilatancy effect gradually increased causing an increase in the slopes of the strain contours until maximum rate of dilatancy occurs at the maximum stress difference. On further straining the rate of dilatancy decreased and therefore the slopes decreased until ultimate conditions

were reached. At ultimate conditions the dilatancy effect is zero and the interlocking is a minimum. At low consolidation pressures all the strain contours converged towards the origin, i.e., tended to have zero effective cohesion intercepts. The Mohr envelope in drained shear therefore represents conditions when the rate of dilatancy is a maximum but not when the interlocking is a maximum.

In undrained shear the Mohr envelopes appeared to occur when the rate of decrease in excess pore pressure with increasing axial strain was a maximum, i.e., when the tendency for change in packing was a maximum. As maximum stress difference was reached grain crushing and localized volume changes caused the excess pore pressures to remain essentially constant with further straining and interlocking reached a maximum.

In summary the following conclusions can be drawn for the strength behavior of the untreated dense sands investigated:

1. The slopes of the drained Mohr envelopes decreased with increasing consolidation pressure.
2. The curvature of the drained envelopes was most pronounced at low consolidation pressures but the curvature could be considerably reduced by using the stress-dilatancy correction suggested by Rowe.

3. The undrained envelopes had higher $\bar{\phi}$ than the drained envelopes at the same void ratio when the stress-dilatancy correction was applied to the drained test results.
4. Increasing the as-molded relative density caused an increase in $\bar{\phi}$ for both tne drained and undrained tests. The increase in ϕ is presumably due to an increase in dilatancy and/or interference during shear.
5. At the same as-molded dry density the coarse Ottawa sand had a flatter drained Mohr envelope than the medium Ottawa sand because it was better rounded and therefore had a lower friction and dilatancy behavior probably due to more rolling of sand grains during shear.
6. At ultimate conditions the effective stress-strength relations in drained shear were independent of as-molded dry density because the void ratios at ultimate were independent of molding conditions.
7. The coarse sand had a slightly lower ultimate shearing resistance than the medium sand even though it was at lower void ratios presumably due to its grains being more rounded and therefore able to roll more easily during shear.

8. The slopes of the axial strain contours on the $\bar{p}$ versus q plots for the drained tests increased with increasing axial strain until the maximum stress difference was reached. The strain contours tended to show zero cohesion intercepts.
9. In drained shear the maximum stress difference and therefore the Mohr envelope was reached when the rate of dilatancy with axial strain was a maximum which did not correspond to maximum interlocking. In undrained shear the Mohr envelope probably corresponded to conditions of maximum tendency for change in packing with increasing axial strain.

5.3 Influence of Artificial Cementation in Coarse-Grained Soils

To examine the effect of cementation on the strength behavior of the sands the density of the sand excluding cement was kept essentially constant so as to have about the same packing of sand grains as in the corresponding untreated samples. This was done to minimize the effect of differences in interlocking on the shearing resistance.

In the case of the cemented coarse Ottawa sand samples the dry density of the sand excluding the cement was kept constant at 102.9 lb/cu ft. For the cemented medium

sand samples the density of the sand was kept at 100.7 ± 0.2 lb/cu ft.

Cementation caused the drained Mohr envelopes to have cohesion intercepts and to be appreciably curved at the lower consolidation pressures (see Figs. 5-8 through 5-10). The pronounced curvatures of the envelopes at low consolidation pressures are believed to be due to premature fracture caused by the presence of submicroscopic shrinkage cracks which develop in the cement during curing. The premature fracture exhibited itself as a sudden catastrophic failure in which the samples shattered without advance warning as can be seen from the stress-strain curves shown in Fig. 5-11. As the consolidation pressure is increased the cracks will close up and the tendency for premature fracture will be reduced because friction will be mobilized between the surfaces of the closed cracks. Such a mechanism was suggested for rocks by McClintock and Walsh (1962). The consolidation pressure required to close the cracks and prevent premature fracture increased as the strength of the samples increased. For example a consolidation pressure of 10 kg/cm^2 was sufficient to prevent premature brittle fracture when 5% cement was used with the medium sand (Fig. 5-9) but nearly 25 kg/cm^2 was required when 10% cement was used with the same sand (Fig. 5-10).

The net effect of premature fracture on the Mohr envelope of the cemented sands at low consolidation pressures was to reduce the cohesion intercept and increase the angle of internal friction.

At the higher consolidation pressures, when premature brittle fracture no longer occurred, the Mohr envelopes of the cemented sands were essentially straight and therefore satisfy the Mohr-Coulomb criterion of failure.

As shown in Fig. 5-12, 5% cement did not alter the effective angle of internal friction of medium Ottawa sand*, and 10% cement increased it only slightly (2 degrees) provided premature fracture did not occur. The cohesion intercept increased substantially with increasing cement content.

As with untreated sand it is of interest to examine the shearing resistance of cemented sands as a function of axial strain. Axial strain contours have been drawn on the $\bar{p}$ versus q plots of medium Ottawa sand cemented with 5% and 10% portland cement in Figs. 5-9 and 5-10 respectively and for coarse Ottawa sand plus 5% cement in Fig. 5-8. From the figures it can be seen that at low strains the shearing resistance is apparently solely due to the cementation between grains and no appreciable friction is

*This was also observed with the coarse Ottawa sand as can be seen by comparing Fig. 5-8 with Fig. 5-1. All these results were for drained tests.

mobilized as demonstrated by the essentially zero slope of the strain contours. At about 0.4% axial strain the frictional resistance due to interlocking and mineral-mineral friction starts being mobilized as indicated by the gradual steepening of the strain contours. By the time 0.6% axial strain has been reached the shearing resistance due to cementation (the cohesion intercept) has reached a maximum and is starting to decrease due to its gradual breakdown, whereas the frictional resistance continues to increase.

The maximum principal stress difference (the Mohr-Coulomb envelope) occurs when the sum of the shearing resistance due to friction and cohesion reaches a maximum. At this time the cohesive resistance has dropped well below its maximum value whereas the frictional resistance due to dilatancy has not yet reached a maximum since the slopes of the $\Delta V/V$ versus ε curves have not yet reached a maximum (see the stress-strain curves in Figs. SC-2, SM-3, and SM-4 of Appendix B). The shearing resistance due to interlocking is close to its maximum value because the maximum principal stress difference occurs at about the same axial strain as the minimum volume. The shearing resistance due to mineral-mineral friction has probably not yet reached its maximum value since, as will be shown later, the slope at ultimate conditions is only slightly

lower than that of the Mohr envelope even though the dilatancy effect is zero and interlocking effect a minimum.

On further straining ultimate conditions are reached at which time the continuous cementation between grains in the failure zone is completely destroyed and the effective stress-strength curve converges towards the origin on a $\bar{p}$ versus q plot (Fig. 5-13). The curvature possibly reflects tne influence of the cement on the friction between grains. At low consolidation pressures the grains are still coated with cement but as the consolidation pressure is increased the coating gets rubbed off the sand grains during shear causing the frictional characteristics of the grains to change with consolidation pressure. The slightly flatter slopes of the effective stress-strength curves at ultimate are due to the dilatancy effect being zero and the lower interlocking since the volume is larger than at maximum principal stress difference.

Fig. 5-14 shows that in undrained shear 5% cement increased the effective cohesion intercept of coarse Ottawa sand without appreciably altering the effective angle of internal friction.

The influence of artificial cementation on the behavior of sands in drained shear can be summarized as follows:

1. Cementation causes the Mohr-Coulomb envelope to have a cohesion intercept, the magnitude of which increases appreciably with increasing cement content.
2. At high consolidation pressures, when premature brittle fracture does not occur, cementation only slightly increases the angle of internal friction of the Mohr envelope provided the density of the sand excluding the cement is kept constant.
3. At low consolidation pressures premature fracture of cemented samples causes the Mohr envelope to have a lower cohesion intercept and higher angle of internal friction than at high consolidation pressures.
4. The Mohr-Coulomb criterion of failure for cemented sands represents conditions when the sum of the shearing resistance due to cohesion and the shearing resistance due to friction, dilatancy, and interlocking is a maximum.
5. The maximum shearing resistance due to the cohesion occurs well before failure as defined by the Mohr-Coulomb criterion.
6. The maximum shearing resistance due to friction per se probably occurs after failure as defined

by the Mohr-Coulomb criterion since at ultimate conditions the slope of the shearing resistance versus effective stress is only slightly below the slope of the Mohr envelope even though the dilatancy effect is zero and the interlocking a minimum.

7. At ultimate conditions the cementation between grains in the failure zone is completely destroyed and therefore the curve of shearing resistance versus effective stress has zero cohesion intercept.

5.4 Behavior of Untreated Fine-Grained Soils

The untreated fine-grained soils were tested in undrained shear with pore pressure measurements. Only one molding water content and dry density are presented for each soil because the Mohr-Coulomb envelopes in terms of effective stresses are not significantly affected by molding conditions even though the excess pore pressures during undrained shear may be quite different (Seed, et al., 1960).

The effective Mohr-Coulomb envelope for the clayey silt (M-21) was straight over the wide range of consolidation pressures investigated (Fig. 5-15). It had zero effective cohesion intercept and an effective angle of internal resistance of 31.5°. The effective Mohr-Coulomb envelope for the plastic clay (VBC) was slightly curved

having $\bar{\phi} = 18.5^{\circ}$ at consolidation pressures between 25 kg/cm^2 and 50 kg/cm^2 and $\bar{\phi} = 22.5^{\circ}$ at 0 to 5 kg/cm^2. The effective cohesion intercept was 0.3 kg/cm^2 (Fig. 5-16).

The use of strain contours to separate the frictional and cohesive resistance is open to question when applied to fine-grained soils since large decreases in void ratio occur with increasing consolidation pressure and therefore the fabric changes appreciably with consolidation pressure. As the void ratio decreases the number of mineral-mineral contacts increases which will increase the frictional resistance during shear. The cohesive resistance will probably also increase with consolidation pressure since it is due to the electrical attraction between particles which increases as the number of contacts increases.

In the case of the clayey silt (M-21) the strain contours are essentially straight lines with zero cohesion intercepts as shown in Fig. 5-15. This is reasonable since this soil contains only a very small percentage of colloidal clay and therefore the cohesion due to interparticle attraction should be negligibly small over a wide range of consolidation pressures. The strain contours are straight probably because no dilatancy effect existed since the samples were sheared at constant volume. The shearing resistance due to interlocking and mineral-

mineral friction as measured by the slopes of the strain contours increased with increasing axial strain and reached a maximum at point of first tangency with the Mohr-Coulomb effective stress envelope.

In the case of the plastic clay, VBC, the strain contours were slightly curved and exhibited a small cohesion intercept (Fig. 5-16). The curvature of the strain contours is probably due to the large changes in void ratio with consolidation pressure which would affect both the frictional and cohesive resistance of the soil.

As will be shown later, the curvature and cohesion intercepts of the strain contours for untreated VBC are insignificant compared to the influence of artificial cementation on the strain contours, and therefore it will be assumed that the strain contours for the untreated soil are straight and have zero cohesion intercept.

In summary as far as this investigation is concerned it will be assumed that both soils have a negligible amount of cohesive resistance and that the shearing resistance is mainly frictional, i.e., due to mineral-mineral friction and interlocking. The maximum frictional resistance occurs at point of first tangency with the Mohr-Coulomb effective stress envelope and then remained essentially constant on further straining.

5.5 Influence of Artificial Cementation in Fine-Grained Soils

Most of the triaxial tests on the artificially cemented fine-grained soils were undrained because of the long testing times which would have been needed to run drained tests. One series of triaxial tests on VBC cemented with 5% hydrated lime was run in drained as well as undrained shear to determine the influence of drainage on the effective stress-strength behavior. The Mohr-Coulomb effective stress envelopes at high consolidation pressures were about the same as can be seen by comparing Figs. 5-17 and 5-18, but the axial strains required to reach the envelope were considerably different. The drained tests required much larger strains probably because of the difference in the effective stress paths, the volume changes during shear, and the difference in rate of straining. The strain contours in the drained tests showed more consistent trends because in the undrained tests small seating effects appreciably influenced the strain contours at small strains and small differences in molding condition influenced the excess pore pressure developed during shear and therefore the effective stress paths.

At low consolidation pressures the cemented samples of the plastic clay, VBC, failed prematurely causing the Mohr-Coulomb effective stress envelope at low consolidation

pressures to have a higher effective angle of internal friction and lower effective cohesion intercept. The premature failures were probably due to the existence of shrinkage cracks which develop during curing. This can be seen from the test results for VBC + 10% cement shown in Figs. 5-19 through 5-21. Fig. 5-19 shows that for 55 days of curing only, the sample consolidated to 0.1 kg/cm^2 failed slightly below the Mohr-Coulomb effective stress envelope but when samples were subjected to severe cycles of wetting and drying prior to shear, as shown in Fig. 5-21, both the sample consolidated to 0.1 kg/cm^2 and the sample consolidated to 5 kg/cm^2 failed appreciably below the envelope. Mild cycles of wetting and drying caused the 0.1 kg/cm^2 sample to fail slightly before the corresponding uncycled sample (Fig. 5-20). The size and intensity of the visible cracks increased with increasing severity of the cycling.

The strain contours at low consolidation pressures were also much steeper than at high consolidation pressures because of the existence of shrinkage cracks and also because drainage occurred during shear due to the boundary conditions of the triaxial test which will be discussed later in Chapter 7.

The following discussion will therefore concentrate on the influence of cementation at high consolidation pressures because the behavior at low consolidation pressures is mainly controlled by premature fracture and drainage conditions in the triaxial cell.

Figs. 5-22 through 5-26 show typical examples of the effective stress-strength behavior of the various soil-stabilizer systems investigated. Also plotted in the figures are the strain contours. The rates at which the cohesive and frictional resistances (intercept and slope of the strain contours) change with increasing axial strain are summarized in Figs. 5-27 and 5-28. For the untreated clayey silt (M-21) the cohesive resistance throughout shear was essentially zero but the frictional resistance gradually increased with increasing axial strain and reached a maximum at point of first tangency with the effective Mohr-Coulomb envelope (Fig. 5-27a). In the case of untreated VBC the frictional resistance also increased gradually with increasing axial strain and reached a maximum at point of first tangency with the effective Mohr-Coulomb envelope. VBC had a small cohesive resistance which increased with increasing consolidation pressure (Figs. 5-28a and 5-28b).

When a cementing material was added to these soils the cohesive resistance increased very rapidly with

increasing axial strain and reached a maximum at a relatively small axial strain (0.3 to 0.7% axial strain). On further straining the cohesive resistance started to decrease probably due to a gradual breakdown of the cementation. By the time the Mohr-Coulomb envelope was reached the cohesive resistance was 30 to 70% of its maximum value (see Figs. 5-27 and 5-28). At very large axial strains (ultimate conditions) the cohesive resistance was completely destroyed probably due to a complete breakdown of the weaker cementation between the strongly cemented aggregates of soil, as shown by the zero cohesion intercepts at ultimate (Figs. 5-29 and 5-30).*

The slopes of the strain contours for the cemented soils have been assumed to be a measure of the frictional resistance since there was only a slight decrease in void ratio with increasing consolidation pressure especially at the higher consolidation pressures when the shrinkage cracks had closed up. When the amount of cementation was small the frictional resistance increased with increasing axial strain in a similar manner to the untreated soils (Figs. 5-27a, 5-27b, and 5-28c). When the amount of

*Not all the results have been shown in these figures because samples which failed prematurely never reached ultimate conditions. Further some of the low consolidation pressure samples shown in Fig. 5-30 were not strained far enough (as can be seen from their corresponding stress-strain curves) and therefore lie above the effective stress-strength relation at ultimate.

cementation was increased (Figs. 5-27d and 5-28d) little or no frictional resistance was mobilized at low strains and the shearing resistance was mainly cohesive. As the cohesive resistance approached its maximum value the frictional resistance mobilized very rapidly and by the time the effective Mohr-Coulomb envelope was reached a large amount of the frictional resistance had been mobilized. On further straining the frictional resistance increased very slowly until at ultimate conditions it reached its maximum value (Figs. 5-29 and 5-30).

The Mohr-Coulomb envelopes for cemented soils therefore represent conditions when the sum of the cohesive resistance and frictional resistance is a maximum. The maximum cohesive resistance occurs with little or no mobilization of friction and at lower strains than the Mohr-Coulomb envelope. The maximum frictional resistance occurs at much higher strains than the Mohr-Coulomb envelope when ultimate conditions are reached and the cohesion in the failure zone completely destroyed.

For any given soil-stabilizer system there should be a relation between the effective stress-strength parameters $\bar{c}$ and $\bar{\phi}$ as determined by the Mohr-Coulomb envelope and the maximum cohesive resistance and frictional resistance as determined from the strain contours and ultimate

conditions respectively, because increasing curing time did not alter $\bar{\phi}$ nor the frictional resistance at ultimate conditions as shown in Figs. 5-31 and 5-29 respectively for M-21 plus 5% lime and Figs. 5-32 and 5-29 respectively for M-21 plus 5% cement. The Mohr-Coulomb effective cohesion intercept increased at a decreasing rate with increasing curing time (Figs. 5-33 and 5-34) but it was not possible to show such a trend with the maximum cohesion because of the large scatter in the results due to seating imperfections which appreciably influence the results at low strains. For example, in Fig. 5-35 is a plot of the cohesive resistance and frictional resistance as a function of axial strain for VBC + 10% cement following 43 and 55 days of curing. It can be seen from the figure that even though the Mohr-Coulomb cohesion intercept increased with increasing curing time the maximum cohesive resistance decreased which is contrary to what would be expected. The other systems also showed no definite trend for the maximum cohesive resistance to increase with increasing curing time.

The maximum frictional resistance of a cemented fine-grained soil is independent of the strength of the cementation, i.e., curing time, probably because no appreciable change in the soil fabric or particle orientation takes place during curing. This is similar to the

behavior of artificially cemented sands where the packing of the sand grains and not the cementation between grains mainly determined the frictional resistance. The maximum cohesive resistance probably should increase with increasing curing time because the strength of the cementation increases.

A few tests run at low consolidation pressure only, suggest that molding conditions can alter the Mohr-Coulomb effective cohesion intercept without altering the effective angle of internal friction (Fig. 5-36) of cemented soils.* The differences in $\bar{c}$ are thought to reflect the differences in volumetric changes, occurring during curing, which are dependent on molding conditions and cause some cracking of the cementation. Similar but more severe detrimental volume changes occurred during cycles of wetting and drying of VBC + 10% cement which also caused a decrease in $\bar{c}$ without affecting $\bar{\phi}$ as can be seen by comparing the Mohr-Coulomb effective stress envelopes shown in Figs. 5-19, 5-20, and 5-21. Fig. 5-37 shows that for untreated M-21 molding conditions have no effect on the Mohr-Coulomb envelope but influence the effective stress paths which is in agreement with Seed et al. (1960).

Unlike the sands, the frictional behavior of fine-grained soils was appreciably affected by cementation.

*See Fig. 4-3 for molding conditions of these samples.

The frictional resistance, especially at ultimate conditions, was usually considerably increased due to the addition of a cementing material. Table 5-1 summarizes the influence of the various stabilizers used in this investigation on the frictional behavior of M-21 and VBC at both point of first tangency with the Mohr-Coulomb envelope and ultimate conditions. The increase in frictional resistance was dependent on the type of soil as well as the type and amount of cementing material added. For example, 5% lime increased the maximum angle of shearing resistance (at ultimate conditions) of M-21 from 30.5° to 35° and that of VBC from 20° to 30.5°. The larger increase in the frictional resistance of VBC is probably due to the fact that lime is more reactive with the colloidal size clay particles in VBC than with the coarse size silt and sand particles in M-21, causing a larger change in surface texture and more aggregation of the fine soil particles in VBC. The existence of strongly cemented aggregates could account for the higher frictional resistance by causing a greater amount of interlocking during shear. The reduction in maximum dry density of the fine-grained soils for a given compactive effort due to the addition of hydrated lime or portland cement suggests that such an aggregation of the clay size

particles occurs (Figs. 4-1 and 4-2). In addition, even after crushing and wet sieving the cemented samples had considerably less fines than the untreated samples (Figs. 5-38 and 5-39). The gradation of the coarser cemented particles was obviously dependent on the method of crushing which for comparison purposes was kept constant for these particle size determinations.

The influence of artificial cementation on the effective stress-strength behavior of fine-grained soils can therefore be summarized as follows:

1. Provided premature fracture does not occur, the Mohr-Coulomb effective stress envelope of cemented fine-grained soils can be represented by the equation:

$$\tau_{ff} = \bar{c} + \bar{\sigma}_{ff} \tan \bar{\phi}$$

where $\bar{c}$ = the effective cohesion intercept and is a function of the soil type, type and amount of cementing materials, molding conditions, and curing history

$\bar{\phi}$ = the effective angle of internal friction and is a function of the soil type and type and amount of cementing material.

2. Both the effective cohesion intercept and the effective angle of internal friction of the Mohr-

Coulomb envelope of a fine-grained soil can be increased by artificial cementation.

3. For a given soil-stabilizer system the effective cohesion intercept increases at a decreasing rate with increasing curing time. Increasing the amount of cementing material increases the magnitude of the cohesion intercept. Volume changes which can occur during curing or weathering (cycles of wet-dry) can damage the cementation and thus reduce the magnitude of the cohesion intercept.
4. For a given soil the effective angle of internal friction, $\overline{\phi}$, increases by increasing the amount of cementing material added to the soil probably due to the formation of strongly cemented soil aggregates. The more clay in the soil the larger is the increase in $\overline{\phi}$ due to cementation, possibly due to the larger reduction in the amount of uncemented clay size particles present. $\overline{\phi}$ is essentially independent of the strength of the cementation (curing time) and it is not influenced by weathering (cycles of wet-dry).
5. The Mohr-Coulomb envelope represents conditions when the <u>sum</u> of the cohesive resistance and frictional resistance is a maximum.

6. The maximum cohesive resistance is greater than $\bar{c}$ and occurs at lower strains.
7. The maximum frictional resistance can be considerably greater than $\bar{\phi}$ and occurs at larger strains.
8. Premature fracture due to the existence of shrinkage cracks which develop during curing and weathering exhibits itself at low consolidation pressures by a decrease in the effective cohesion intercept and an increase in the effective angle of internal friction. At high consolidation pressures cracking lowers the effective cohesion intercept without altering the effective angle of internal friction.
9. At ultimate conditions the shearing resistance in the failure zone is solely frictional and can be represented by the equation:

$$\tau_{ult} = \bar{\sigma}_{ult} \tan \bar{\phi}_{ult}$$

where $\bar{\tau}_{ult}$ = the ultimate shear stress on the failure plane assumed to be oriented at $45^{\circ} + \bar{\phi}_{ult}/2$ to the major principal plane.

$\bar{\sigma}_{ult}$ = the ultimate effective normal stress on the failure plane assumed at $45^{\circ} + \bar{\phi}_{ult}/2$ to the major principal plane.

$\bar{\phi}_{ult}$ = the effective angle of shearing resistance at ultimate conditions and is the maximum angle of internal friction of the system. It is independent of molding and curing conditions. Artificial cementation may considerably increase $\bar{\phi}_{ult}$.

Table 5-1

INFLUENCE OF CEMENTATION ON THE FRICTIONAL RESISTANCE OF THE FINE-GRAINED SOILS

System	$\bar{\phi}$	$\bar{\phi}_{ult}$
Untreated M-21	30.5°	30.5°
M-21 + 5% Lime	31.5°	25.5°
M-21 + 3% Cement	32°	-
M-21 + 5% Cement	37°	38°
Untreated VBC	18.5°-22.5°	18.5°
VBC + 5% Lime	20°-22.5°	32°
VBC + 10% Cement + 0.5 N. NaOH	32°	37°

Note: The Monr-Coulomb effective cohesion intercepts of the fine-grained cemented soils were a function of the curing time whereas at ultimate conditions they were zero.

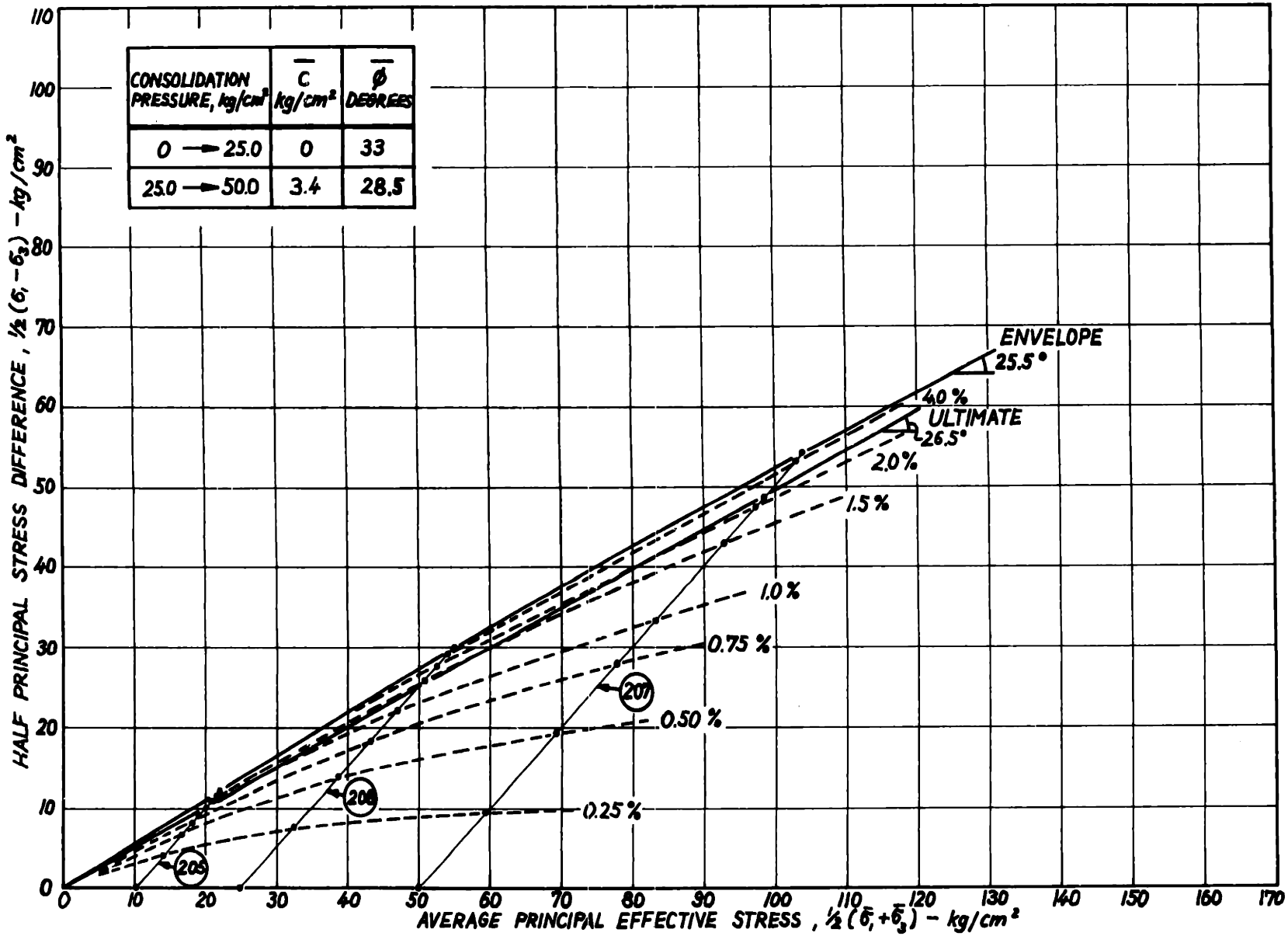

FIG 5-I. EFFECTIVE STRESS–STRENGTH BEHAVIOR IN DRAINED SHEAR OF UNTREATED COARSE OTTAWA SAND (RELATIVE DENSITY OF SAND = 42 %).

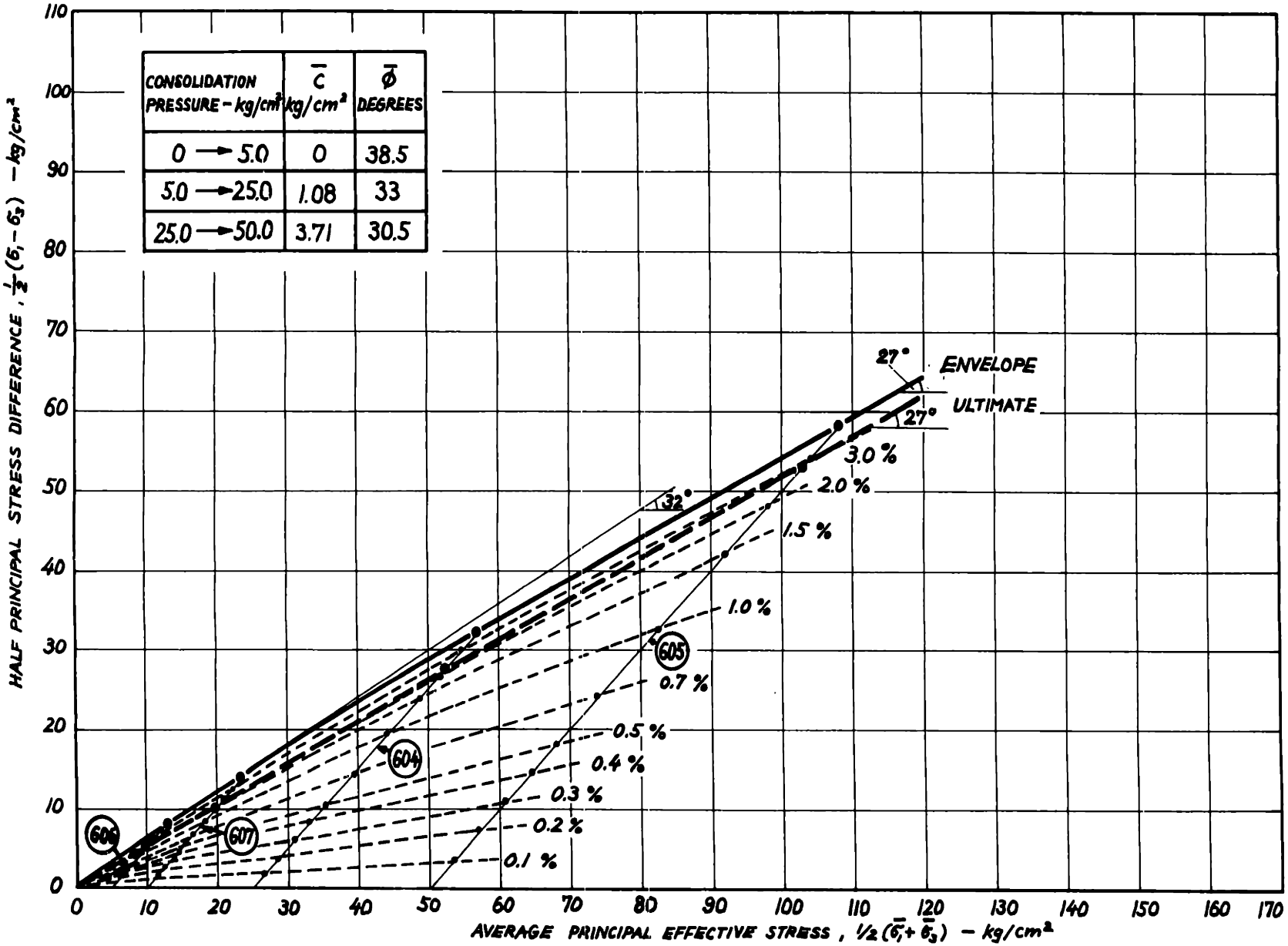

FIG. 5-2. EFFECTIVE STRESS - STRENGTH BEHAVIOR OF UNTREATED MEDIUM OTTAWA SAND IN DRAINED SHEAR AT A RELATIVE DENSITY OF 62% .

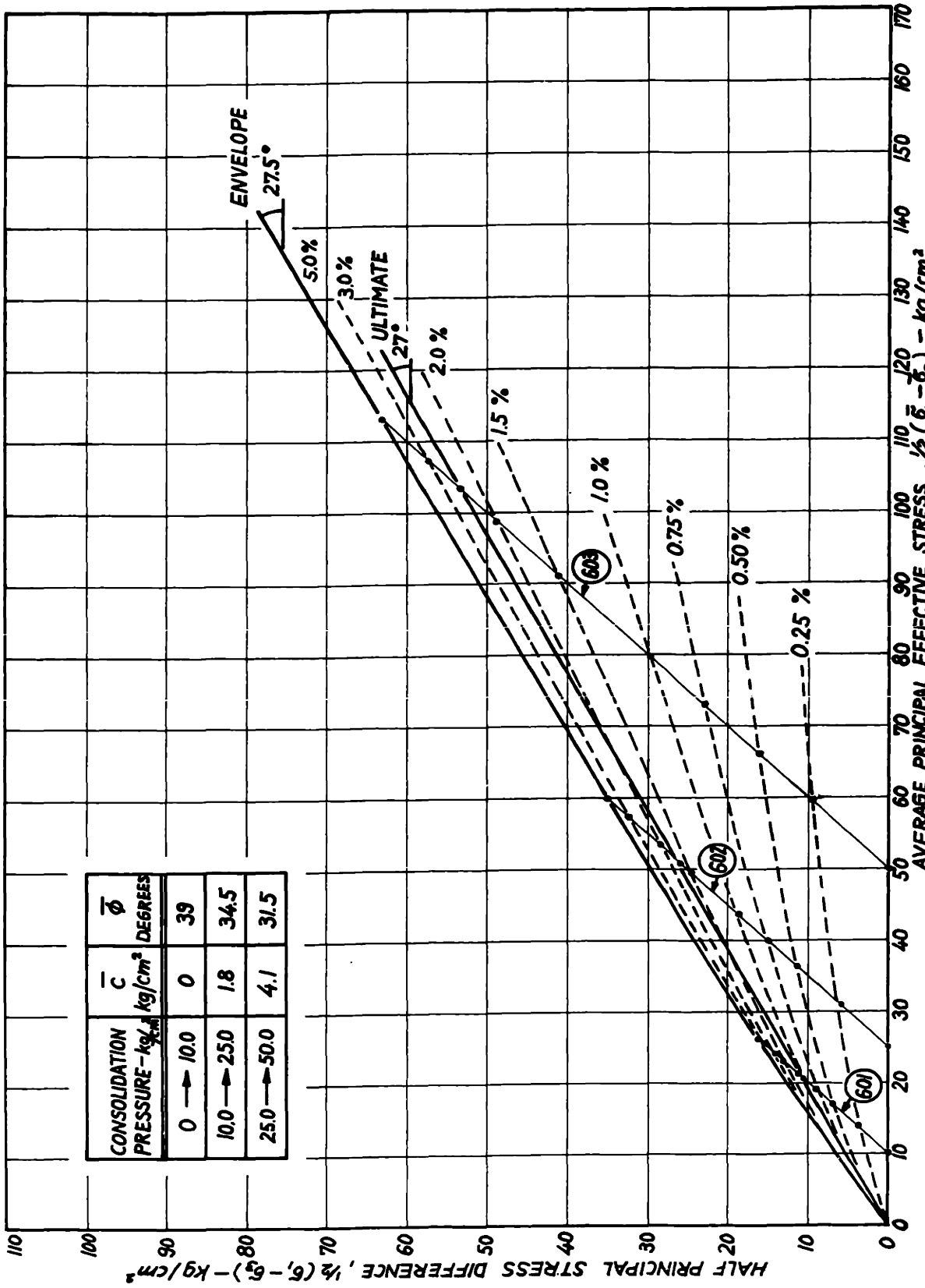

FIG. 5-3. EFFECTIVE STRESS—STRENGTH BEHAVIOR IN DRAINED SHEAR OF UNTREATED MEDIUM OTTAWA SAND (RELATIVE DENSITY OF SAND = 75 %).

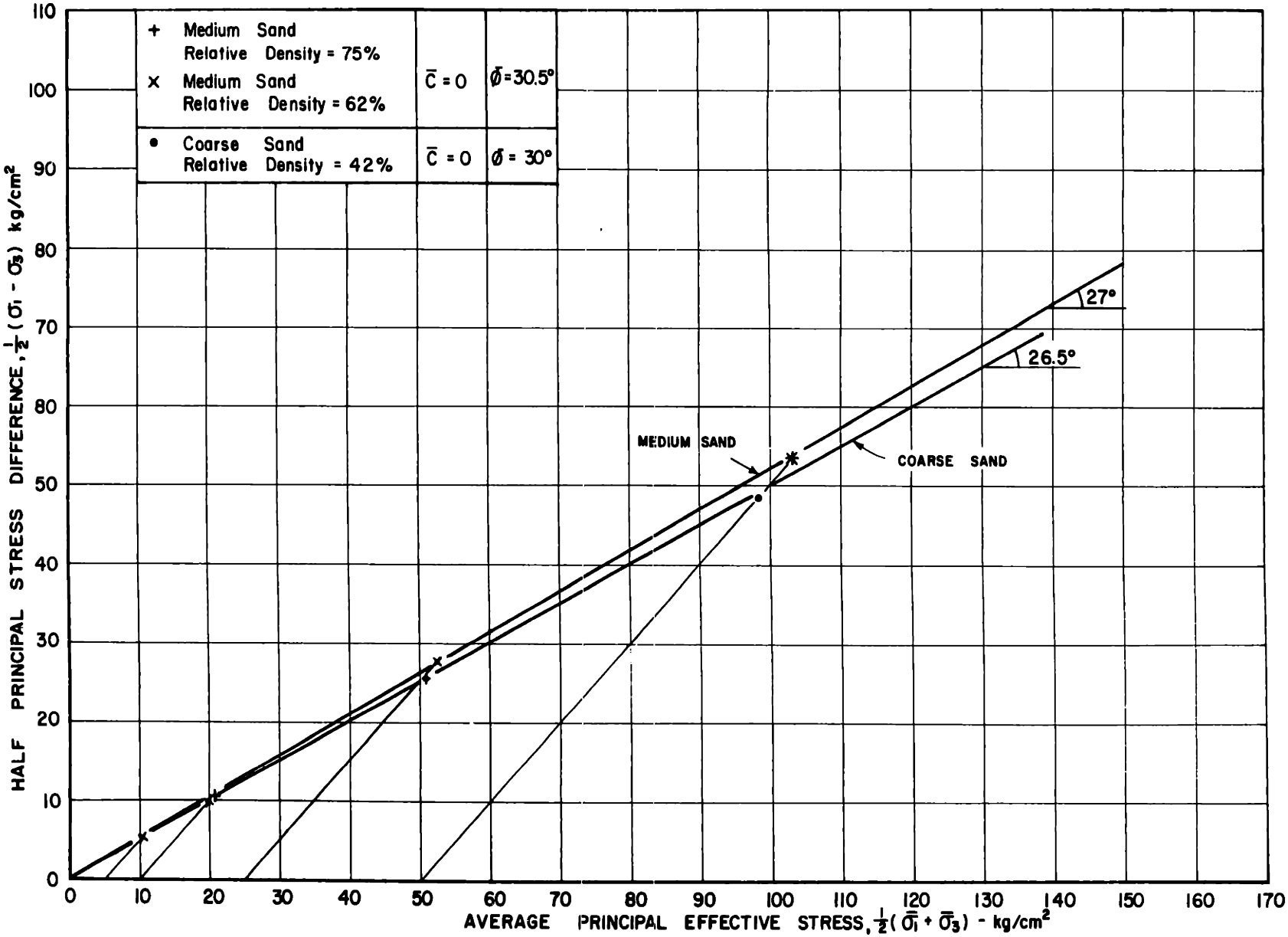

FIG. 5-4. EFFECTIVE STRESS - STRENGTH BEHAVIOR OF UNTREATED COARSE AND MEDIUM OTTAWA SAND IN DRAINED SHEAR AT ULTIMATE CONDITIONS.

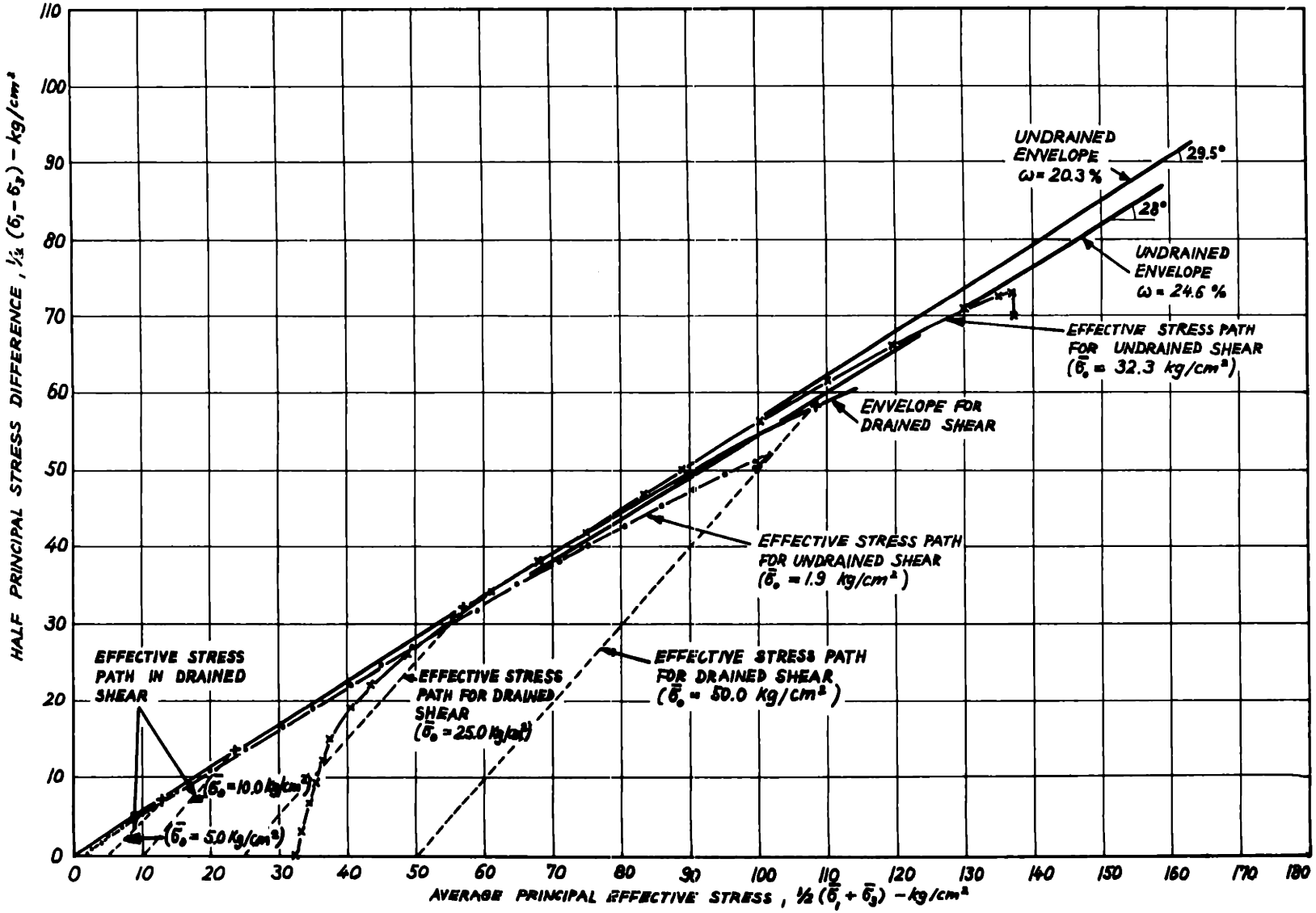

FIG. 5-5. COMPARISON OF EFFECTIVE STRESS-STRENGTH OF MEDIUM OTTAWA SAND IN DRAINED AND UNDRAINED SHEAR. (AS-MOLDED DRY DENSITY = 100.5 lb/cu ft).

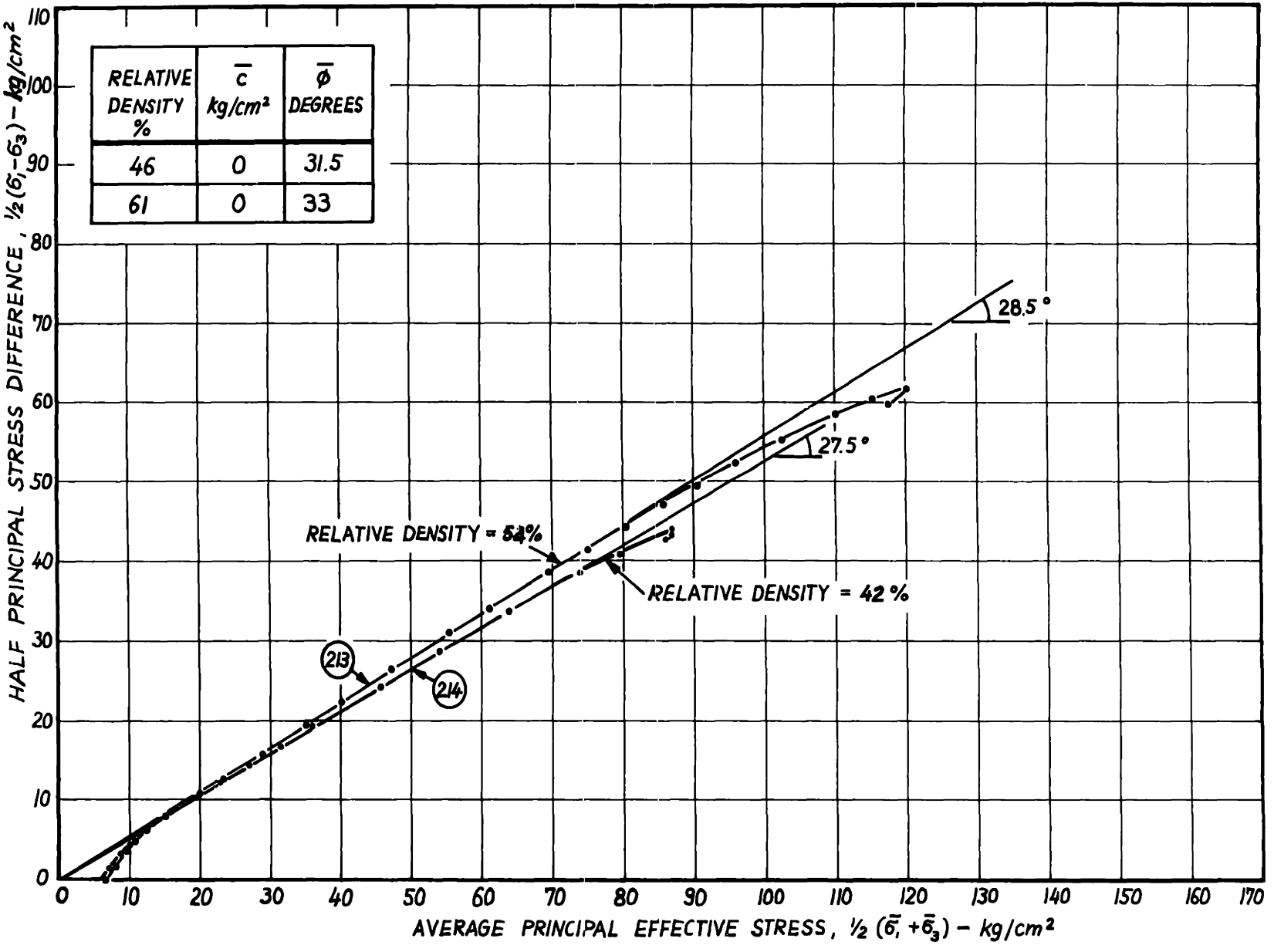

FIG. 5-6. INFLUENCE OF AS-MOLDED RELATIVE DENSITY ON THE EFFECTIVE STRESS-STRENGTH BEHAVIOR OF UNTREATED COARSE OTTAWA SAND IN UNDRAINED SHEAR.

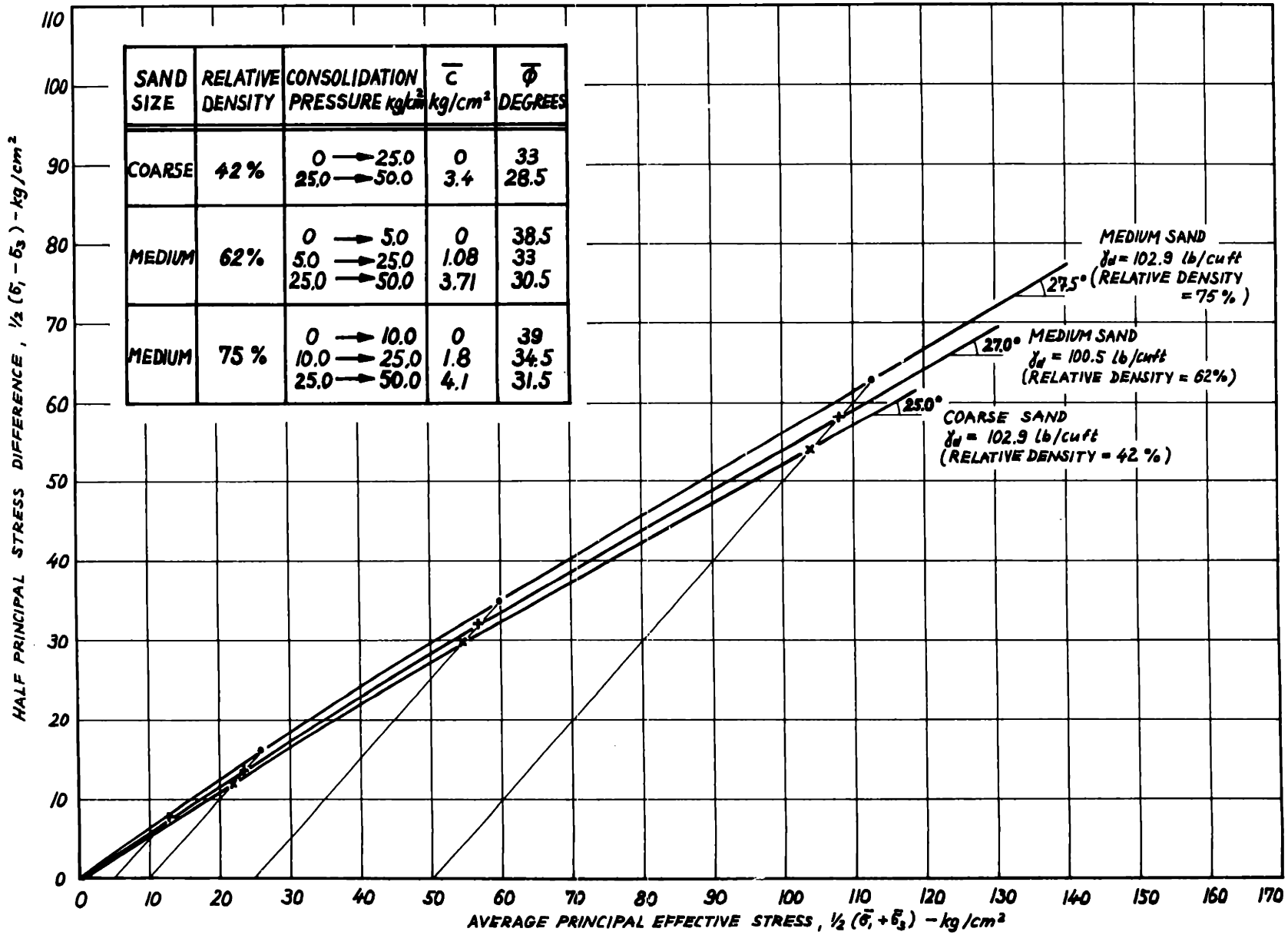

FIG. 5-7. INFLUENCE OF GRAIN SIZE AND RELATIVE DENSITY ON THE DRAINED EFFECTIVE STRESS ENVELOPE OF UNTREATED OTTAWA SAND.

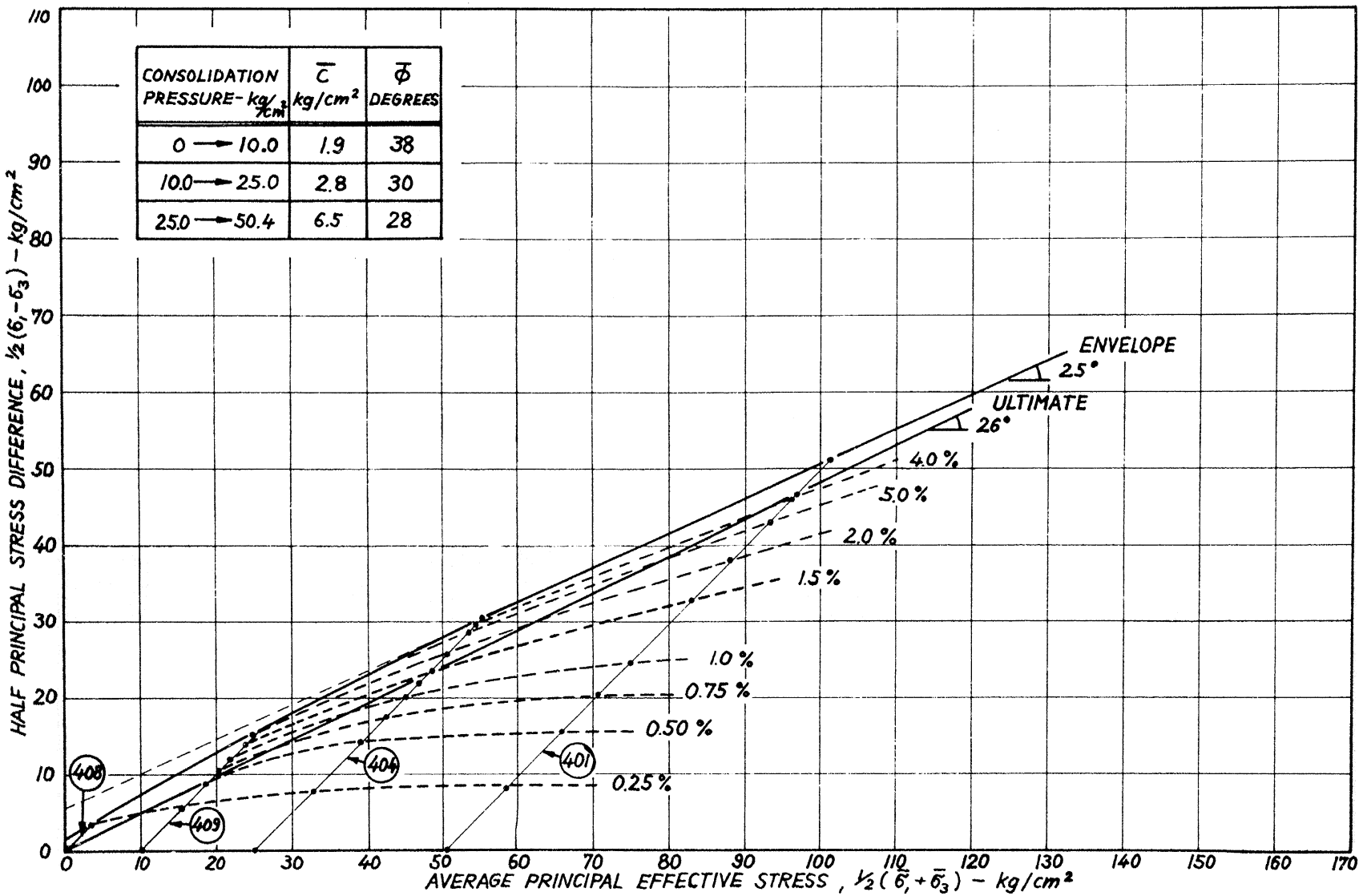

FIG. 5-8. EFFECTIVE STRESS-STRENGTH BEHAVIOR IN DRAINED SHEAR OF COARSE OTTAWA SAND STABILIZED WITH 5% CEMENT AND CURED FOR 28 DAYS.

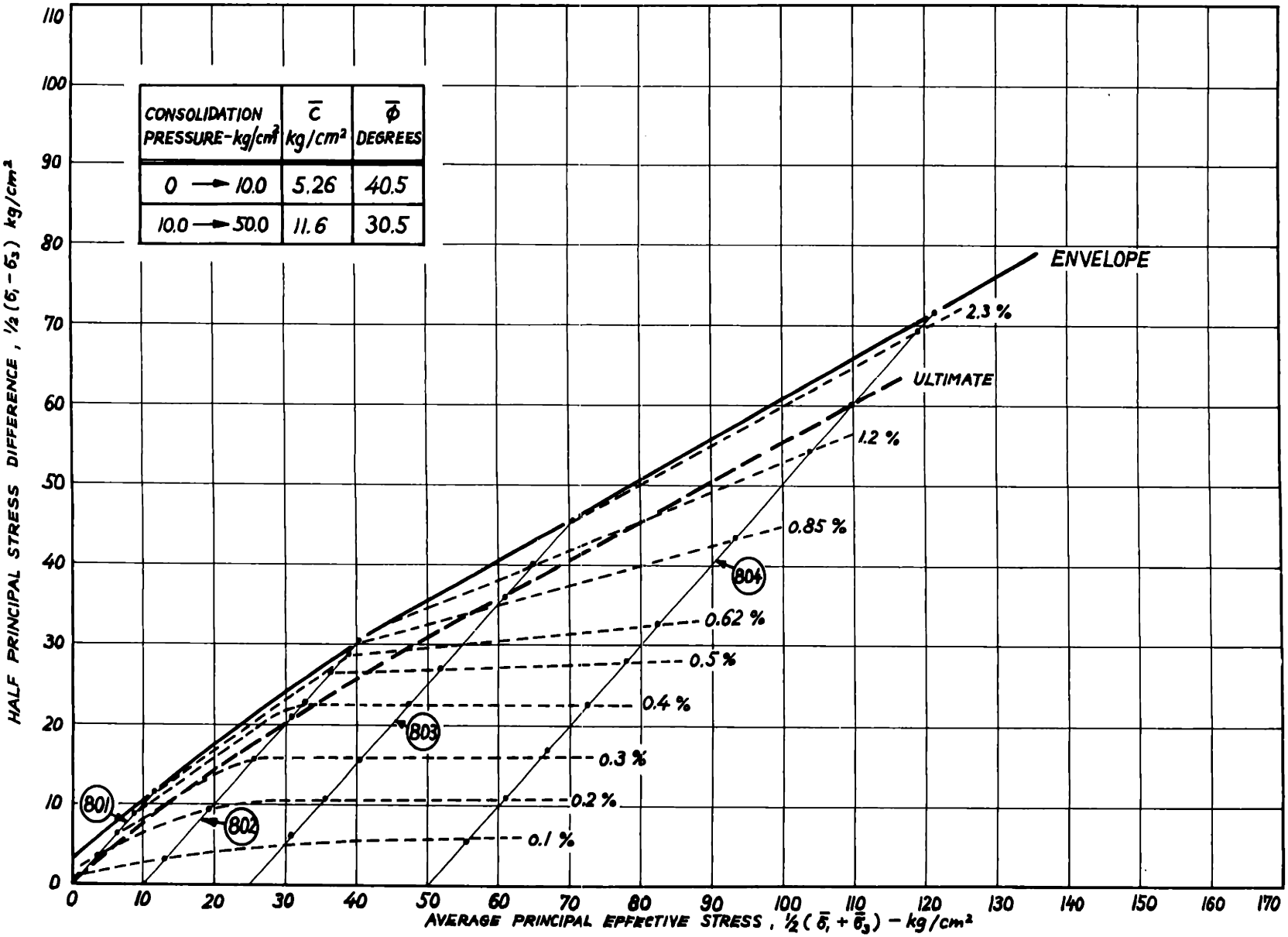

FIG. 5-9. EFFECTIVE STRESS-STRENGTH BEHAVIOR OF MEDIUM OTTAWA SAND STABILIZED WITH 5 % PORTLAND CEMENT CURED FOR 32-33 DAYS IN DRAINED SHEAR.

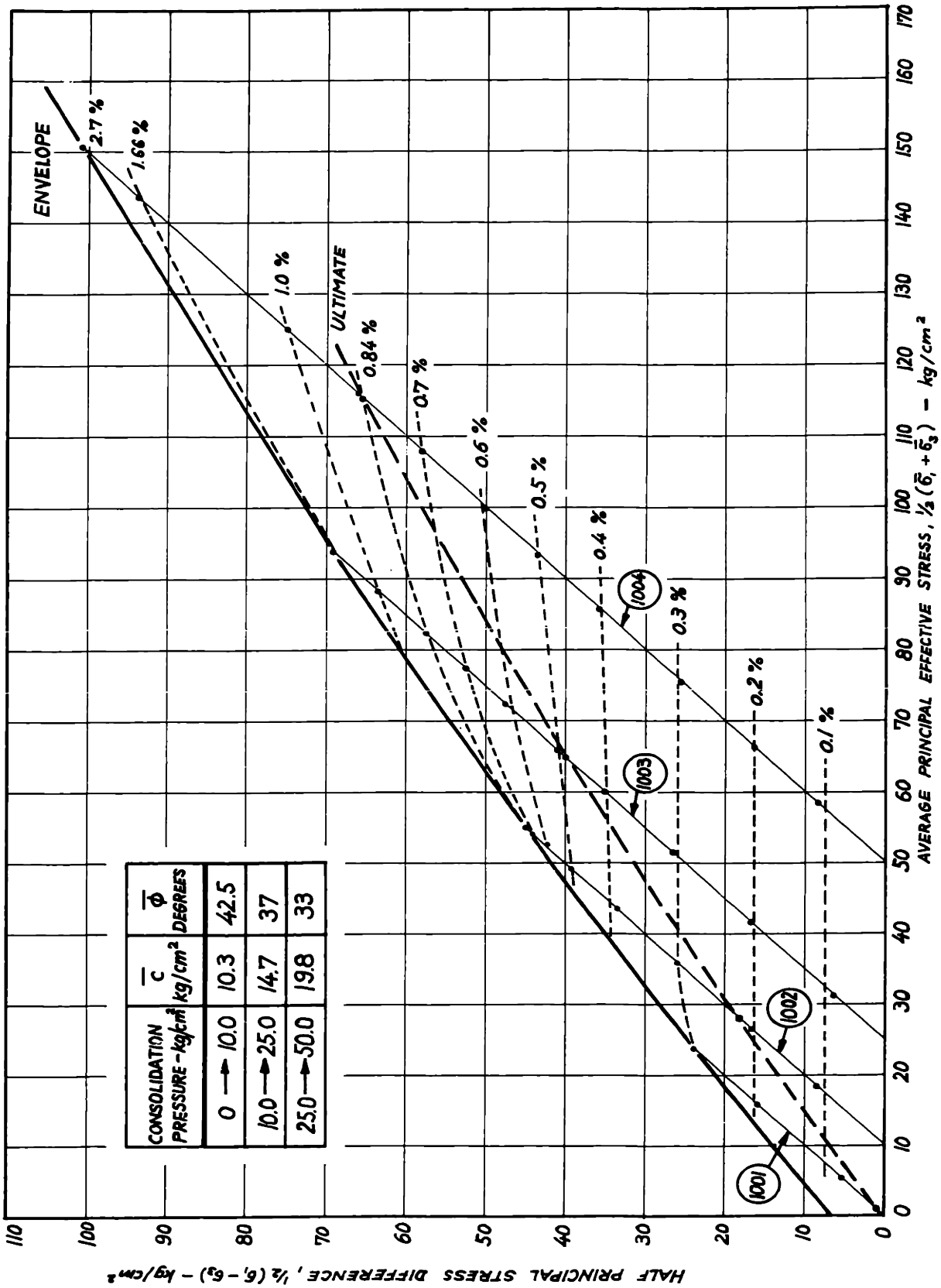

FIG. 5-10. EFFECTIVE STRESS–STRENGTH BEHAVIOR OF MEDIUM OTTAWA SAND STABILIZED WITH 10 % PORTLAND CEMENT CURED FOR 21–22 DAYS IN DRAINED SHEAR.

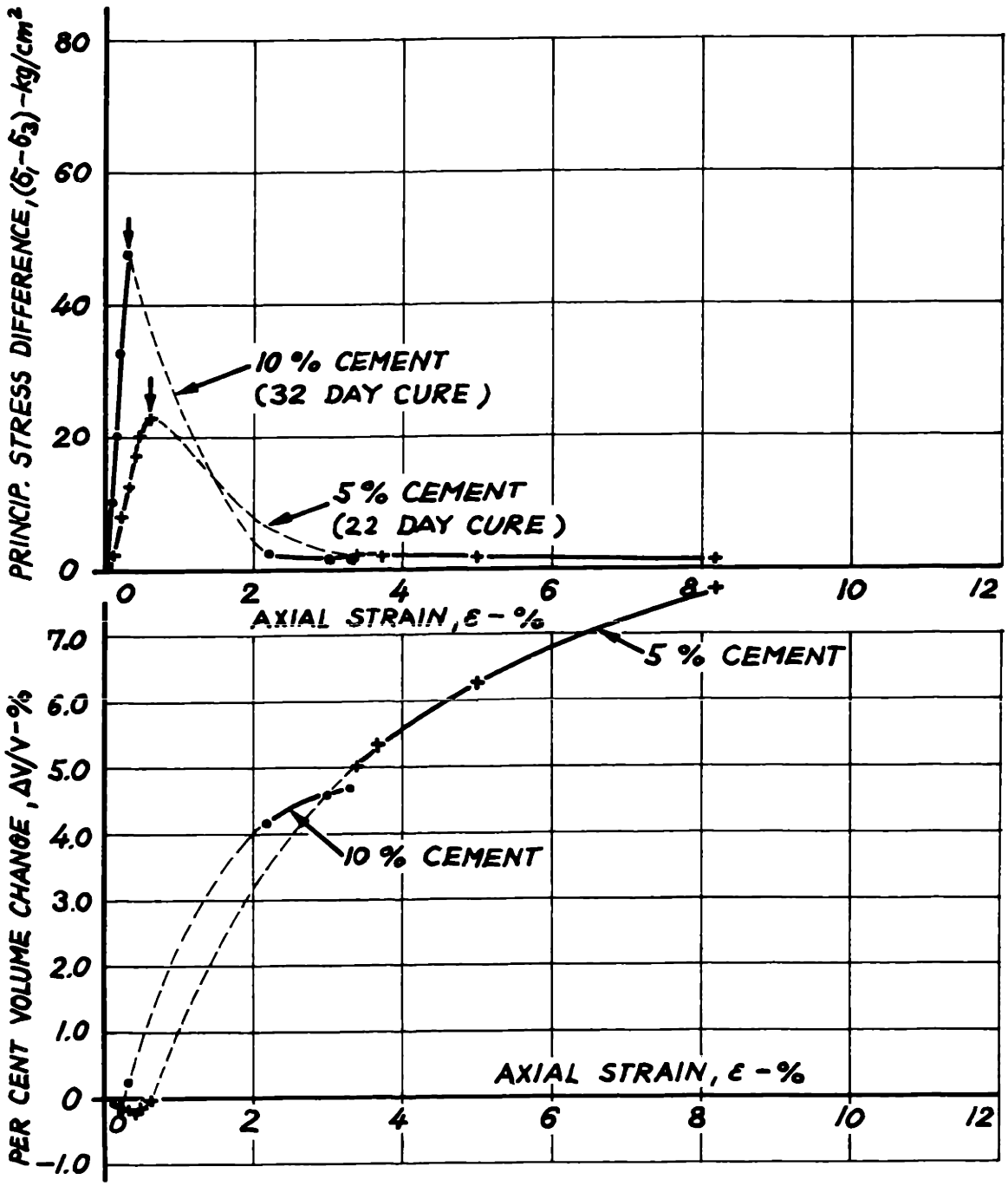

FIG. 5-11. *INFLUENCE OF CEMENT CONTENT ON THE STRESS - STRAIN BEHAVIOR OF MEDIUM OTTAWA SAND CONSOLIDATED TO 0.07 kg/cm².*

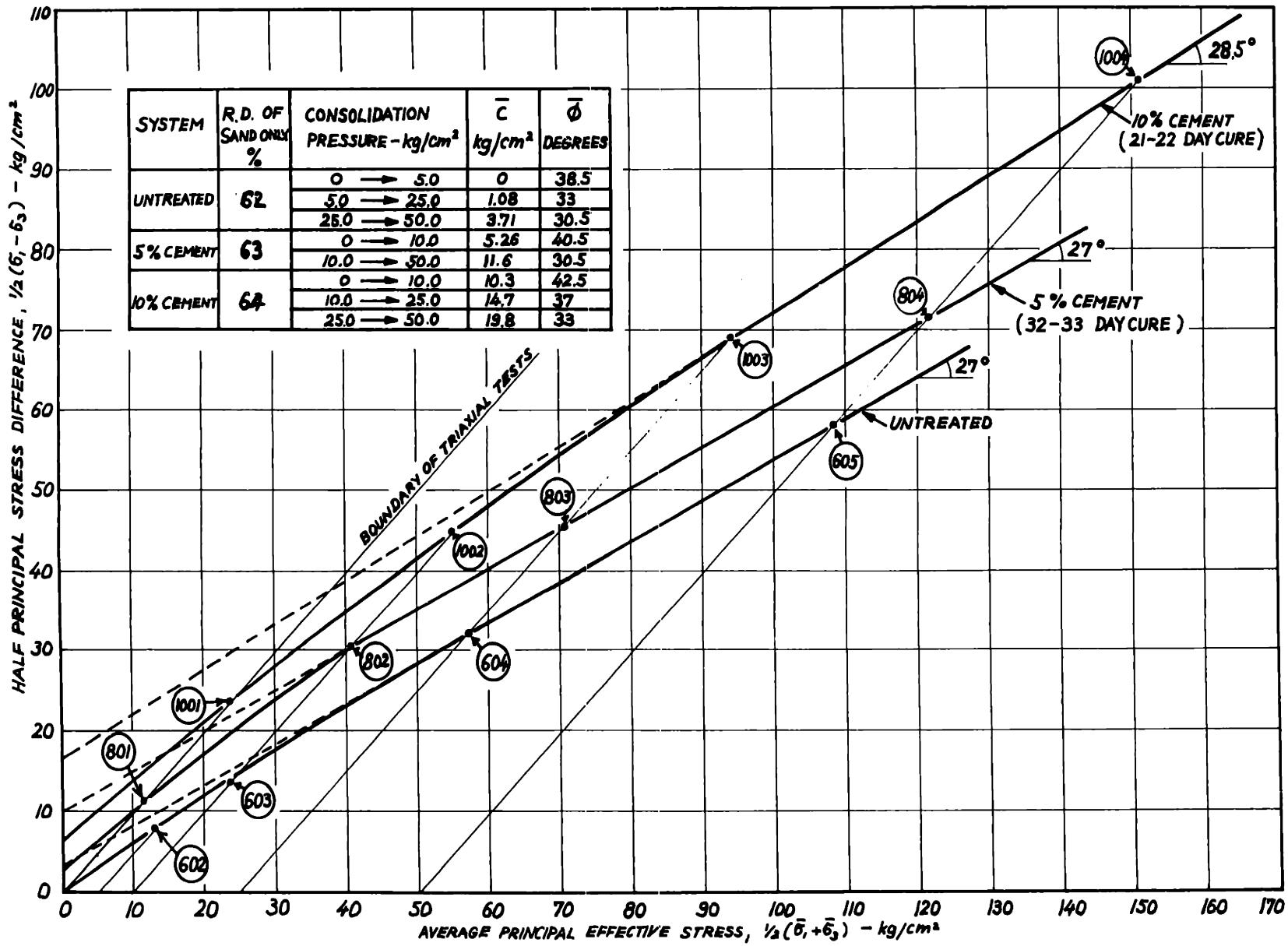

FIG. 5-12. INFLUENCE OF CEMENT CONTENT ON THE EFFECTIVE STRESS–STRENGTH ENVELOPE OF MEDIUM OTTAWA SAND IN DRAINED SHEAR.

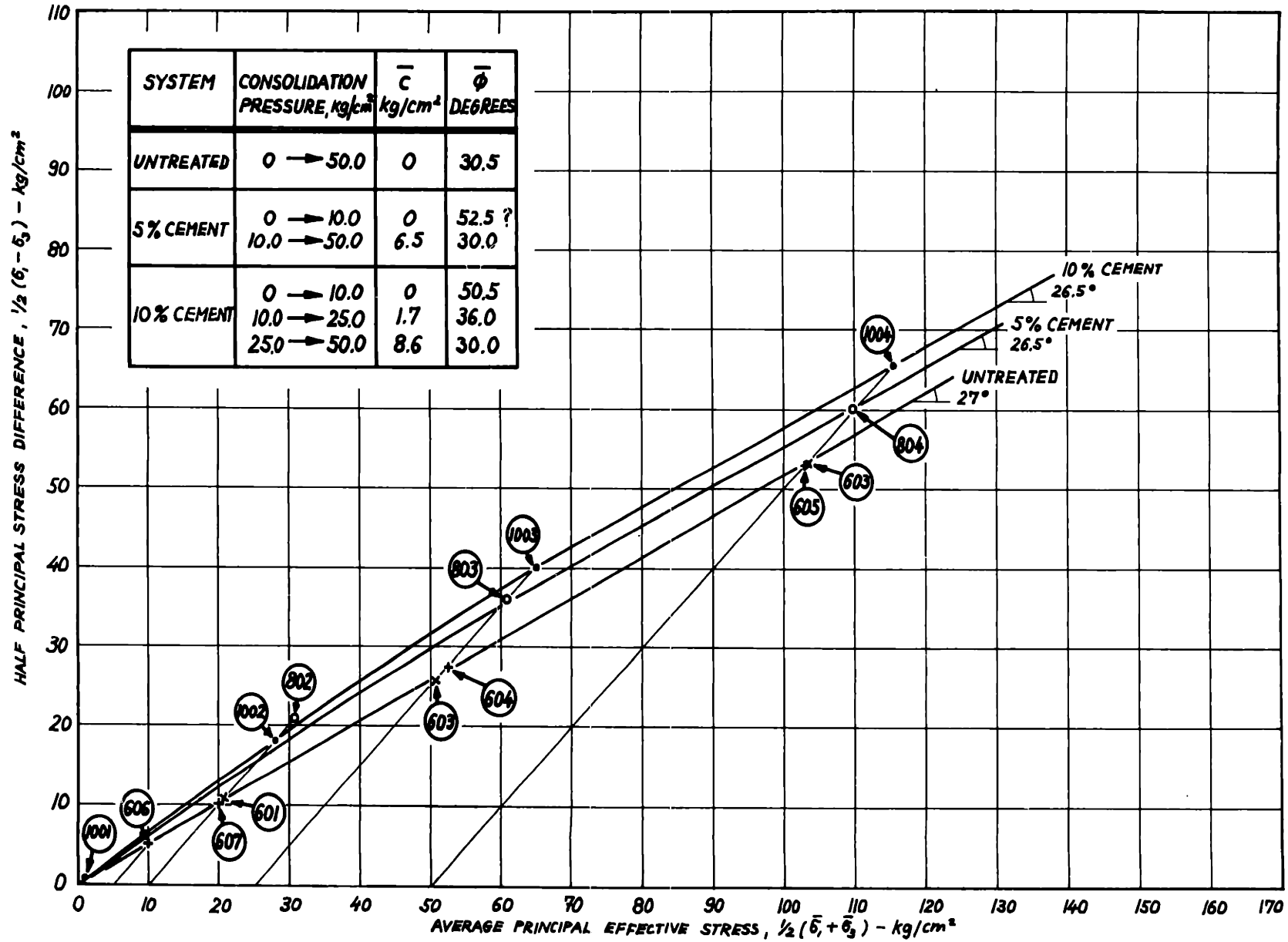

FIG. 5-13. INFLUENCE OF CEMENTATION ON THE EFFECTIVE STRESS-STRENGTH RELATIONS OF MEDIUM OTTAWA SAND IN DRAINED SHEAR AT ULTIMATE.

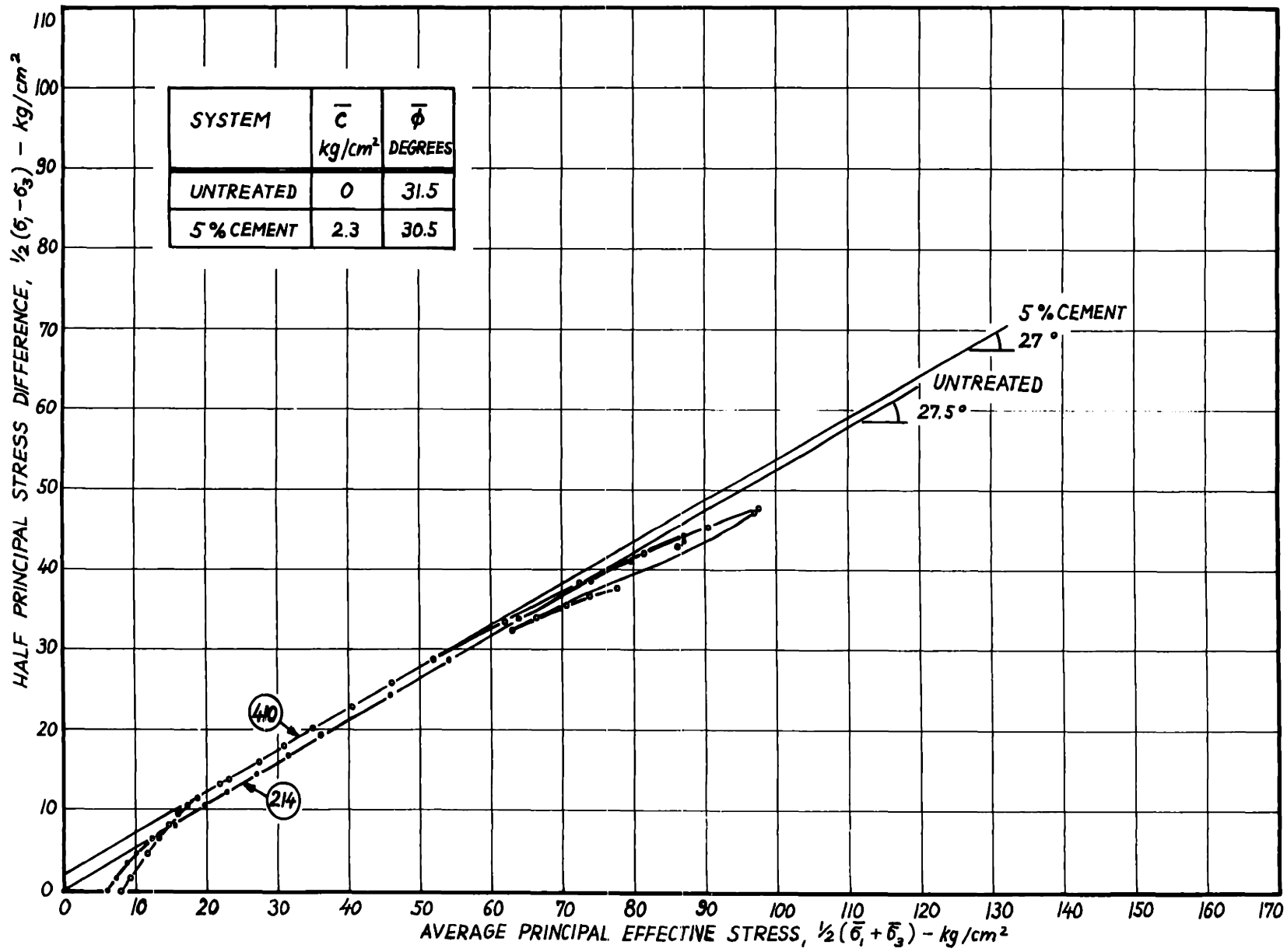

FIG. 5-14. INFLUENCE OF 5% CEMENT ON THE EFFECTIVE STRESS-STRENGTH BEHAVIOR OF COARSE OTTAWA SAND IN UNDRAINED SHEAR (RELATIVE DENSITY OF SAND EXCLUDING CEMENT = 54 %).

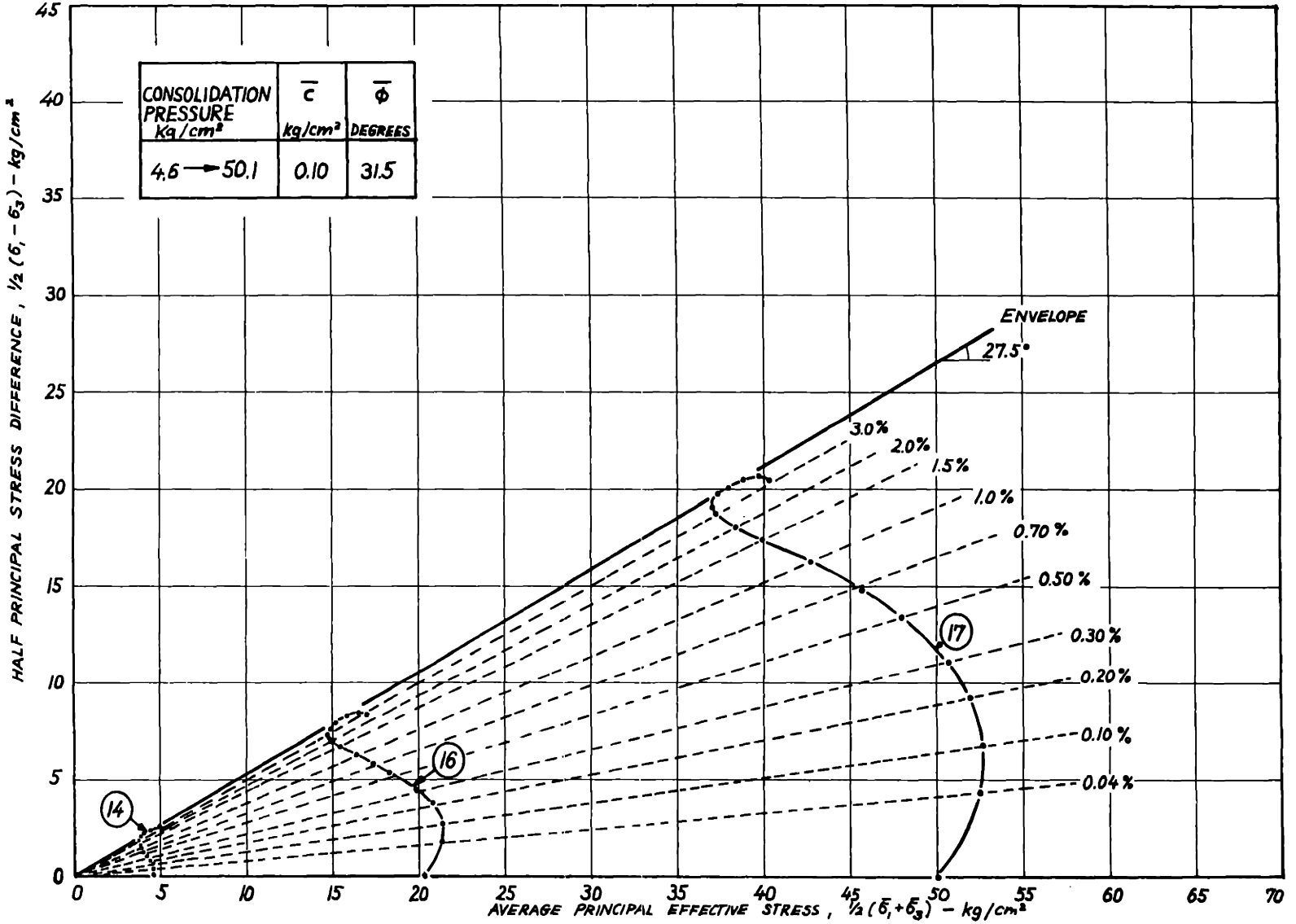

FIG. 5-15. EFFECTIVE STRESS–STRENGTH BEHAVIOR IN UNDRAINED SHEAR OF UNTREATED MASSACHUSETTS CLAYEY SILT.

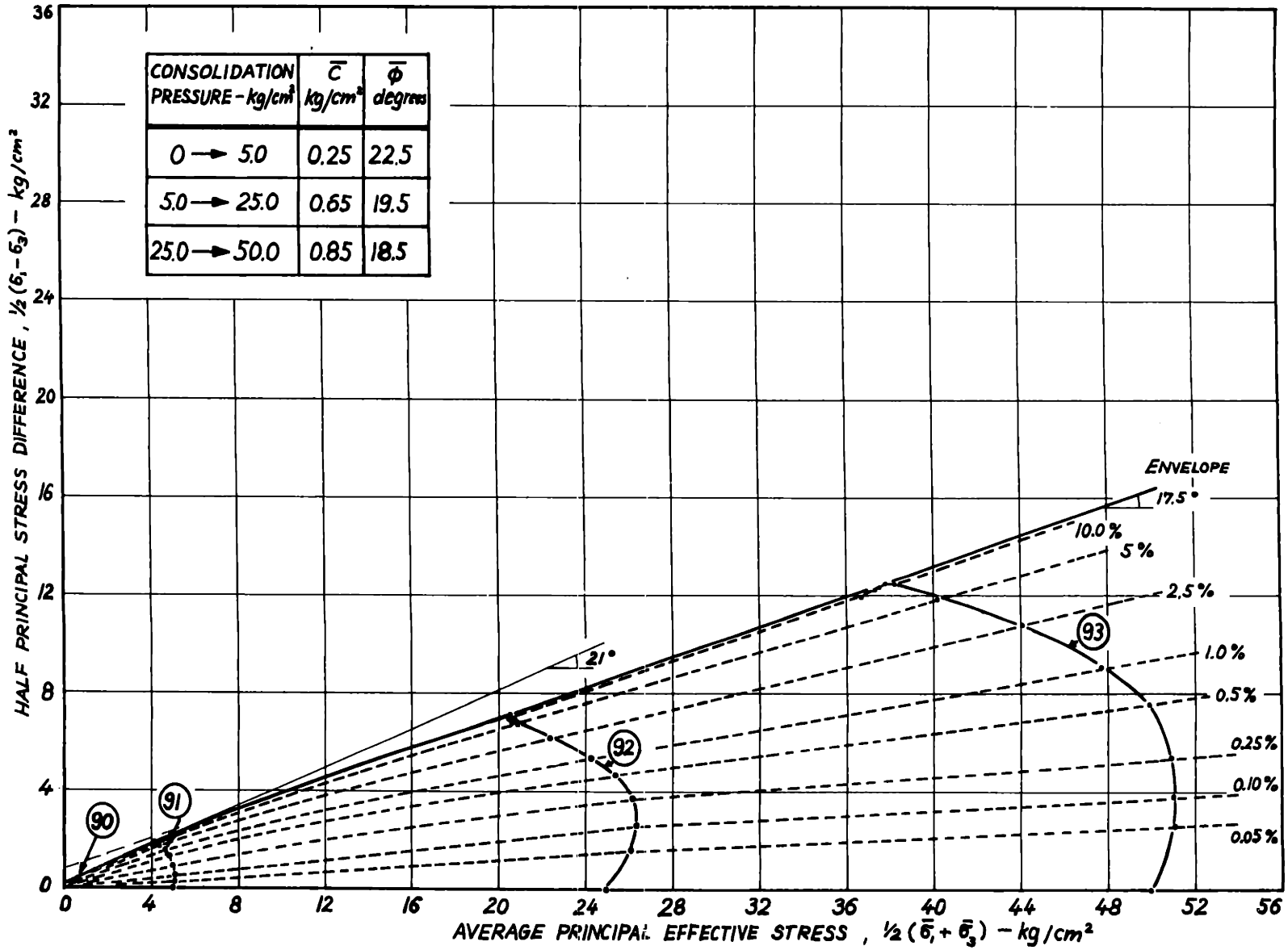

FIG. 5-16. EFFECTIVE STRESS-STRENGTH BEHAVIOR IN UNDRAINED SHEAR OF UNTREATED VICKSBURG BUCKSHOT CLAY

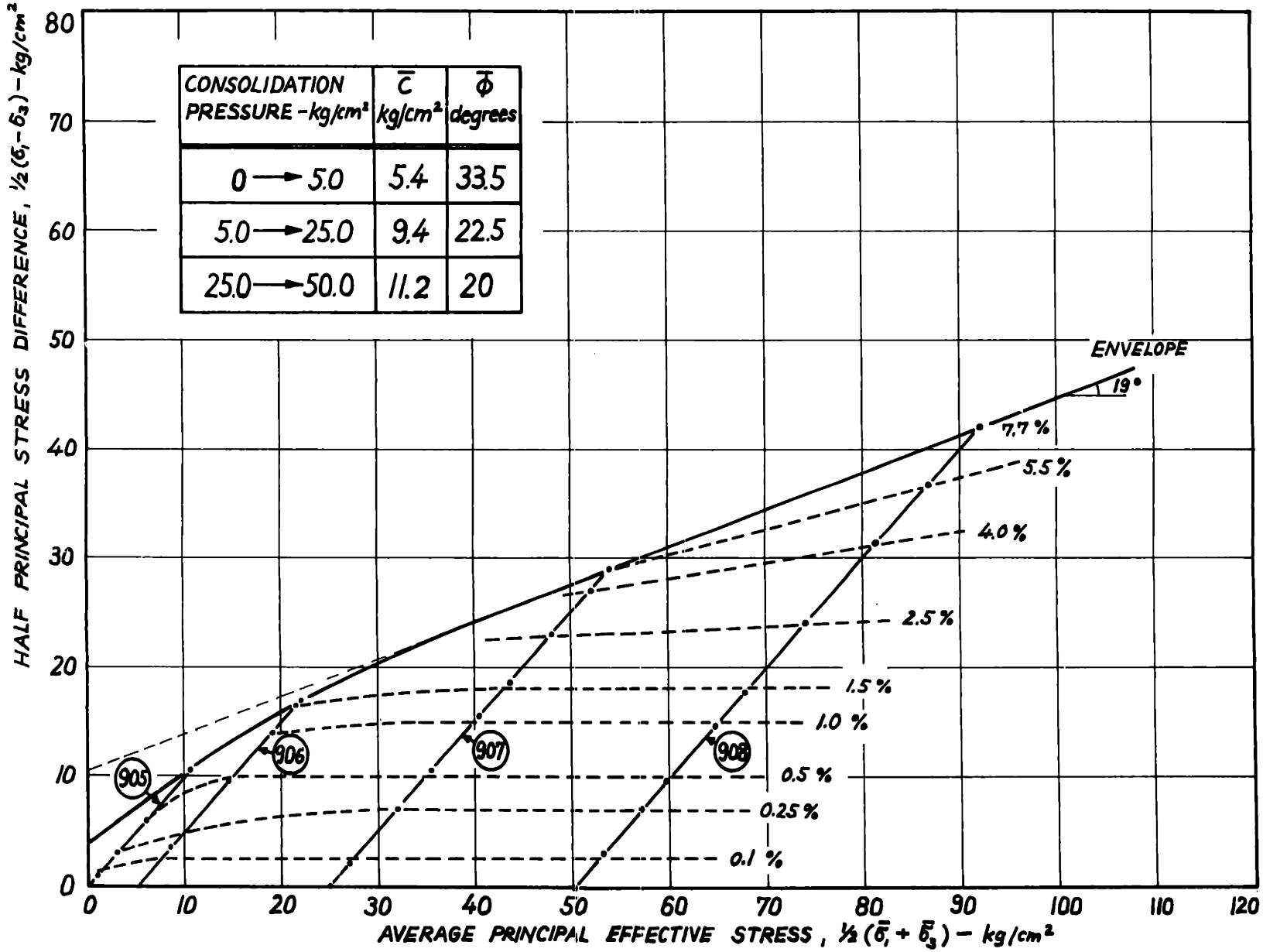

FIG. 5-17. EFFECTIVE STRESS-STRENGTH BEHAVIOR IN DRAINED SHEAR OF VICKSBURG BUCKSHOT CLAY STABILIZED WITH 5 % LIME AND CURED FOR ONE YEAR

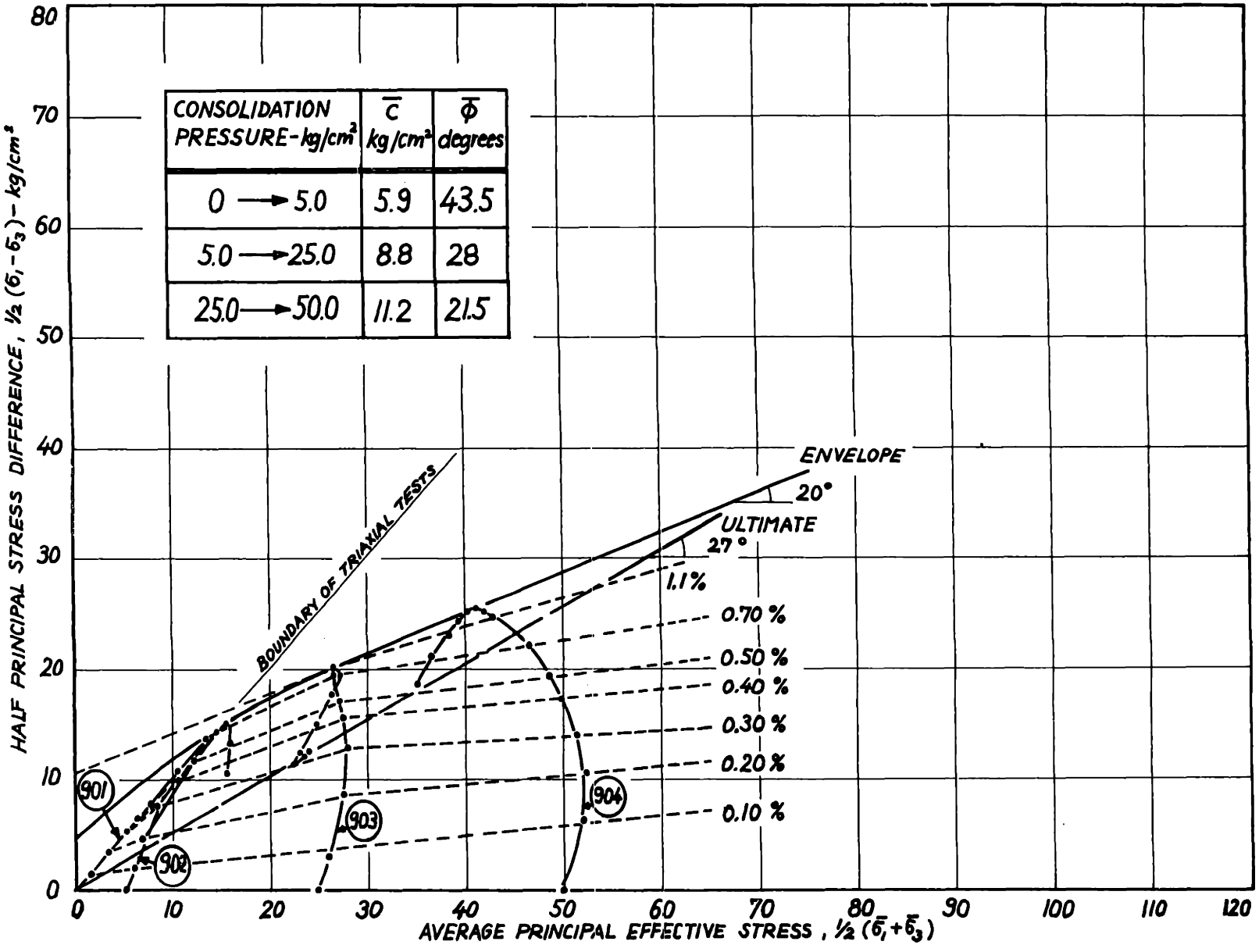

FIG. 5-18. EFFECTIVE STRESS-STRENGTH BEHAVIOR IN UNDRAINED SHEAR OF VICKSBURG BUCKSHOT CLAY STABILIZED WITH 5 % LIME AND CURED FOR ONE YEAR

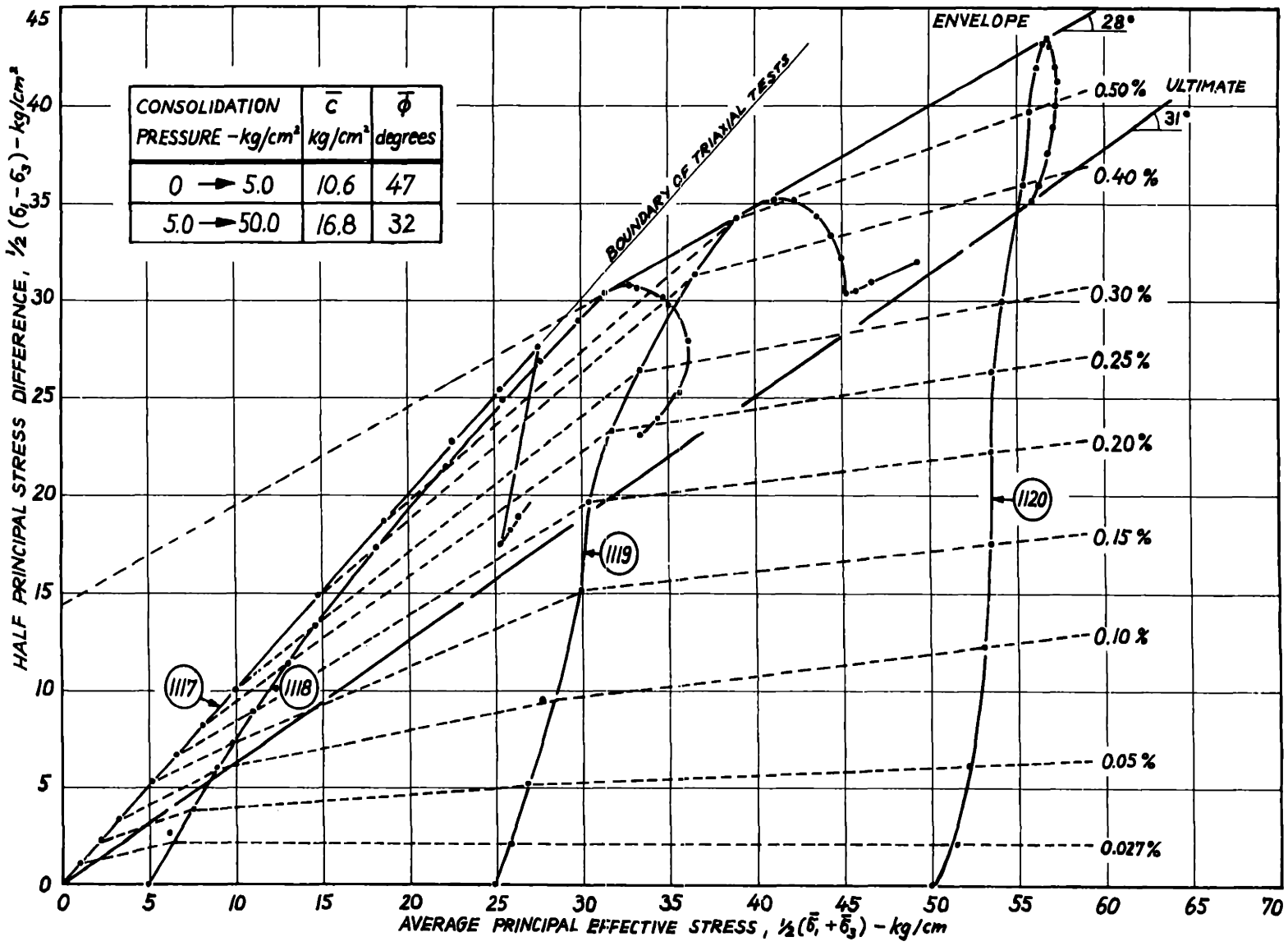

FIG. 5-19. EFFECTIVE STRESS-STRENGTH BEHAVIOR IN UNDRAINED SHEAR OF VICKSBURG BUCKSHOT CLAY STABILIZED WITH 10 % CEMENT + 0.5 N NaOH AND CURED FOR 55 DAYS

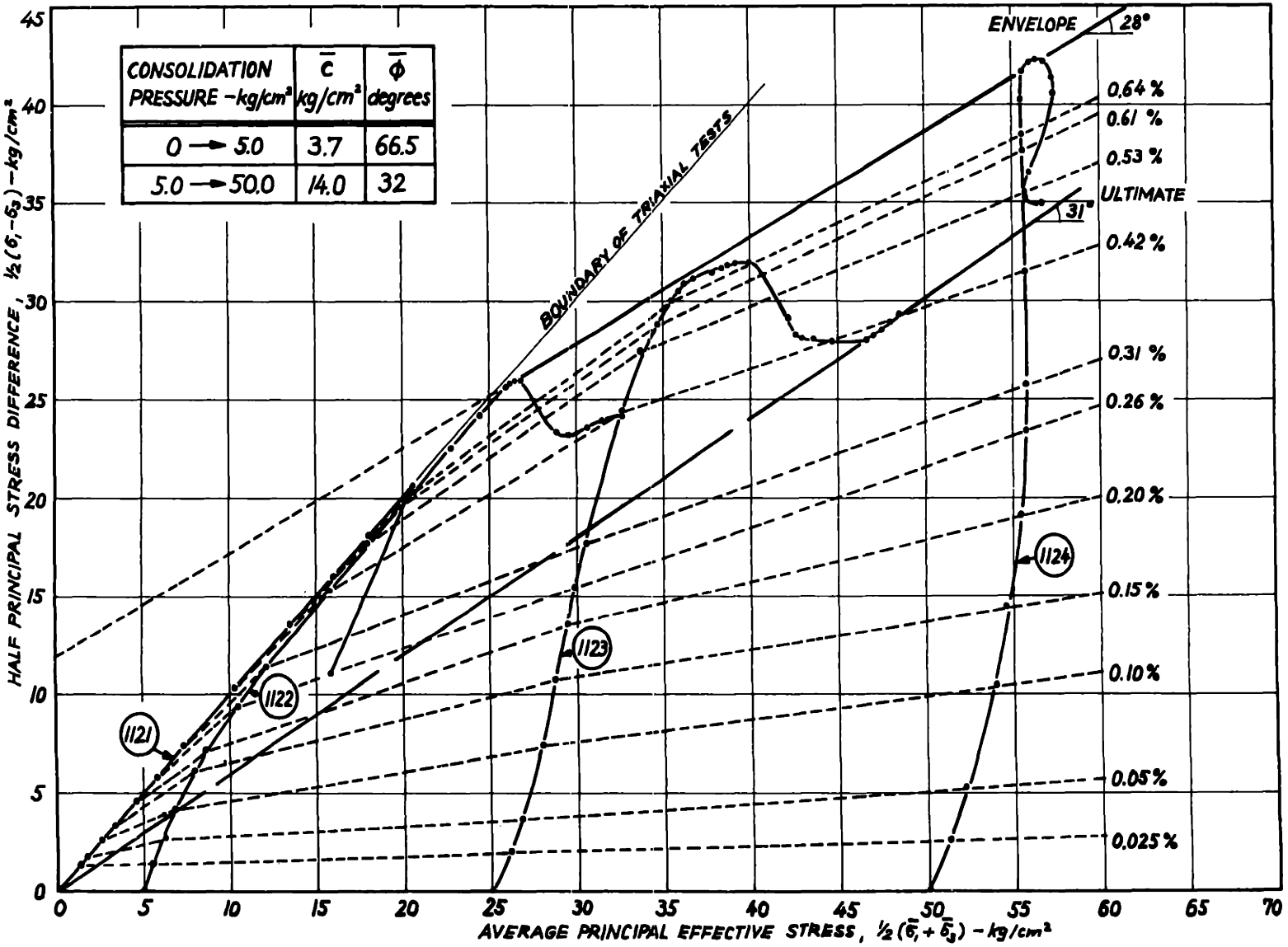

FIG. 5-20. EFFECTIVE STRESS-STRENGTH BEHAVIOR IN UNDRAINED SHEAR OF VICKSBURG BUCKSHOT CLAY STABILIZED WITH 10% CEMENT + 0.5 N NaOH AFTER CYCLES OF MILD WETTING AND DRYING. 55 DAYS CURING

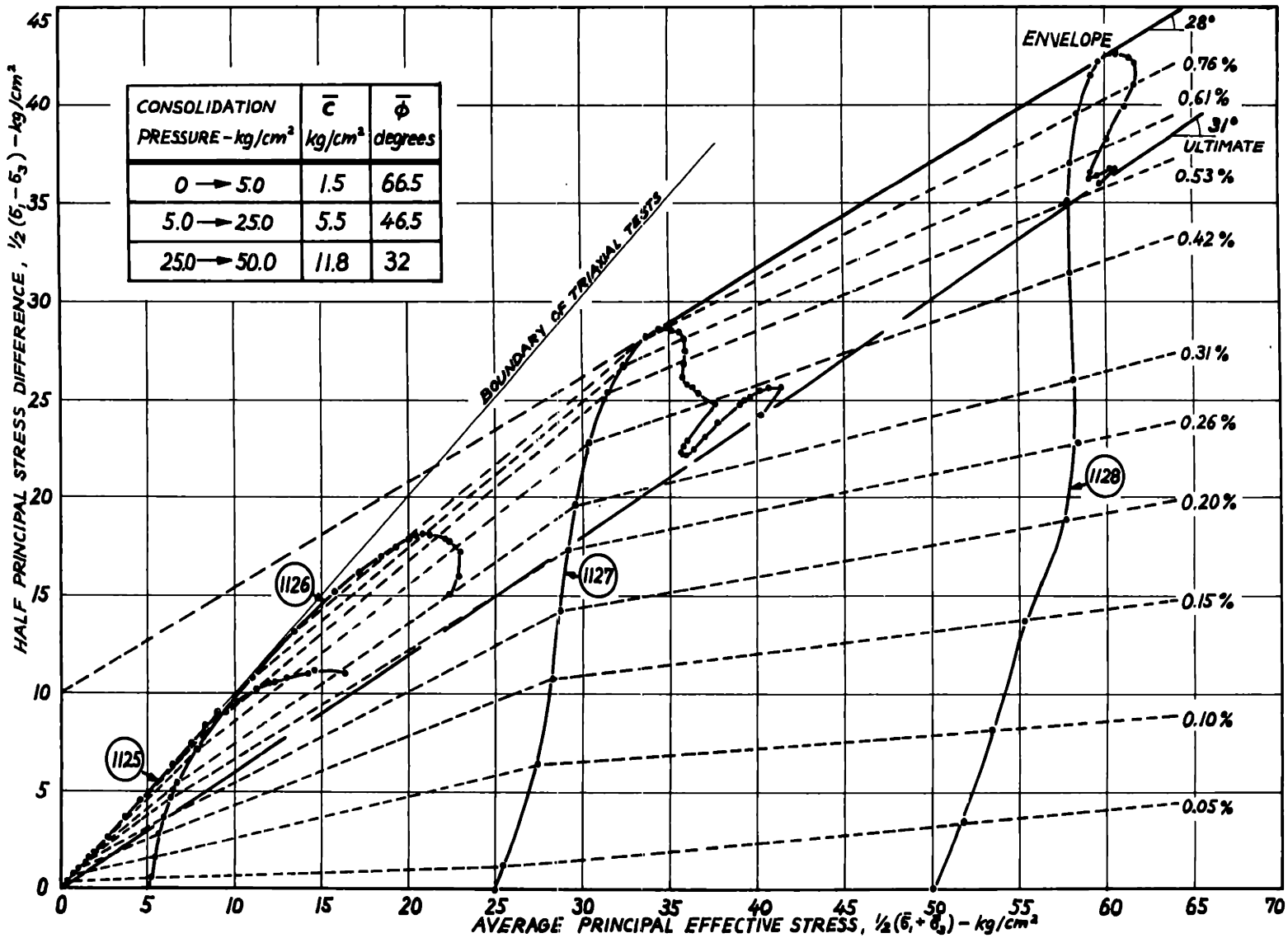

FIG. 5-21. EFFECTIVE STRESS-STRENGTH BEHAVIOR IN UNDRAINED SHEAR OF VICKSBURG BUCKSHOT CLAY STABILIZED WITH 10 % CEMENT + 0.5 N NaOH AFTER CYCLES OF SEVERE WETTING AND DRYING. 90DAYS CURING

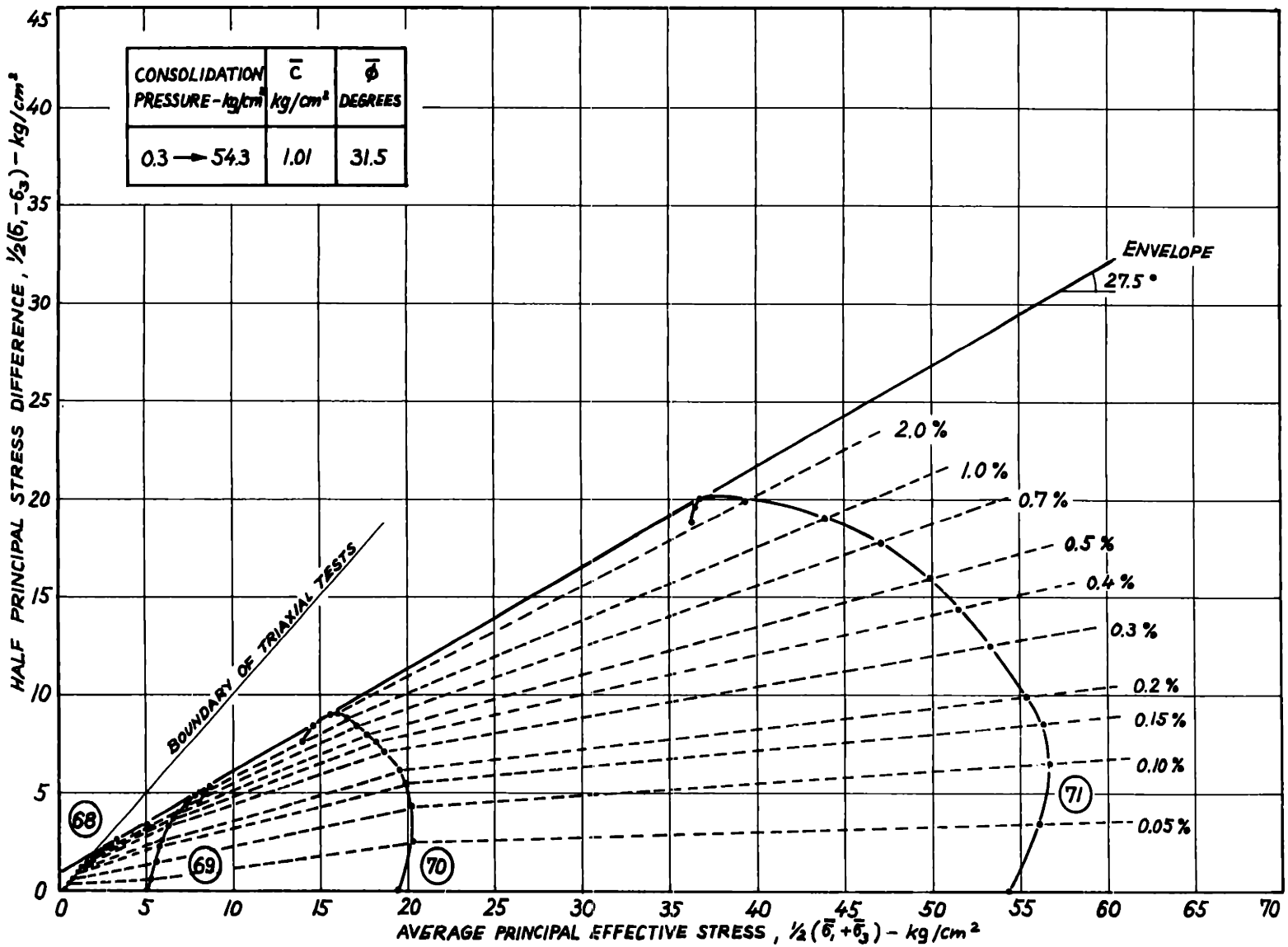

FIG. 5-22. EFFECTIVE STRESS-STRENGTH BEHAVIOR IN UNDRAINED SHEAR OF MASSACHUSETTS CLAYEY SILT STABILIZED WITH 5 % LIME AND CURED FOR 20 DAYS.

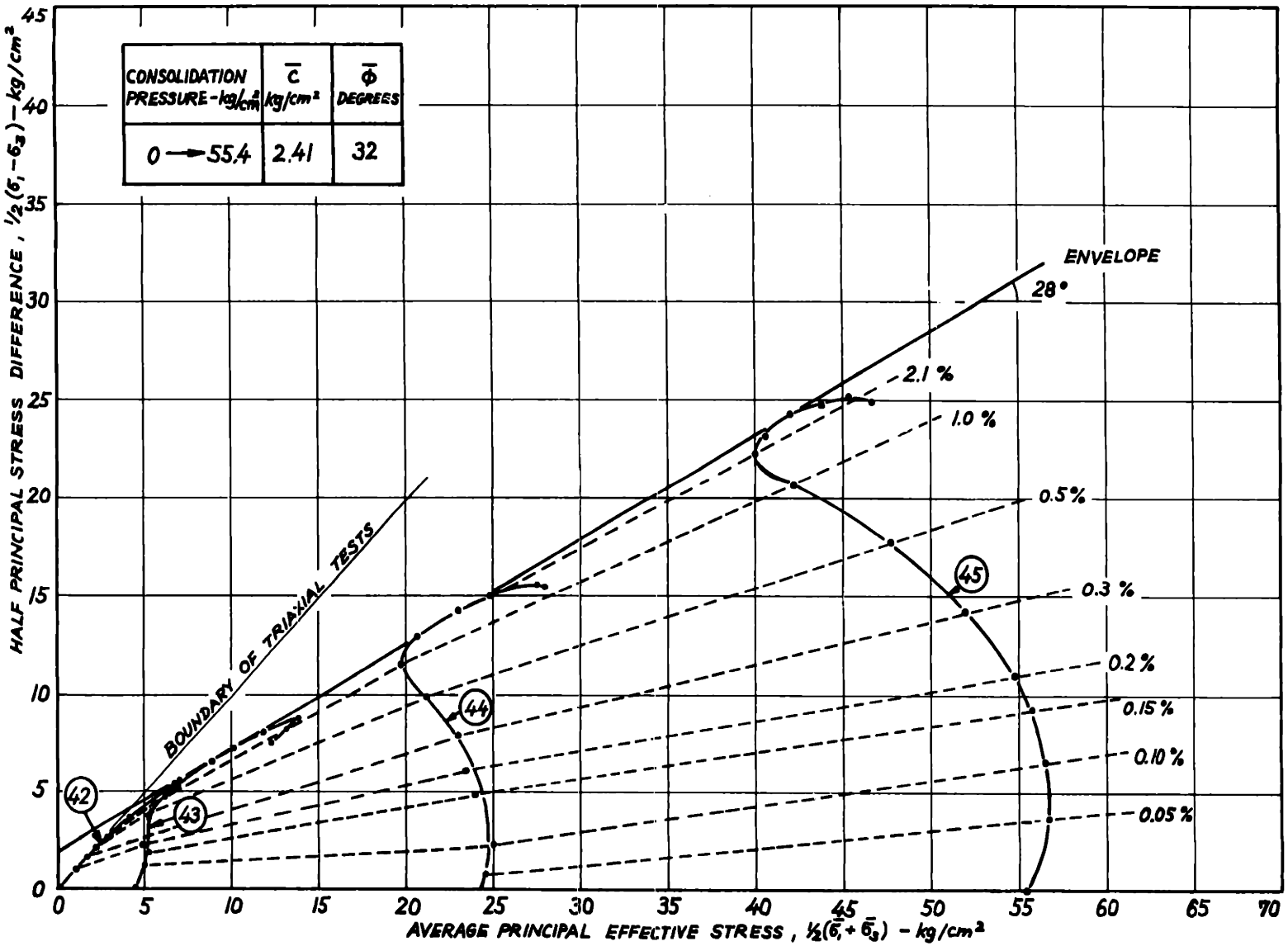

FIG. 5-23. EFFECTIVE STRESS–STRENGTH BEHAVIOR IN UNDRAINED SHEAR OF MASSACHUSETTS CLAYEY SILT STABILIZED WITH 3 % CEMENT AND CURED FOR 21 DAYS.

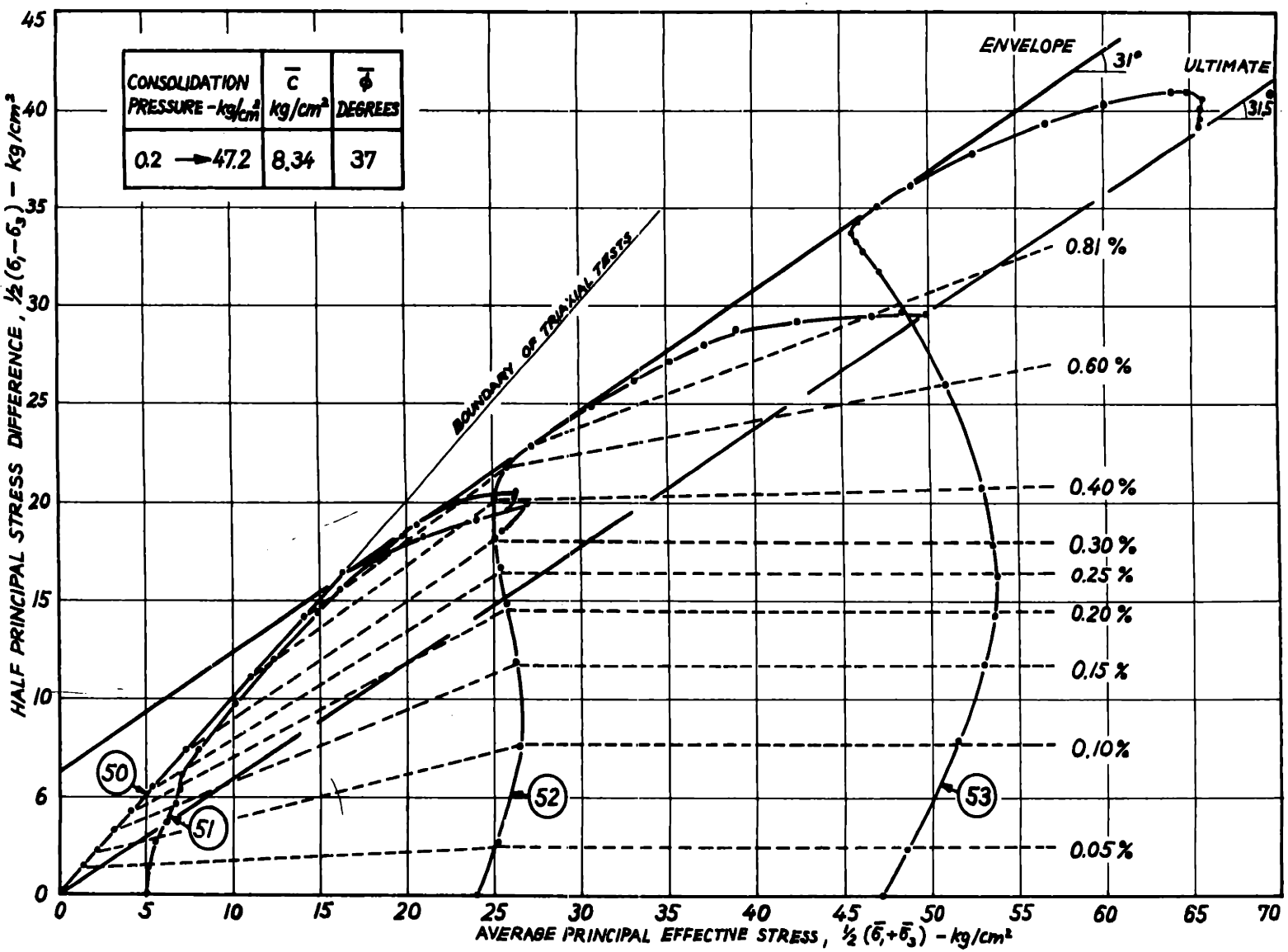

FIG. 5-24. EFFECTIVE STRESS-STRENGTH BEHAVIOR IN UNDRAINED SHEAR OF MASSACHUSETTS CLAYEY SILT STABILIZED WITH 5 % CEMENT AND CURED FOR 50 DAYS.

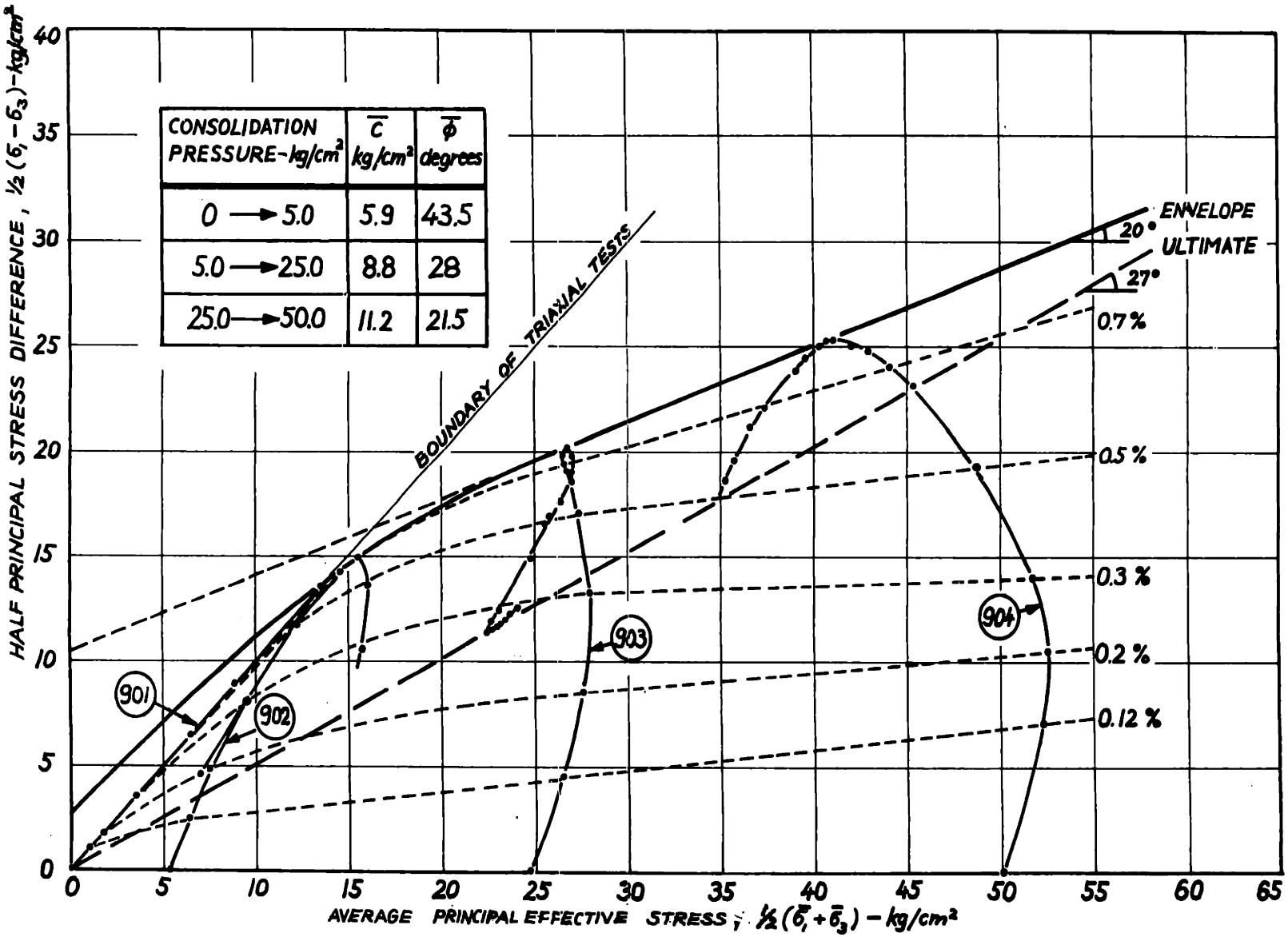

FIG. 5-25. EFFECTIVE STRESS–STRENGTH BEHAVIOR IN UNDRAINED SHEAR OF VICKSBURG BUCKSHOT CLAY STABILIZED WITH 5% LIME AND CURED FOR ONE YEAR

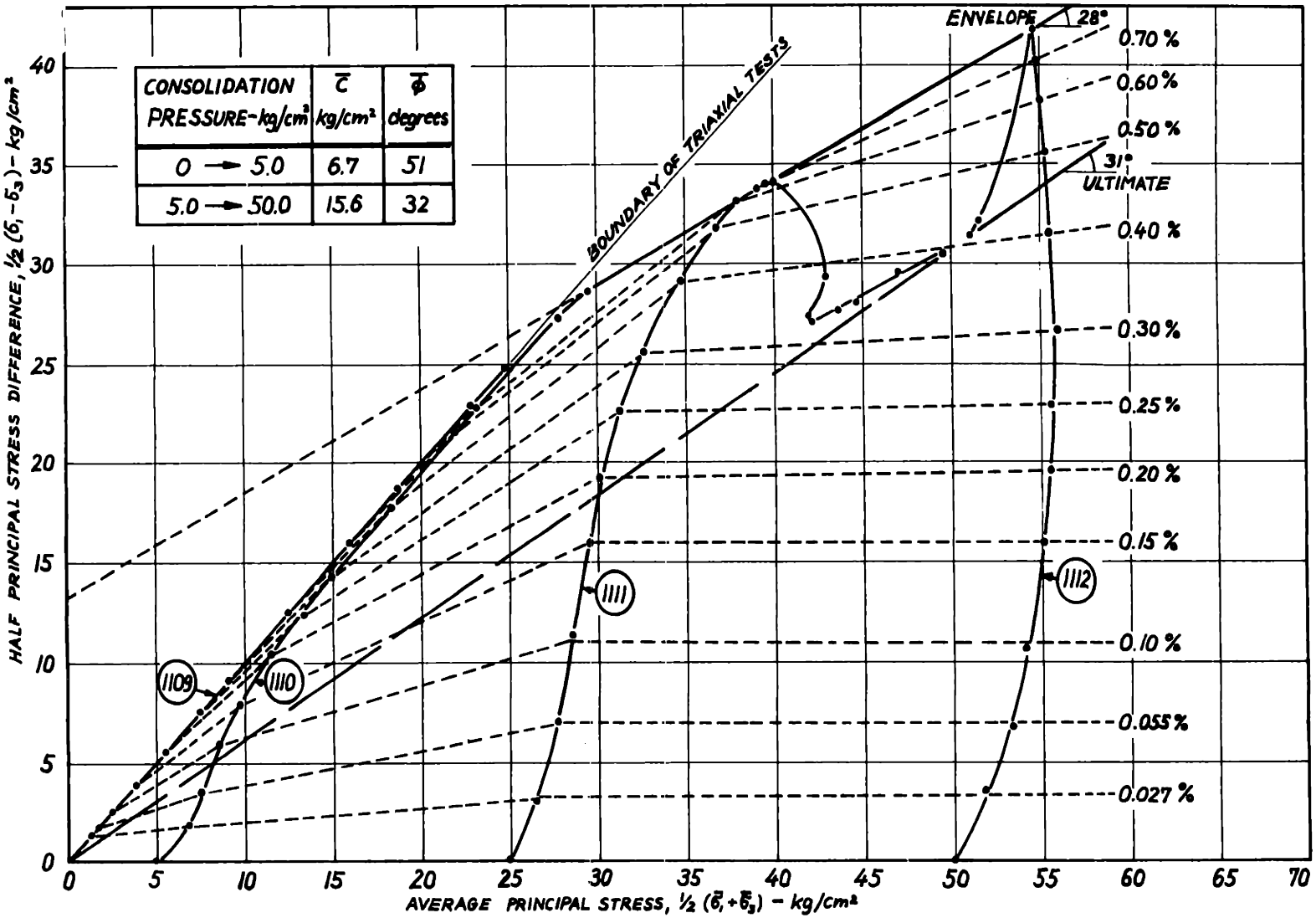

FIG. 5-26. EFFECTIVE STRESS–STRENGTH BEHAVIOR IN UNDRAINED SHEAR OF VICKSBURG BUCKSHOT CLAY STABILIZED WITH 10% CEMENT + 0.5 N NaOH AND CURED FOR 43 DAYS

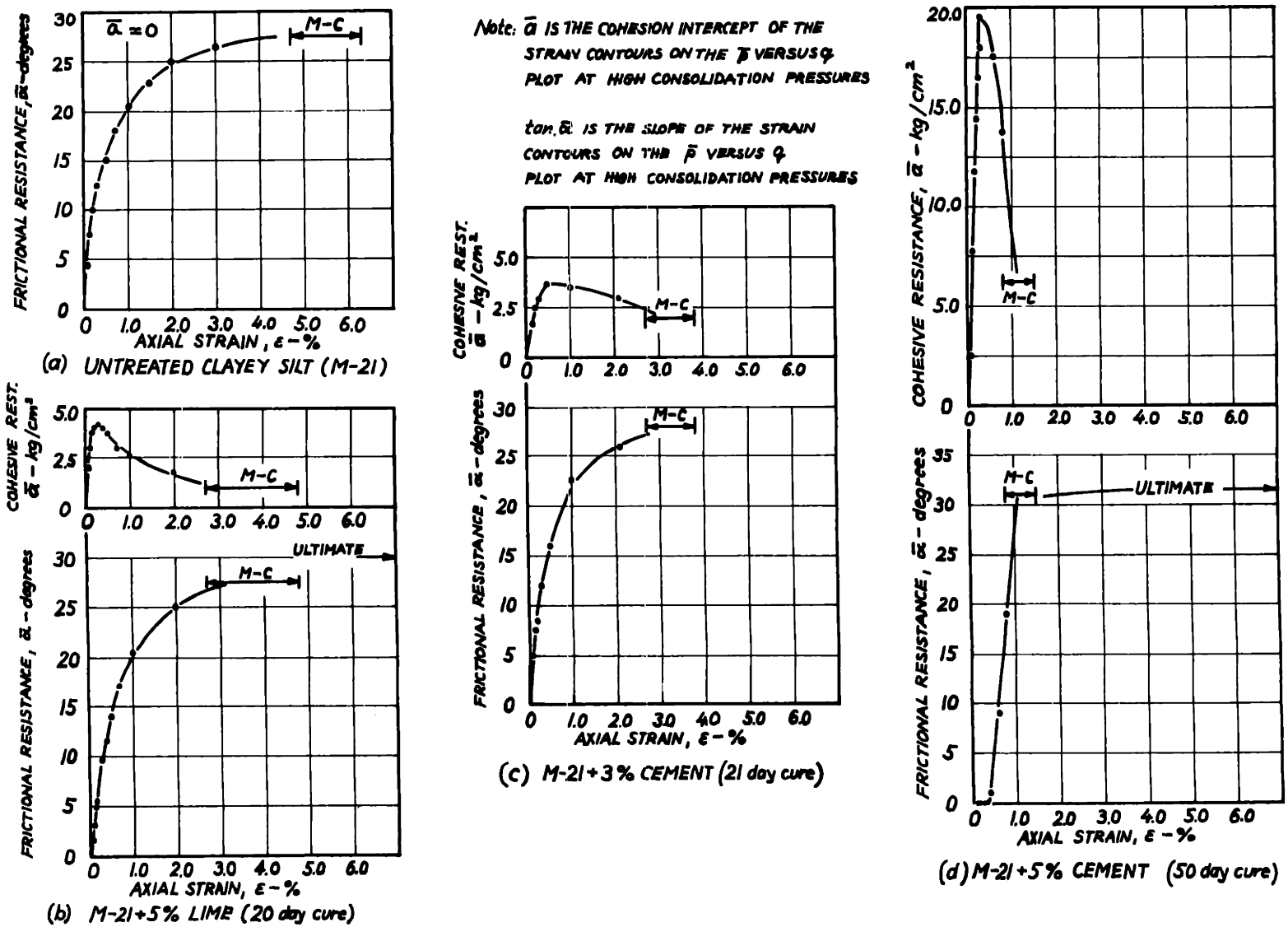

FIG. 5-27. INFLUENCE OF CEMENTATION ON THE FRICTIONAL AND COHESIVE RESISTANCE OF MASSACHUSETTS CLAYEY SILT AS DETERMINED FROM AXIAL STRAIN CONTOURS.

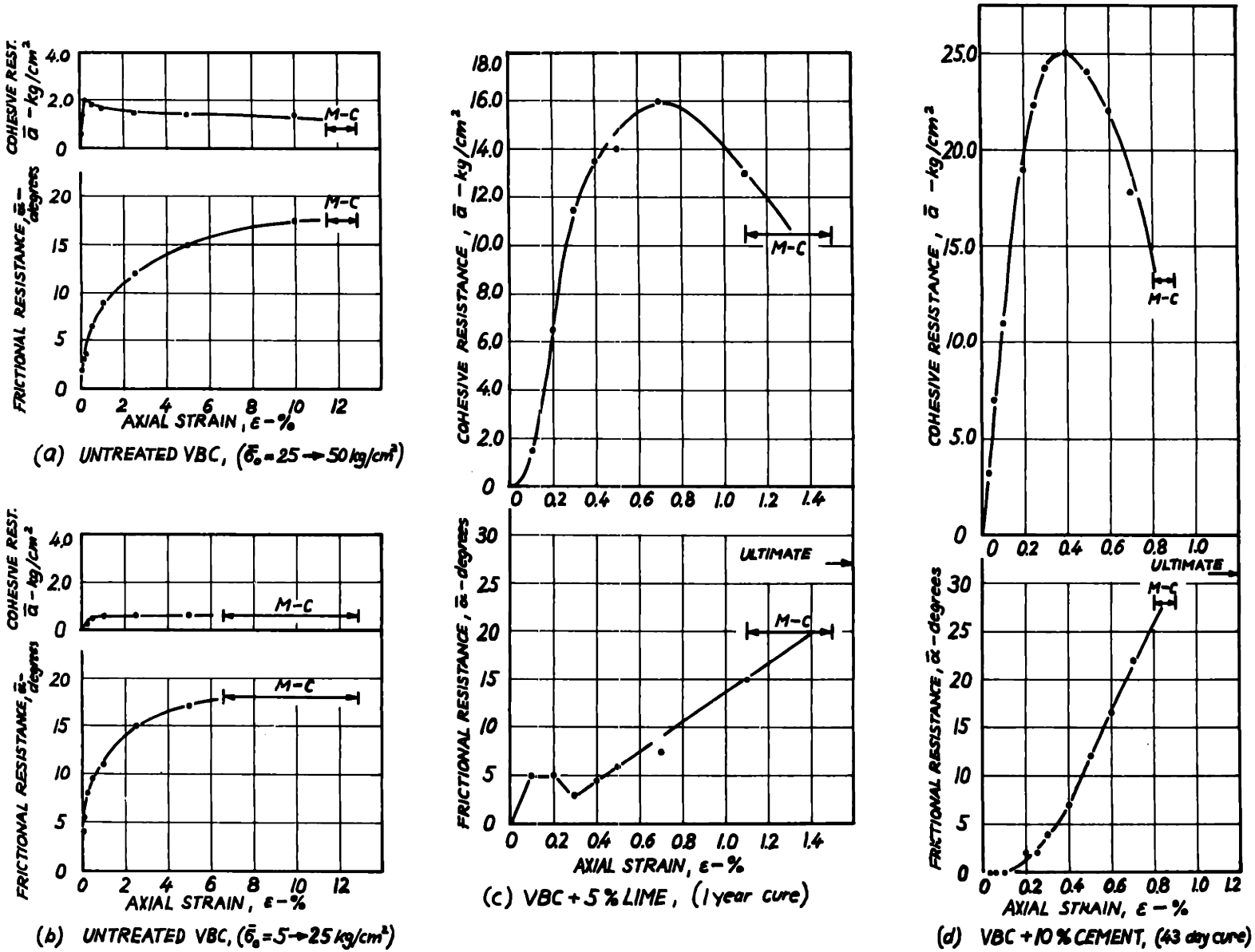

FIG. 5-28. INFLUENCE OF CEMENTATION ON THE FRICTIONAL AND COHESIVE RESISTANCE OF VICKSBURG BUCKSHOT CLAY AS DETERMINED FROM AXIAL STRAIN CONTOURS.

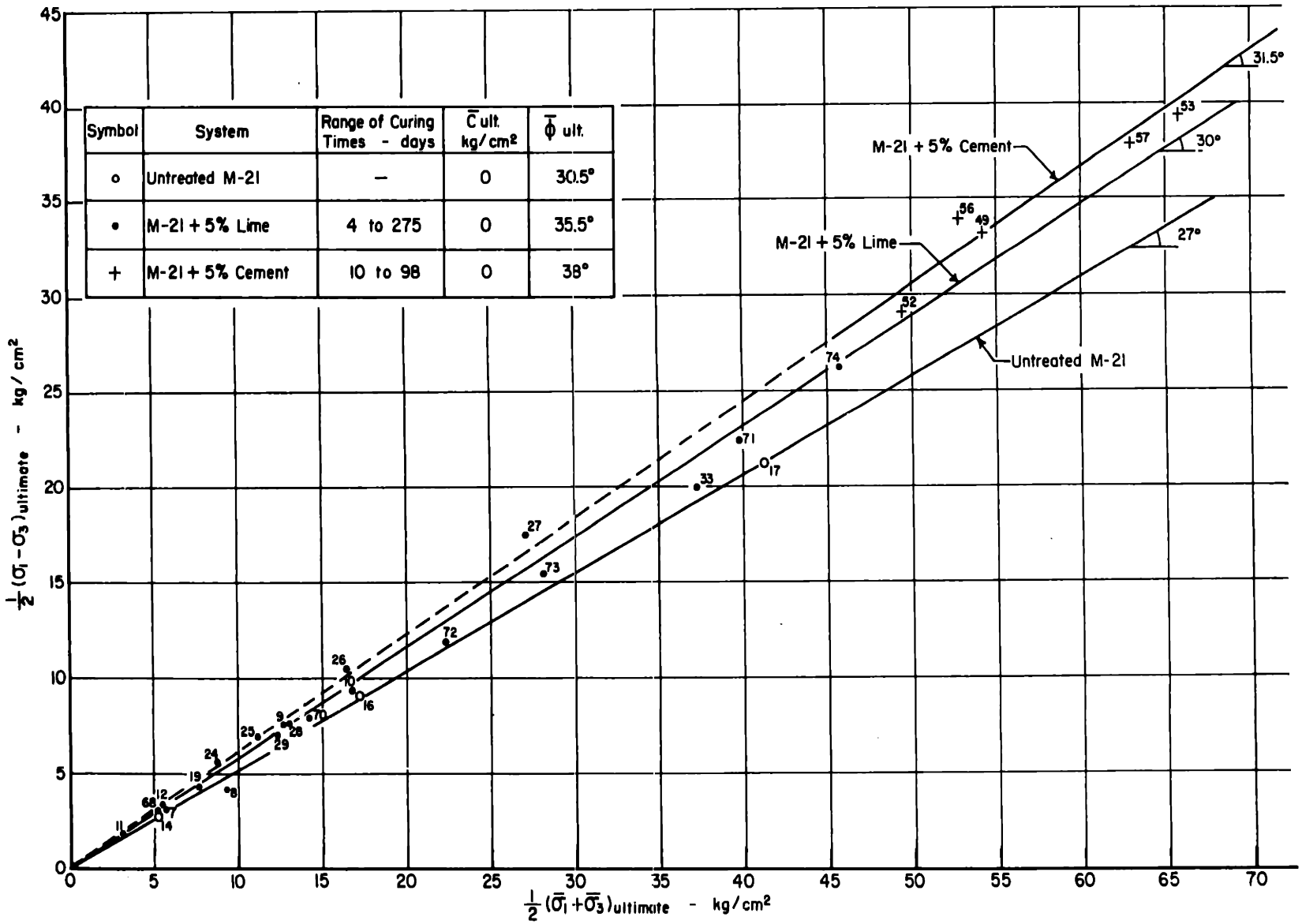

FIGURE 5-29. ULTIMATE EFFECTIVE STRESS-STRENGTH RELATIONS FOR UNTREATED M-21, M-21+5% LIME AND M-21+5% CEMENT AT ULTIMATE

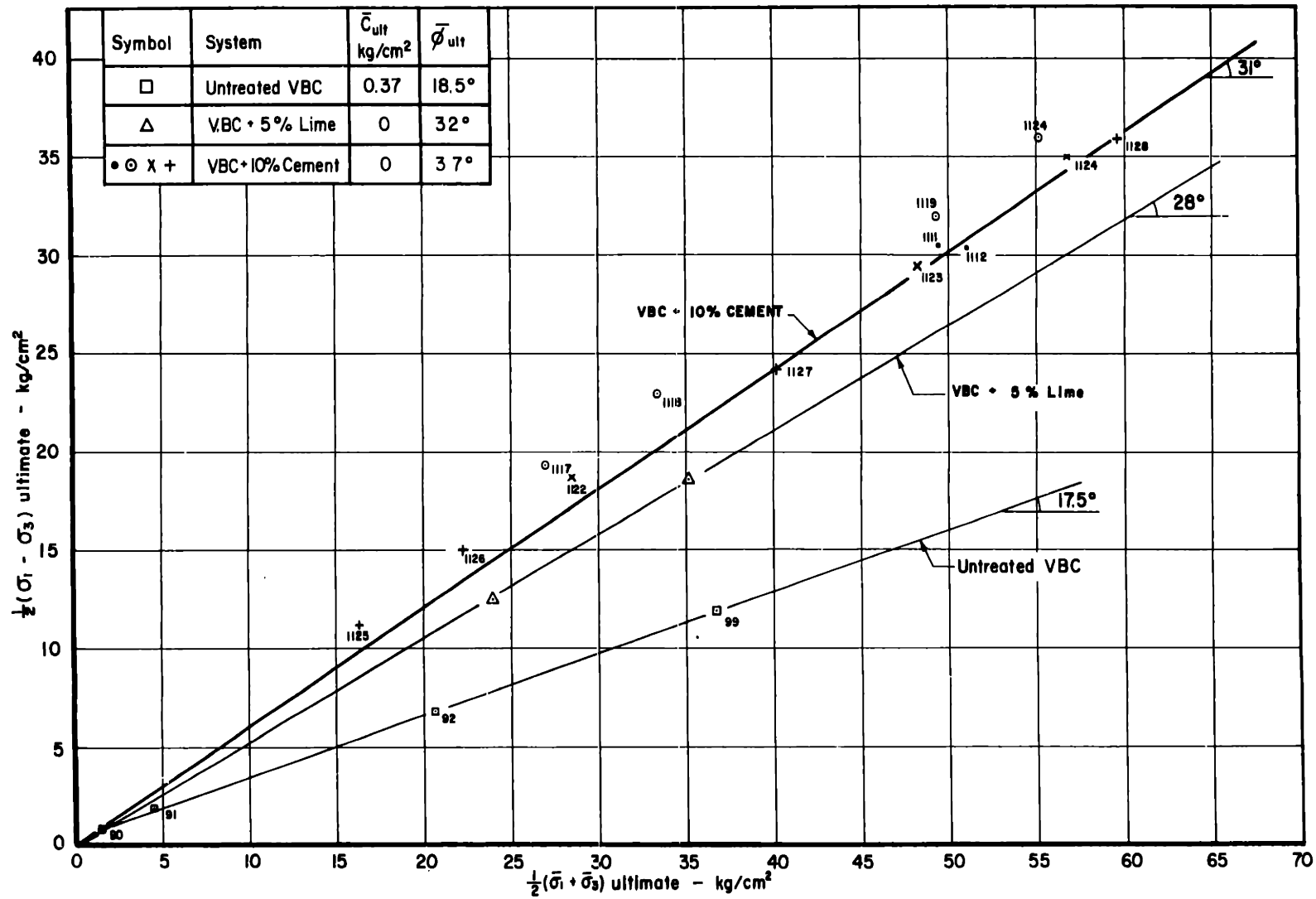

FIG. 5-30 EFFECTIVE STRESS - STRENGTH RELATIONS FOR UNTREATED VBC, VBC + 5% LIME, AND VBC + 10% CEMENT AT ULTIMATE

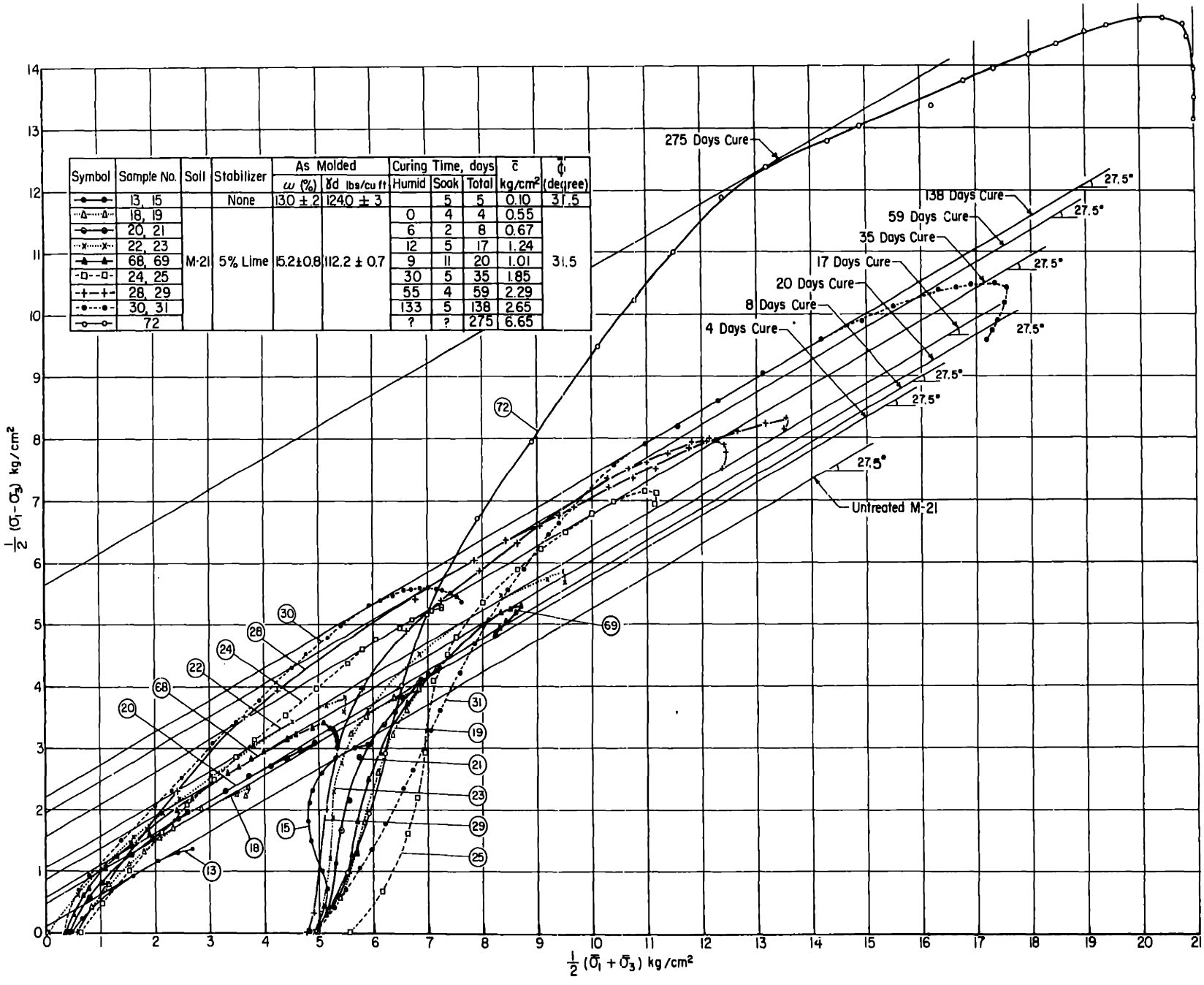

FIGURE 5-31a. EFFECT OF CURING TIME ON THE EFFECTIVE STRESS-STRENGTH ENVELOPE OF M-21 + 5% LIME (for low consolidation pressures only)

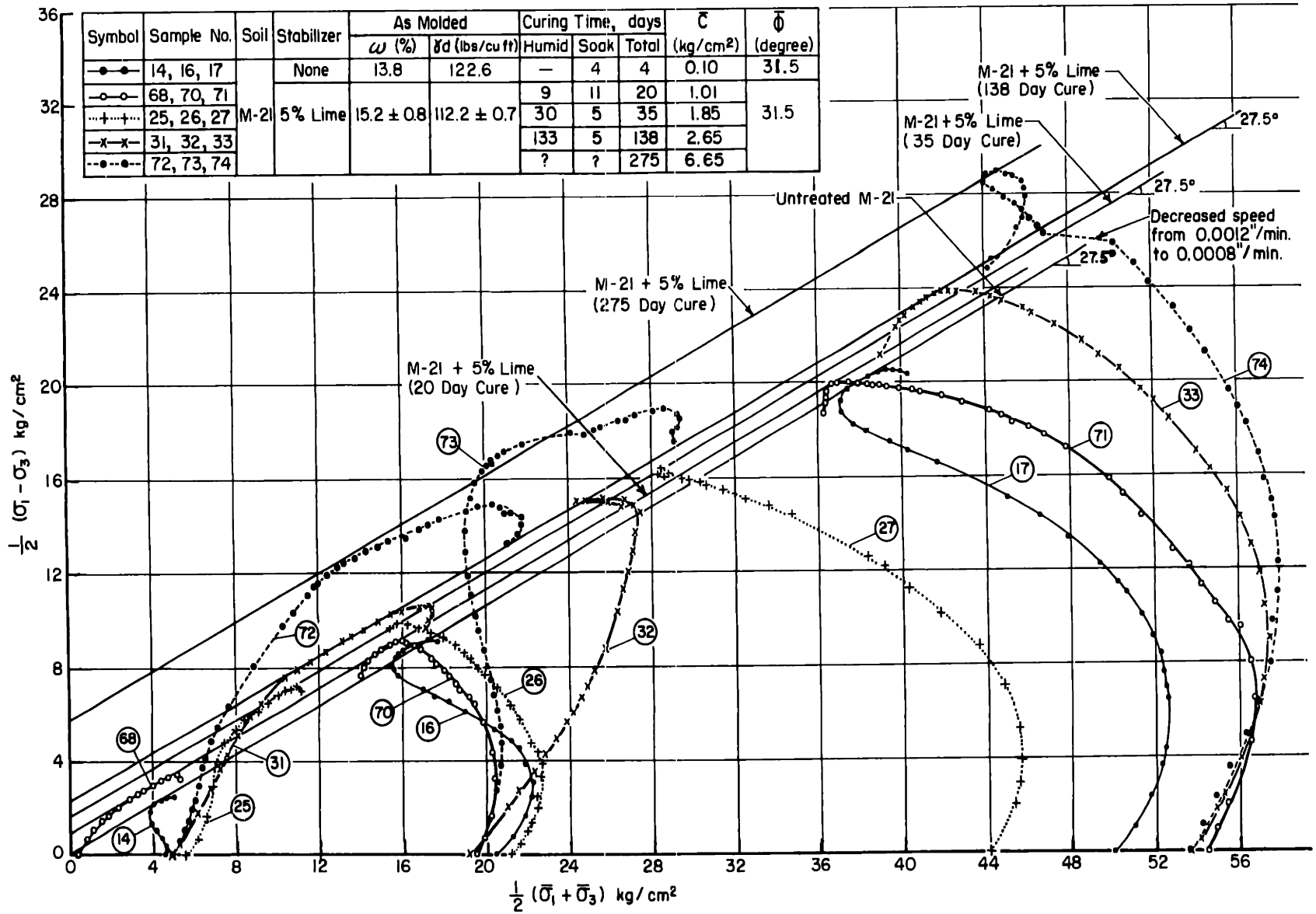

FIGURE 5-31b EFFECT OF CURING TIME ON THE EFFECTIVE STRESS-STRENGTH ENVELOPE OF M-21 + 5% LIME

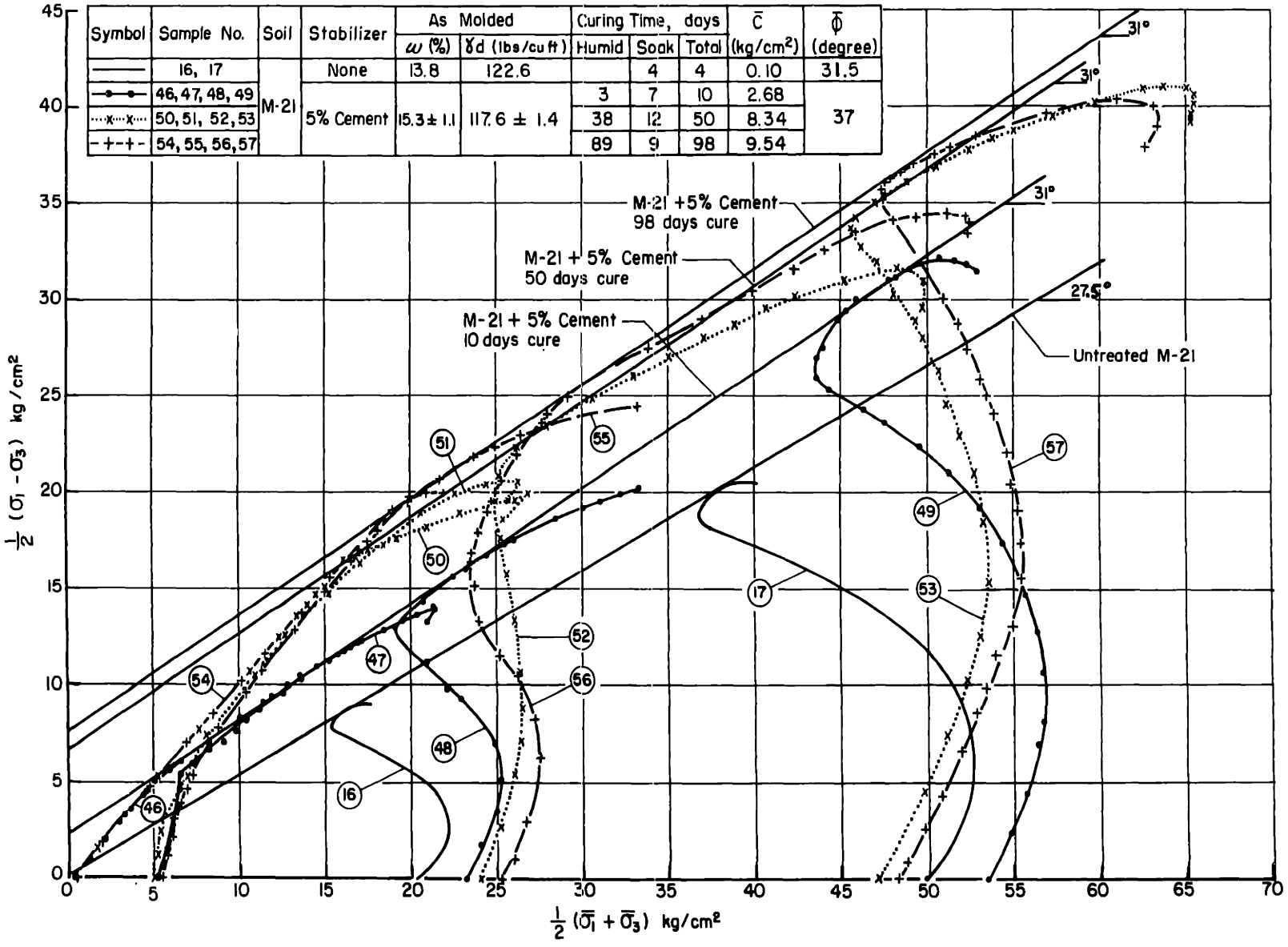

FIGURE 5-32 EFFECT OF CURING TIME ON THE EFFECTIVE STRESS-STRENGTH ENVELOPE OF M-21 + 5% CEMENT

FIGURE 5-33. EFFECT OF CURING TIME ON EFFECTIVE STRESS PARAMETERS OF M-21 + 5% LIME

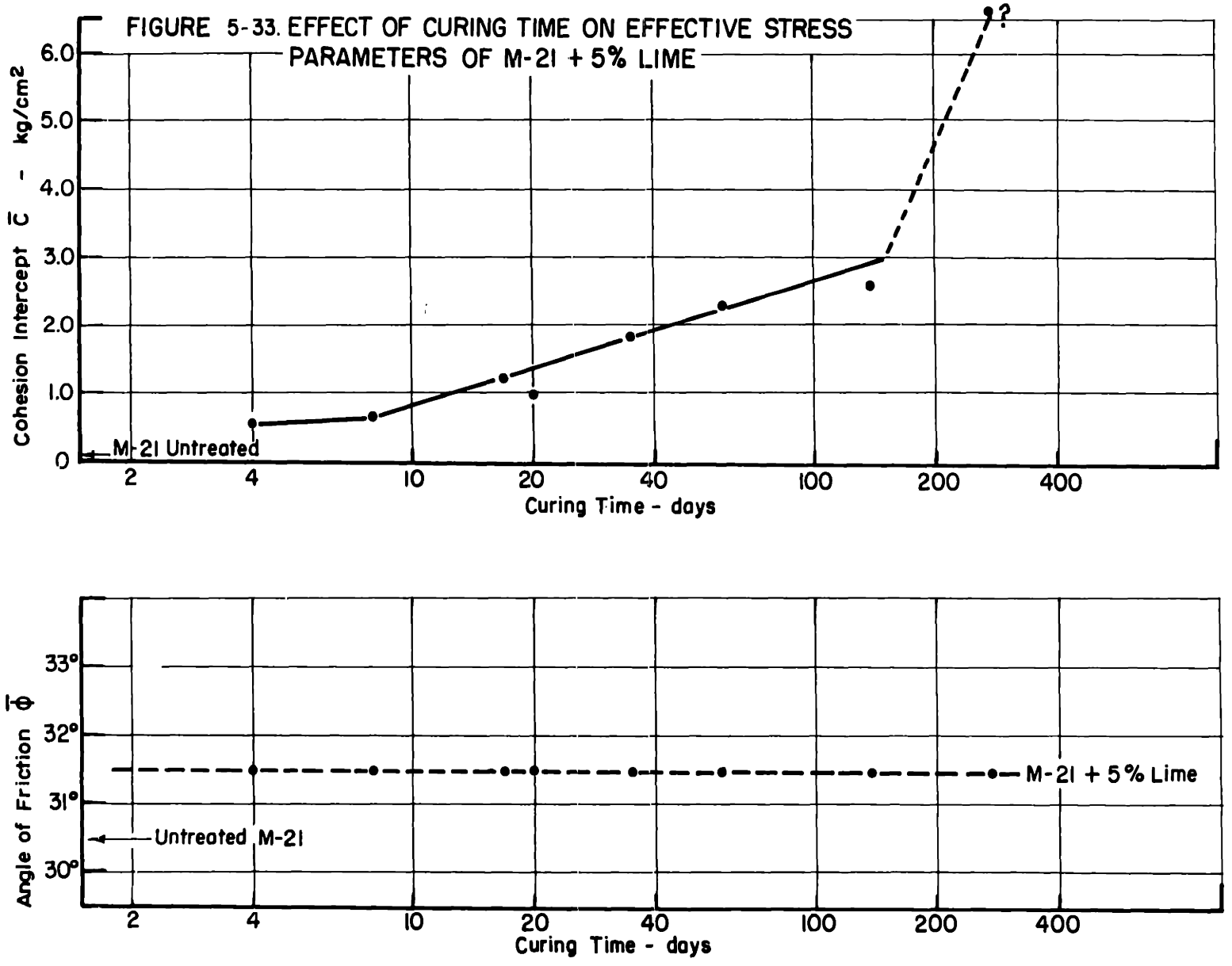

FIGURE 5-34. EFFECT OF CURING TIME ON EFFECTIVE STRESS PARAMETERS OF M-21 + 5% CEMENT

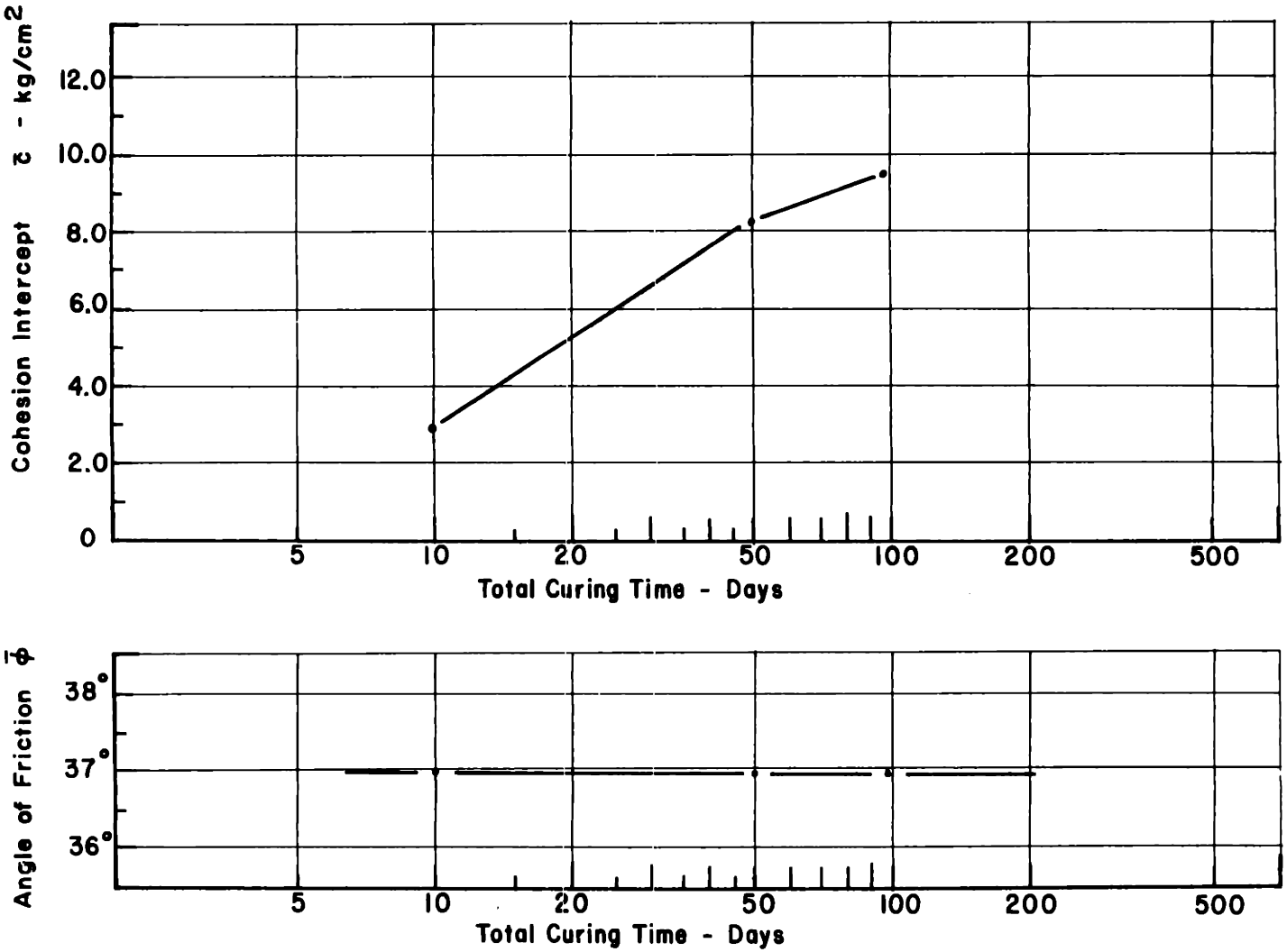

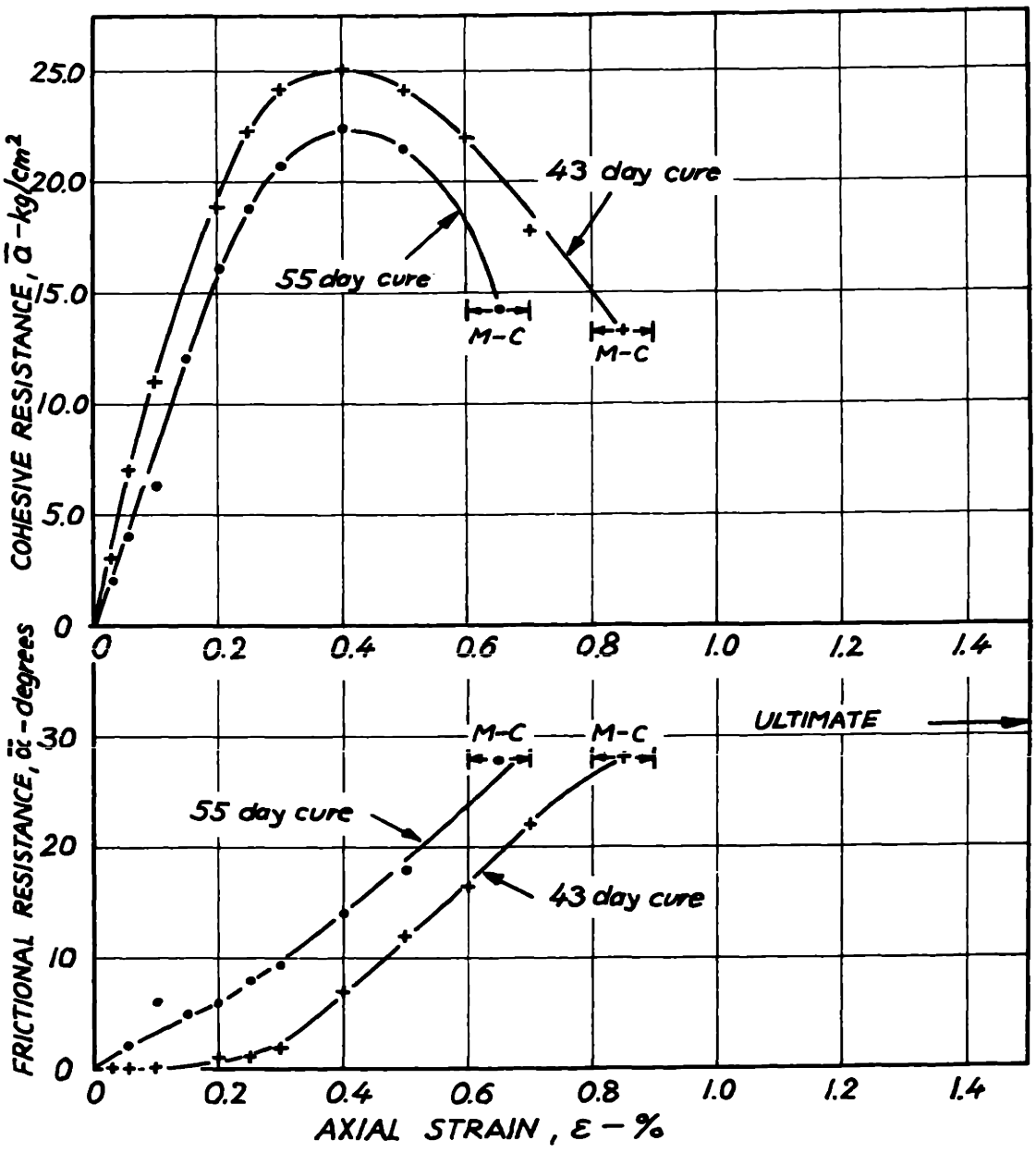

FIG. 5-35. *INFLUENCE OF CURING TIME ON THE FRICTIONAL AND COHESIVE RESISTANCE OF VBC + 10 % CEMENT*

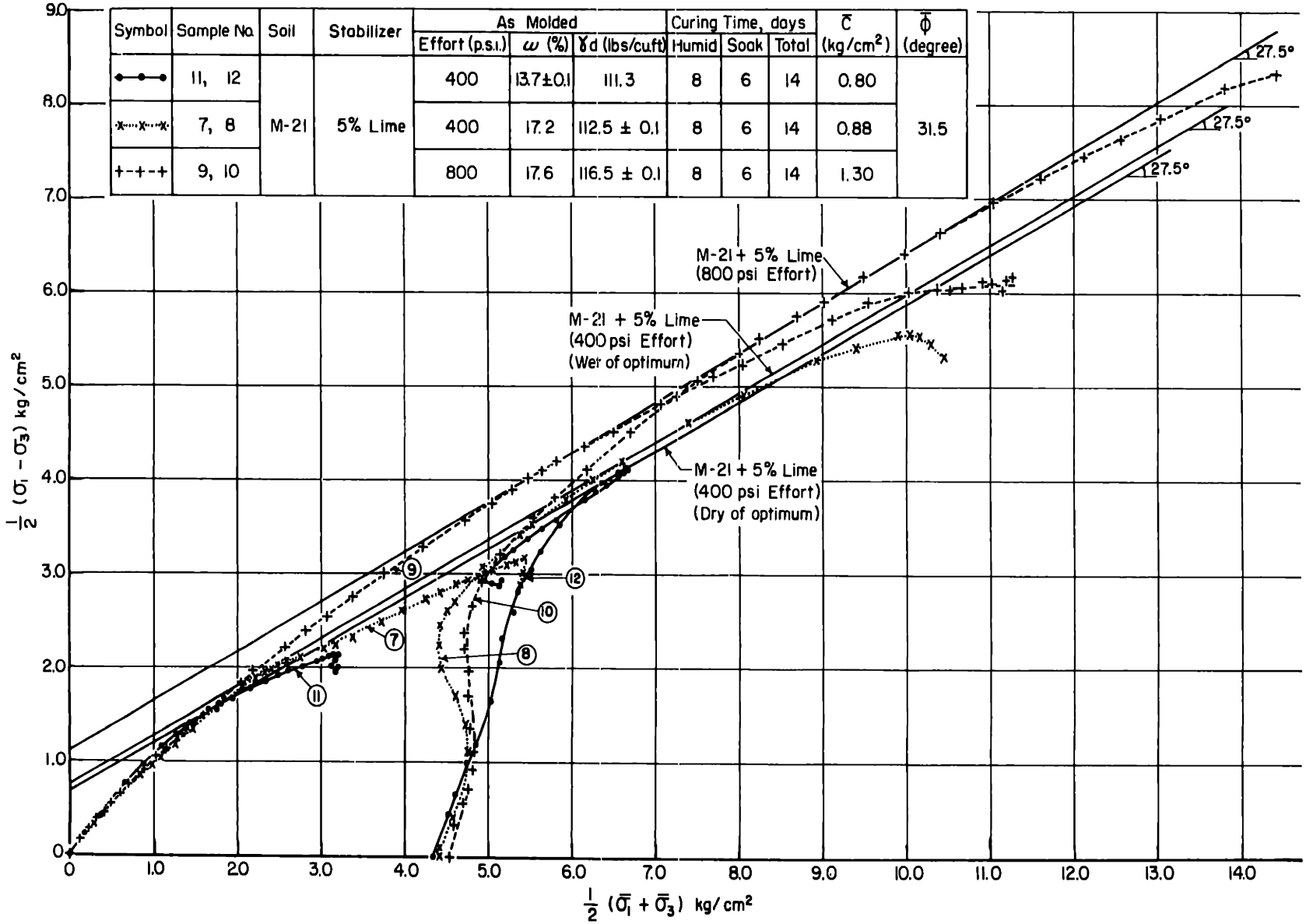

FIGURE 5-36 EFFECT OF MOLDING WATER AND MOLDING DRY DENSITY ON EFFECTIVE STRESS-STRENGTH ENVELOPE OF M – 21 + 5 % LIME

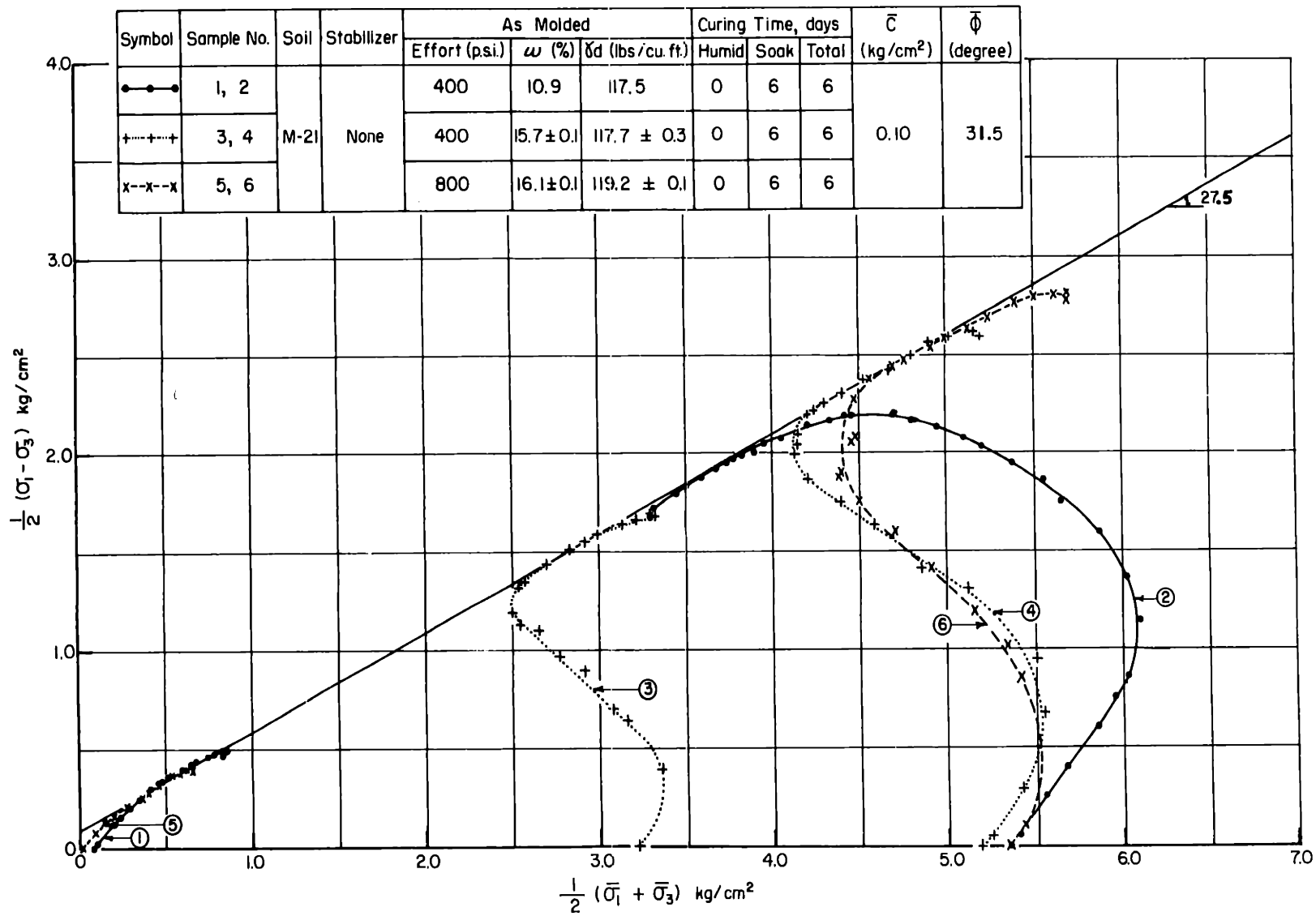

FIGURE 5-37 EFFECT OF MOLDING WATER CONTENT AND MOLDING DRY DENSITY ON THE EFFECTIVE STRESS—STRENGTH ENVELOPE OF M-21

FIGURE 5-38. **GRAIN SIZE DISTRIBUTION**
FOR VBC STABILIZED WITH 5 % LIME AND 10 % CEMENT

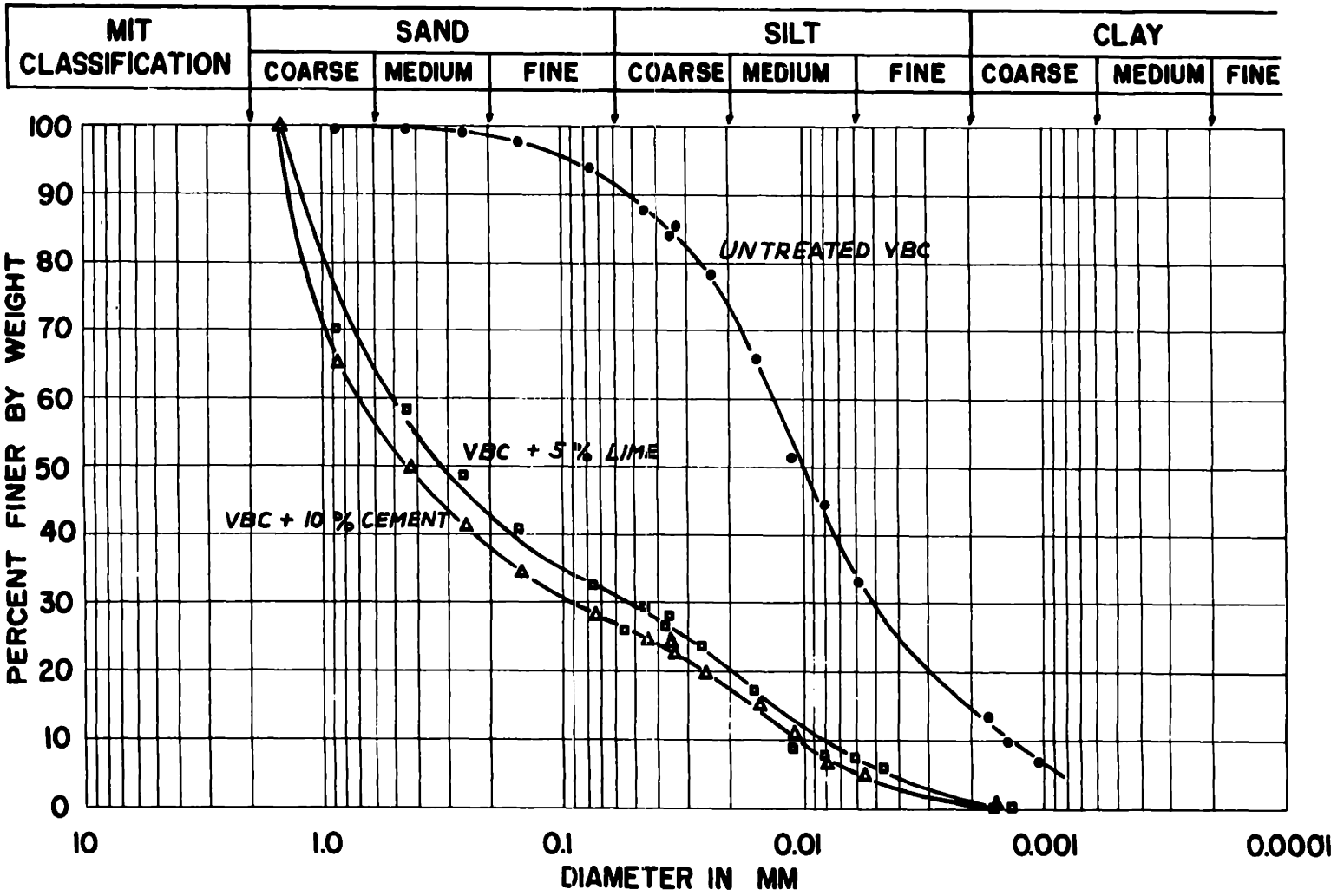

FIGURE 5-39. GRAIN SIZE DISTRIBUTION

FOR M-21 STABILIZED WITH 3% CEMENT AND 5% LIME AND 5% CEMENT RESPECTIVELY.

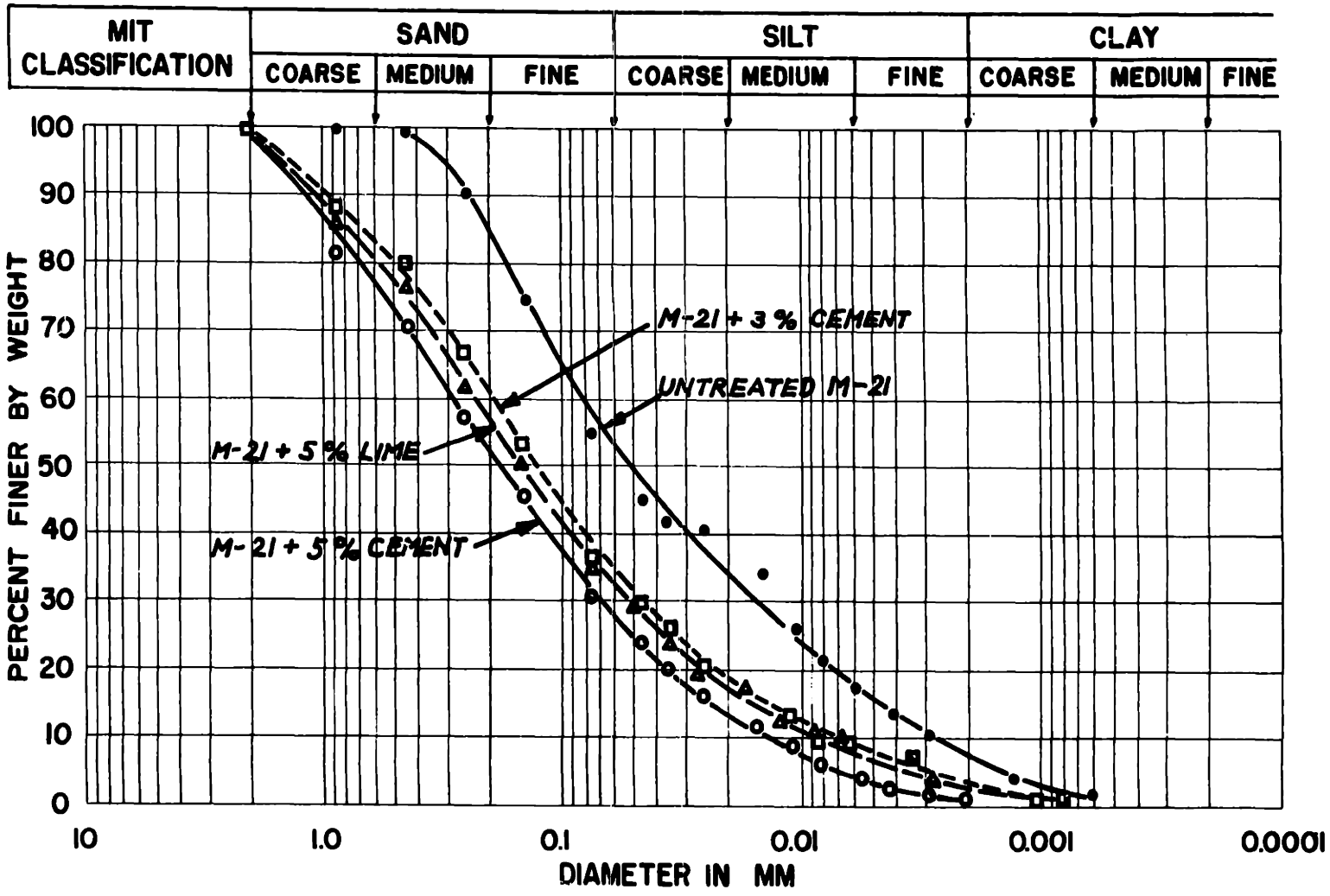

Chapter 6

PORE PRESSURE RESPONSE IN STABILIZED SOILS

6.1 Background

Skempton (1954) derived the following equation relating the change in pore pressure, Δu, to a change in all-round total stress, $\Delta\sigma_o$, for no drainage:

$$\frac{\Delta u}{\Delta\sigma_o} = B = \frac{1}{1 + \frac{nC_w}{C_c}} \qquad (6.1)$$

where $\Delta\sigma_o$ = the change in the all-round total stress

Δu = the change in pore pressure corresponding to $\Delta\sigma_o$

B = the Skempton pore pressure coefficient B or B factor

n = the porosity of the soil

C_c = the compressibility of the soil skeleton

C_w = the compressibility of the pore fluid (liquid and gas)

For most saturated untreated soils at low consolidation pressures, the compressibility of the pore fluid is very much lower than the compressibility of the soil skeleton since there are no compressible air voids in the fluid phase. The ratio C_w/C_c is then approximately zero and Eq. 6.1 becomes:

$$\frac{\Delta u}{\Delta\sigma_o} = B \simeq 1.0 \qquad (6.1a)$$

If the soil is not saturated the compressibility of the pore fluid increases substantially because of the presence of air. In this case the ratio C_w/C_c is no longer approximately zero and Eq. 6.1 becomes:

$$\frac{\Delta u}{\Delta \sigma_o} = B < 1.0 \qquad (6.1b)$$

The relation given in Eq. 6.1a is often used to check that triaxial samples and the pore pressure measuring systems are saturated prior to shear. The results are often given as a percentage and they are then called pore pressure responses.

For stabilized soils or untreated soil at very high consolidation pressures the compressibility of the soil skeleton may be of the same order of magnitude as that of water. The value of C_w/C_c is then no longer approximately zero and the B factor can be substantially less than 1.0 even though the system is completely saturated.

6.2 Test Results

The pore pressure responses of most of the $\overline{CU}$ triaxial tests on the fine-grained samples have been listed in Tables 4-2 and 4-3. For the lower consolidation pressure samples (0 - 6 kg/cm^2) the response was determined for an increment of cell pressure, ($\Delta\sigma_o$), of 10 psi (0.7 kg/cm^2). The results show that for the low consolidation

pressure tests the responses varied from 90% to 99% with an average of 95.5%. For the high consolidation pressure tests the pore pressure responses ranged between 55% and 90% with an average of 76% for a cell pressure increment of 20 psi.

A plot of pore pressure response versus initial tangent modulus for all the triaxial tests on the fine-grained samples prior to shear is given in Fig. 6-1. Even though there is a large scatter in the results there is a definite trend for the B factor to decrease with increasing initial tangent modulus.

Figs. 6-2b, 6-3b, and 6-4b show the effect of consolidation pressure on the pore pressure responses of the untreated and the stabilized fine-grained soils. The B factors decreased with increasing consolidation pressure. The effect of curing time on the B factors of M-21 + 5% lime is given in Fig. 6-5b. The results show that B de-decreases with increasing curing time. The influence of wet-dry cycles on the pore pressure response of VBC + 10% cement is shown in Fig. 6-6b.

6.3 Discussion

A pore pressure response of less than 1.0 can be due to a low compressibility of the soil skeleton and/or a high compressibility of the pore fluid (due to the presence of air in the soil or pore pressure measuring

device). It was therefore necessary, especially with the high pressure samples, to check that responses much less than unity were due to the rigidity of the soil skeletons and not due to the presence of air bubbles. This was achieved by measuring the pore pressure response for several consecutive 20-psi increments of cell pressure. In a saturated system the compressibility of the pore fluid is essentially independent of the pore water pressure and therefore the B factor remains constant as the cell pressure is increased. However if air bubbles are present in the system, the compressibility of the pore fluid decreases with increasing pore pressure since the air bubbles decrease in volume. This would cause the B factor to increase with each successive increment of cell pressure.

In all the high pressure tests, after equilibrium had been reached under a back pressure of 150 psi, the B factor, i.e., pore pressure response, remained essentially constant with increasing increments of cell pressure. It was therefore assumed that the samples and pore pressure measuring devices were saturated and free of air bubbles, and that the low pore pressure responses were due to the high rigidity of soil skeletons.

If the compressibility of the soil skeleton is known and S = 100% it is then possible to compute the B

factor using Eq. 6.1. No attempt was made to measure the compressibility of the soil skeleton since this would have involved the development of a very sensitive device to measure the small amounts of water which flow out of the soil when a small increment of cell pressure is applied. The increment of consolidation pressure $\Delta\bar{\sigma}_o$ should be equal to the increment of effective stress induced when the B factor is determined, i.e., $(1-B)\Delta\sigma_o$, where $\Delta\sigma_o$ is the increment of cell pressure used to determine the B factor under conditions of no drainage. For B = 0.76, which was the average value for the high pressure tests, the increment of consolidation pressure used to determine the compressibility would have been 0.24 x 20 or 4.8 psi at a consolidation pressure of over 700 psi (the increment of cell pressure used to determine B in these tests was 20 psi).

It is theoretically possible to compute the compressibility of the soil skeleton from the initial tangent modulus during triaxial compression if the soil skeleton is assumed to be linearly elastic and isotropic and if the Poisson ratio, ν, is known. This can be done using the following equation:

$$\frac{1}{C_c} = K = \frac{E}{3(1-2\nu)} \qquad (6.2)$$

where C_c = the compressibility of the soil skeleton

K = the bulk modulus of the soil skeleton

E = the initial tangent modulus (Young's modulus)

ν = the Poisson ratio

In using Eq. 6.2 an apparent porosity must be used to take into account the compressibility of the volume of water in the pore pressure lines and measuring device.* A typical value for the actual porosity of the M-21 systems at high pressures is 0.30 but when the 8.5 cc of water which was in the pore pressure lines is included the apparent porosity becomes 0.40. Similarly for the VBC systems the actual porosity was about 0.41 and the apparent porosity 0.52.

B factors versus initial tangent moduli for all the triaxial tests are plotted in Fig. 6-1. Also included in the figure are theoretical lines of B factors versus initial tangent moduli for a range of Poisson ratios, computed using Eqs. 6.1 and 6.2 and an apparent porosity of 0.40 and 0.52 for the M-21 and VBC systems respectively. There is a large scatter in the results but there is a definite trend for the B factors to decrease with increasing moduli. The results suggest that the equivalent ν lies between 0.25 and 0.45. It is believed that the measured moduli obtained from the stress-strain curves

*See Appendix A for a discussion of the influence of the flexibility of the pore pressure measuring equipment on the pore pressure response.

given in Appendix B are too low, especially at the higher modulus values, because of seating imperfections of the samples. The Poisson ratios may therefore actually be lower than the values suggested in Fig. 6-1.

A decrease in pore pressure response with increasing consolidation pressure and curing time (Figs. 6-2b, 6-3b, 6-4b, and 6-5b) simply reflects their effect on increasing the initial tangent moduli as shown in Figs. 6-2a, 6-3a, 6-4a, and 6-5a.

6.4 Conclusions

For stabilized soils and untreated soils at high consolidation pressures, pore pressure responses of less than 100% are not caused by a high compressibility of the pore fluid, due to the presence of air in the system, but rather due to the high rigidity of the soil skeletons.

The decrease in B factor with increasing consolidation pressure and curing time is further evidence of the effect of the rigidity of the soil skeletons on the pore pressure response.

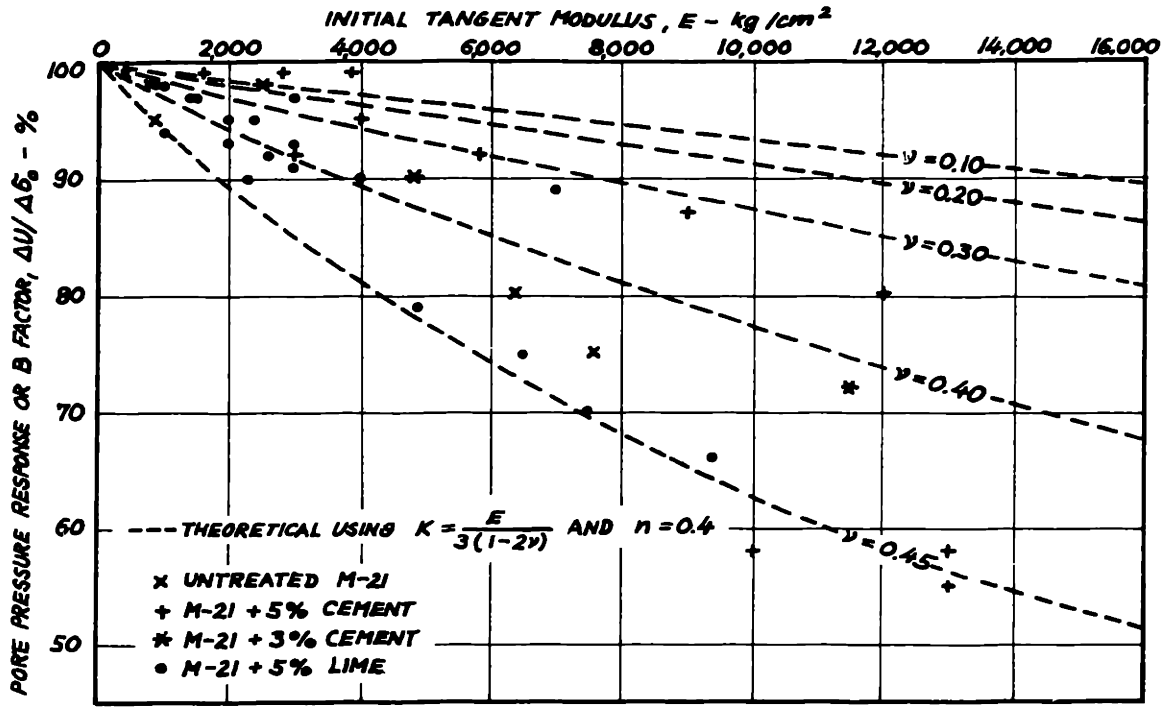

THEORETICAL AND MEASURED VALUES OF B FACTOR VERSUS INITIAL TANGENT MODULUS FOR MASSACHUSETTS CLAYEY SILT SYSTEMS.

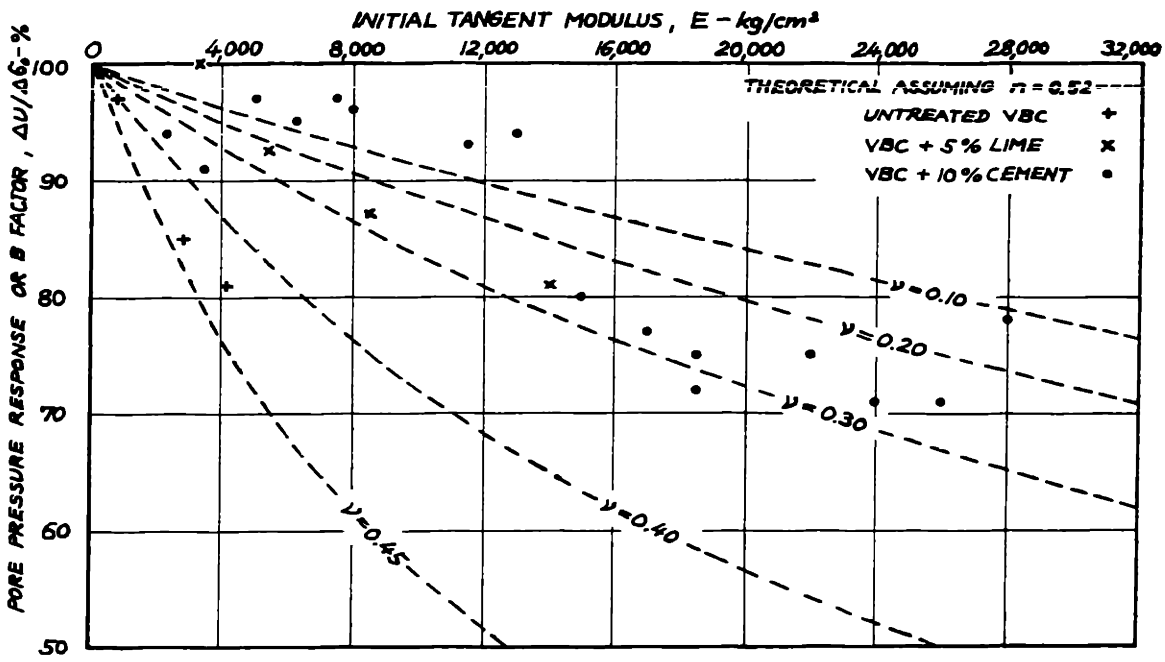

THEORETICAL AND MEASURED VALUES OF B FACTOR VERSUS INITIAL TANGENT MODULUS FOR VICKSBURG BUCKSHOT CLAY SYSTEMS.

FIG. 6-I. INFLUENCE OF INITIAL TANGENT MODULUS ON THE PORE PRESSURE RESPONSE OF THE FINE GRAINED SYSTEMS.

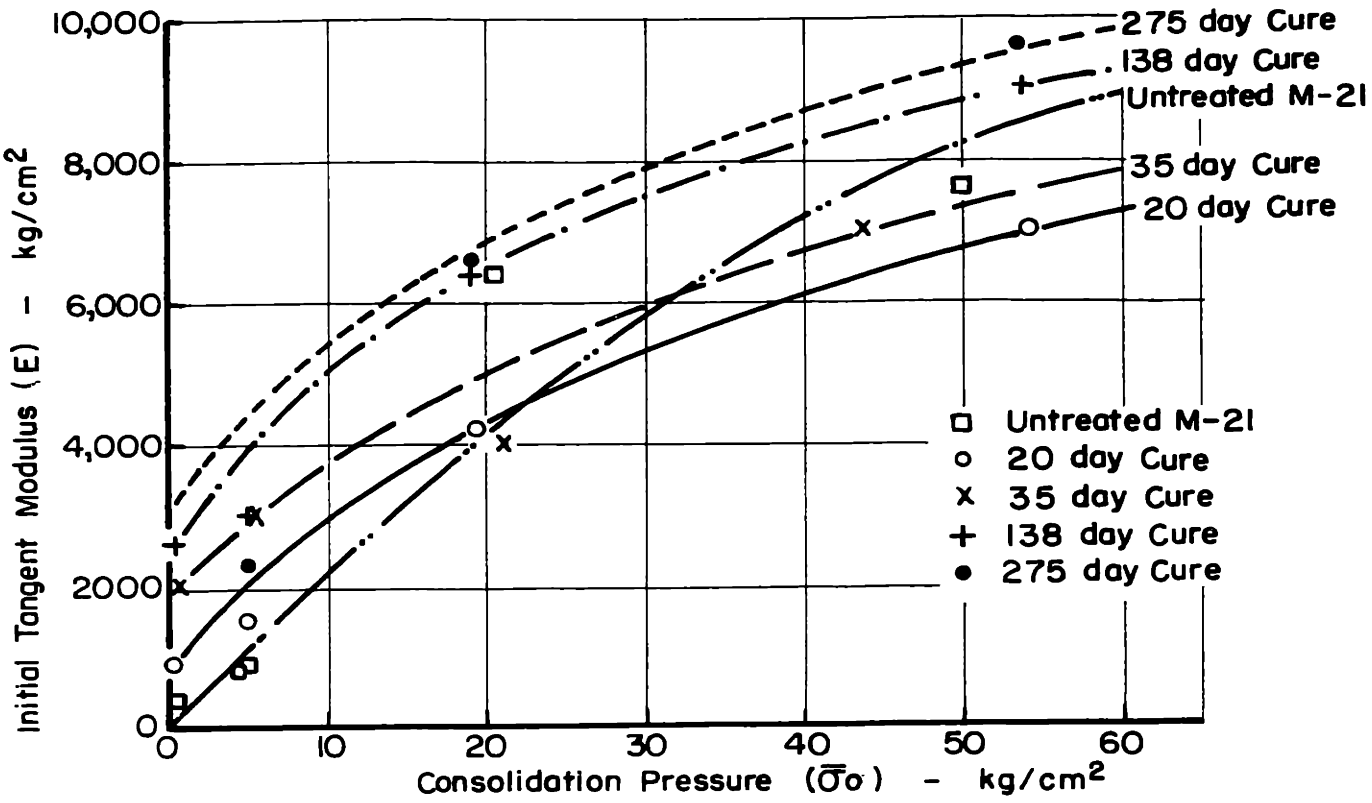

FIGURE 6-2a. INITIAL TANGENT MODULUS vs CONSOLIDATION PRESSURE FOR M-21 + 5% LIME

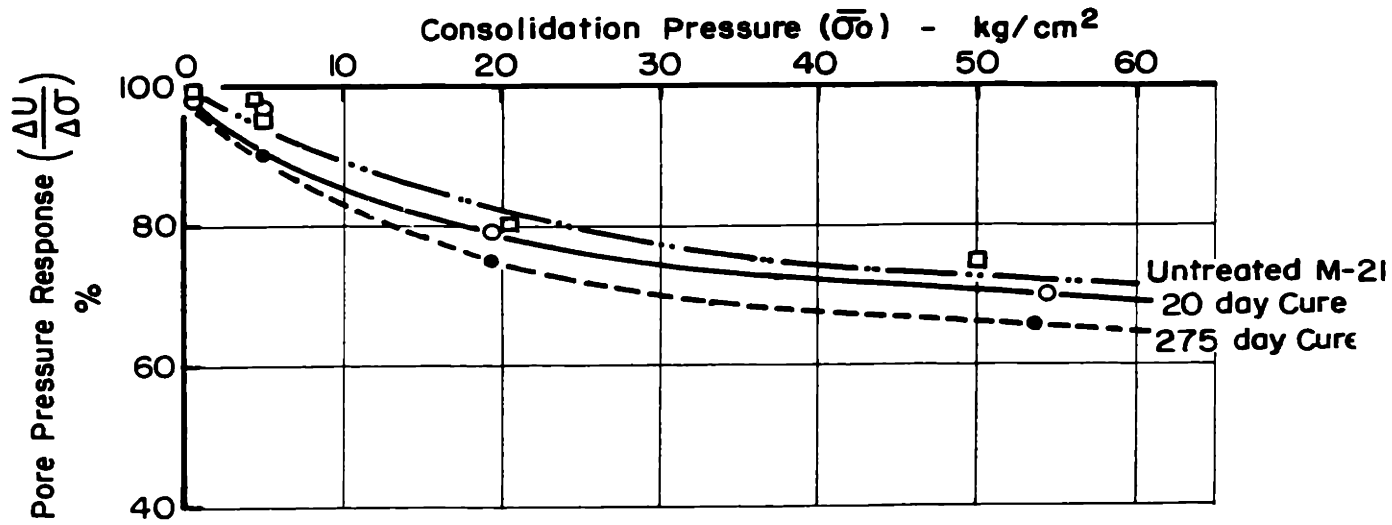

FIGURE 6-2b. PORE PRESSURE RESPONSE vs CONSOLIDATION PRESSURE FOR M-21 + 5% LIME

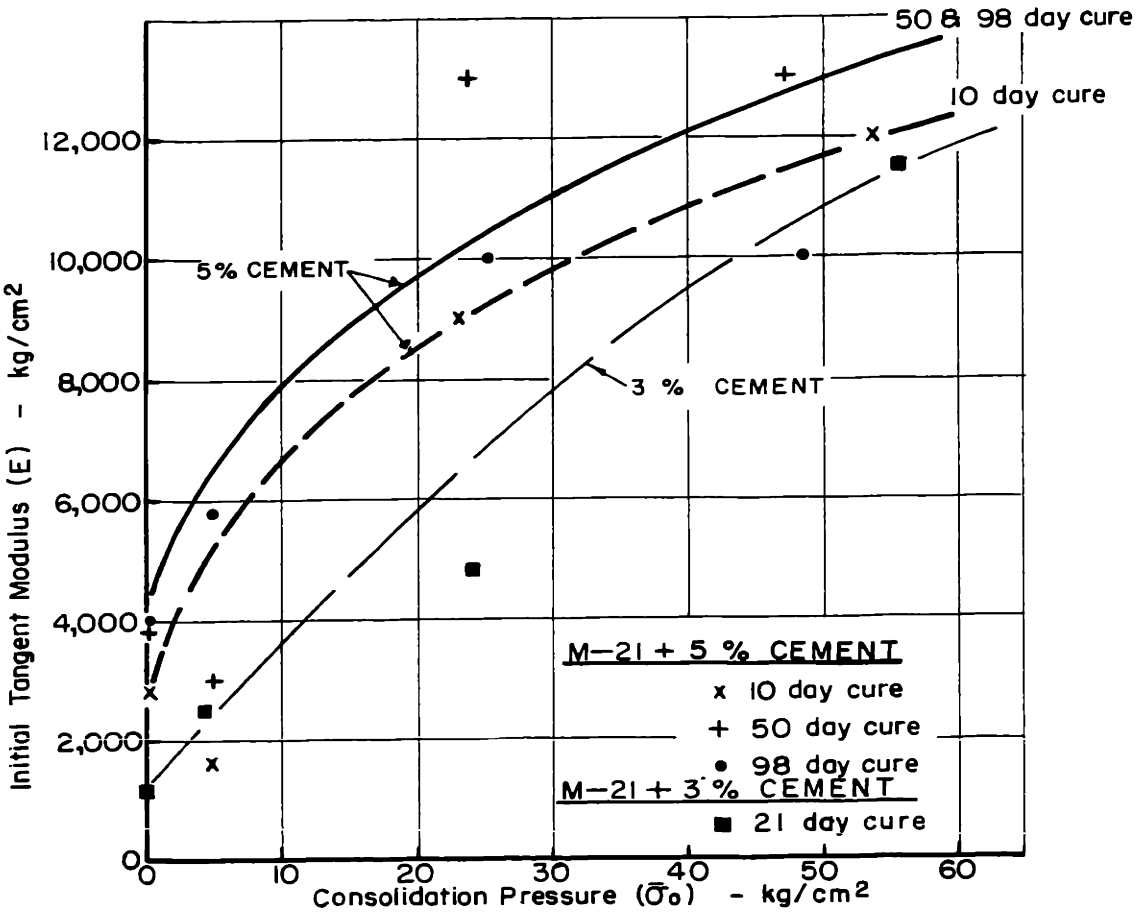

FIGURE 6-3a. INITIAL TANGENT MODULUS vs CONSOLIDATION PRESSURE FOR M-21 + 5% CEMENT AND M—21 + 3 % CEMENT

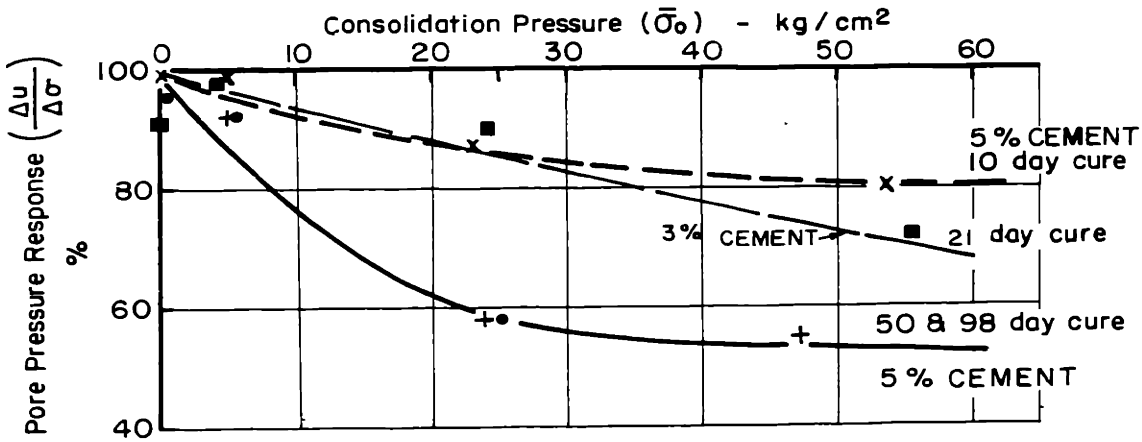

FIGURE 6-3b. PORE PRESSURE RESPONSE vs CONSOLIDATION PRESSURE FOR M-21 + 5% CEMENT AND M-21 + 3 % CEMENT

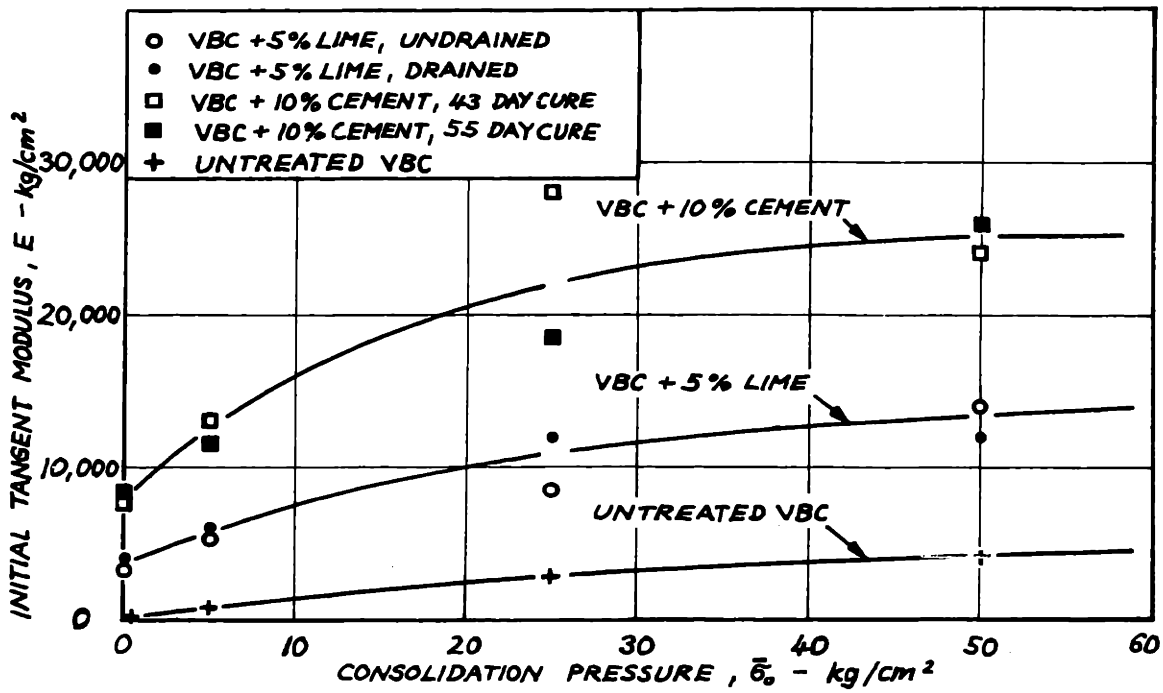

FIG. 6-4a. *INITIAL TANGENT MODULUS VERSUS CONSOLIDATION PRESSURE FOR VICKSBURG BUCKSHOT CLAY SYSTEMS.*

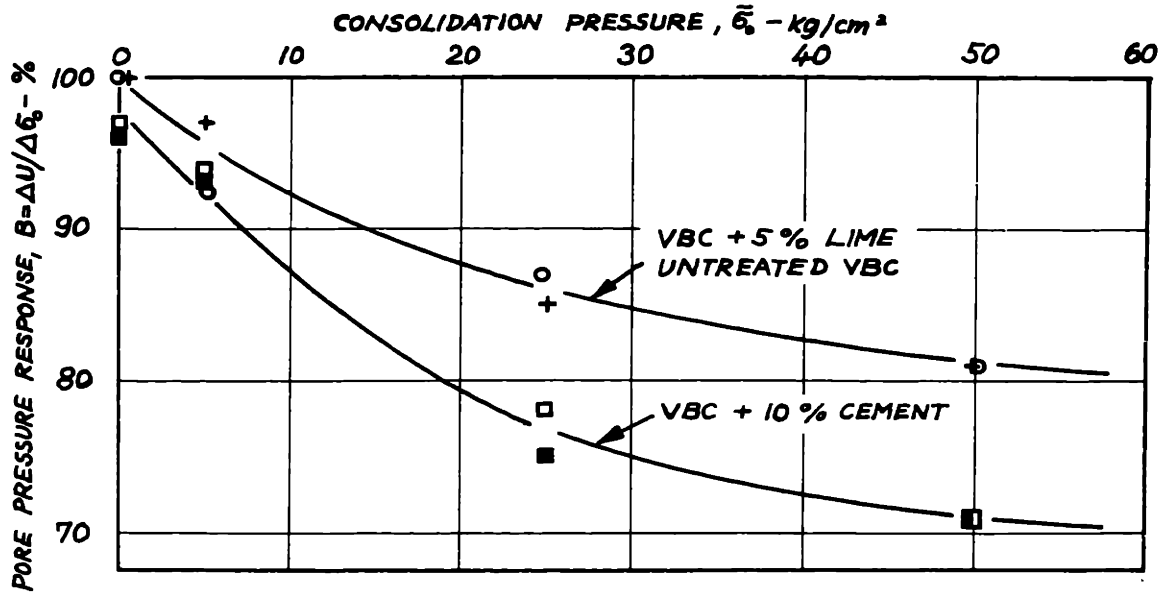

FIG. 6-4b. *PORE PRESSURE RESPONSE VERSUS CONSOLIDATION PRESSURE FOR VICKSBURG BUCKSHOT CLAY SYSTEMS.*

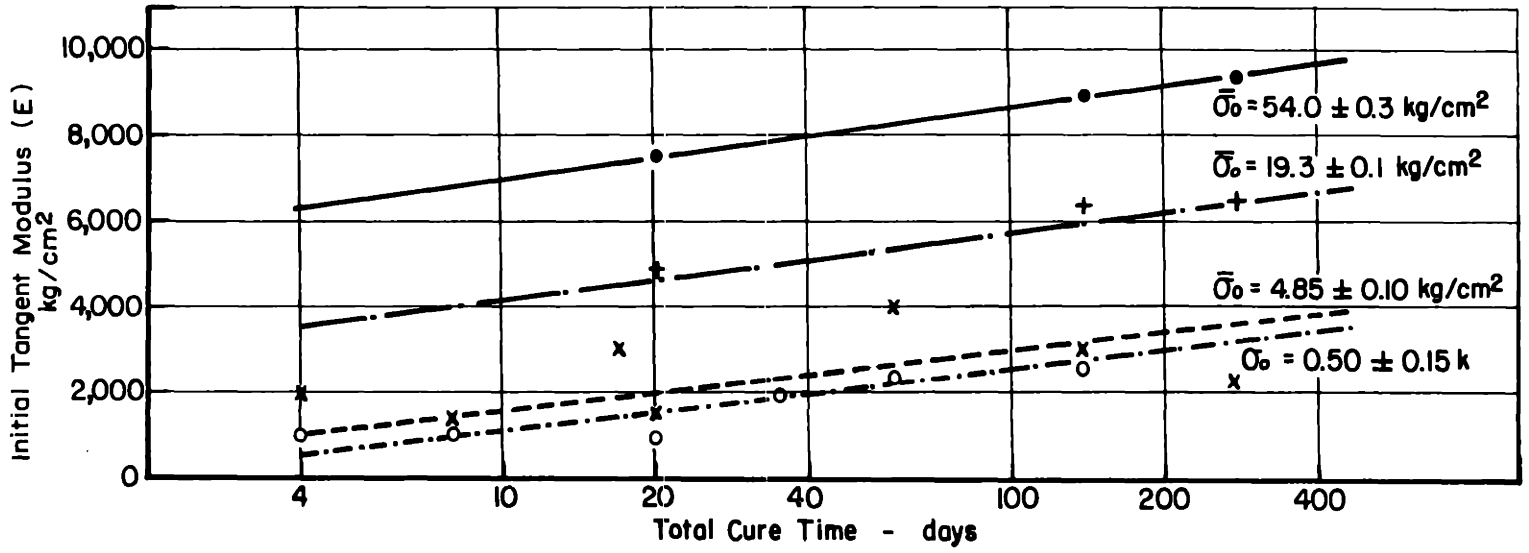

FIGURE 6-5a. EFFECT OF TOTAL CURE TIME ON INITIAL TANGENT MODULUS OF M-21 + 5% LIME

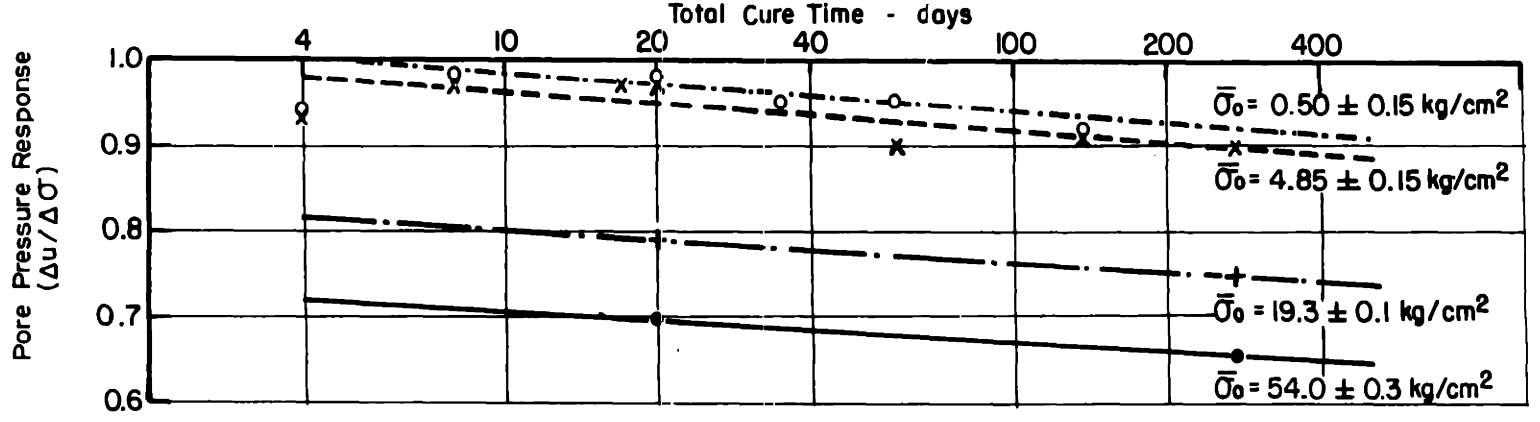

FIGURE 6-5b. EFFECT OF TOTAL CURE TIME ON PORE PRESSURE RESPONSE OF M-21 + 5% LIME

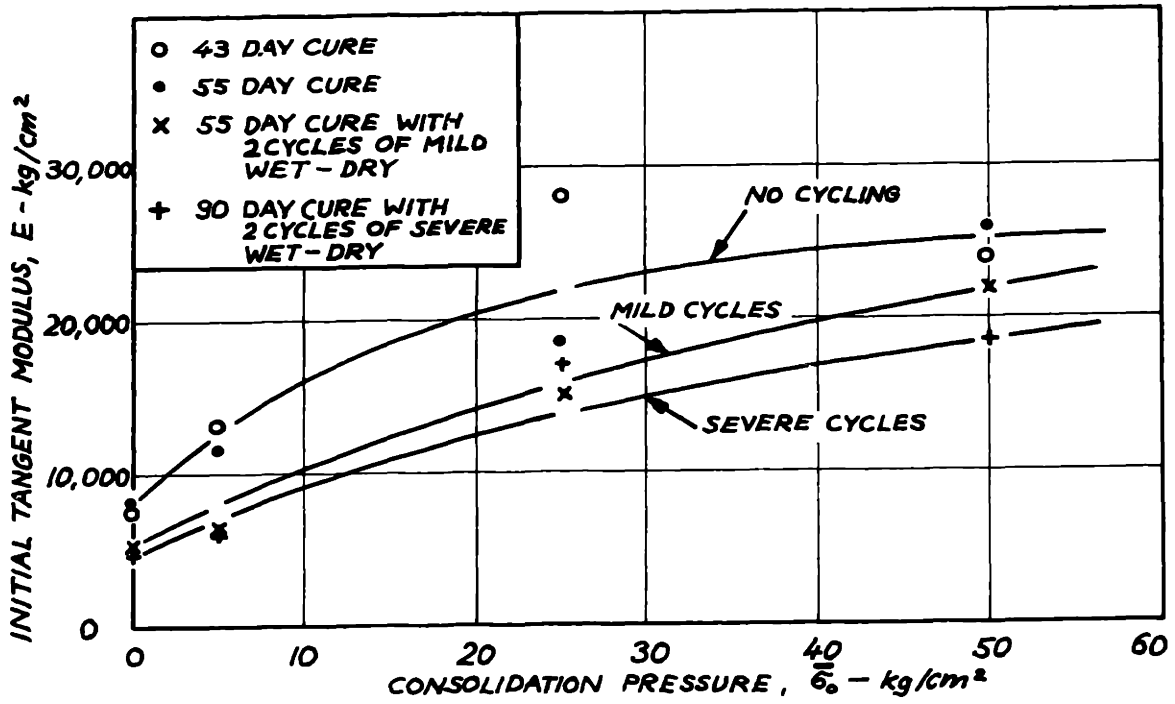

FIG. 6-6a. INFLUENCE OF CYCLES OF WET-DRY ON THE INITIAL TANGENT MODULUS OF VICKSBURG BUCKSHOT CLAY STABILIZED WITH 10 % CEMENT + 0.5 N. NaOH.

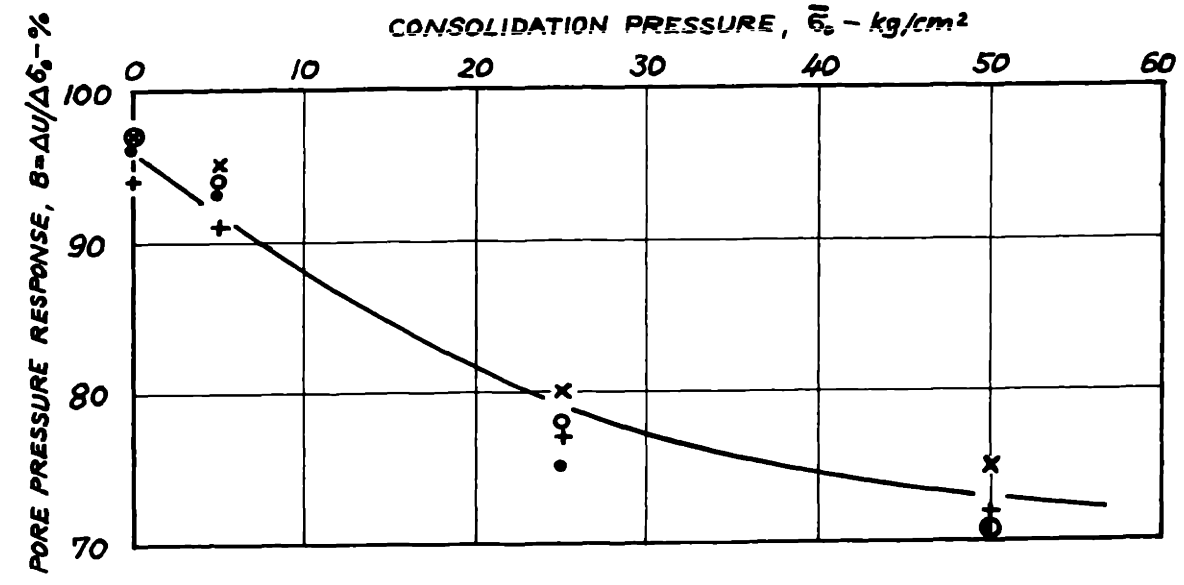

FIG. 6-6b. INFLUENCE OF CYCLES OF WET-DRY ON THE PORE PRESSURE RESPONSE OF VICKSBURG BUCKSHOT CLAY STABILIZED WITH 10 % CEMENT + 0.5 N. NaOH.

Chapter 7

EFFECTIVE STRESS-VOLUME CHANGE BEHAVIOR DURING SHEAR

7.1 Introduction

The volume change behavior of a saturated porous material can be determined during drained shear by measuring the quantity of water flowing into or out of the pores of the test specimen. In undrained shear the sample is kept at constant volume and the volume change tendency is reflected as a change in effective stress.

The effective stress-volume change behaviors of soils during shear are a function of the strain and they can be compared in a number of ways. From a practical point of view it is usual to speak about conditions at failure, i.e., at maximum principal stress difference or point of first tangency with Mohr-Coulomb effective stress envelope. Another interesting case is at ultimate conditions when the effective stress or volume remains constant with further straining.

Skempton (1954) has shown that for an elastic material the pore pressure developed during undrained shear is solely dependent on the change in mean principal stress, i.e., $1/3\ (\sigma_1 + 2\sigma_3)$, whereas for a soil it is also a function of the change in principal stress difference. To take this into account Skempton proposed the pore pressure

parameter A given by the following equation:

$$\Delta u = B[\Delta\sigma_3 + A(\Delta\sigma_1 - \Delta\sigma_3)] \qquad (7.1)$$

where Δu = the change in pore water pressure

B = the pore pressure parameter B or B factor as defined in Chapter 6.

$\Delta\sigma_3$ = the change in total minor principal stress

$\Delta\sigma_1$ = the change in total major principal stress

A = the Skempton pore pressure coefficient A or A factor

In an undrained triaxial test in which the cell pressure is kept constant during shear $\Delta\sigma_3 = 0$ and Eq. 7.1 becomes

$$\Delta u = AB\ (\Delta\sigma_1) \qquad (7.1a)$$

and for isotropic consolidation, $\Delta\sigma_1 = (\sigma_1 - \sigma_3)$ so that

$$\Delta u = AB\ (\sigma_1 - \sigma_3) = \bar{A}\ (\sigma_1 - \sigma_3) \qquad (7.1b)$$

where $\bar{A} = AB$

For most saturated uncemented soils at low consolidation pressures B is approximately equal to unity and then Eq. 7.1b becomes

$$\Delta u = A\ (\sigma_1 - \sigma_3)$$

or $$A = \Delta u/(\sigma_1 - \sigma_3) \qquad (7.1c)$$

It has been shown in Chapter 6 that at the higher consolidation pressures B was appreciably less than unity due to the rigidity of the soil skeleton and therefore Eq. 7.1c is not applicable.

In this investigation the B factor was determined prior to shear but it was not measured during shear. The B factor will change during shear because the rigidity of the soil skeleton changes due to changes in effective stress and, in the case of stabilized soils, due to partial breakdown of the cemented skeleton. The A factors were therefore not known during shear and only the product AB could be determined. The product of AB which is denoted by $\bar{A}$ will therefore be used in the following.

In undrained shear the $\bar{A}$ factor relates the pore pressure change to the change in principal stress difference and similarly in drained shear the volume change should be related to the principal stress difference. This can be done by dividing the per cent volume change, $\Delta V/V \times 100$, by the principal stress difference, i.e.,

$$W = \frac{-\Delta V/V \times 100}{(\sigma_1 - \sigma_3)} \qquad (7.2)$$

To keep the volume change parameter dimensionless the stress difference can be normalized by dividing it by the consolidation pressure $\bar{\sigma}_o$, or

$$\bar{W} = \frac{-\Delta V/V \times 100}{(\sigma_1 - \sigma_3)/\bar{\sigma}_o} \qquad (7.3)$$

The negative sign has been used in the above equation to make the sign of $\bar{W}$ compatible with the Skempton $\bar{A}$ parameter, since dilation in a drained test corresponds to a pore pressure decrease in an undrained test.

In this investigation most of the tests on the fine-grained soils were undrained because of the time involved in running completely drained tests. The cell pressure was usually kept constant and the changes in pore water pressure measured.

Drained tests were usually run on the sand systems since it is difficult to prevent the pore water from cavitating during undrained shear especially when the sand is in a dense state. The cell pressure was kept constant and the volume change during shear determined by measuring the flow of the pore water under a constant back pressure.

7.2 Volume Change Behavior of the Saturated Untreated Soils

Before examining the influence of artificial cementation on the effective stress-volume change behavior it is desirable to summarize some of the more important pore water characteristics observed during shear of the untreated compacted soils.

7.2.1 Volume Change Characteristics of the Compacted Fine-Grained Soils

The single most important factor influencing the volume change behavior of the compacted fine-grained soils during shear was the consolidation pressure. Molding water content and dry density probably influence the volume change behavior (Seed, et al., 1960) but their effect was eliminated by considering only one set of molding conditions for each soil and each soil-stabilizer system.

At low consolidation pressures (below 5 kg/cm^2) the compacted uncemented soils, VBC and M-21, behaved like heavily overconsolidated clays, i.e., in undrained shear the pore pressure started off by increasing with strain until it reached a relatively small maximum positive excess pore pressure. On further straining the pore pressure dropped gradually and the excess pore pressure became negative. At very large strains the pore pressure reached a minimum value which remained constant with further straining.*

At high consolidation pressures (above 20 kg/cm^2) the compacted fine-grained soils behaved like normally consolidated clays. Large positive excess pore pressures developed during undrained shear. The pore pressure increased at a decreasing rate with increasing axial strain

*The observed pore pressure behavior was for triaxial compression in which the lateral confining pressure was kept constant during shear.

until it reached a maximum value after which it remained essentially constant with further straining.*

The influence of consolidation pressure on the stress-strain behavior of the compacted VBC samples is shown in Fig. 7-1. The untreated M-21 samples exhibited a similar behavior.

At low consolidation pressures the $\bar{A}$ factors increased rapidly with increasing consolidation pressure which is typical of overconsolidated clays. At high consolidation pressures the $\bar{A}$ values approached a constant value which is characteristic of normally consolidated clays (Fig. 7-2).

7.2.2 Effective Stress-Volume Change Behavior of the Untreated Sands

In the case of the untreated sands the volume change behavior during shear was also dependent on the consolidation pressure but an equally important factor was the relative density of the sand prior to shear.

Figs. 7-3a and 7-3b show the influence of consolidation pressure on the volume change of medium Ottawa sand at maximum stress difference and ultimate (20% strain) respectively. As the consolidation pressure was increased the dilation during shear decreased. Also shown in Fig. 7-3 is the influence of as-molded relative

*See footnote, p. 144.

density on the volume change. The sand at a relative density of 62% (γ_d = 100.5 lb/cu ft) dilated considerably less than the sand at a relative density of 75% (γ_d = 102.9 lb/cu ft). A 2.4-lb/cu ft increase in as-molded dry density (13% increase in relative density) was equivalent to 10-15 kg/cm^2 decrease in consolidation pressure as far as the volume change during drained shear was concerned. The dilation of the medium sands was such that at ultimate conditions the void ratios (water contents) reached a constant value which were essentially independent of initial dry density but they were a function of the consolidation pressure as shown in Fig. 7-4. The volume change behavior of this sand as a function of strain is shown in Figs. 7-5a through 7-5c.

The volume change behavior of the coarse Ottawa sand as a function of axial strain is shown in Figs. 7-6a through 7-6c. At an initial dry density of 102.9 lb/cu ft the coarse sand dilated considerably less than the medium sand at the same dry density. Its dilation was about the same as the medium sand at a density of 100.5 lb/cu ft. The difference in dilation between the two sands at the same dry density is probably not due to the difference in grain size but rather due to a difference in grain shape. The coarse sand was well rounded while the medium

sand was sub-rounded. The void ratios of the coarse Ottawa sand at ultimate conditions were also lower than those for the medium sand at the same consolidation pressure (Fig. 7-4).

A few undrained tests were run on the untreated sands. The volume of the samples was kept constant by preventing the pore water from cavitating during shear. This was achieved by using a very high back pressure which in some cases approached 70 kg/cm^2. The back pressure was always high enough to prevent the pore pressure during shear to drop below 10 kg/cm^2. The pore pressure behavior of the sands during undrained shear is shown in Fig. 7-7. In all cases very large negative excess pore pressures developed during shear, the magnitude of which was a function of consolidation pressure and as-molded density. The magnitude of the maximum negative excess pore pressure increased as the as-molded dry density increased and decreased as the consolidation pressure increased. Negative excess pore pressures in excess of 50 kg/cm^2 were measured and $\bar{A}$ factors as low as -0.5 were obtained.

7.3 Influence of Artificial Cementation in Coarse-Grained Soils

It was shown in Art. 7.2.2 that the volume change of the untreated sands during shear was very sensitive to

molding dry density, i.e., the packing of the sand grains; therefore the packing of the sand grains in the cemented samples was kept about the same as the corresponding uncemented samples. This was achieved by testing cemented samples having the same density of sand (excluding cement) as the untreated samples.

The influence of cement content on the volume change of medium Ottawa sand during drained shear is shown in Figs. 7-8a through 7-8c. There is a considerable scatter in the results as a function of strain probably due to small variations in the as-molded density of the sand in the cemented samples. The smaller volume changes of the cemented samples at maximum stress difference could be due to a number of reasons: (1) the maximum principal stress difference of the cemented samples occurred at a much smaller axial strain than the uncemented samples and therefore the packing of the sand grains in the cemented samples would not have changed (dilated) as much, (2) the cementation between grains tended to oppose the volume change, (3) at maximum principal stress difference the zone of shearing was more localized in the cemented samples, (4) the mean principal stress was much larger for the cemented samples at the maximum stress difference.

Probably all the factors mentioned above have an effect on reducing the volume change of a sand at the maximum stress difference when it is cemented.

At ultimate conditions the volume change tended to approach a constant value which was independent of cementation (Fig. 7-9) because the cementation between grains was completely destroyed in the zone of shearing which now covered a much larger portion of the samples. The mean principal stresses of the cemented samples were still higher than those of the corresponding untreated samples which could account for the numerically smaller volume change parameters, $\overline{W}$, of the cemented samples (Fig. 7-10). Apparently the physical presence of the cement did not increase the dilation at ultimate conditions since a decrease in the void ratio of an untreated sand produces an increase in the numerical value of $\overline{W}$ as shown in Fig. 7-11 and this was definitely not the case for the cemented samples which were at a lower void ratio than the uncemented samples.

Fig. 7-12 shows that 5% cement did not appreciably affect the pore pressure behavior of coarse Ottawa sand in undrained shear.

In summary cementation alters the volume change behavior of a sand at small axial strains but at ultimate conditions it has only a minor influence on the maximum dilation. The controlling factor is the density of the sand excluding the cement, i.e., the relative packing of the sand grains.

7.4 Influence of Artificial Cementation in Fine-Grained Soils

In general the pore pressure behavior of the cemented samples was very similar to that of the untreated samples during undrained shear. At low consolidation pressures the cemented samples started out by tending to contract slightly followed by a strong tendency to dilate as the maximum stress difference was reached. Increasing the consolidation pressure caused the pore water pressure to increase during undrained shear or the volumetric contraction to increase during drained shear. Fig. 7-13 shows the influence of consolidation pressure on the pore pressure behavior of VBC + 10% cement in undrained shear. A similar behavior was observed with the other soil-stabilizer systems.

The influence of consolidation pressure on the pore pressure behavior of the various soil-stabilizer systems investigated is summarized in Figs. 7-14 through 7-16. The figures show that at maximum stress difference and at point of first tangency with effective Mohr-Coulomb envelope the excess pore pressures were dependent on the cementing agent as well as consolidation pressure. In general the excess pore pressures of the stabilized soils were 10-15% higher than those of the corresponding untreated soils at the same consolidation pressure. The

higher excess pore pressures could be due to the higher void ratios* of the cemented samples during shear and/or the higher mean principal stresses.

Fig. 7-17 shows the effect of lime and cement on the principal stress difference and excess pore pressure of VBC consolidated to 50 kg/cm^2. It is apparent from the figure that the change in mean principal stress, $1/3(\Delta\sigma_1)$** , cannot fully account for the differences in the excess pore pressures since the lime and cement samples had about the same excess pore pressures at maximum principal stress difference but considerably different mean principal stresses. Further it will be shown later that for a given soil-stabilizer system increasing the curing time, which increases the mean principal stress, does not influence the excess pore pressure at the maximum stress difference.

The differences in the void ratios during shear could possibly account for the differences in excess pore pressures since the untreated VBC had the lowest excess pore pressure and the lowest water content during shear (17.8%). VBC plus 5% lime had the highest excess pore

---

*Note that for S = 100%, e = Gw, thus e $\propto$ w. See Tables 4-2 and 4-3 for final water contents of the test specimens.

**For $\Delta\sigma_3 = 0$, i.e., constant cell pressure $1/3(\Delta\sigma_1) = 1/3(\sigma_1 - \sigma_3)$

pressure and the highest water content (27.0%) and VBC plus 10% cement at a water content of 24.4% had a slightly lower excess pore pressure than VBC plus 5% lime.

Even though the cemented soils had higher excess pore pressures during shear their $\bar{A}$ factors were usually lower than those of the untreated samples (Figs. 7-18 through 7-20). This means that for the same shear stress the cemented samples produced less excess pore pressure than the corresponding uncemented samples. This stands to reason since a cemented soil structure would require a higher shear stress for the same deformation. However at the same axial strain the cemented samples still usually had lower $\bar{A}$ factors (e.g., Fig. 7-17) even though they were at higher void ratios. This could possibly be due to a change in the effective particle size of the soil caused by the formation of strongly cemented aggregates of clay size particles. These aggregates would interlock during shear and produce a dilation tendency which opposes some of the tendency for the soil skeleton to contract.

To determine the influence of cementation per se on the pore water behavior samples having identical molding conditions were tested after various curing times. This eliminated variations in soil fabric due to the different cementing agents and molding conditions

which would have had some influence on the pore water behavior. For a given soil-stabilizer system and a fixed set of molding conditions the excess pore pressures developed during undrained shear were essentially independent of curing time at the high consolidation pressures. For example Fig. 7-21 shows the stress-strain behavior of M-21 + 5% lime after 20 days and 138 days curing at a consolidation pressure of 54 kg/cm^2. At these high consolidation pressures the excess pore pressures developed during shear were essentially independent of curing time whereas the maximum stress difference increased with increasing curing time. The net effect was for the $\bar{A}$ factors to decrease with increasing curing time. Figs. 7-22 and 7-23 summarize the influence of curing time on the excess pore pressures of the M-21 + 5% lime and M-21 + 5% cement systems respectively at maximum stress difference and point of first tangency with the effective Mohr-Coulomb envelopes. Over the wide range of curing times investigated the excess pore pressures were essentially constant but the $\bar{A}$ factors decreased with increasing curing time because the stress differences were increasing* (Figs. 7-24 and 7-25).

*See Chapter 8.

In undrained shear the pore pressure behavior of the cemented samples at low consolidation pressures as a function of curing time was erratic especially at $(\sigma_1 - \sigma_3)$ maximum as shown in Fig. 7-26. This was probably due to boundary drainage conditions which are inherent in the triaxial test. At low consolidation pressures the tendency to contract initially can be fully observed in drained shear; however in undrained shear the excess pore pressure increases with strain until it is equal to the consolidation pressure, i.e., $\bar{\sigma}_3$ tends to zero, and then remains constant until the sample starts to dilate at larger strains. This is due to the fact that the pore pressure cannot become greater than the consolidation pressure. The additional tendency to contract causes water to be squeezed out of the sample by pushing the rubber membrane surrounding the sample away from the sides of the sample and the water drains into the space between the membrane and sample. Fig. 7-27 shows this effect for a cemented soil by comparing the volume change behavior during drained shear with the pore pressure behavior in undrained shear. At about 0.5% axial strain the excess pore pressure in the undrained shear test reached the consolidation pressure of 0.1 kg/cm^2 and then remained constant until failure. The drained specimen continued to decrease in volume until failure was reached. The

behavior after failure has not been shown in the figure but there always is a large tendency to dilate on further straining. This effect becomes more pronounced as the cementation increases. In other words it is not possible at low consolidation pressures to run a completely undrained test on a cemented soil. In actual fact the tests are always partially drained.

In summary the pore water behavior of cemented fine-grained soils is similar to that of untreated soils. In undrained shear at constant cell pressure, the excess pore pressure increases rapidly with consolidation pressure and is independent of curing time, i.e., of the strength of the cementation. The addition of a cementing agent, such as hydrated lime or portland cement, alters the fabric of a fine-grained soil probably by the production of cemented aggregates of the clay particles. This change in fabric alters the rate at which the excess pore pressure develops with strain. At the same axial strain cemented samples have higher excess pore pressure than corresponding untreated samples probably because they usually have higher void ratios during shear and higher mean principal stresses especially at small axial strains. For a given soil-stabilizer system the $\bar{A}$ factors decrease with increasing strength of the cementation (curing time)

because the cemented aggregates get stronger and therefore will deform less during shear.

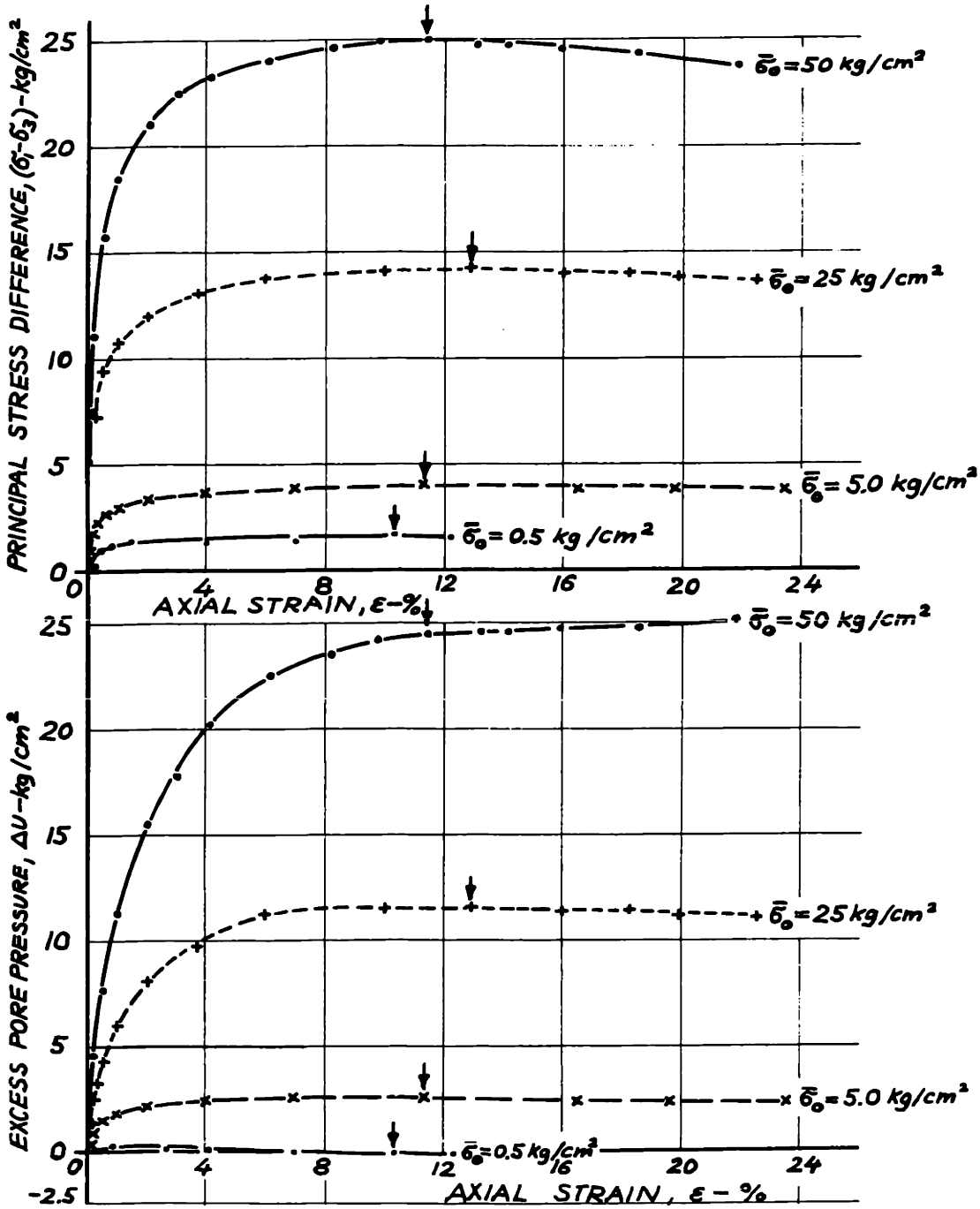

FIG. 7-1. *INFLUENCE OF CONSOLIDATION PRESSURE ON THE STRESS-STRAIN BEHAVIOR OF COMPACTED VICKSBURG BUCKSHOT CLAY*

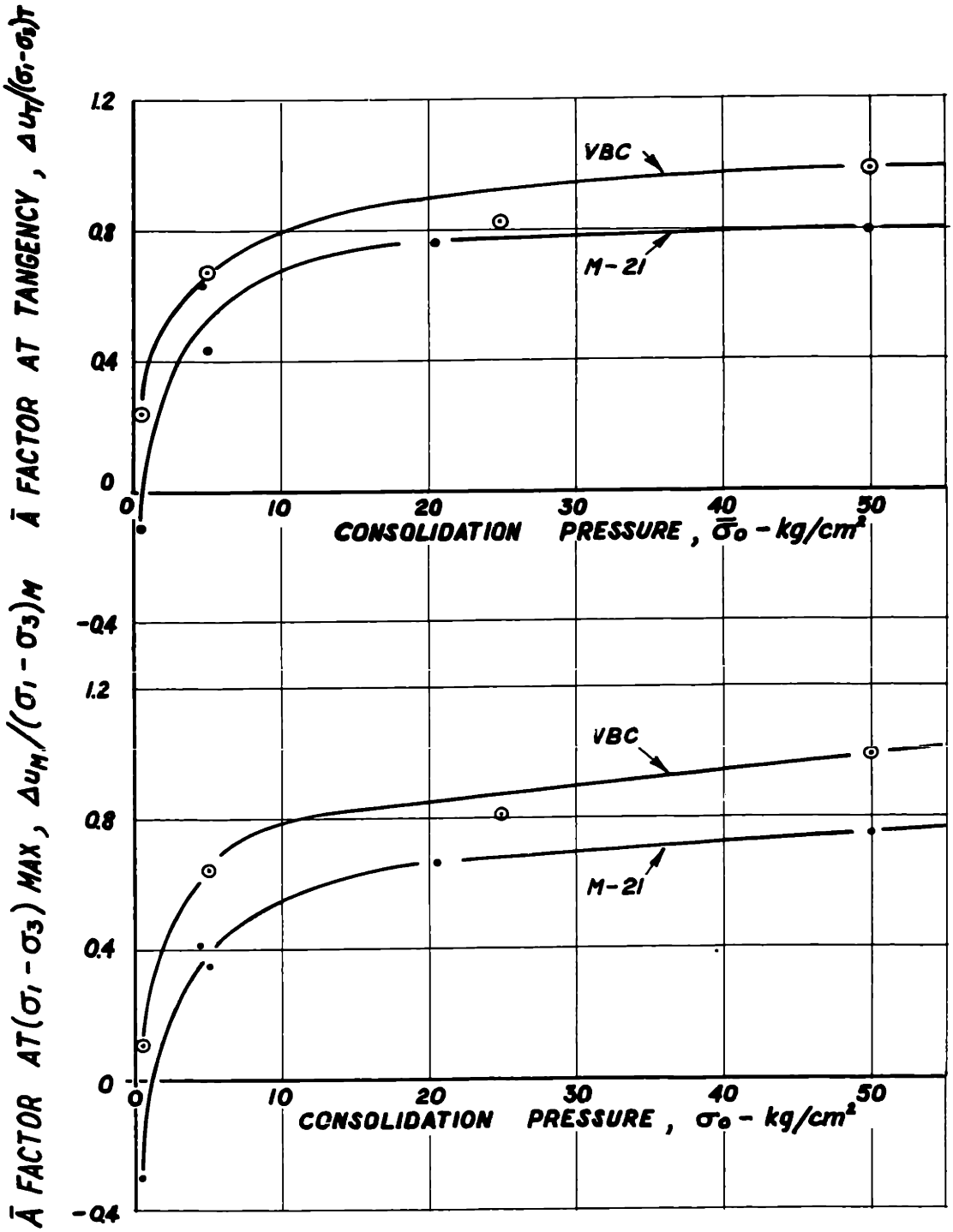

FIG. 7-2. **INFLUENCE OF CONSOLIDATION PRESSURE ON THE Ā FACTORS OF THE UNTREATED FINE-GRAINED SOILS.**

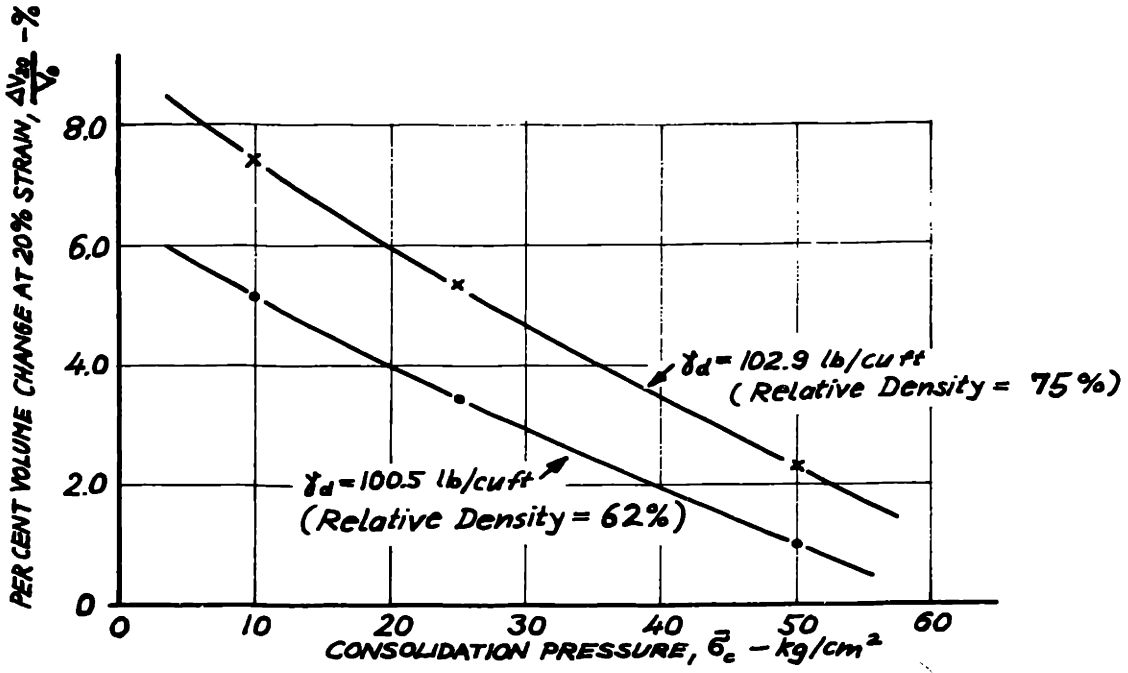

FIG. 7-3b. INFLUENCE OF INITIAL DRY DENSITY AND CONSOLIDATION PRESSURE ON THE VOLUME CHANGE BEHAVIOR OF MEDIUM OTTAWA SAND AT 20% STRAIN

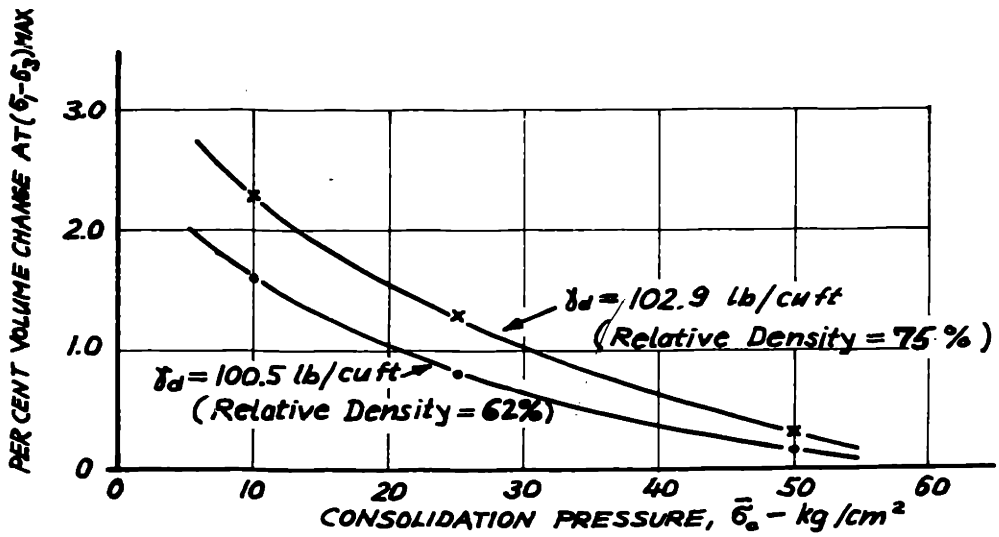

FIG. 7-3a. INFLUENCE OF INITIAL DRY DENSITY AND CONSOLIDATION PESSURE ON THE VOLUME CHANGE BEHAVIOR OF MEDIUM OTTAWA SAND AT $(\bar{\sigma}_1 - \bar{\sigma}_3)$ MAX.

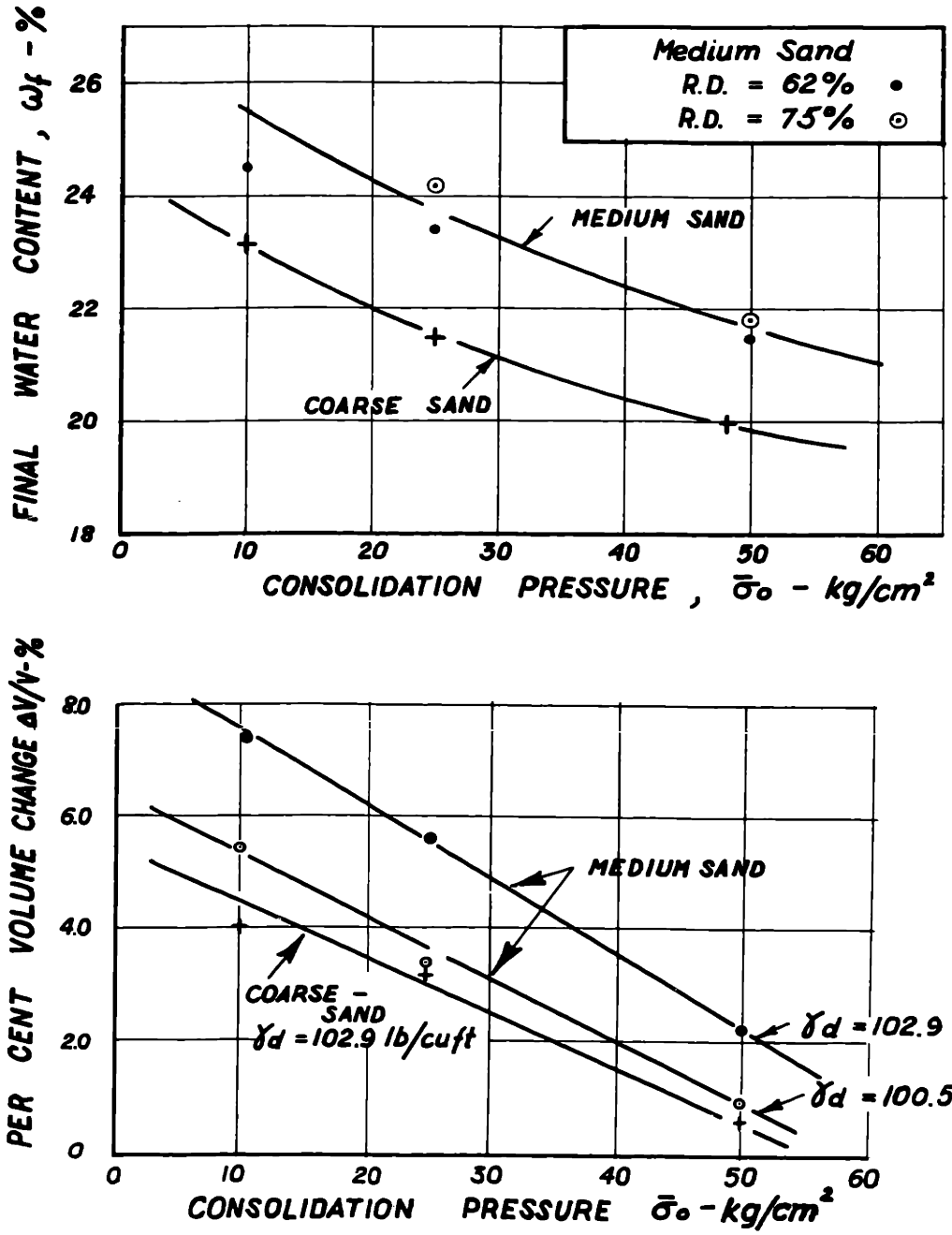

FIG.7-4. INFLUENCE OF INITIAL DRY DENSITY AND GRAIN SIZE ON THE MAXIMUM DILATENCY OF OTTAWA SAND

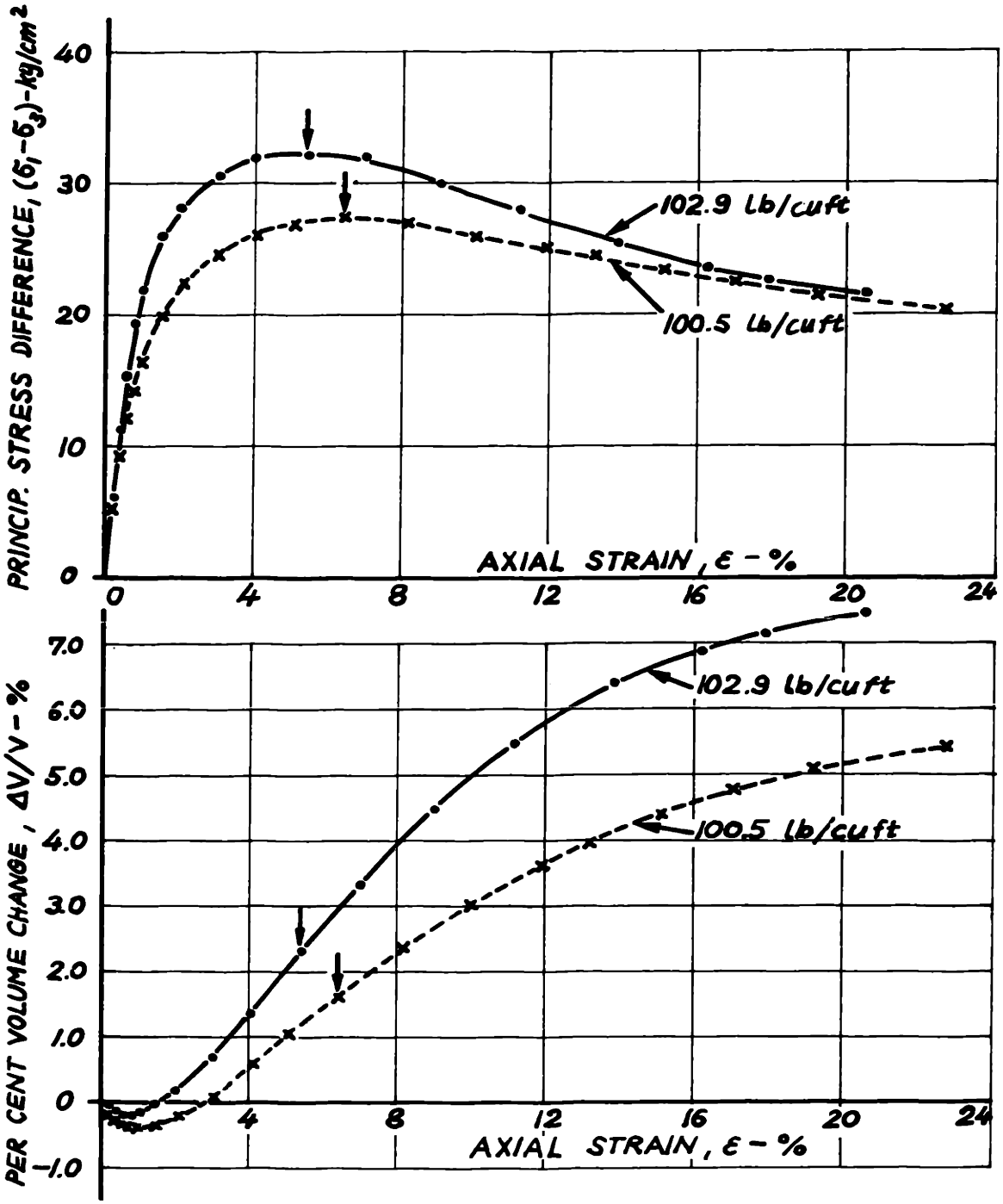

FIG. 7-5a EFFECT OF INITIAL DRY DENSITY ON THE STRESS - STRAIN BEHAVIOR OF MEDIUM OTTAWA SAND CONSOLIDATED TO 10 kg/cm².

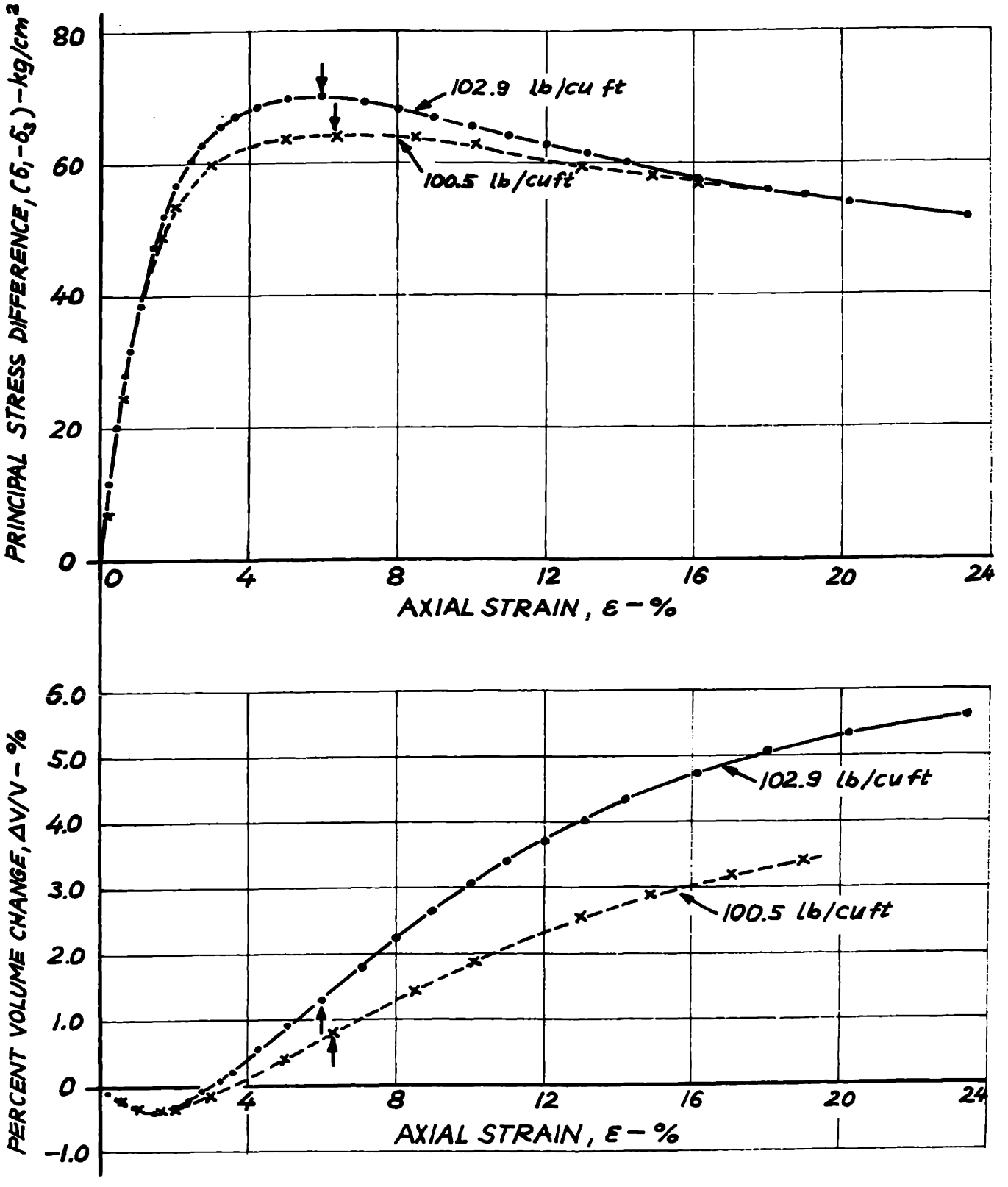

FIG. 7-5b EFFECT OF INITIAL DRY DENSITY ON THE STRESS–STRAIN BEHAVIOR OF MEDIUM OTTAWA SAND CONSOLIDATED TO 25 kg/cm²

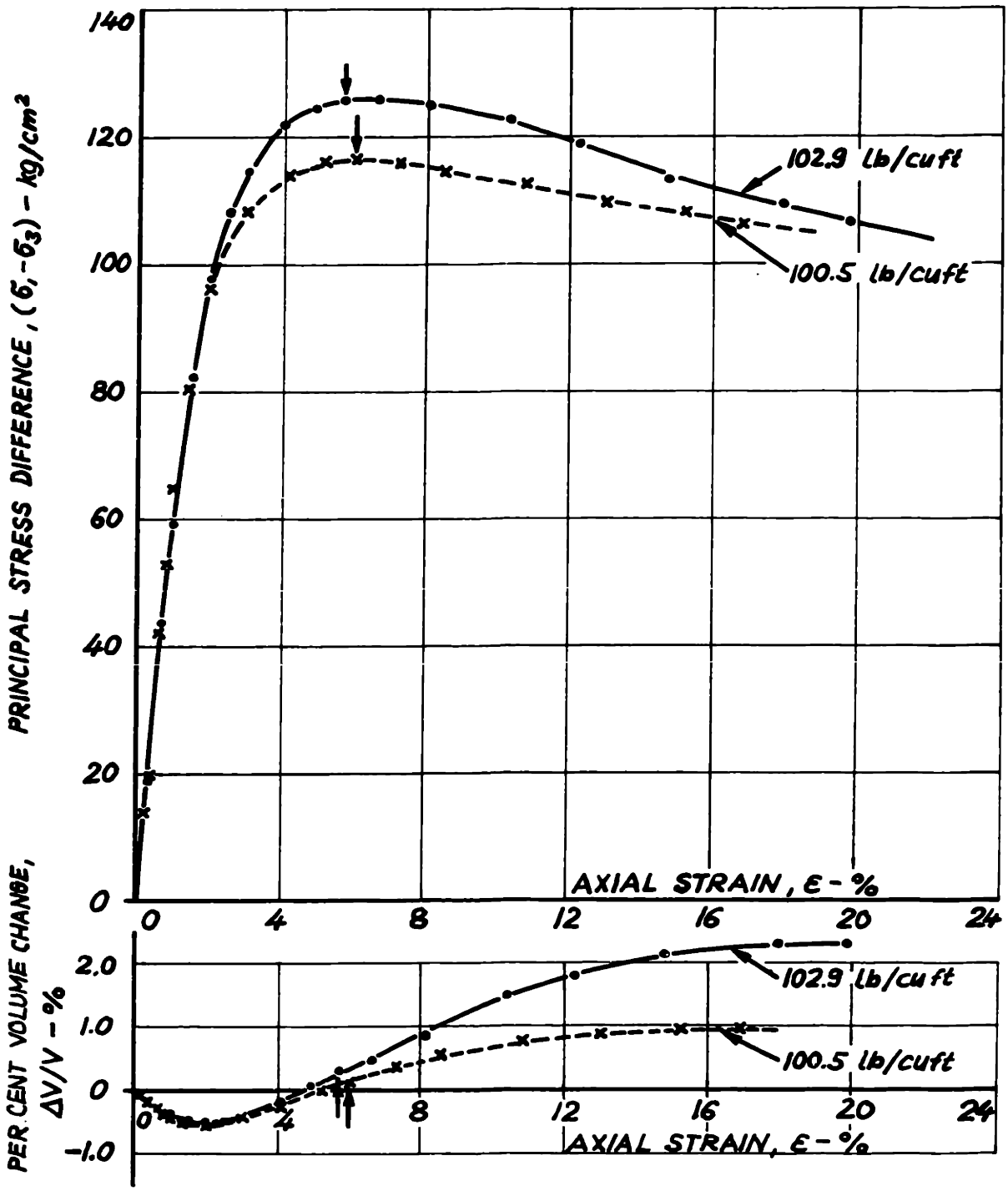

FIG. 7-5c EFFECT OF INITIAL DRY DENSITY ON THE STRESS - STRAIN BEHAVIOR OF MEDIUM OTTAWA SAND CONSOLIDATED TO 50 kg/cm².

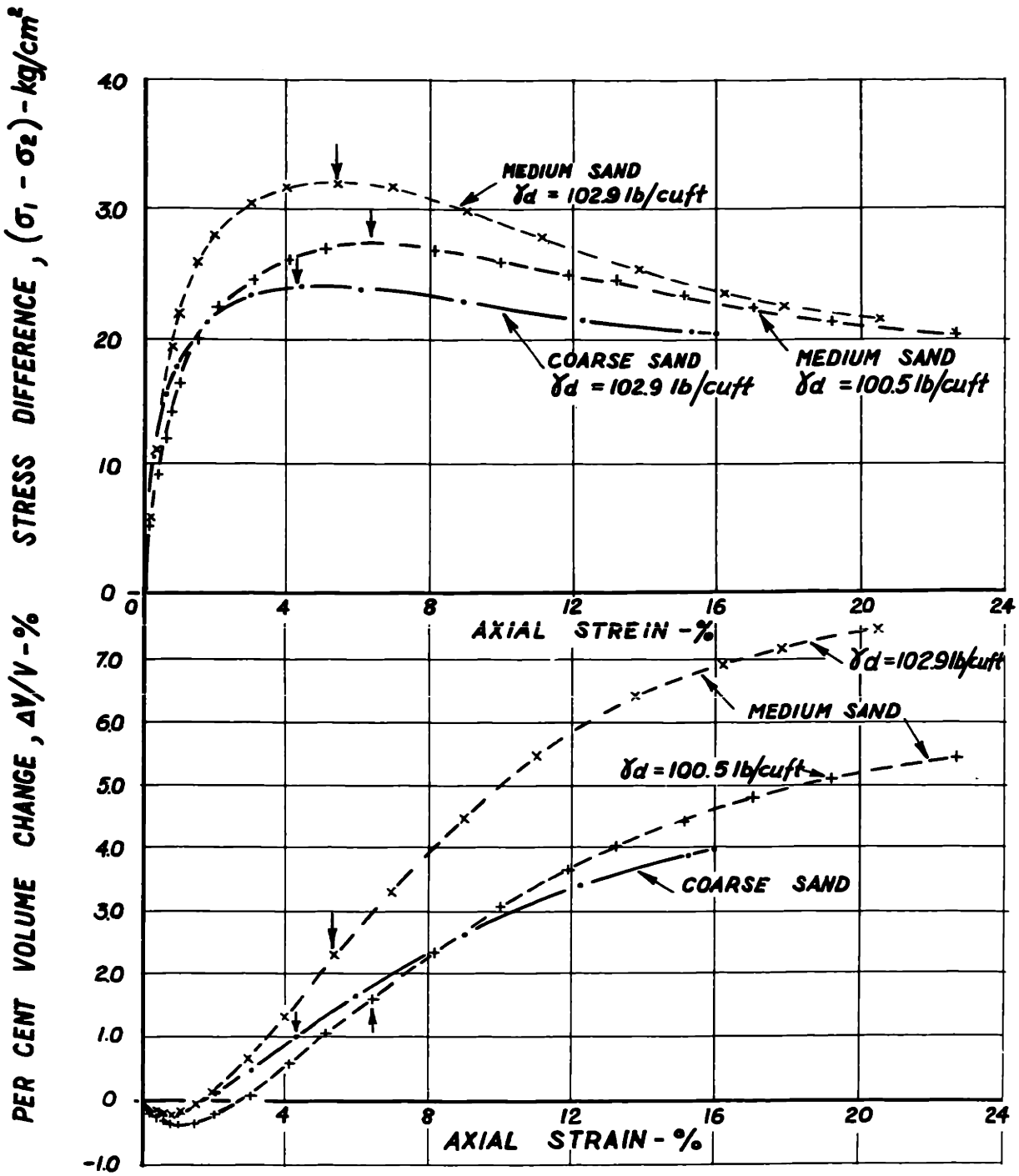

FIG. 7-6a. **INFLUENCE OF GRAIN SIZE ON THE STRESS - STRAIN BEHAVIOR OF OTTAWA SAND CONSOLIDATED TO 10kg/cm²**

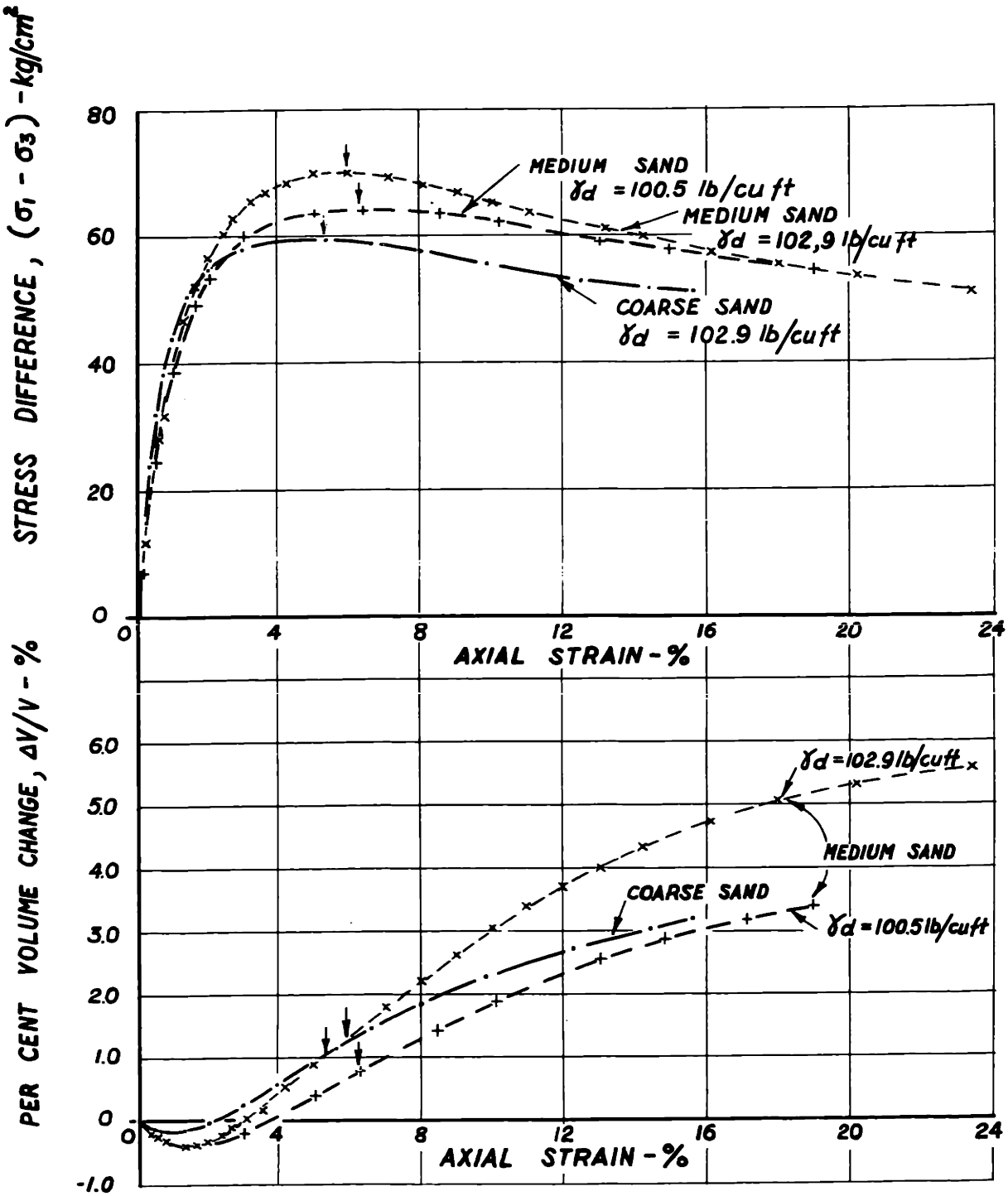

FIG.7-6b. **INFLUENCE OF GRAIN SIZE ON THE STRESS - STRAIN BEHAVIOR OF OTTAWA SAND CONSOLIDATED TO 25kg/cm²**

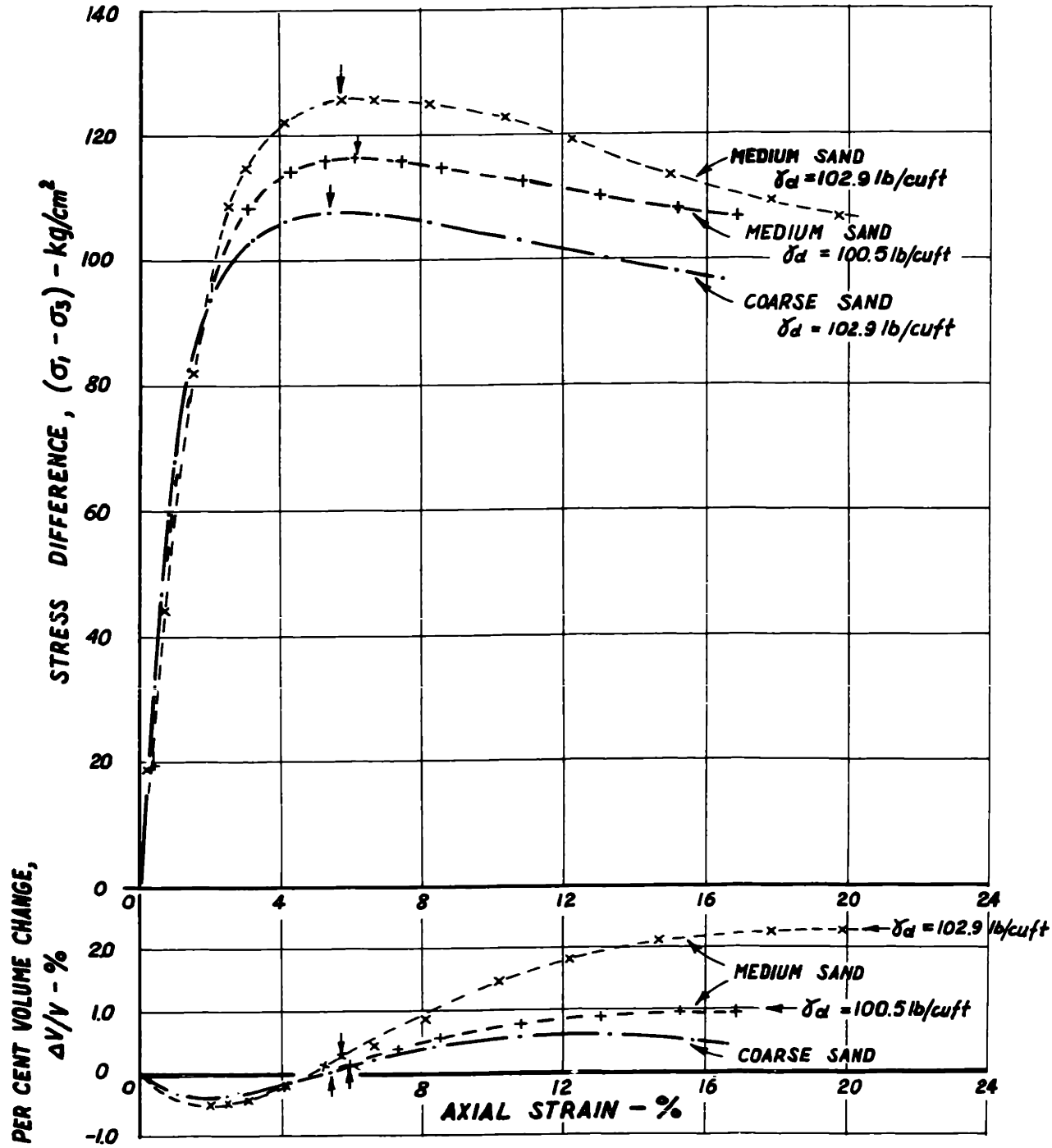

FIG. 7-6c **INFLUENCE OF GRAIN SIZE ON THE STRESS - STRAIN BEHAVIOR OF OTTAWA SAND CONSOLIDATED TO 50 kg/cm²**

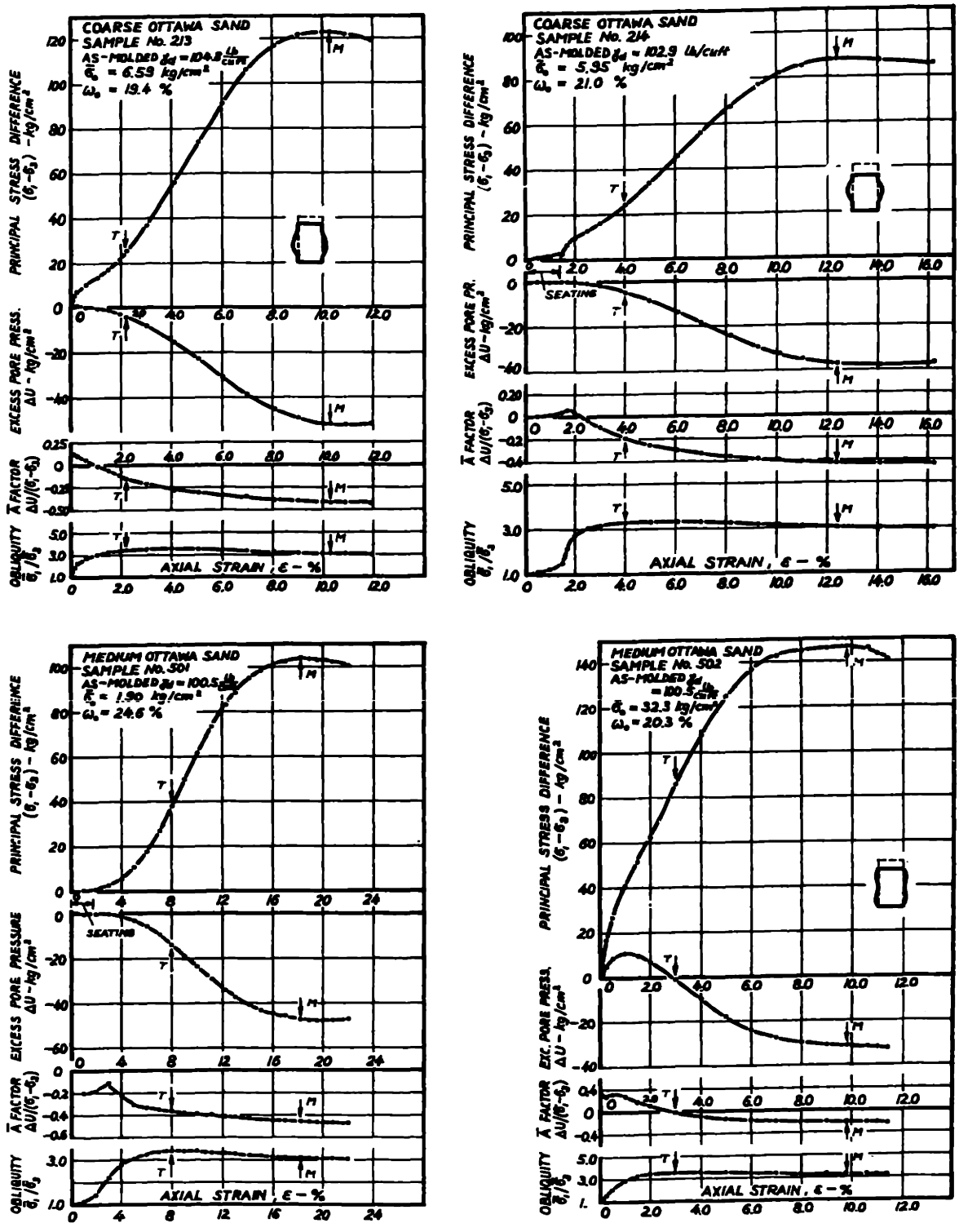

FIG. 7-7 STRESS-STRAIN BEHAVIOR OF UNTREATED OTTAWA SAND IN UNDRAINED SHEAR.

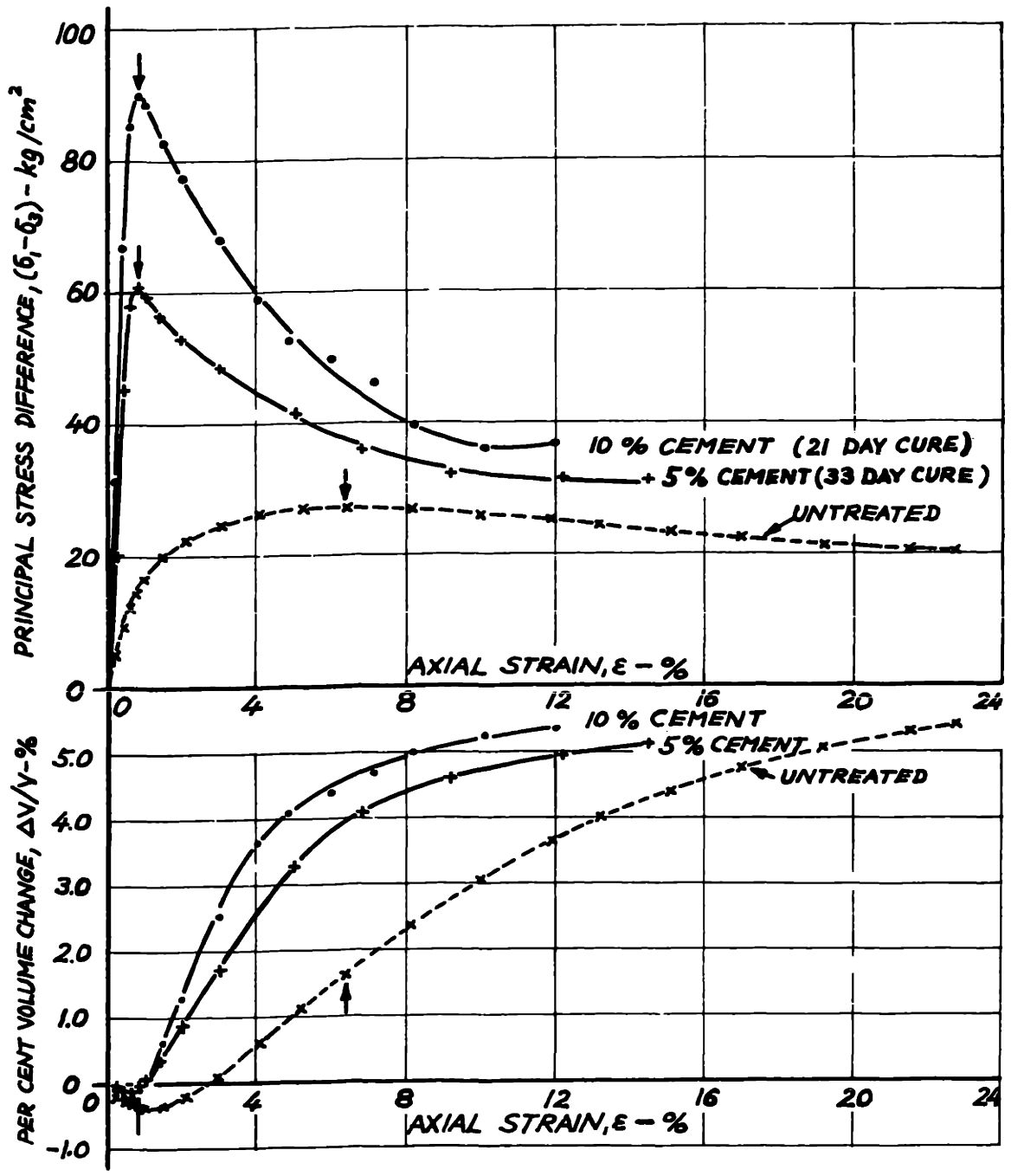

FIG. 7-8a. INFLUENCE OF CEMENT CONTENT ON THE STRESS-STRAIN BEHAVIOR OF MEDIUM OTTAWA SAND CONSOLIDATED TO 10 kg/cm²

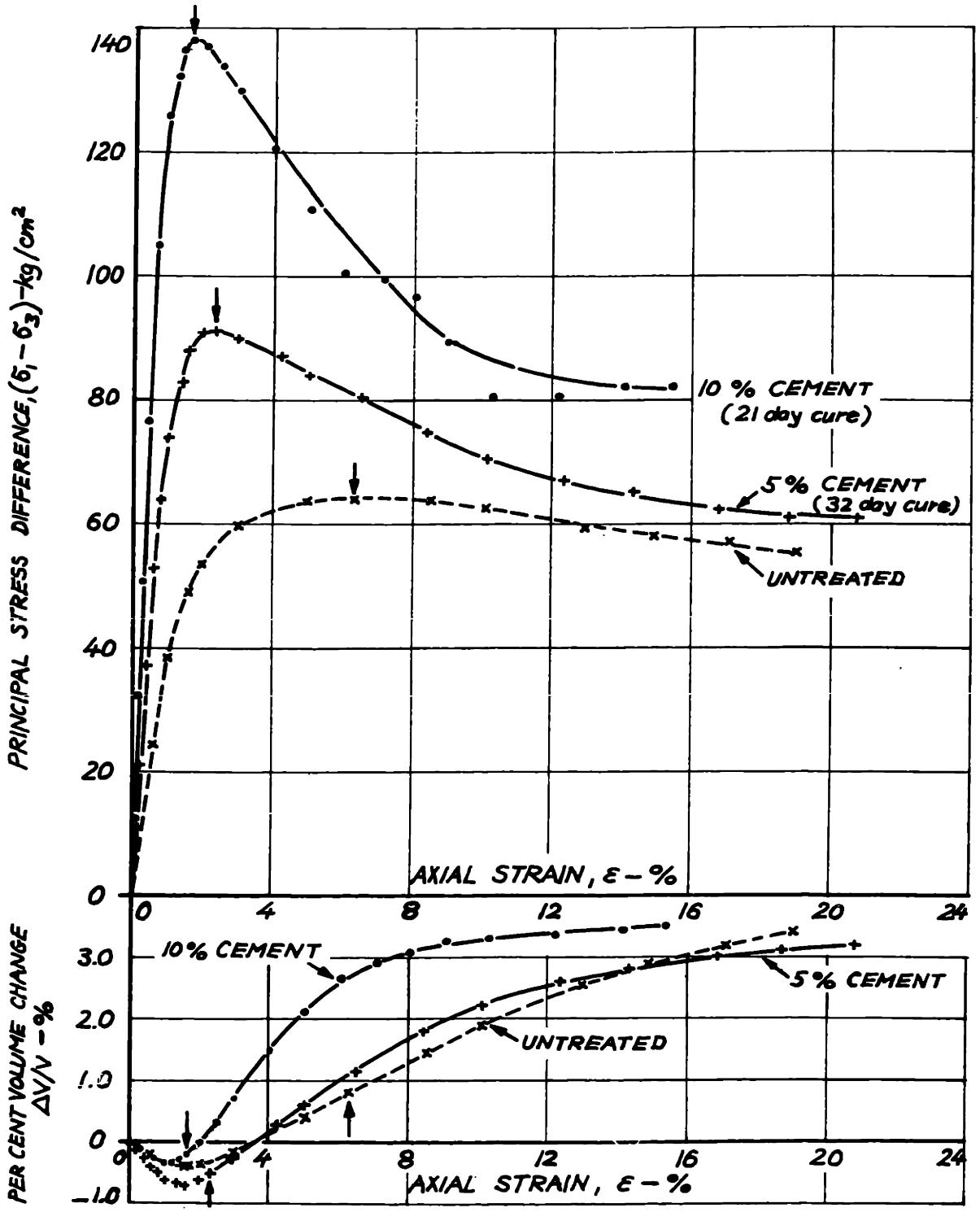

FIG. 7-8 b. *INFLUENCE OF CEMENT CONTENT ON THE STRESS-STRAIN BEHAVIOR OF MEDIUM OTTAWA SAND CONSOLIDATED TO 25 kg/cm²*

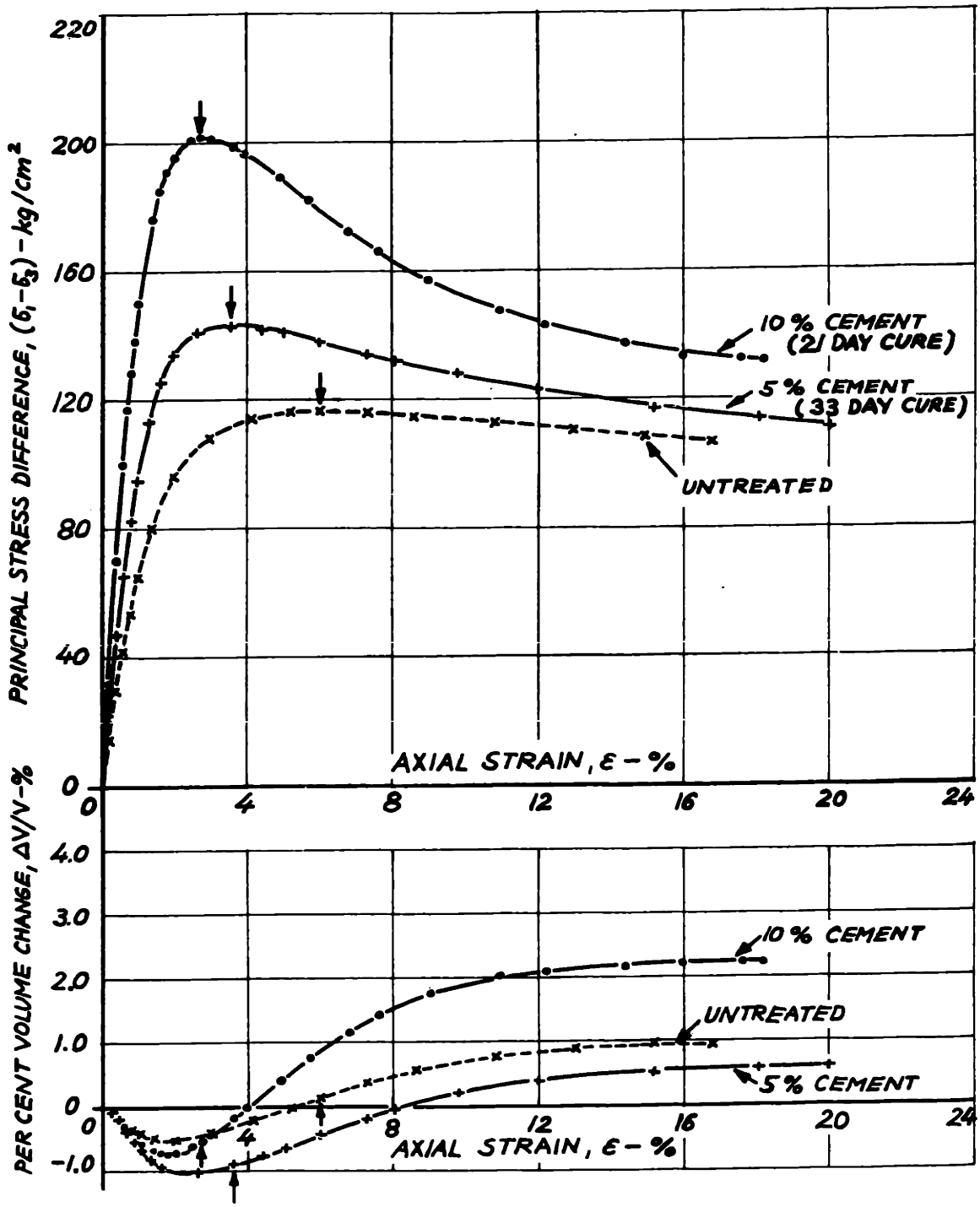

FIG. 7-8c. INFLUENCE OF CEMENT CONTENT ON THE STRESS-STRAIN BEHAVIOR OF MEDIUM OTTAWA SAND CONSOLIDATED TO 50 kg/cm²

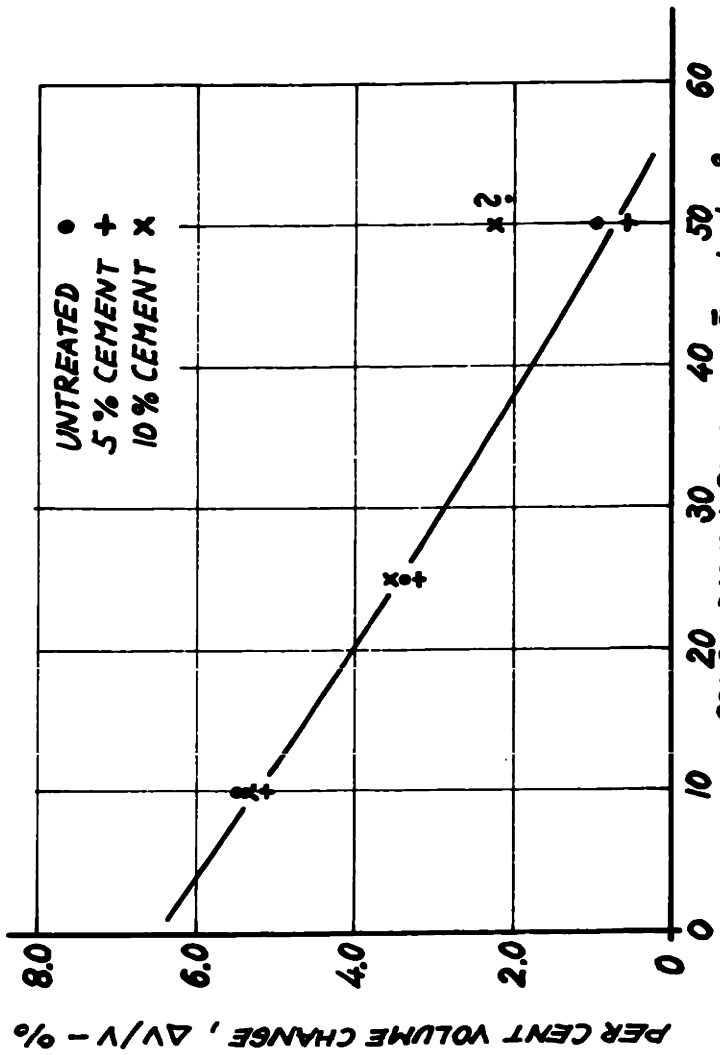

FIG.7-9. INFLUENCE OF CEMENT CONTENT ON THE MAXIMUM DILATENCY OF MEDIUM OTTAWA SAND IN DRAINED SHEAR

FIG. 7-10. *INFLUENCE OF CEMENTATION ON THE VOLUME CHANGE PARAMETER, $\bar{W}$, OF MEDIUM OTTAWA SAND AT ULTIMATE CONDITIONS*

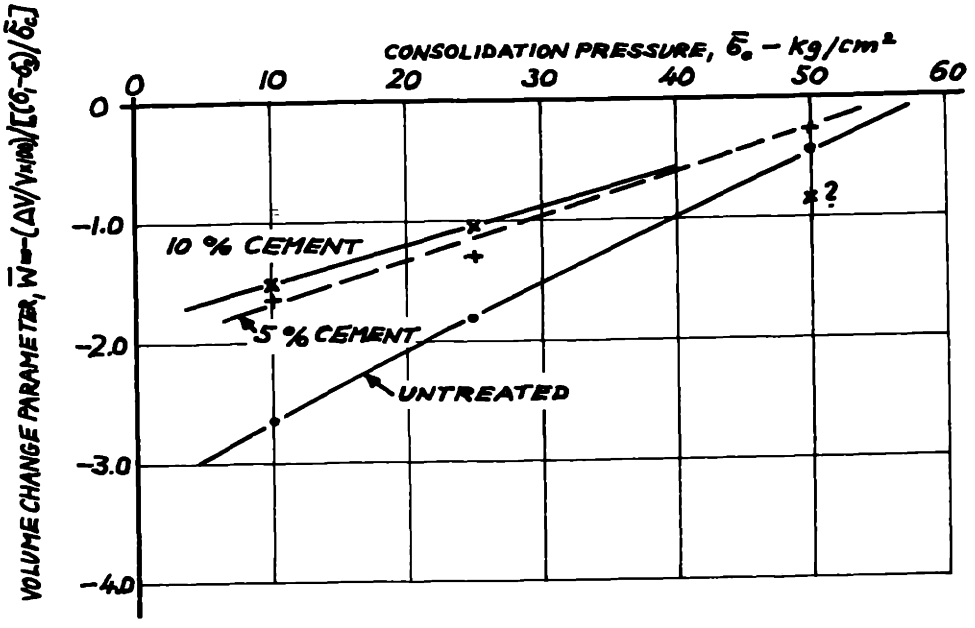

FIG. 7-11. *INFLUENCE OF INITIAL DRY DENSITY AND GRAIN SIZE ON THE VOLUME CHANGE PARAMETER, $\bar{W}$, OF OTTAWA SAND AT ULTIMATE*

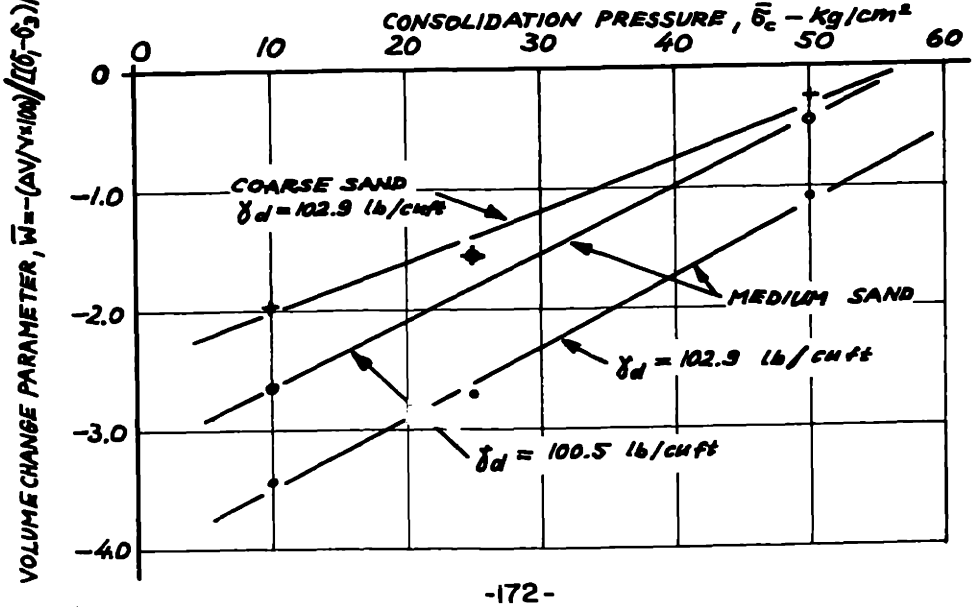

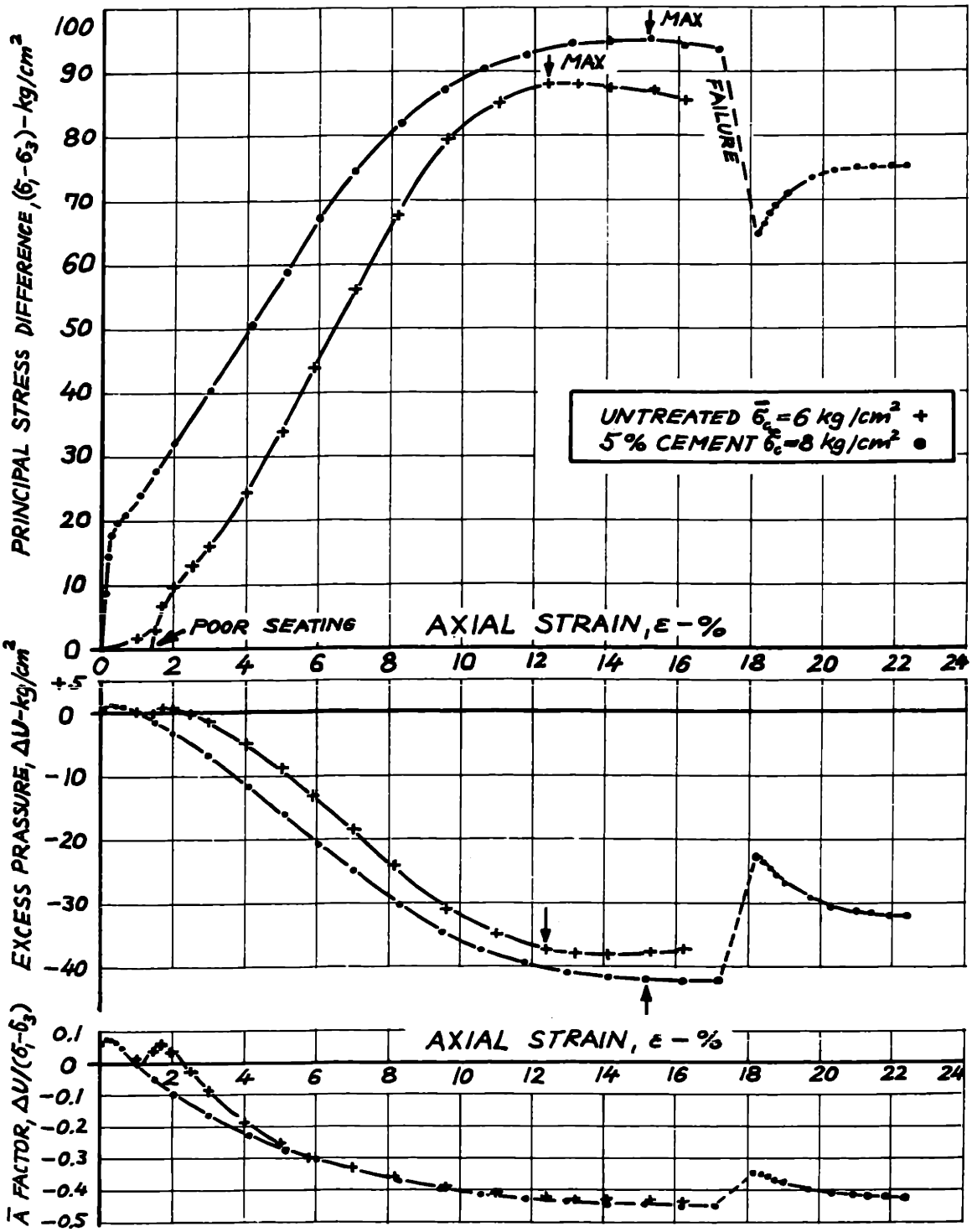

FIG. 7-12. STRESS-STRAIN BEHAVIOR OF UNTREATED AND CEMENTED COARSE OTTAWA SAND IN UNDRAINED SHEAR

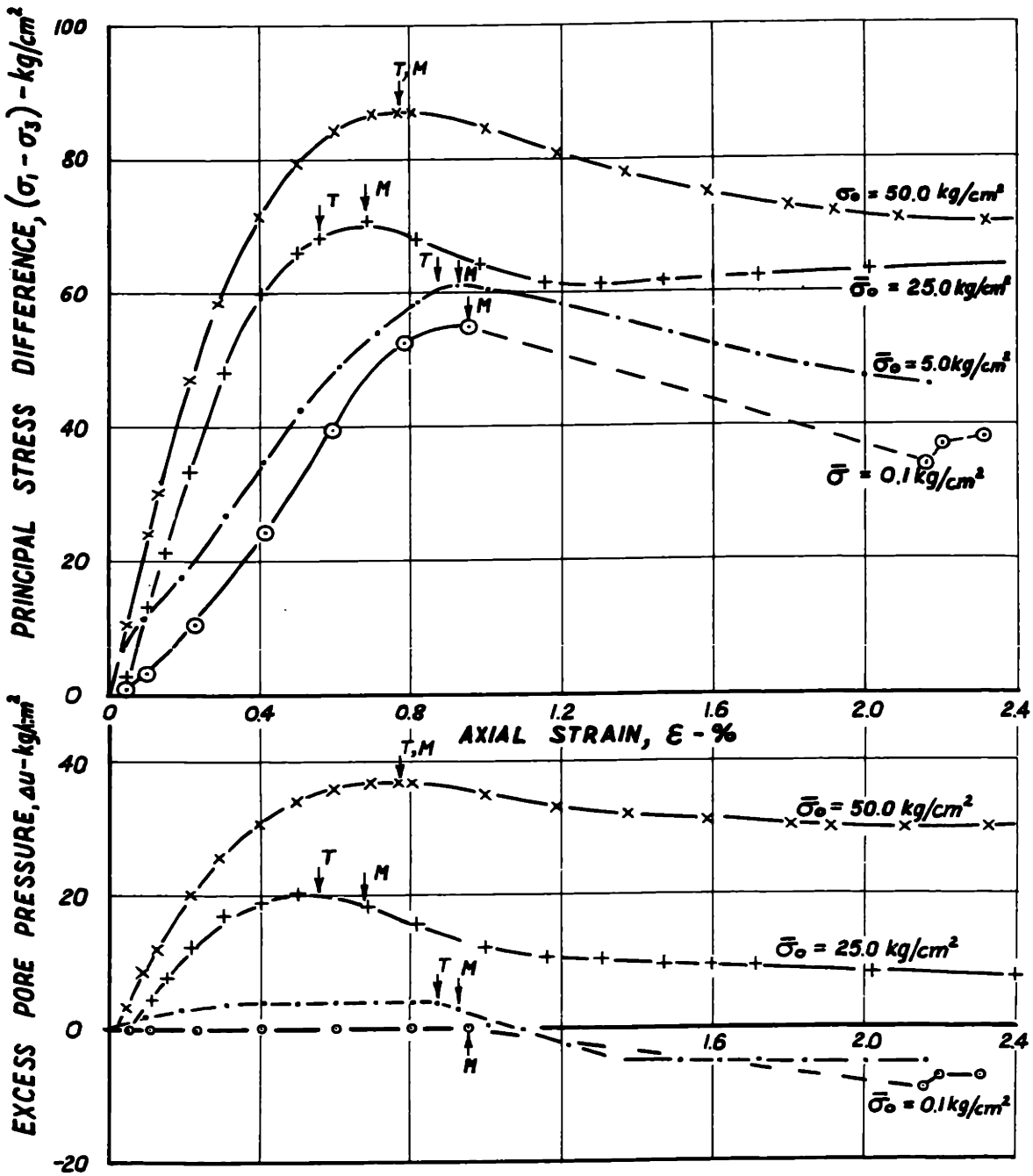

FIG. 7-13. INFLUENCE OF CONSOLIDATION PRESSURE ON THE STRESS-STRAIN BEHAVIOR OF VBC + 10% CEMENT AFTER 55 DAYS CURING

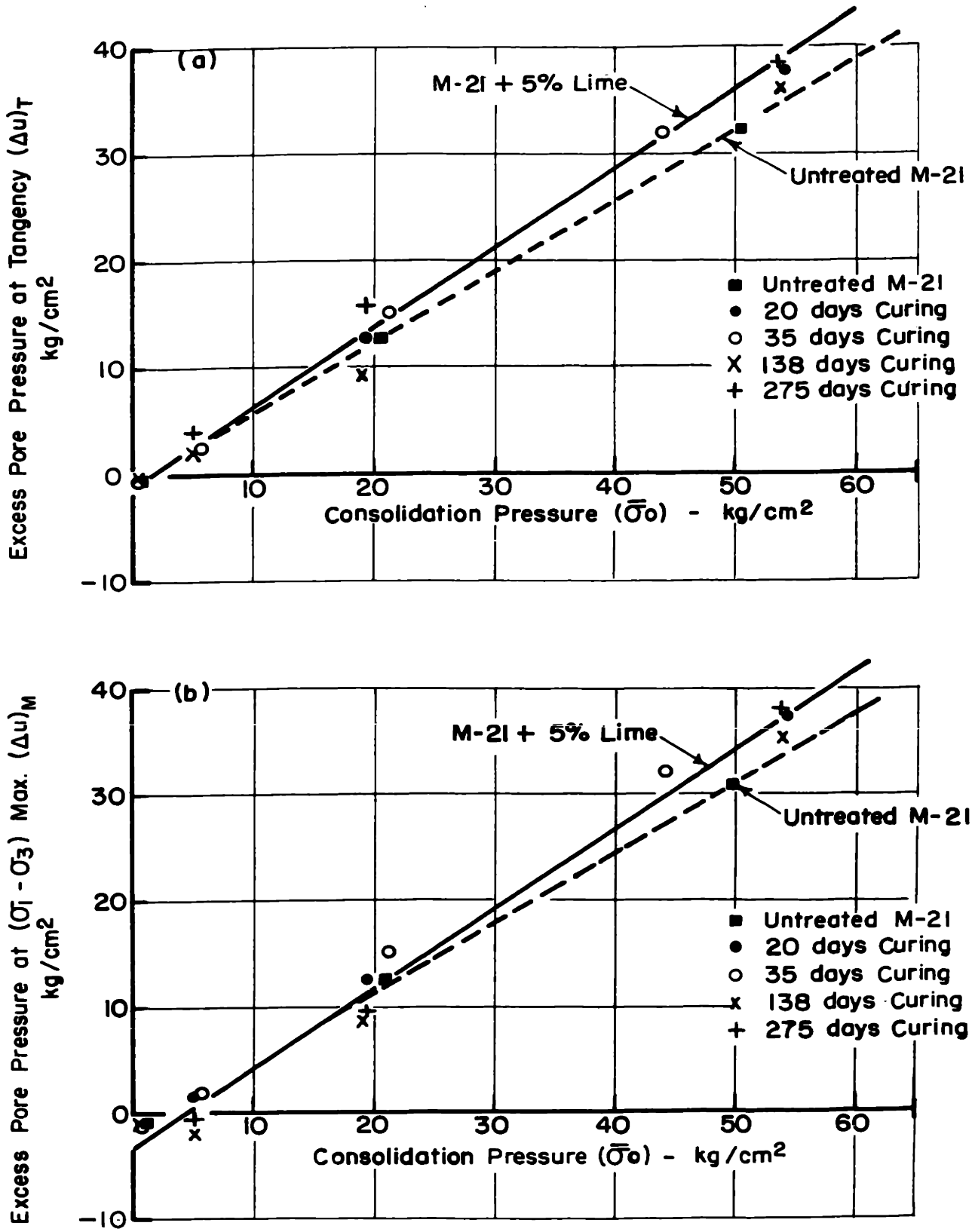

FIGURE 7-14. EFFECT OF CONSOLIDATION PRESSURE ON EXCESS PORE PRESSURE OF M-21 + 5% LIME

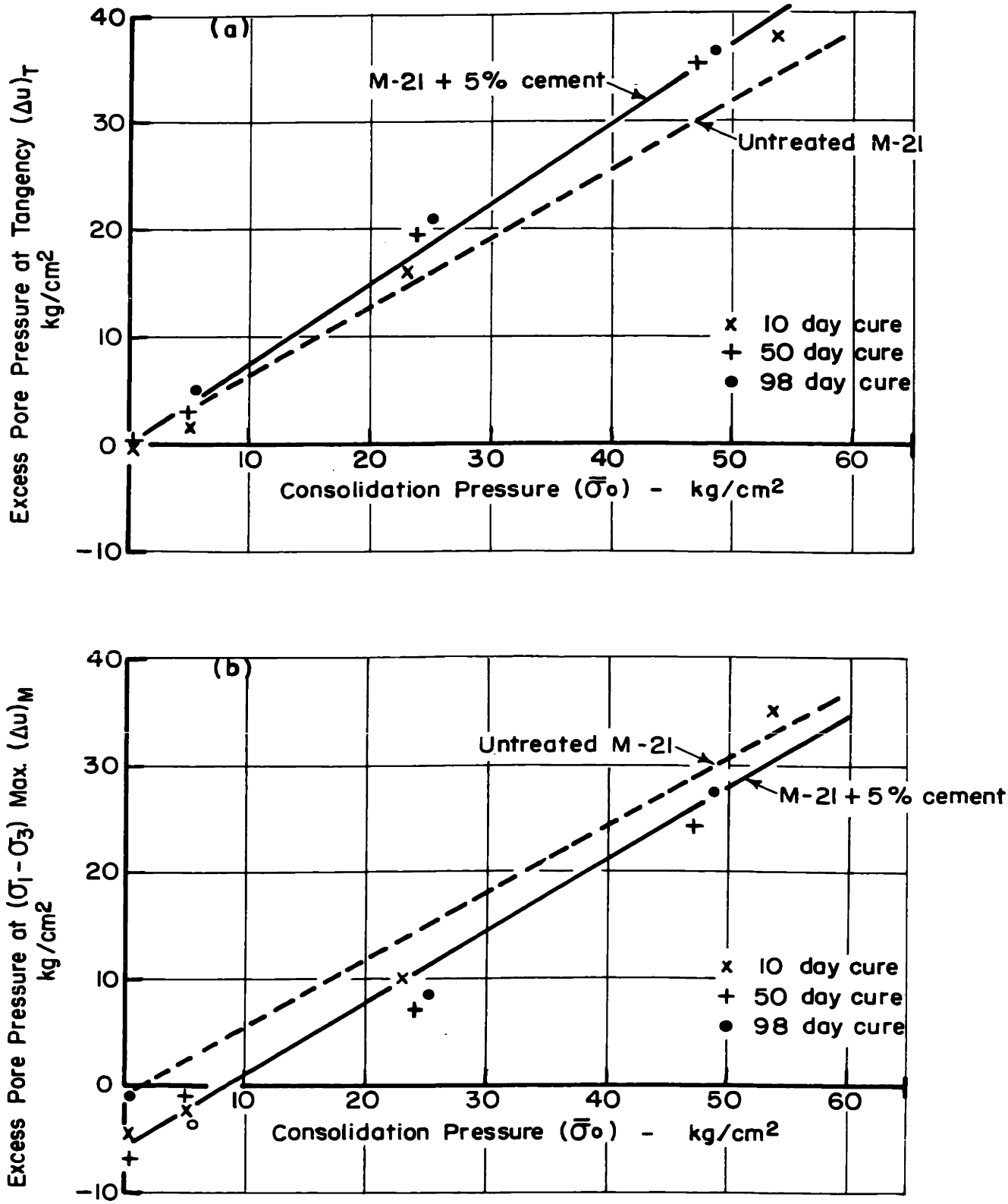

FIGURE 7-15. EFFECT OF CONSOLIDATION PRESSURE ON EXCESS PORE PRESSURE OF M-21 + 5% CEMENT

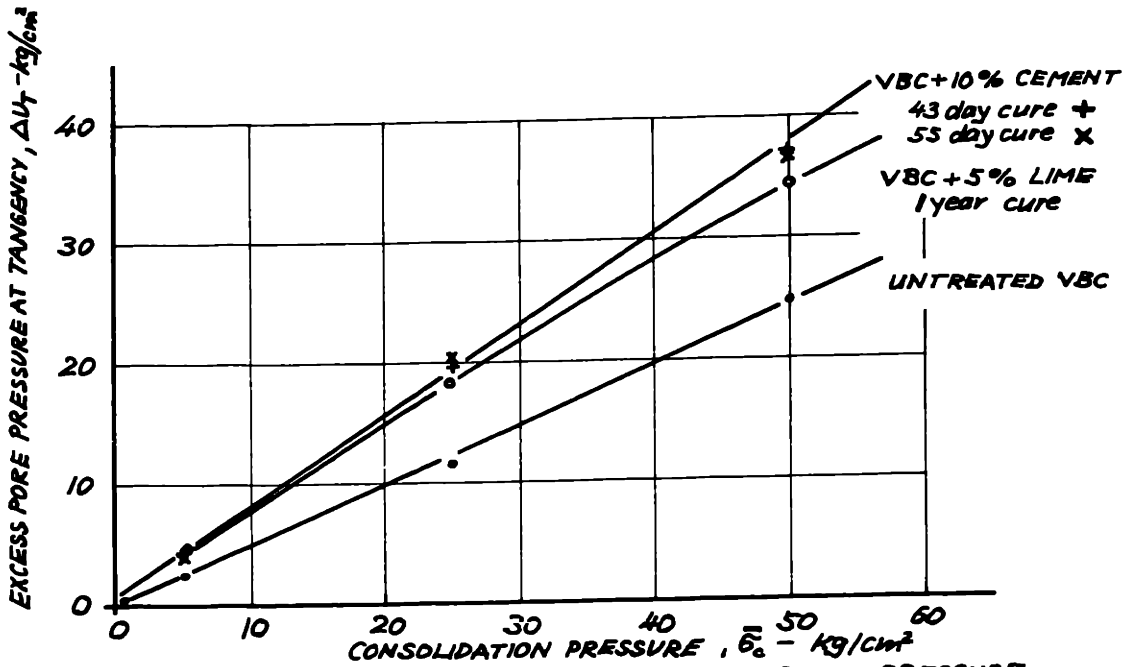

FIG. 7-16a. *INFLUENCE OF CEMENTATION ON THE EXCESS PORE PRESSURE OF VBC AT TANGENCY.*

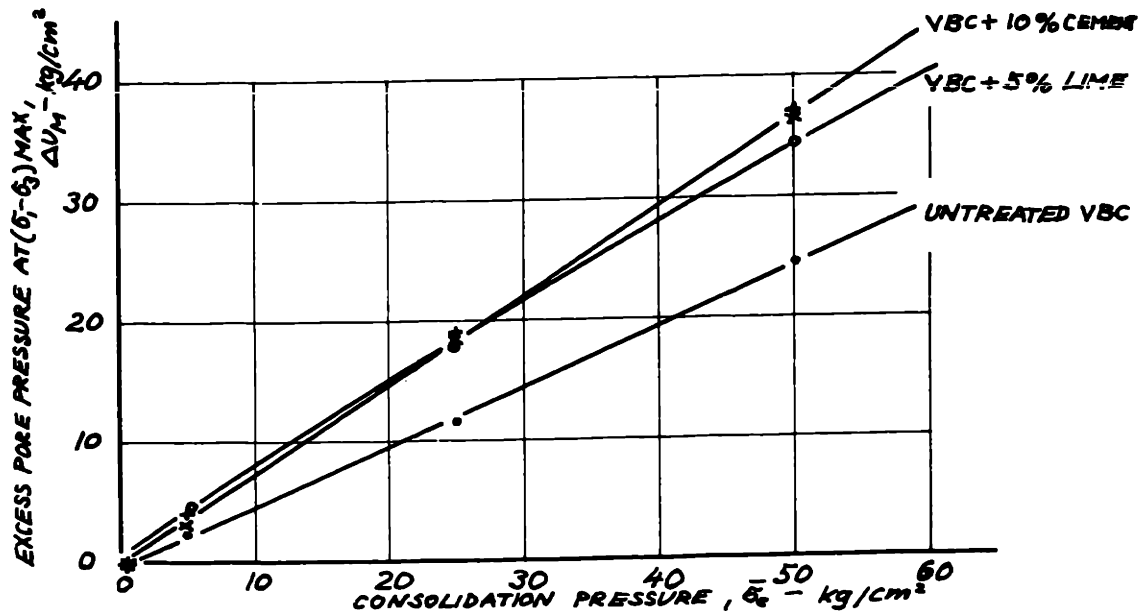

FIG. 7-16b. *INFLUENCE OF CEMENTATION ON THE EXCESS PORE PRESSURE OF VBC AT $(\sigma_1-\sigma_3)$ MAX.*

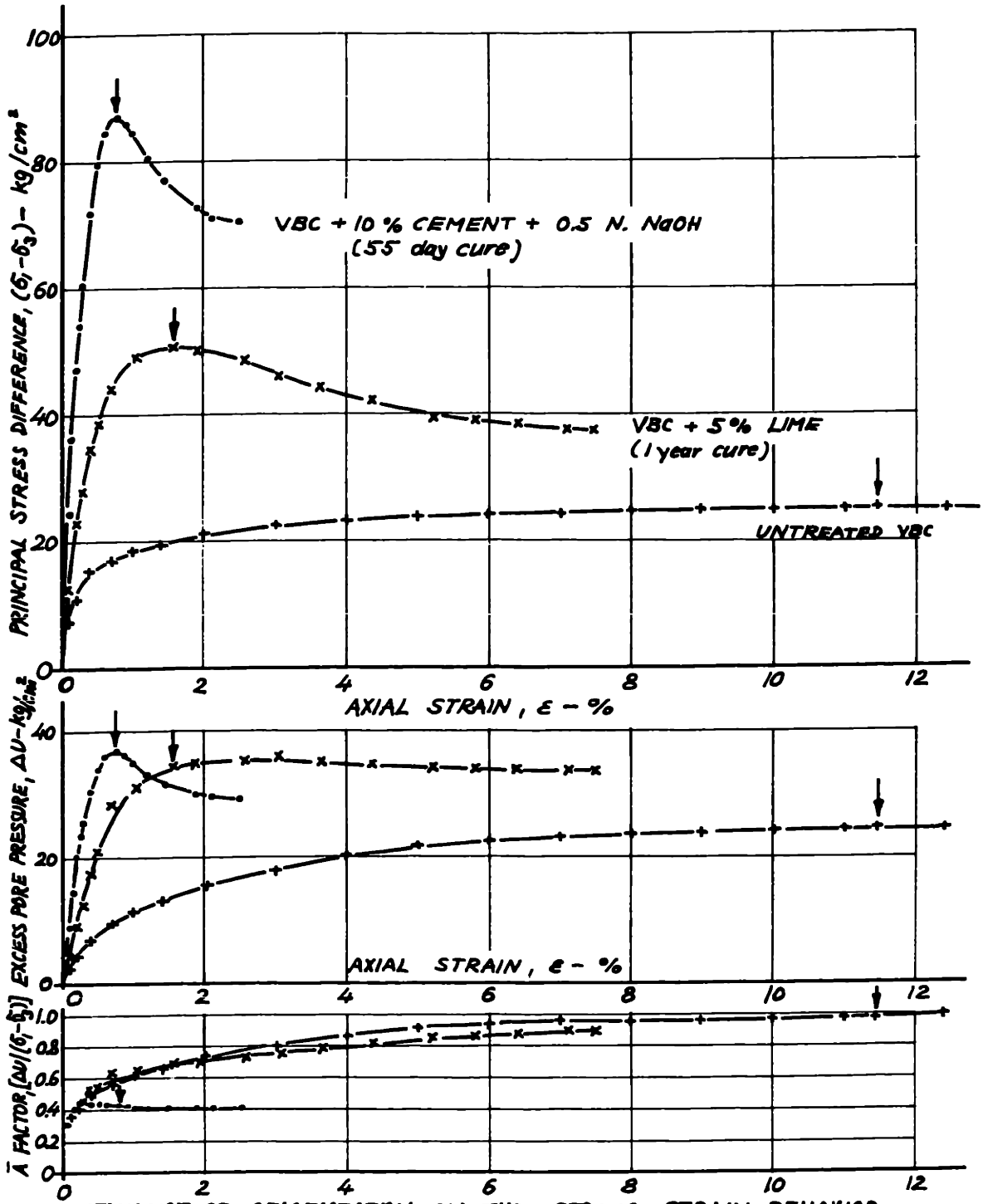

FIG. 7-17. INFLUENCE OF CEMENTATION ON THE STRESS-STRAIN BEHAVIOR OF VBC CONSOLIDATED TO 50 kg/cm².

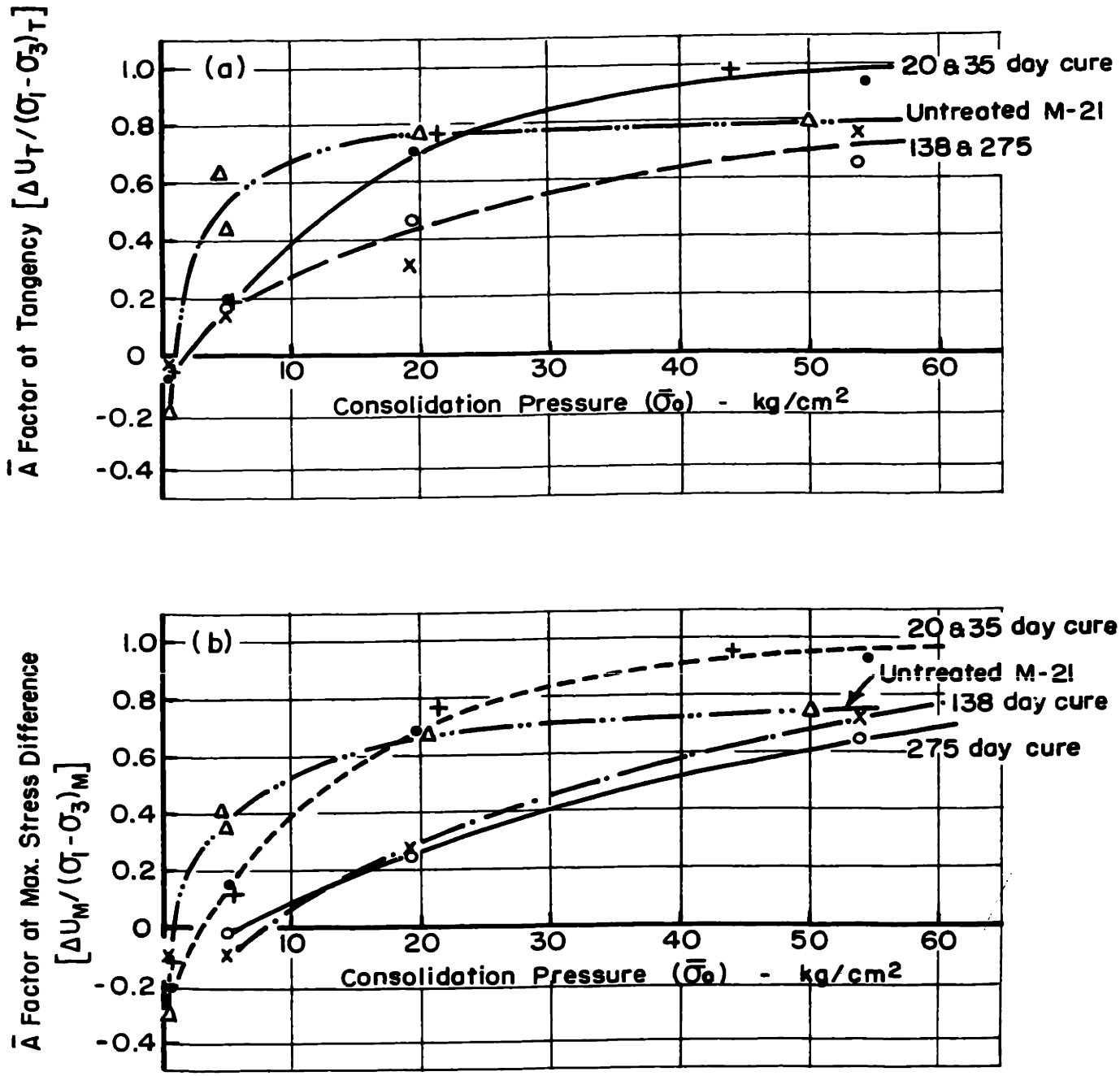

FIGURE 7-18. $\bar{A}$ FACTORS vs CONSOLIDATION PRESSURE FOR M-21 + 5% LIME

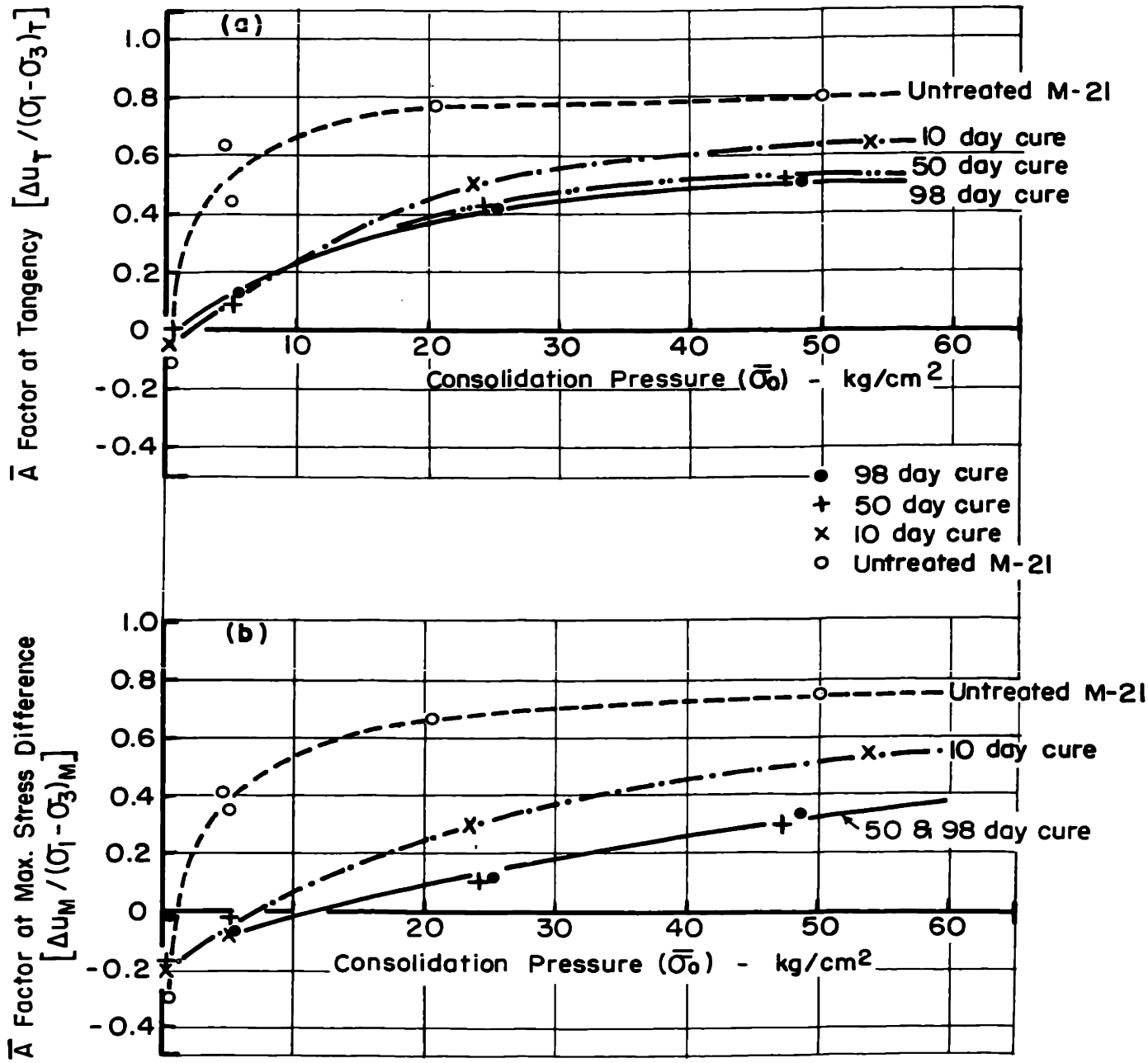

FIGURE 7-19. $\bar{A}$ FACTOR vs CONSOLIDATION PRESSURE FOR M-21 + 5% CEMENT

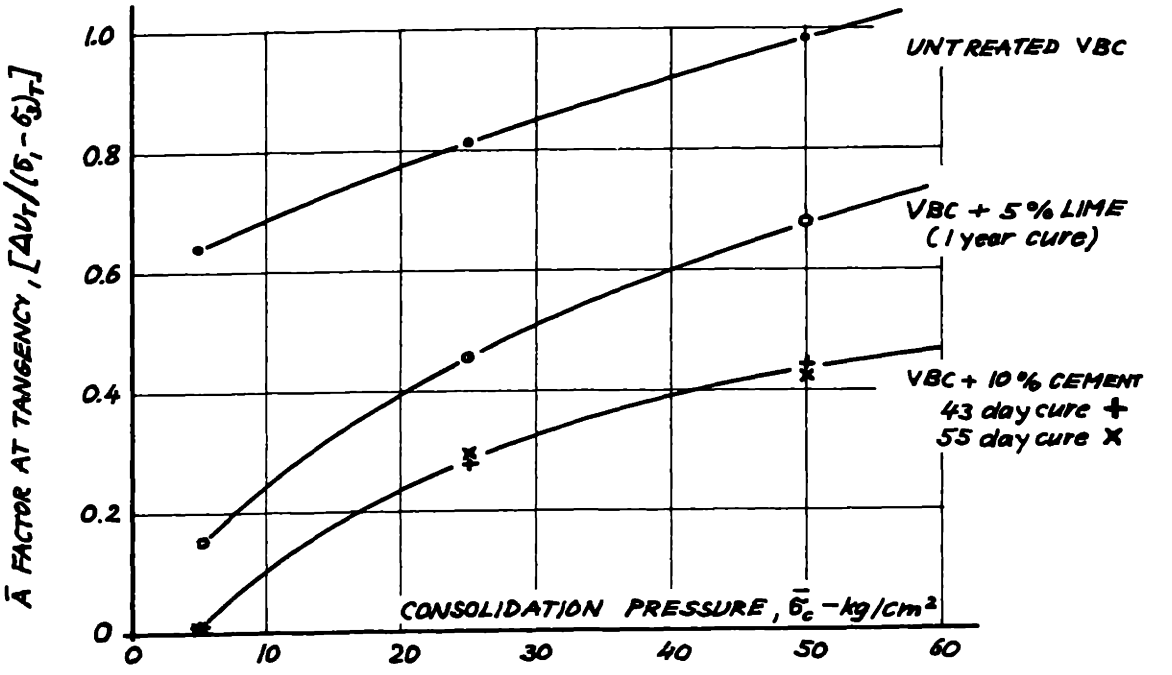

FIG. 7-20a. INFLUENCE OF CEMENTATION ON THE $\bar{A}$ FACTOR OF VICKSBURG BUCKSHOT CLAY AT TANGENCY

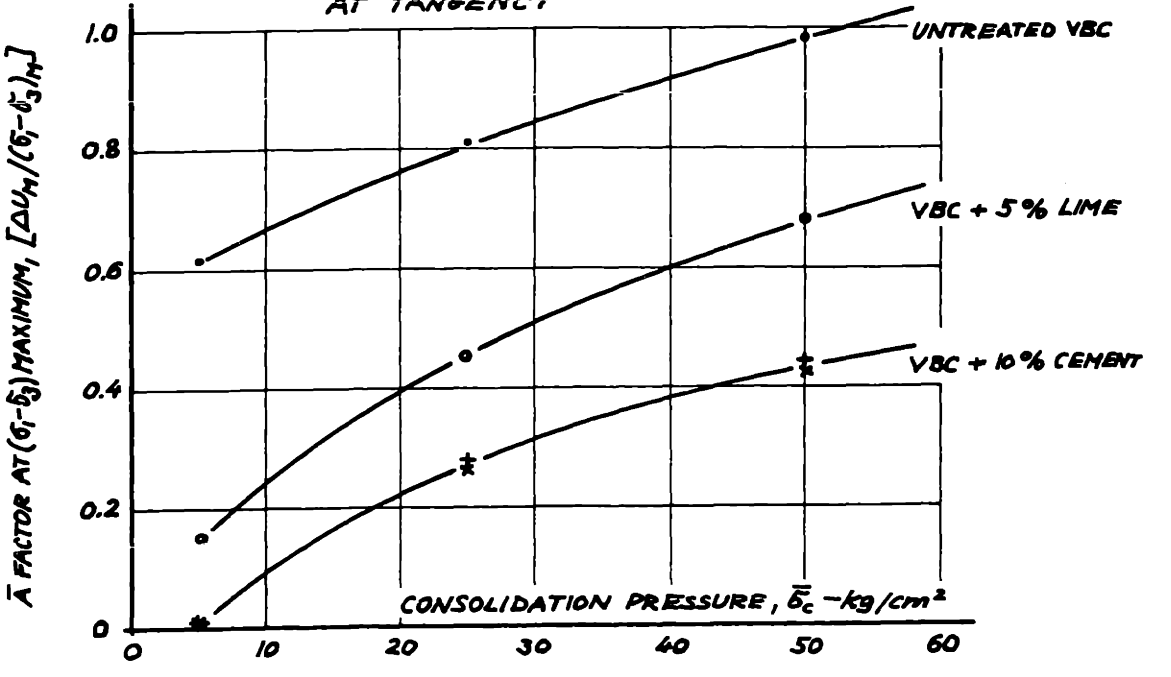

FIG. 7-20b. INFLUENCE OF CEMENTATION ON THE $\bar{A}$ FACTOR OF VICKSBURG BUCKSHOT CLAY AT $(\sigma_1 - \sigma_3)$ MAX.

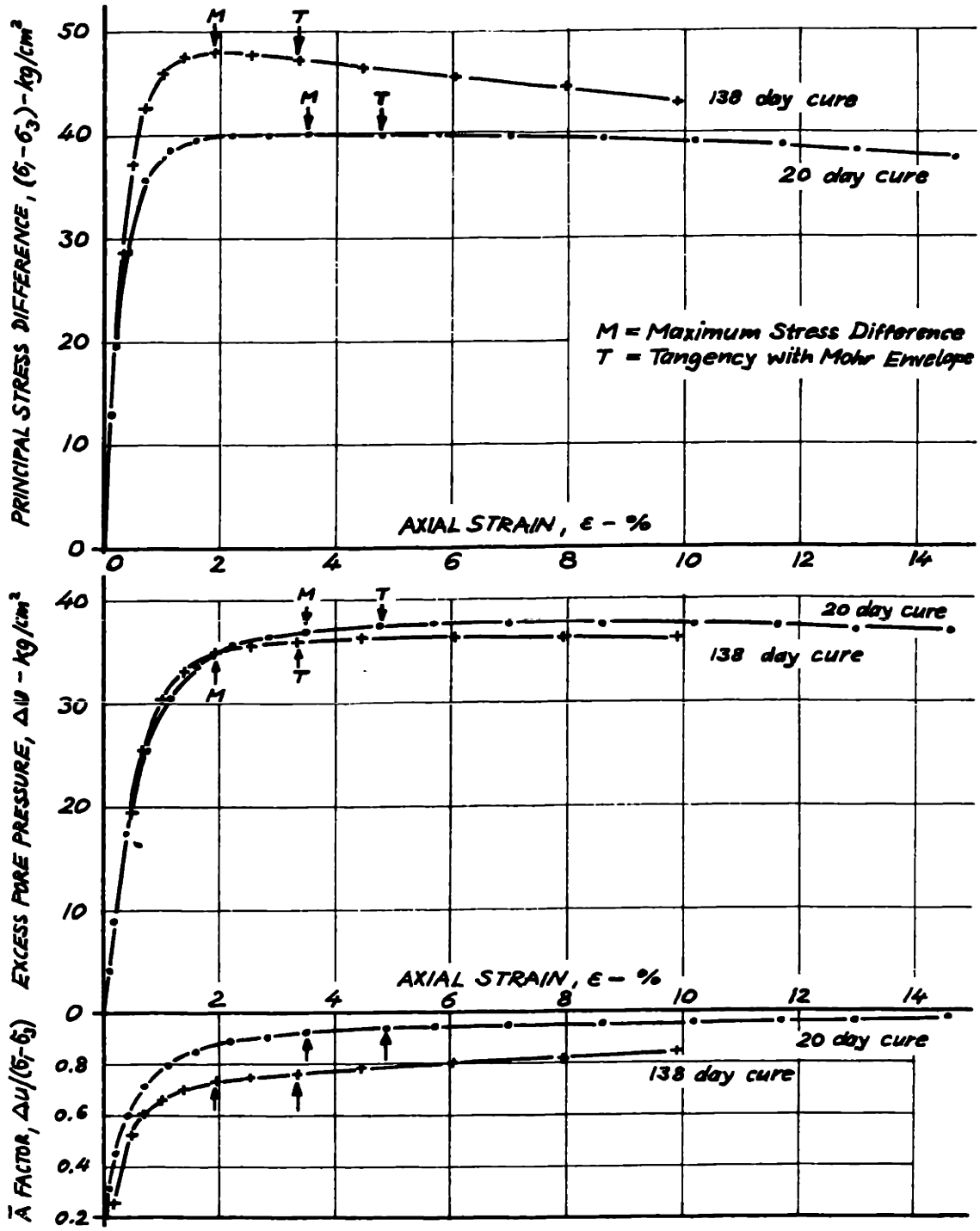

FIG. 7-21. INFLUENCE OF CURING TIME ON THE STRESS-STRAIN BEHAVIOR OF M-21 CEMENTED WITH 5% LIME (Consolidation Pressure = 54 ± 0.2 kg/cm²).

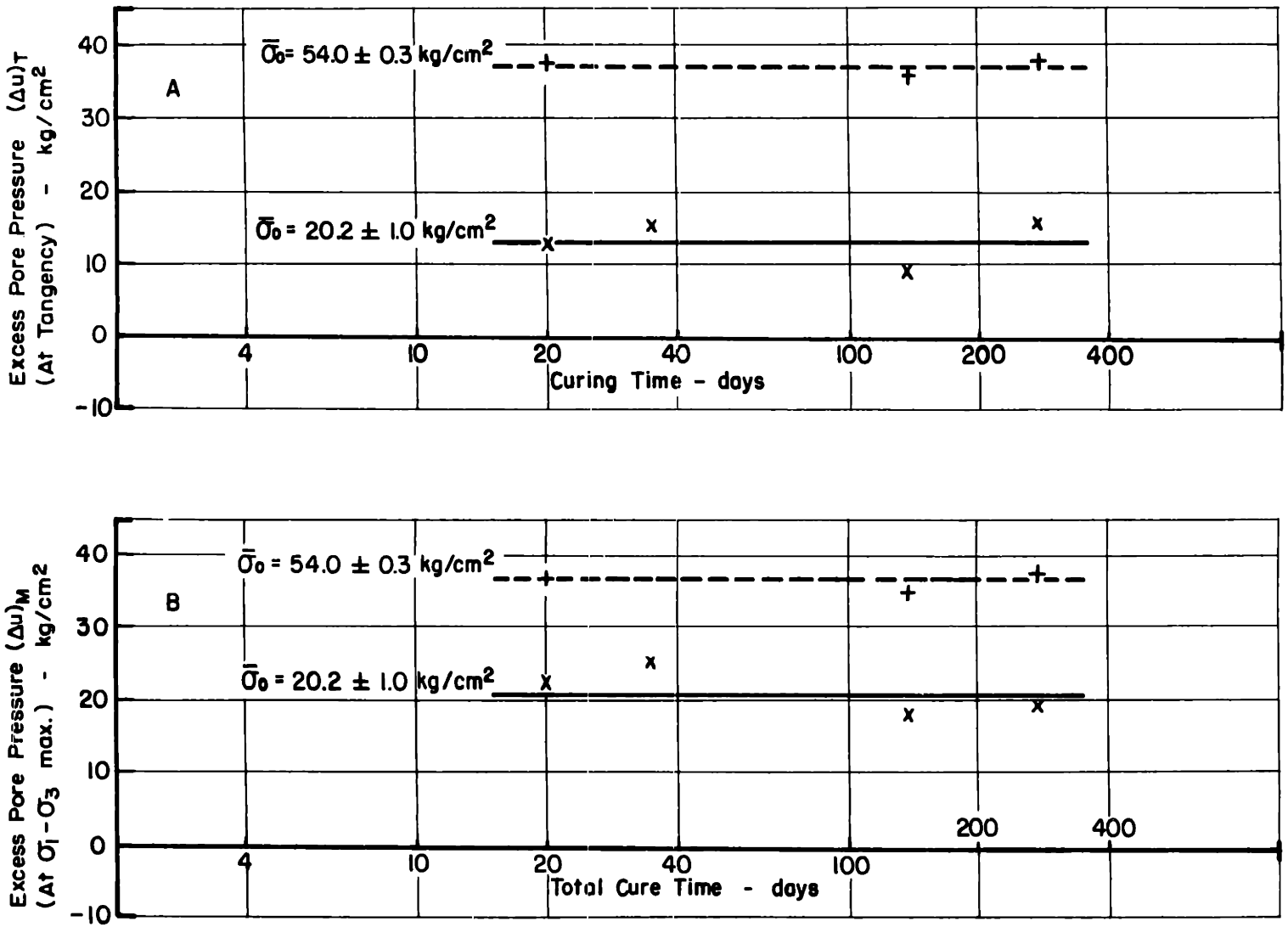

FIGURE 7-22. VARIATION OF EXCESS PORE PRESSURE WITH TOTAL CURE TIME FOR M-21 + 5% LIME AT HIGH CONSOLIDATION PRESSURES

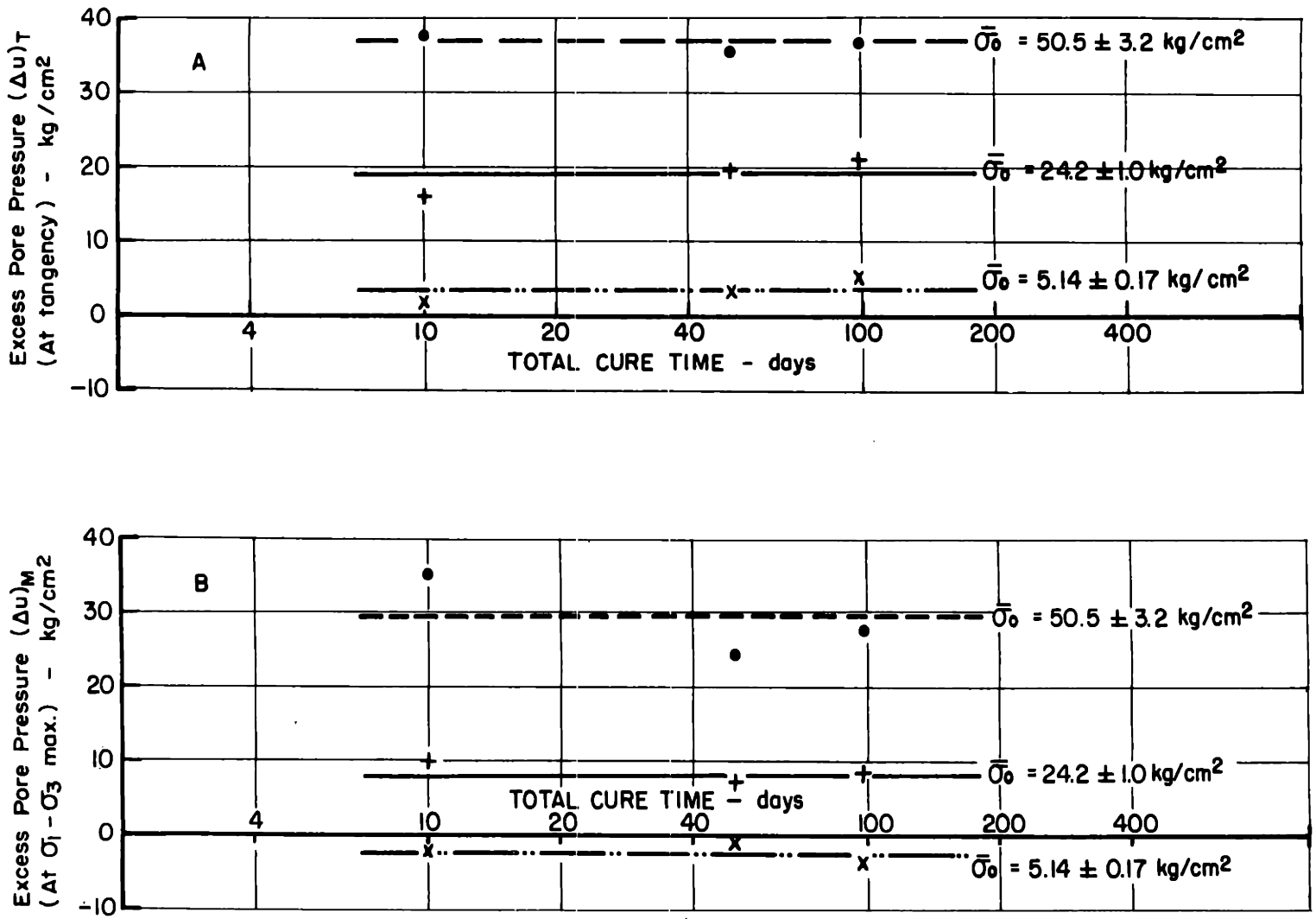

FIGURE 7-23. VARIATION OF EXCESS PORE PRESSURE WITH TOTAL CURE TIME FOR M-21 + 5% CEMENT

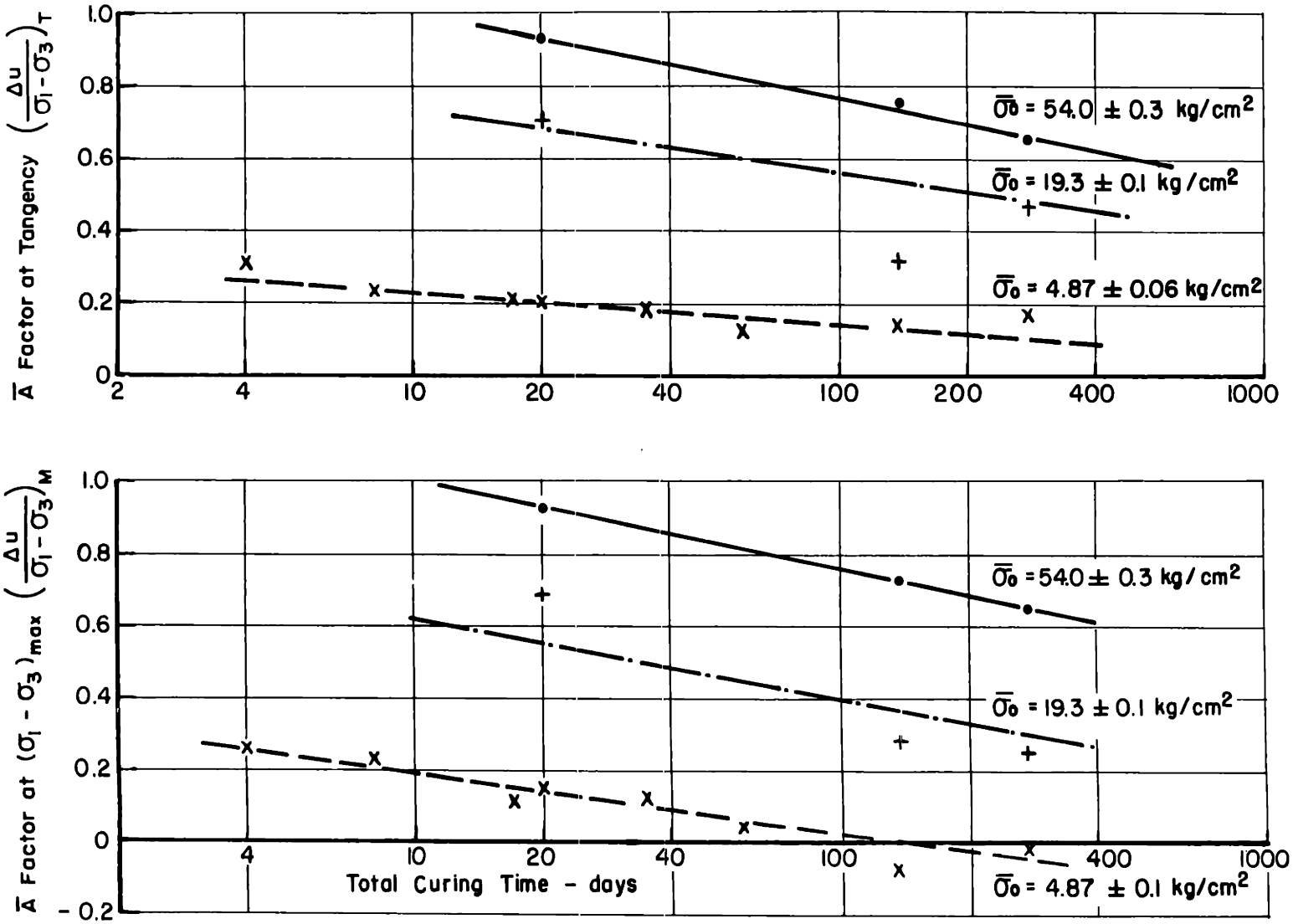

FIGURE 7-24. EFFECT OF TOTAL CURE TIME ON $\bar{A}$ FACTORS OF M-21 + 5% LIME

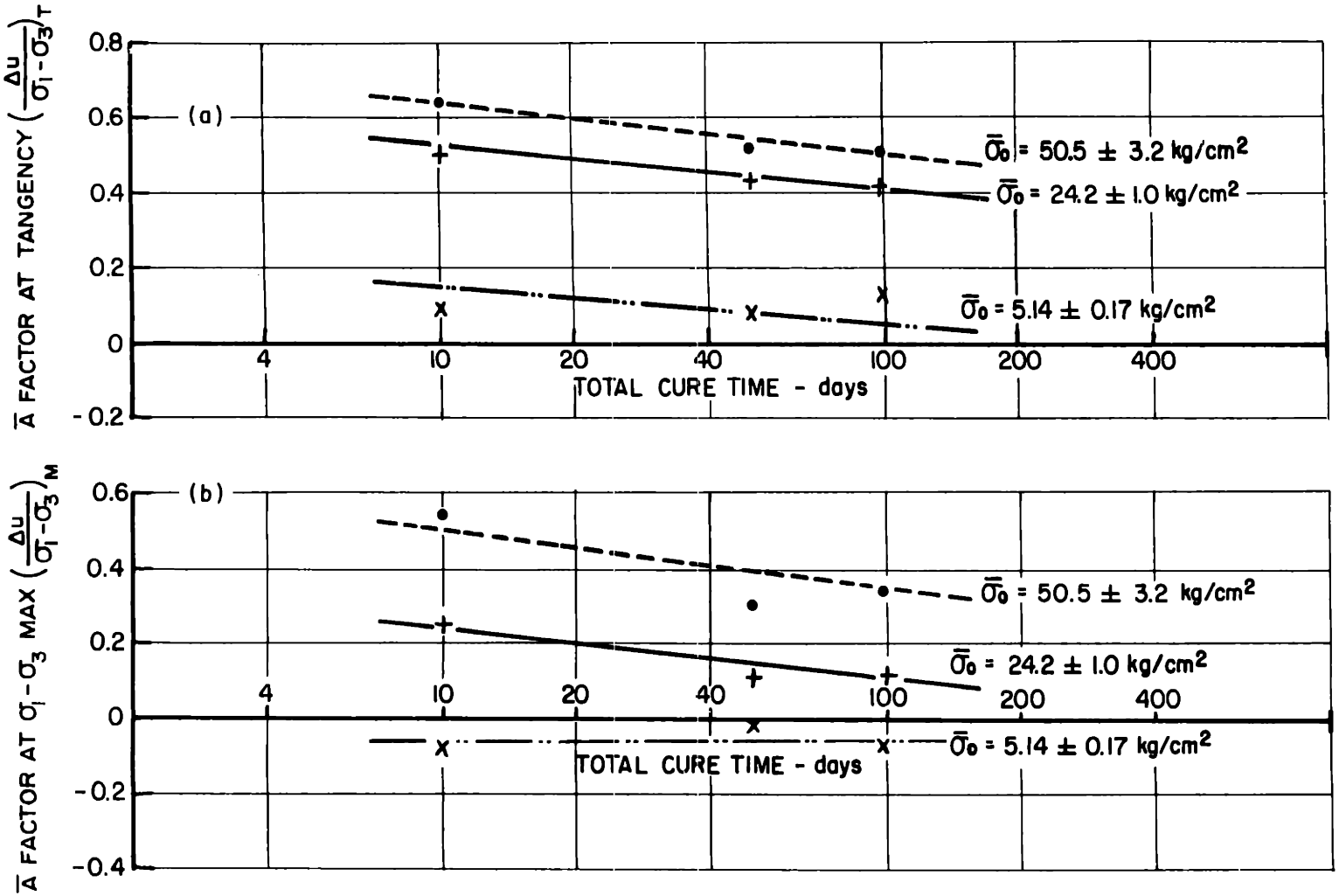

FIGURE 7-25. EFFECT OF TOTAL CURE TIME ON $\bar{A}$ FACTORS OF M21 + 5% CEMENT

FIGURE 7-26. VARIATION OF EXCESS PORE PRESSURE WITH TOTAL CURE TIME FOR M-21+ 5% LIME - (low consolidation pressures only)

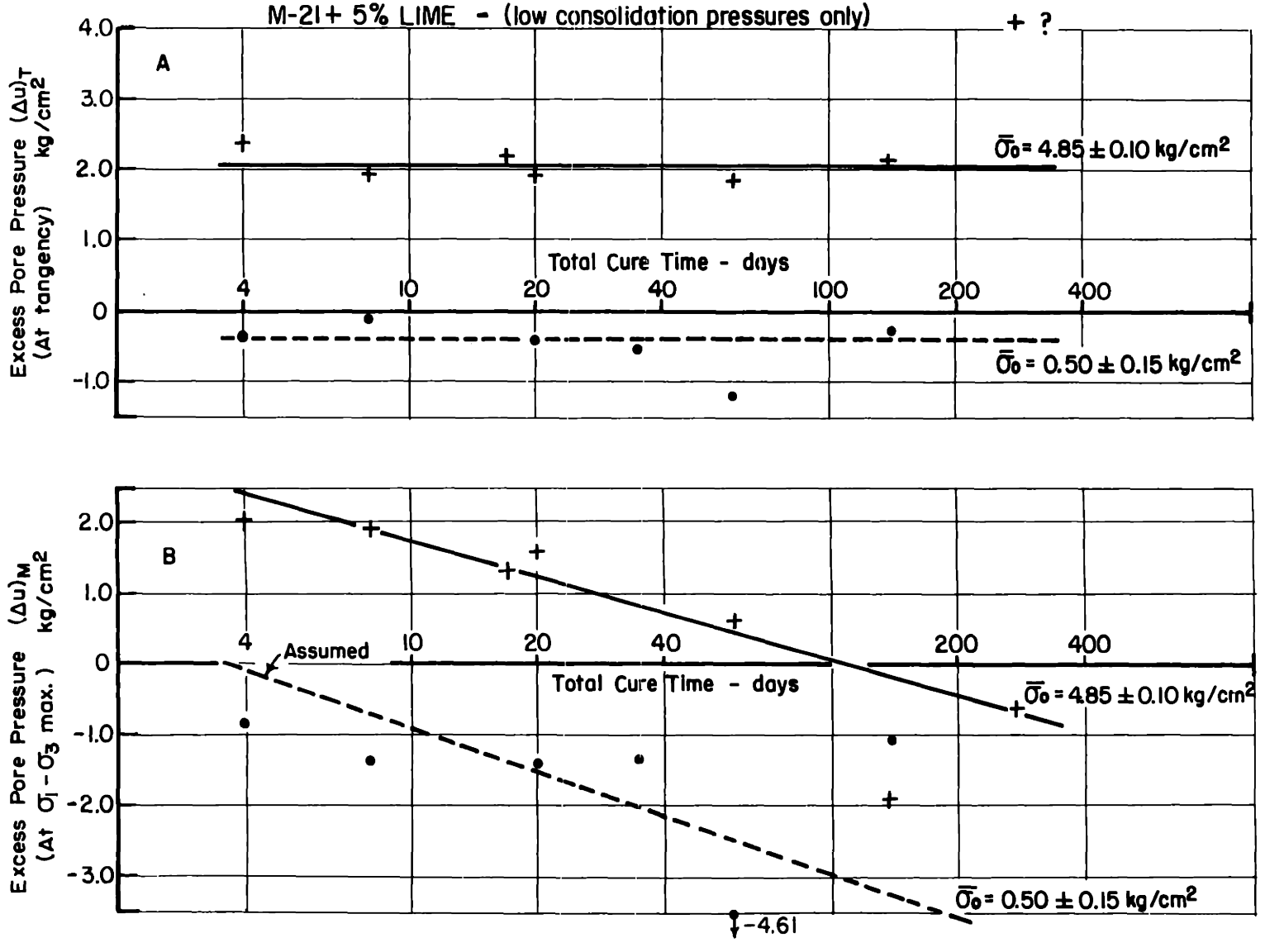

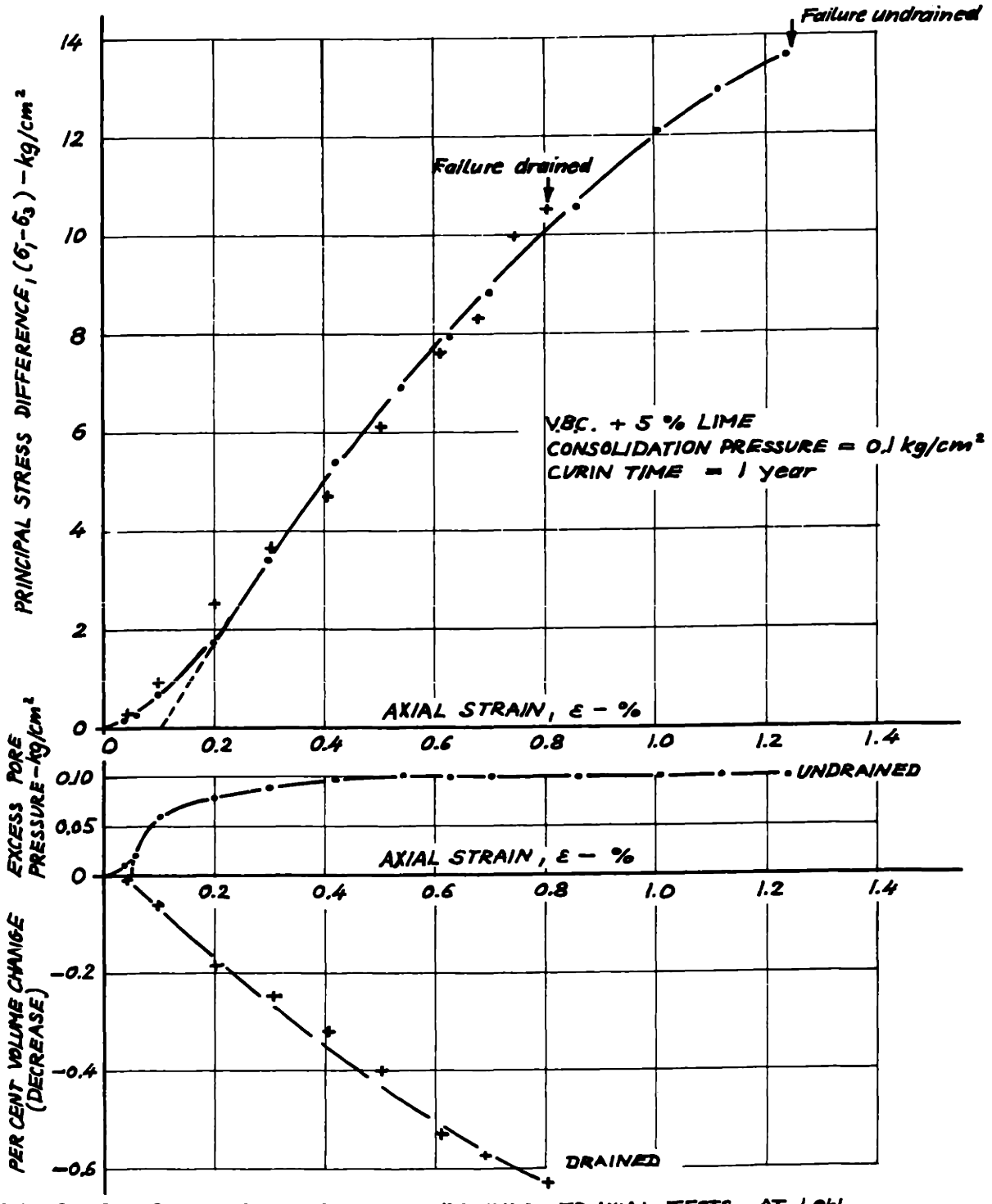

FIG. 7-27. COMPARISON OF DRAINED AND UNDRAINED TRIAXIAL TESTS AT LOW CONSOLIDATION PRESSURES FOR A CEMENTED SOIL.

Chapter 8

SHEAR STRENGTH OF STABILIZED SOILS

8.1 Introduction

The shear strength of a soil is usually defined as the maximum shear stress which can be carried on the failure plane. Its magnitude is therefore dependent on the assumed orientation of the failure plane with respect to the principal planes since:

$$s = (\sigma_1 - \sigma_3)_M \sin\theta \cos\theta \qquad (8.1)$$

where s = the shear strength

$(\sigma_1 - \sigma_3)_M$ = the maximum principal stress difference

θ = the angle of inclination of the assumed failure plane with respect to the major principal plane

If the Mohr-Coulomb criterion of failure is assumed, then

$$\theta = 45^\circ + \phi/2 \qquad (8.2)$$

where ϕ = the angle whose tangent is equal to the slope of Mohr-Coulomb envelope

and $$s = \frac{1}{2}(\sigma_1 - \sigma_3)_M \cos\phi \qquad (8.3)$$

In drained shear the maximum principal stress difference occurs at point of first tangency with the effective Mohr-Coulomb envelope and ϕ is equal to $\overline{\phi}$, the

effective angle of internal friction. In this case s is the drained shear strength of the soil, s_d, and Eq. 8.3 becomes:

$$s_d = \frac{1}{2} (\sigma_1 - \sigma_3)_M \cos \bar{\phi} \qquad (8.3a)$$

In undrained shear the undrained shear strength, s_u, is usually given by the equation:

$$s_u = \frac{1}{2} (\sigma_1 - \sigma_3)_M \cos \phi \qquad (8.3b)$$

where ϕ = the angle whose tangent is equal to the slope of the consolidated-undrained total stress envelope

In Eq. 8.3b ϕ is usually used instead of $\bar{\phi}$ because, more often than not, pore pressures are not measured during undrained shear and therefore $\bar{\phi}$ is unknown. Even when $\bar{\phi}$ is known there is some doubt as to the validity of its use in Eq. 8.3b since in undrained shear the maximum stress difference does not necessarily occur at point of tangency with the effective stress envelope.

To simplify the following presentation of results and discussion of the influence of artificial cementation, the shear strength will be assumed to be equal to half the maximum principal stress difference, q_{max}, i.e., the maximum shear stress on the plane of maximum shear ($\theta = 45^\circ$).

This choice has been made for convenience only and is not intended to suggest that $\bar{\phi}$ and ϕ in Eqs. 8.3a and 8.3b respectively are zero.

The shear strength of an untreated soil is dependent on the effective stress path during shear even though the Mohr-Coulomb effective stress envelope may be independent of the effective stress path. This can be shown by comparing the shear strengths of two identical samples consolidated to the pressure $\bar{\sigma}_o$, and then tested in triaxial compression with σ_3 being kept constant at $\bar{\sigma}_o$ during shear. One sample could be tested in drained shear to get s_d and the other in undrained shear to get s_u. Let it be assumed that both samples have the same effective stress envelope which is given by the equation:

$$q_M = \bar{a} + \bar{p}_M \tan \bar{\alpha} \qquad (8.4)$$

where $q_M = \frac{1}{2}(\sigma_1 - \sigma_3)$ maximum

$\bar{a}$ = the effective cohesion intercept of the Mohr-Coulomb envelope on the p versus q plot*

$\bar{p}_M = \frac{1}{2}(\bar{\sigma}_1 + \bar{\sigma}_3)$ at q_M conditions

$\tan \bar{\alpha}$ = the slope of the effective Mohr-Coulomb envelope on the $\bar{p}$ versus q plot*

*Note that $\bar{a}$ and $\bar{\alpha}$ are uniquely related to $\bar{c}$ and $\bar{\phi}$.

Then the strength of the samples tested in drained shear would be:

$$s_d = (\bar{\sigma}_o \tan \bar{\alpha} + \bar{a}) \frac{1}{1 - \tan \bar{\alpha}} \qquad (8.5)$$

and the strength of the sample tested in undrained shear would for constant σ_3 be:

$$s_u = \left[(\bar{\sigma}_o - \Delta u_M) \tan \bar{\alpha} + \bar{a}\right] \frac{1}{1 - \tan \bar{\alpha}} \qquad (8.6a)$$

where Δu_M = the excess pore pressure at $(\sigma_1 - \sigma_3)_{max.}$

or $$s_u = (\bar{\sigma}_o \tan \bar{\alpha} + \bar{a}) \frac{1}{1 - \tan \bar{\alpha} (1-2\bar{A}_M)} \qquad (8.6b)$$

where $\bar{A}_M$ is the Skempton $\bar{A}$ factor at $(\sigma_1 - \sigma_3)$ max and is equal to $\Delta u_M/(\sigma_1 - \sigma_3)_M$ when $\sigma_3 = \bar{\sigma}_o$ during shear.

It can be seen from the above that, even when the effective stress-strength parameters $\bar{a}$ and $\bar{\alpha}$ (or $\bar{c}$ and $\bar{\phi}$) are the same in drained and undrained shear, the shear strength is dependent on the pore pressures developed during shear, i.e., the effective stress path. Eq. 8.6 also shows that a change in the undrained shear strength, s_u, can be due to either a change in the effective stress-strength parameters, $\bar{a}$ and $\bar{\alpha}$, and/or a change in the excess pore pressure developed during shear.

8.2 Influence of Drainage Conditions on the Strength of Stabilized Soils

8.2.1 Coarse-Grained Soils

In both the untreated and cemented sands the shear strengths in undrained shear were considerably larger than in drained shear mainly due to the very large negative excess pore pressures which developed during undrained shear. It was shown in Art. 5.2 that $\bar{\phi}$ for the untreated sands was not exactly the same in drained and undrained shear even when the stress-dilatancy correstion was applied to the results of the drained tests.* However a few degrees difference in $\bar{\phi}$ has only a negligible effect compared to the large differences in the pore water pressures and therefore effective stress paths during shear.

It should be noted that the undrained shear strength of dense sands is usually only of academic interest since in the field full drainage takes place under most loading conditions or cavitation of the pore water when its pressure approaches zero absolute.

8.2.2 Fine-Grained Soils

To investigate the influence of drainage conditions on the shear strength of stabilized fine-grained soils,

*Strictly speaking, in undrained shear $\bar{\phi}$ at $(\sigma_1 - \sigma_3)$ maximum should be used in Eq. 8.6 instead of $\bar{\phi}$ of the Mohr envelope but the differences between the two values were small (not more than two degrees).

two sets of identical samples of VBC cemented with 5% lime were tested after one year of curing. One set was tested in undrained shear whereas the other set was tested in drained shear. Both sets had about the same effective stress-strength envelopes but the strengths were considerably different as can be seen from Fig. 8-1. At the lowest consolidation pressure of 0.1 kg/cm^2 the undrained sample was stronger than the drained sample because negative excess pore pressures probably started to develop within the undrained sample as $(\sigma_1 - \sigma_3)$ maximum was reached. At the higher consolidation pressures the drained strengths were considerably higher than the undrained strengths because of the large positive excess pore pressures which developed during undrained shear. The rate of increase in strength with increasing consolidation pressure was lower for the undrained tests because Δu_M increased with increasing consolidation pressure.

The results in Fig. 8-1 clearly show that drainage conditions during shear have a major influence on the strength behavior of stabilized soils. This is similar to the effect of drainage conditions on the strength behavior of untreated soils. It is therefore essential to take into consideration drainage conditions during shear when determining the strength of a stabilized soil.

8.3 Influence of Consolidation Pressure on the Undrained Shear Strength

Both the untreated and the stabilized fine-grained soils showed an increase in undrained shear strength with increasing consolidation pressure as shown in Figs. 8-2 through 8-4.

At the higher consolidation pressures the increase in s_u was directly proportional to the increase in $\bar{\sigma}_o$ because $\bar{a}$ and $\bar{\alpha}$ were independent of consolidation pressure provided the curing time was kept constant, and the excess pore pressure, Δu_M, increased linearly with increasing $\bar{\sigma}_o$ (see Figs. 7-14 through 7-16). The net effect was therefore a linear increase in $(\bar{\sigma}_o - \Delta u_M)$ with increasing consolidation pressure such that s_u in Eq. 8-6a increased linearly with increasing $\bar{\sigma}_o$.

It should be noted that to be consistent the values in Eqs. 8.6a for $\bar{\alpha}$ and $\bar{a}$ should represent conditions at $(\sigma_1 - \sigma_3)_M$* and not at tangency. The slopes of the effective stress-strength relations at $(\sigma_1 - \sigma_3)_M$ were the same as at $(\sigma_1 - \sigma_3)_T$ which can be seen by comparing the $\bar{\alpha}$ values in Figs. 5-31 and 5-32 with the corresponding $\bar{\alpha}_M$ values given in Figs. 8-5a and 8-5b for the various M-21 systems. The cohesion intercepts $\bar{a}_M$ were usually

*Subscript M represents conditions at $(\sigma_1 - \sigma_3)$ maximum whereas subscript T represents conditions at point of first tangency with the effective Mohr-Coulomb envelope.

lower than $\bar{a}_T$ but the excess pore pressures at $(\sigma_1 - \sigma_3)_M$ were also lower than at tangency. The decrease in strength at $(\sigma_1 - \sigma_3)_M$ due to lower $\bar{a}_M$ values was less important than the increase in strength due to the lower excess pore pressures which accounts for the lower $(\sigma_1 - \sigma_3)$ values at tangency (Figs. 8-2 through 8-4 also show plots of $(\sigma_1 - \sigma_3)_T$ versus consolidation pressure).

The linear relations between undrained shear strength and consolidation pressure which existed at the higher consolidation pressures did not exist at the low consolidation pressure because of the effects of premature fracture and/or small variations in molding conditions which at these low pressures caused a large scatter in the pore pressure behavior.*

For a given soil-stabilizer system the increase in s_u with increasing $\bar{\sigma}_o$ was independent of curing time because $\bar{\alpha}$ and Δu were essentially independent of curing time. At any given consolidation pressure the increase in strength with increasing curing time was solely due to the increase in $\bar{a}$ with increasing curing time and $\bar{a}$ is independent of consolidation pressure.

Fig. 8-6 shows the influence of cycles of wet-dry on the undrained shear strength of VBC stabilized with

*The erratic pore pressure behavior was also caused by partial drainage as discussed in Art. 7.4.

10% cement. The decrease in strength due to cycling was most pronounced at the lower consolidation pressures. Cycling caused a decrease in $\bar{a}$ without altering $\bar{\alpha}$ at the higher consolidation pressures but at the lower pressures both $\bar{a}$ and $\bar{\alpha}$ were affected which in part accounts for the different rates of increase in s_u with increasing $\bar{\sigma}_o$. Cycling also affected the change in Δu_M with $\bar{\sigma}_o$ which also influenced the rate of increase in s_u with increasing $\bar{\sigma}_o$.

8.4 Influence of Curing Time on the Undrained Shear Strength

The influence of curing time on the undrained shear strength of M-21 stabilized with 5% lime and 5% cement respectively is shown in Figs. 8-7 and 8-8. At the higher consolidation pressures the undrained shear strengths increased linearly with increasing log. curing time because the increase in strengths were solely due to the increase in cohesion intercept, $\bar{c}$, which increased linearly with log. curing time.* The rates of increase in strength with increasing curing time were independent of consolidation pressure because $\bar{a}$ is independent of consolidation pressure.

---

*Note that Δu_M and Δu_T at a given consolidation pressure were independent of curing time.

At low consolidation pressures the effects of premature fracture, molding variations, and drainage caused the results to be erratic.

8.5 Unconfined Shear Strength

In the case of the stabilized soils, the unconfined shear strength, i.e., half the unconfined compressive strength, was obtained on samples which had been subjected to unconfined soaking in water for a number of days prior to testing and therefore the samples were at zero consolidation pressure prior to shear. The main difference between the unconfined compression samples and the corresponding triaxial samples consolidated to near zero pressure was the degree of saturation. The triaxial samples were completely saturated by a back pressure whereas soaking of the unconfined samples produced degrees of saturation ranging from 87% to 97%. The low degrees of saturation of the unconfined samples caused them to have lower B factors and therefore numerically smaller negative pore pressures at $(\sigma_1 - \sigma_3)$ max which in turn caused them to have lower strengths.

In Figs. 8-9 and 8-10 are plotted the effective cohesion intercepts of the Mohr-Coulomb envelopes and the unconfined shear strengths, P/2A, of the M-21 systems as a function of curing time. There was no direct relation between $\bar{c}$ and P/2A because the degree of saturation

of the unconfined samples prior to shear varied considerably. There was however a definite trend for $\bar{c}$ to increase as P/2A increased because the unconfined shear strength is in part due to cohesion.

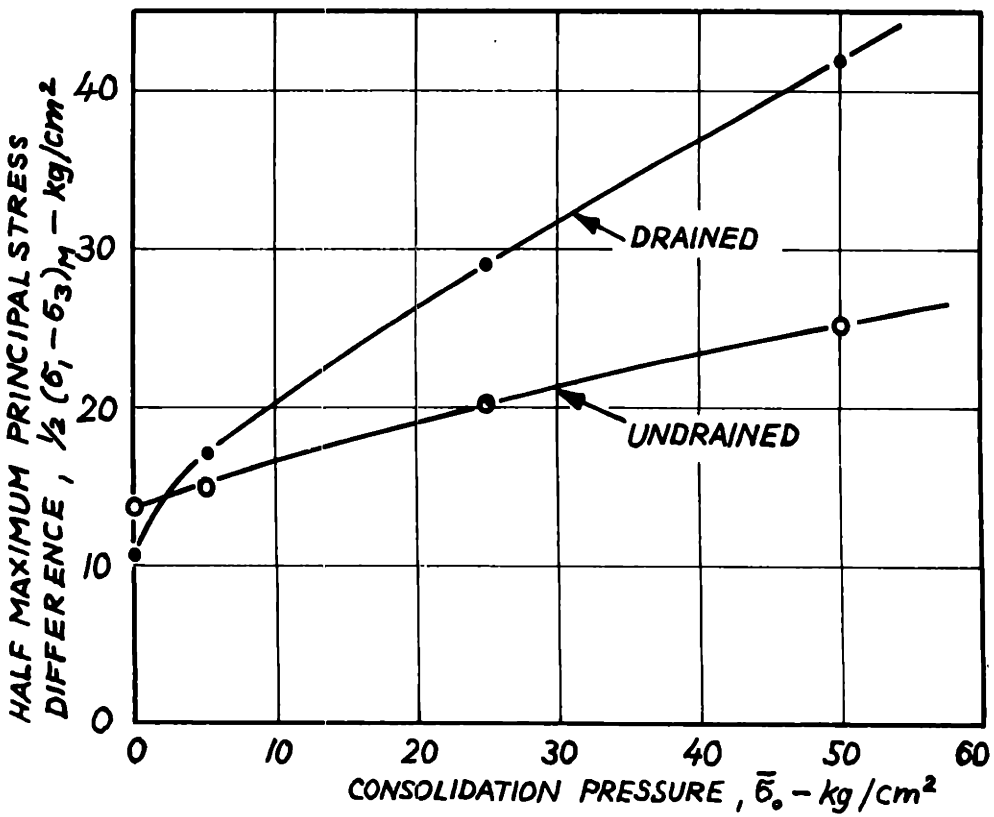

FIG. 8-1. INFLUENCE OF DRAINAGE CONDITIONS ON THE MAXIMUM SHEAR STRENGTH OF VICKSBURG BUCKSHOT CLAY STABILIZED WITH 5% LIME AND CURED FOR ONE YEAR.

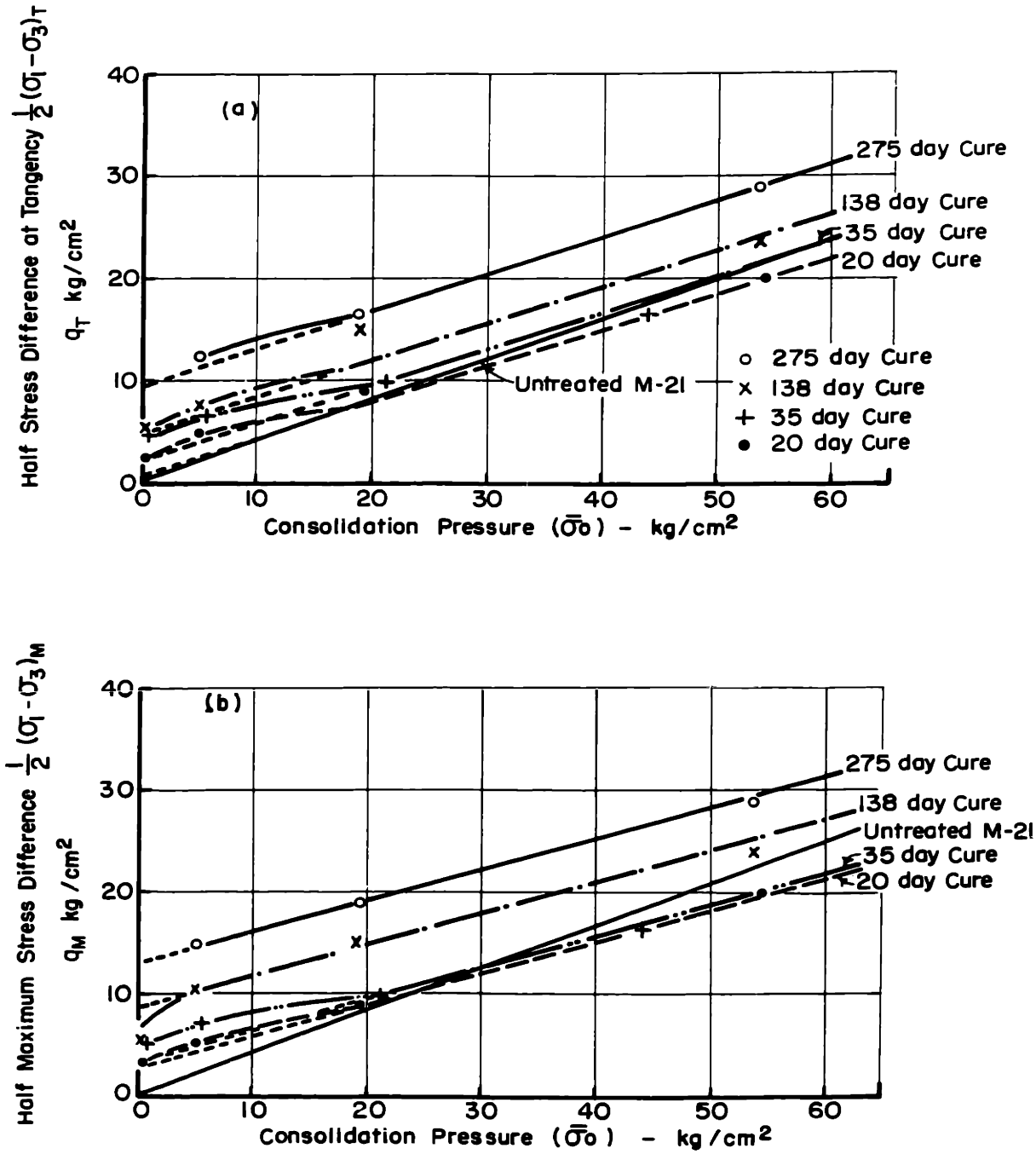

FIGURE 8-2. STRESS DIFFERENCE vs CONSOLIDATION PRESSURE FOR M-21 + 5% LIME

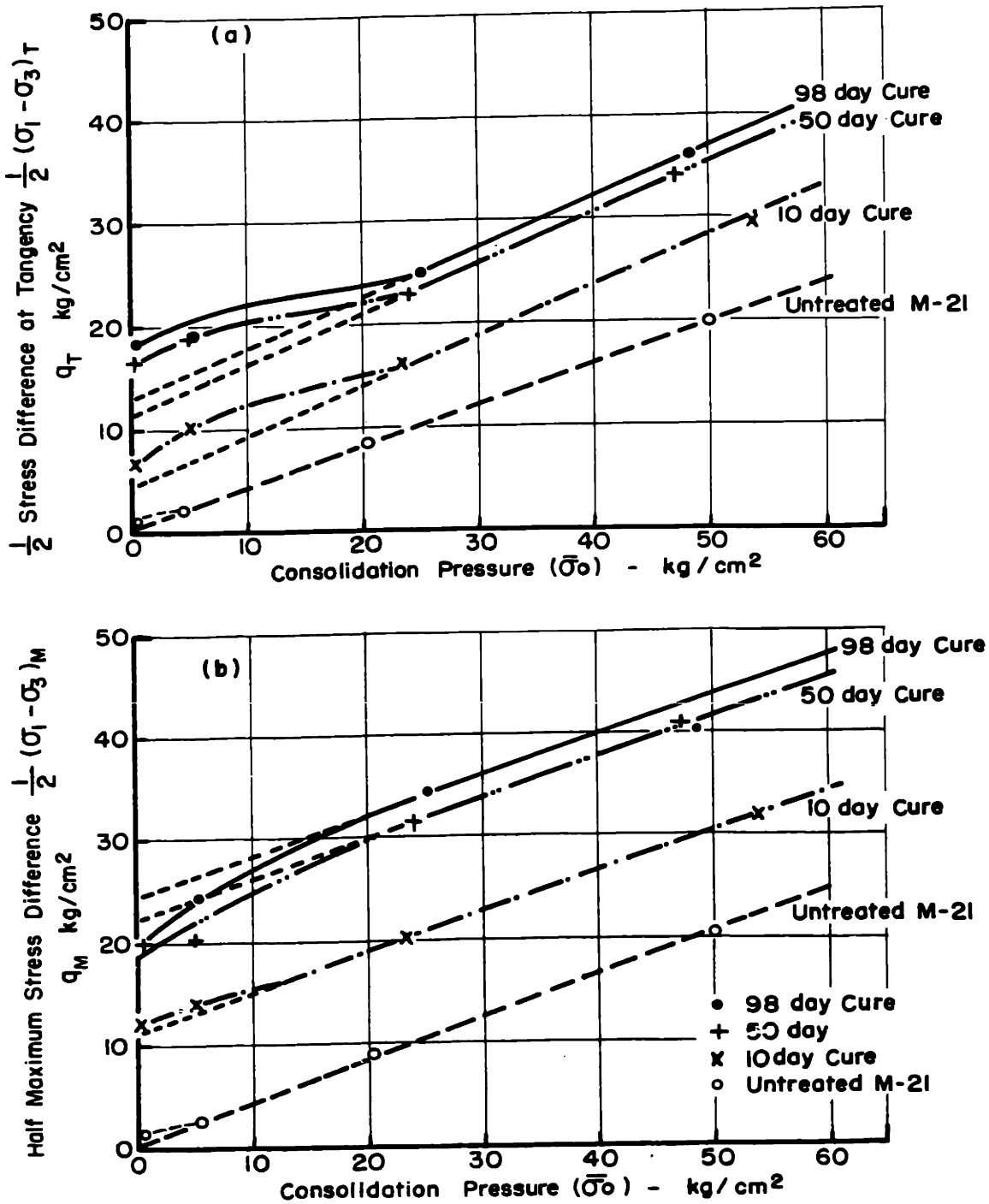

FIGURE 8-3. STRESS DIFFERENCES vs CONSOLIDATION PRESSURE FOR M-21 + 5% CEMENT

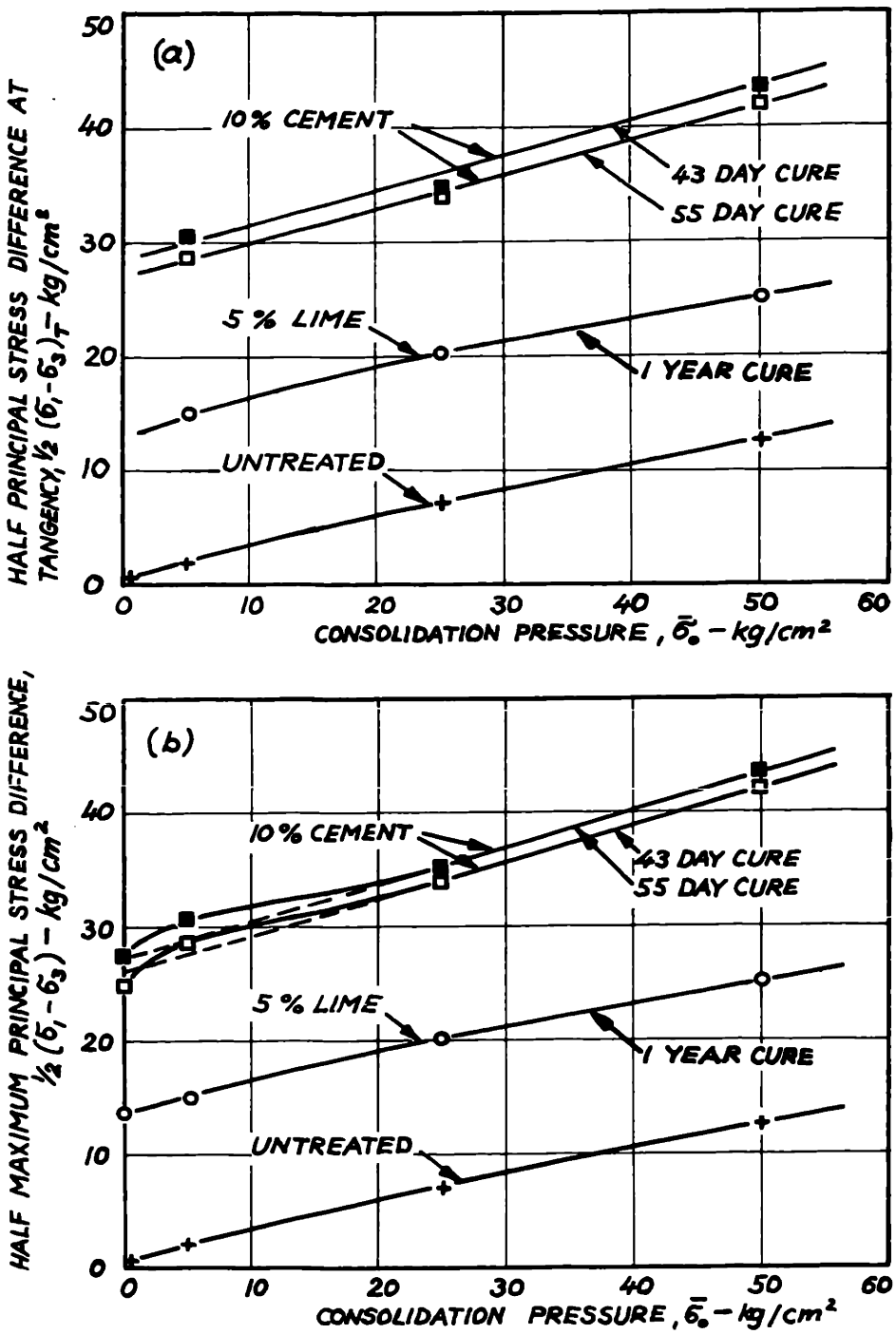

FIG. 8-4. *STRESS DIFFERENCES VERSUS CONSOLIDATION PRESSURE FOR VICKSBURG BUCKSHOT CLAY SYSTEMS.*

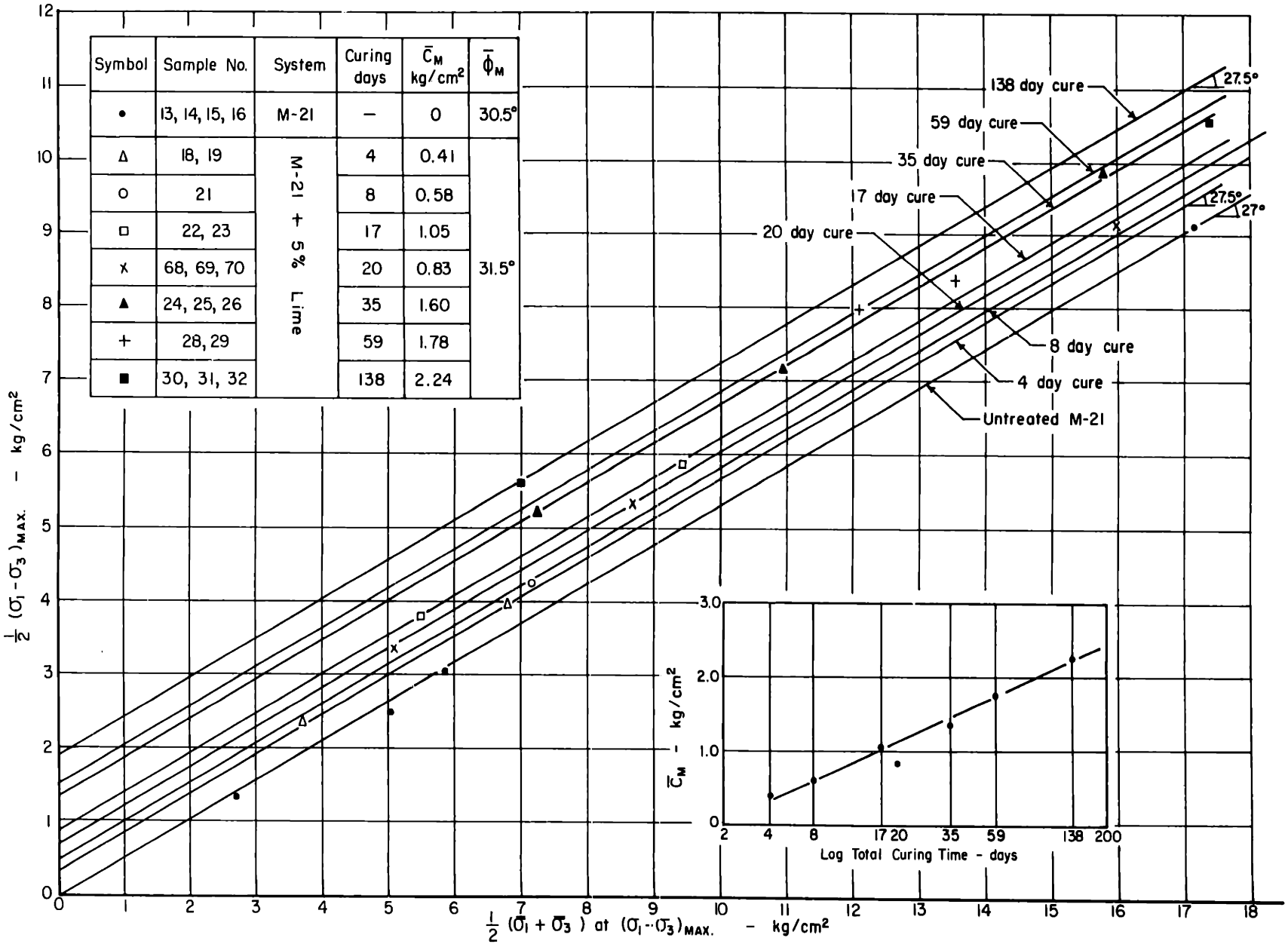

FIGURE 8-5a. EFFECTIVE STRESS-STRENGTH RELATIONS AT MAXIMUM STRESS DIFFERENCE FOR UNTREATED M-21 AND M-21 STABILIZED WITH FIVE PER CENT LIME (see Fig. 8-5b for results of higher effective stresses)

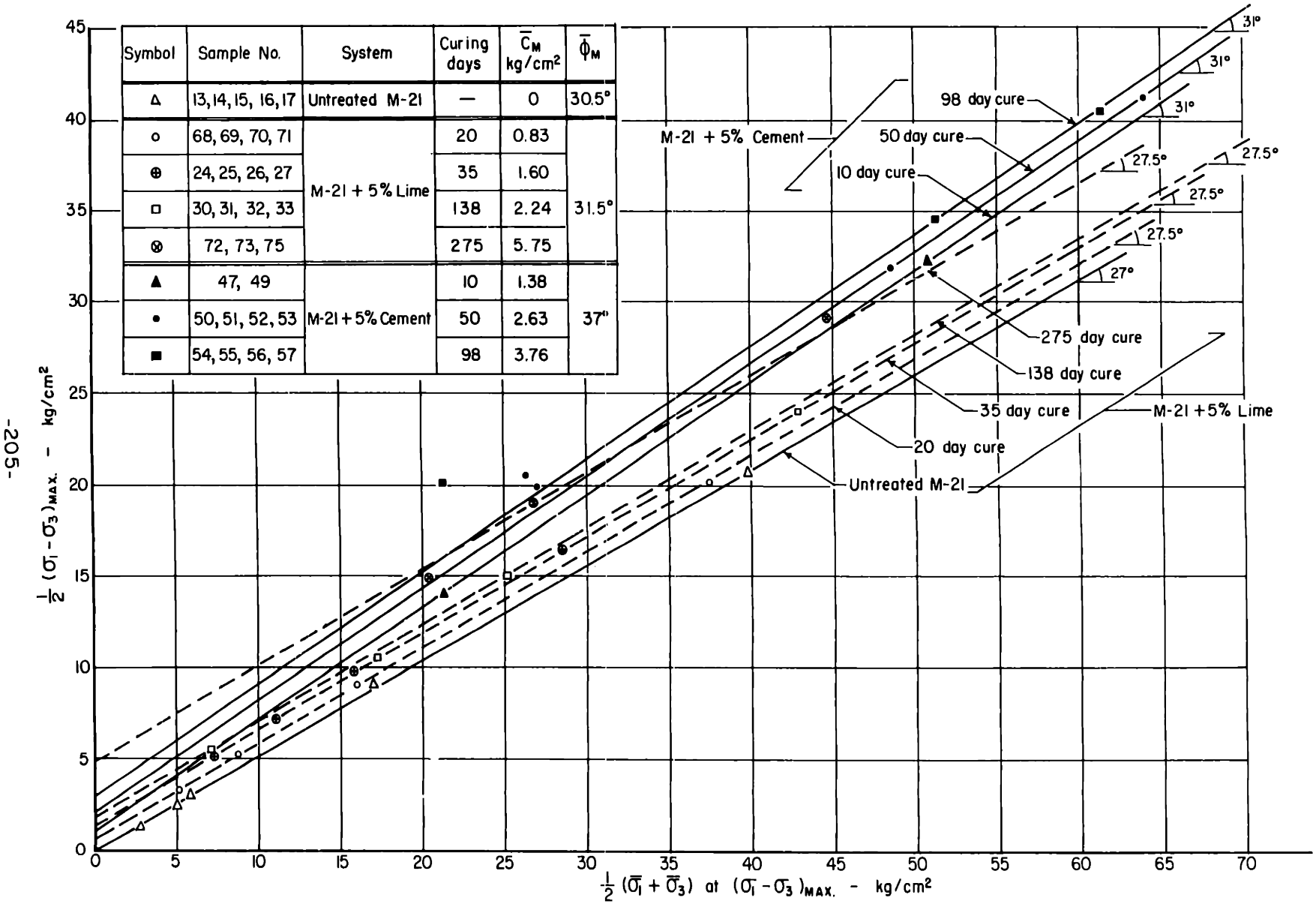

FIGURE 8-5b. EFFECTIVE STRESS-STRENGTH RELATIONS AT MAXIMUM STRESS DIFFERENCE FOR M-21 STABILIZED WITH FIVE PER CENT LIME AND FIVE PER CENT CEMENT RESPECTIVELY

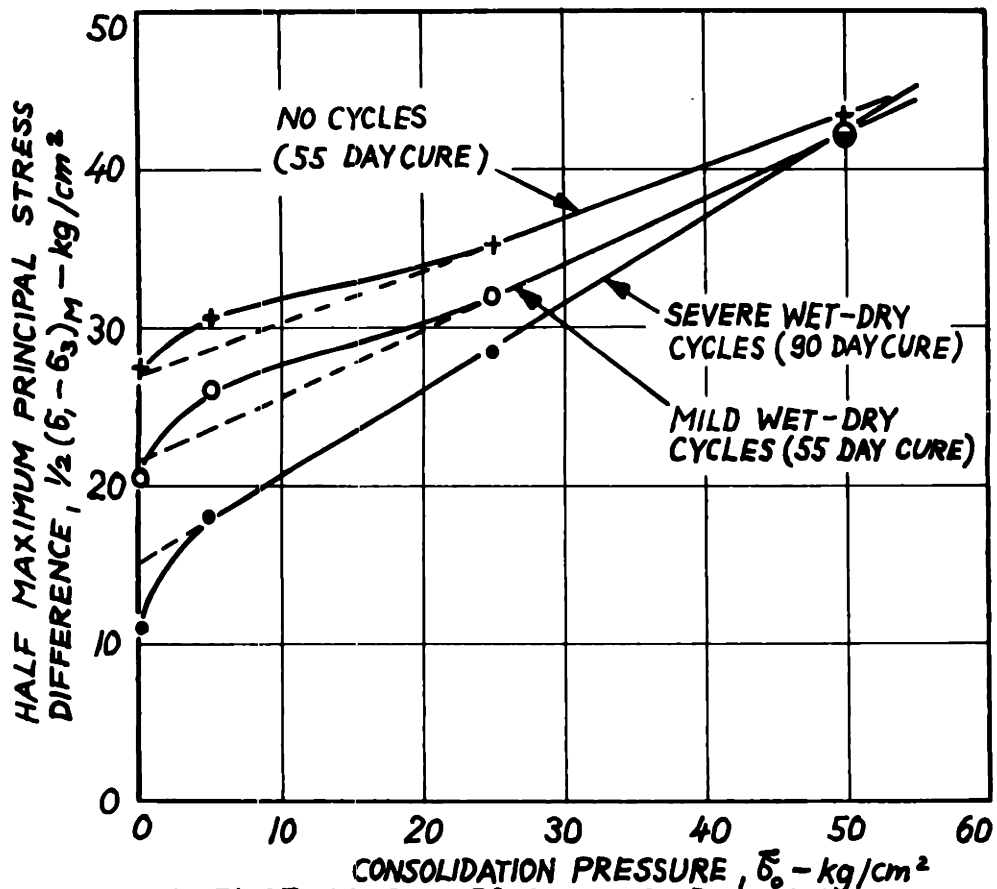

FIG. 8-6. INFLUENCE OF CYCLES OF WET-DRY ON THE UNDRAINED STRENGTH OF VICKSBURG BUCKSHOT CLAY STABILIZED WITH 10 % CEMENT.

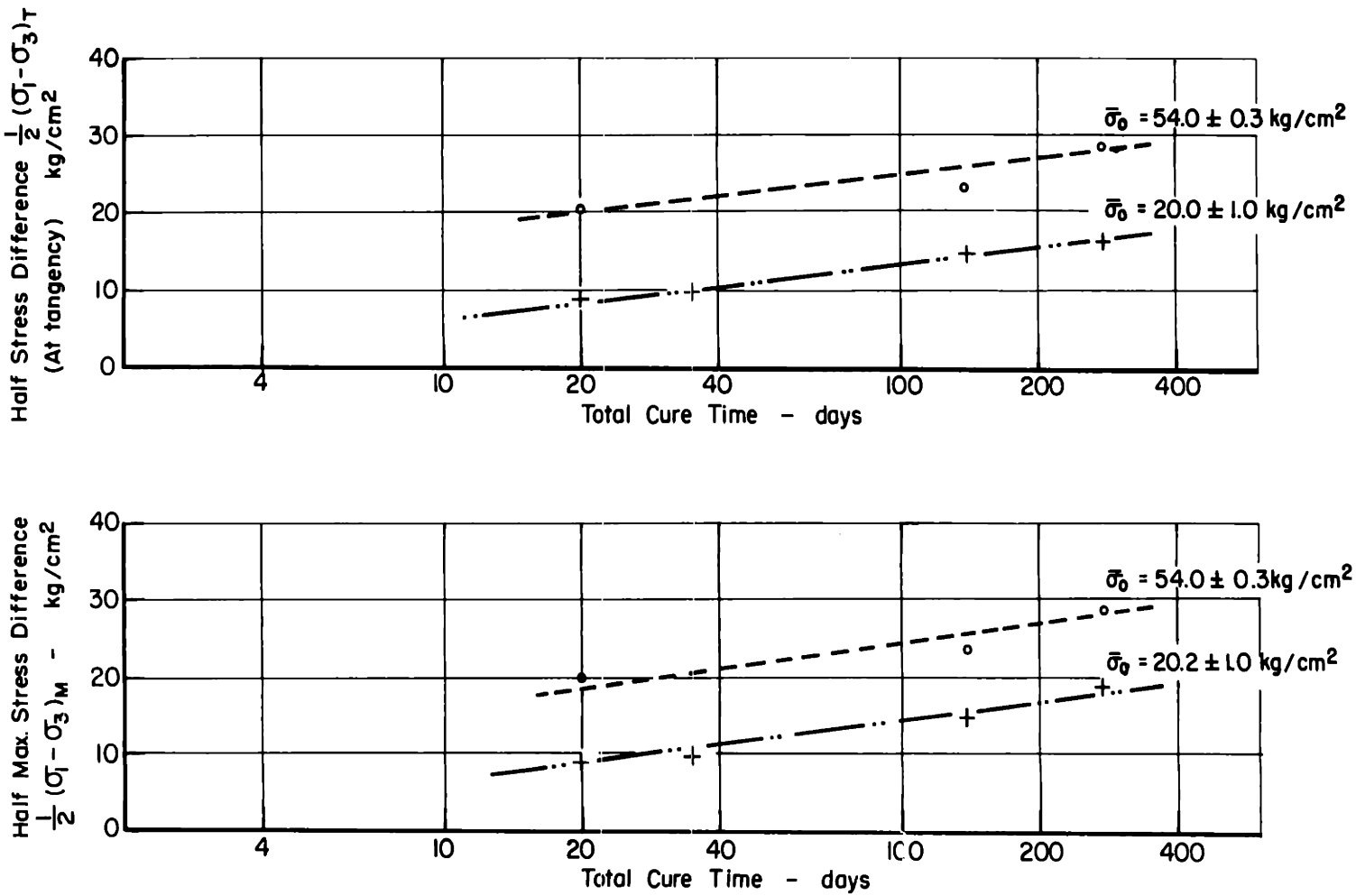

FIGURE 8-7. EFFECT OF TOTAL CURE TIME ON STRESS DIFFERENCES OF M-21 + 5% LIME AT HIGH CONSOLIDATION PRESSURES

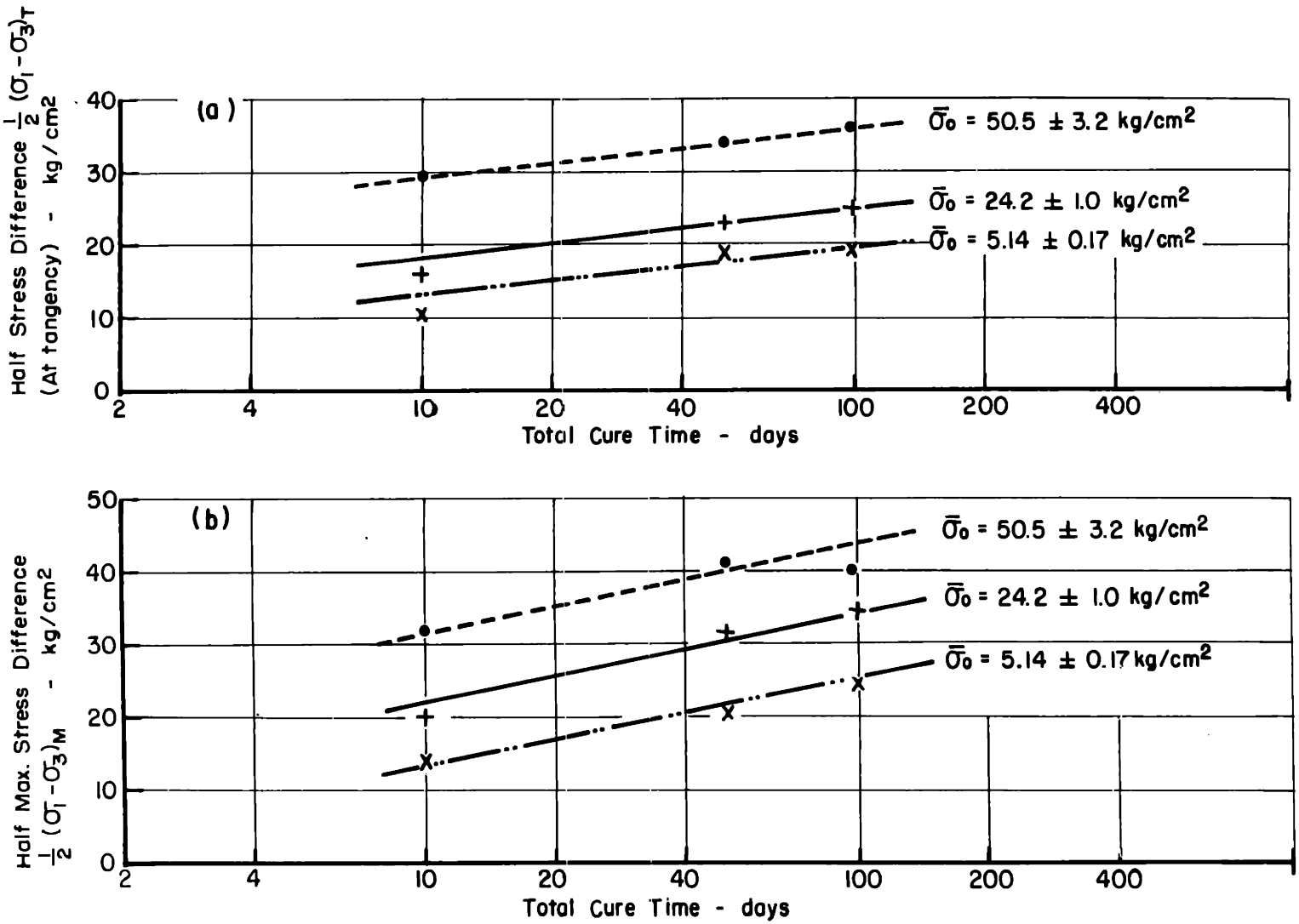

FIGURE 8-8. EFFECT OF TOTAL CURE TIME ON STRESS DIFFERENCES OF M-21 + 5% CEMENT

FIGURE 8-9. COMPARISON BETWEEN COHESION INTERCEPT AND UNCONFINED SHEAR STRENGTH OF M-21 + 5% LIME

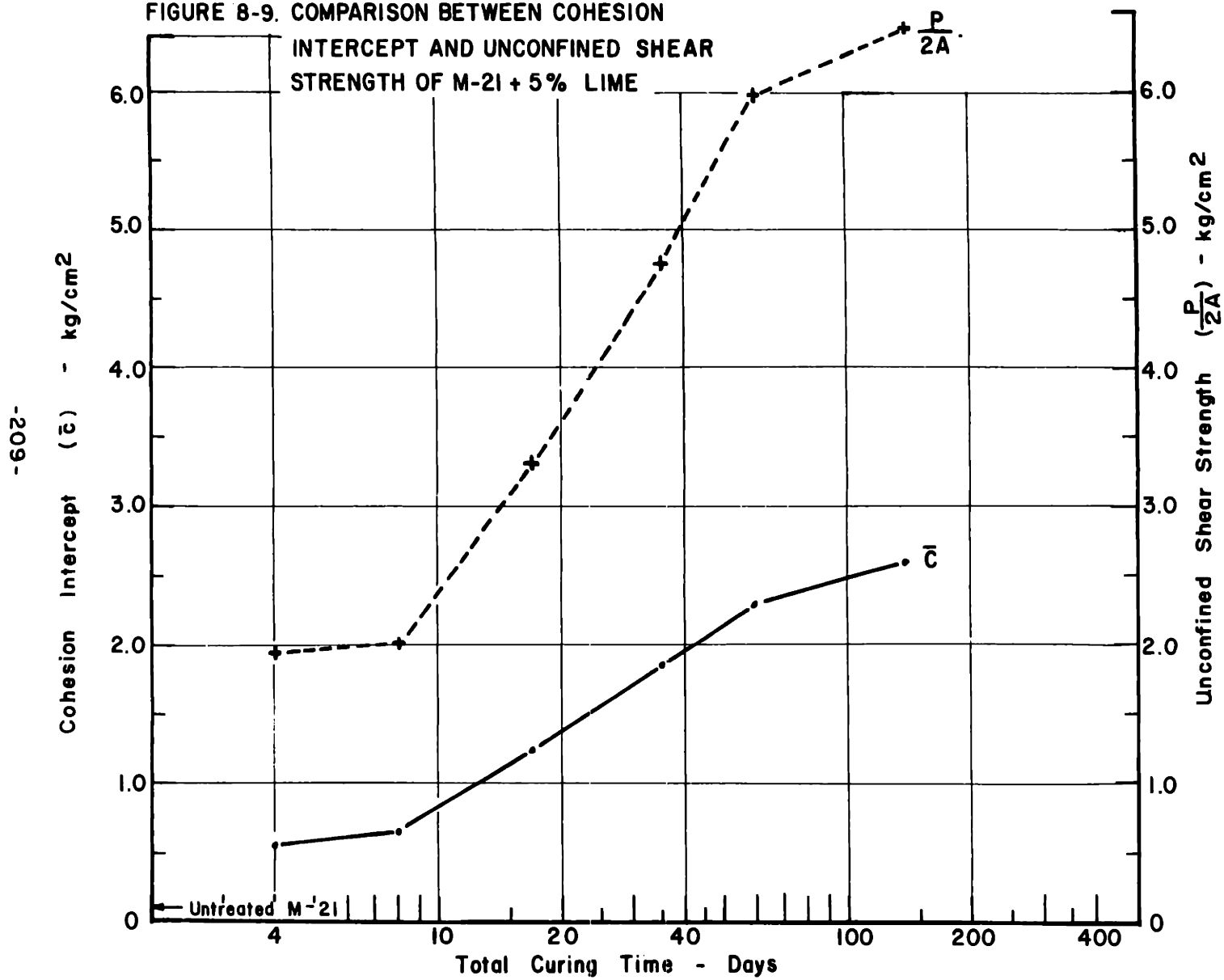

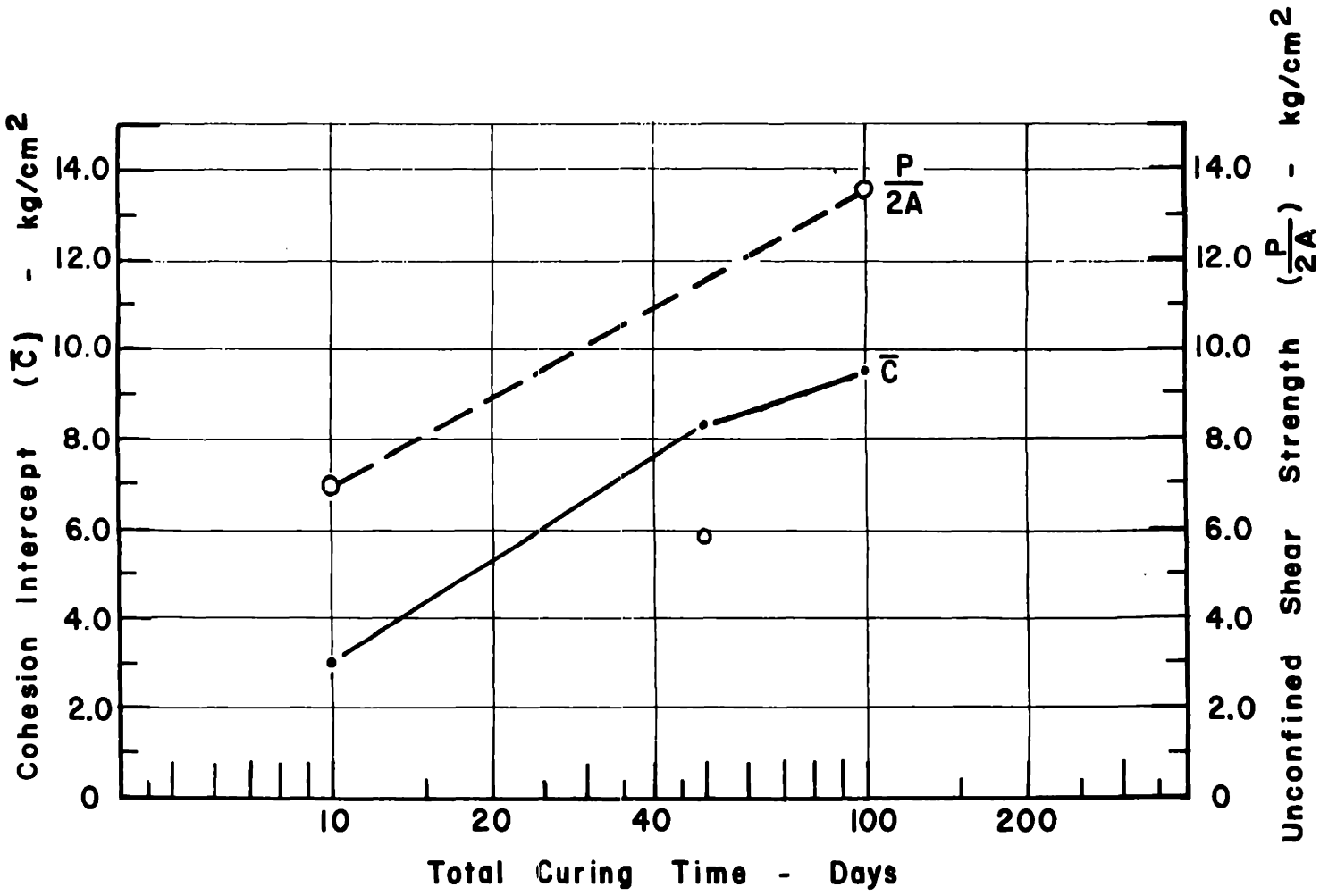

FIGURE 8-10. COMPARISON BETWEEN COHESION INTERCEPT AND UNCONFINED SHEAR STRENGTH OF M-21 + 5% CEMENT

Chapter 9

STRESS-STRAIN CHARACTERISTICS OF STABILIZED SOILS

9.1 Introduction

The stress-strain behavior of an isotropic, linear-elastic material is completely defined by two elastic constants, such as Young's modulus, E, and Poisson's ratio, ν. Soils do not have such a simple stress-strain behavior. Their behavior is approximately linear-elastic only at small stress levels compared to their strengths and their initial tangent moduli are not unique but depend to a large extent on the stress history to which the soils have been subjected (Ladd, 1964).

In order to determine stresses and deformations in soil masses it is usually necessary to assume that soils possess linear-elastic properties. For undrained conditions (constant volume) Poisson's ratio is equal to 0.5 and Young's modulus is usually obtained from laboratory tests. It is often assumed to be equal to the initial tangent modulus of the stress-strain curves obtained from undrained triaxial compression tests. For drained conditions Poisson's ratio can be obtained in the laboratory by methods described in Chapter 6 and Young's modulus from drained triaxial compression tests.

This chapter discusses the influence of artificial cementation on the initial tangent modulus of soils

obtained from triaxial compression tests. Also included in this chapter are the relations between initial tangent modulus and shear strength for the stabilized soils as well as the axial strains required to reach $(\sigma_1 - \sigma_3)$ maximum.

9.2 Behavior of the Coarse-Grained Soil-Stabilizer Systems

The influence of consolidation pressure on the initial tangent modulus, E, of the untreated sands in drained shear is shown in Fig. 9-1. The modulus increased at a decreasing rate with increasing consolidation pressure. At a given consolidation pressure increasing the as-molded relative density of the medium sand from 62% to 75% caused only a slight increase in E. The coarse sand had higher E values than the medium sand at the same dry density even though the coarse sand was at a lower relative density.

The influence of 5% and 10% cement respectively on the initial tangent modulus of the medium sand is shown in Fig. 9-3. E increased substantially with increasing cement content. The cementation caused E to be essentially independent of consolidation pressure. This strongly suggests that the initial resistance to deformations was solely due to the cohesion between particles produced by the cementation.

Fig. 9-2 shows that for the untreated sands the axial strain required to reach $(\sigma_1 - \sigma_3)$ maximum was

essentially independent of consolidation but was dependent on the molding dry density and grain size and/or grain shape of the sand. In the case of the cemented sands the axial strain required to reach $(\sigma_1 - \sigma_3)_M$, ε_M, increased with increasing consolidation pressure but it was always considerably less than that for the untreated sand having the same packing of grains (Fig. 9-4).

It is of interest to note that both the untreated and the cemented sands had essentially straight stress-strain curves until at least half the maximum stress difference was reached. This was however not the case in undrained shear as shown by the stress-strain curves given in Fig. S-1 of Appendix B.

9.3 Behavior of the Fine-Grained Soil-Stabilizer Systems

The initial tangent moduli of both the untreated and the cemented fine-grained soils increased at a decreasing rate with increasing consolidation pressure as can be seen from Figs. 6-2a, 6-3, and 6-4a of Chapter 6. Cementation caused a substantial increase in E.

At any given consolidation pressure the initial tangent modulus of M-21 stabilized with 5% lime increased linearly with increasing log. curing time and the rate of increase was essentially independent of consolidation pressure (Fig. 6-5a). This suggests that at any consolidation pressure the increase in E was due solely to an

increase in the strength of the cementation due to curing since the $\bar{c}$ of M-21 + 5% lime also increased linearly with increasing log curing time. There was considerable scatter in the results at low consolidation pressures probably due to large seating imperfections of the samples at these pressures.

Fig. 6-6a showed that for VBC + 10% cement cycles of wet-dry caused a decrease in E at any given consolidation pressure. This is due to the detrimental effects of cycling on the cohesive resistance of cemented VBC.

Fig. 9-5 suggests that for VBC stabilized with 5% lime drainage conditions during shear have at most only a minor influence on the initial tangent modulus. This is slightly misleading since the slopes of the stress-strain curves in drained shear decrease much more rapidly with increasing load than in undrained shear as can be seen from the stress-strain curves given in Figs. V-2 and V-3 of Appendix B.

Fig. 9-6 shows that drainage conditions had a large influence on the axial strain required to reach $(\sigma_1 - \sigma_3)_M$. In the case of untreated VBC and VBC + 5% lime in undrained shear ε_M was independent of consolidation pressure but in drained shear ε_M for VBC + 5% lime increased rapidly with increasing consolidation pressure.

The increase in ε_M with increasing $\bar{\sigma}_o$ was probably due to the volumetric strains which occurred during drained shear. Fig. 9-6 also shows that ε_M for the untreated soil was a magnitude higher than for the stabilized soil. Cycles of wet-dry caused an increase in ε_M as can be seen from Fig. 9-7.

Reasonably good relations existed between initial tangent modulus and undrained shear strength taken as $\frac{1}{2}(\sigma_1 - \sigma_3)_M$ for each of the soil-stabilizer systems investigated. The relationships were not always linear but they were independent of curing time and cycles of wet-dry as can be seen from Figs. 9-8 through 9-10. These figures also show that ε_M was essentially independent of curing conditions excluding cycles of wet-dry.

Drainage conditions did have an effect on the relation between E and $(\sigma_1 - \sigma_3)_M$ for VBC + 5% lime as shown in Fig. 9-8.

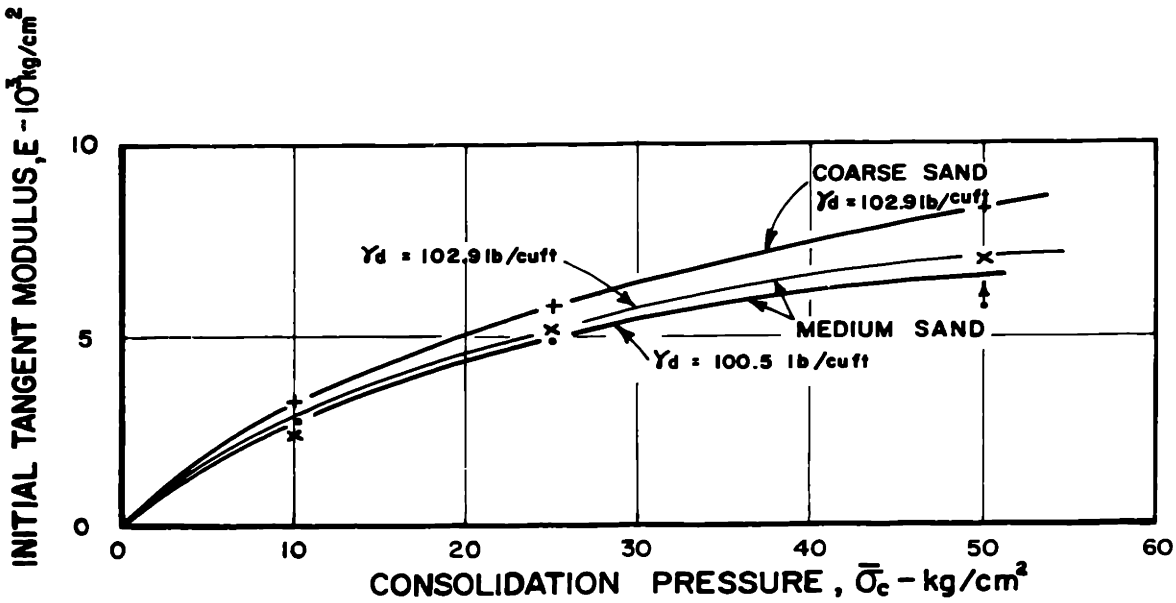

Fig. 9-1. INFLUENCE OF GRAIN SIZE ON THE INITIAL TANGENT MODULUS OF OTTAWA SAND AS A FUNCTION OF CONSOLIDATION PRESSURE

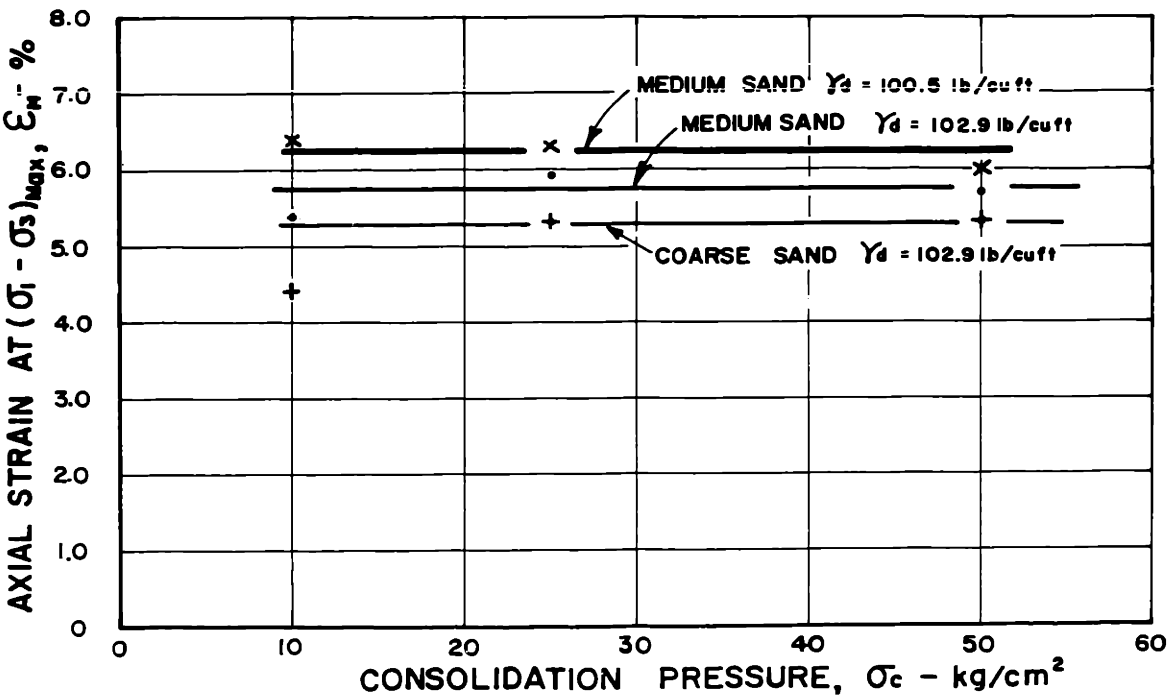

Fig. 9-2 INFLUENCE OF GRAIN SIZE ON THE AXIAL STRAIN AT $(\sigma_1 - \sigma_3)$ MAXIMUM OF OTTAWA SAND AS A FUNCTION OF CONSOLIDATION PRESSURE

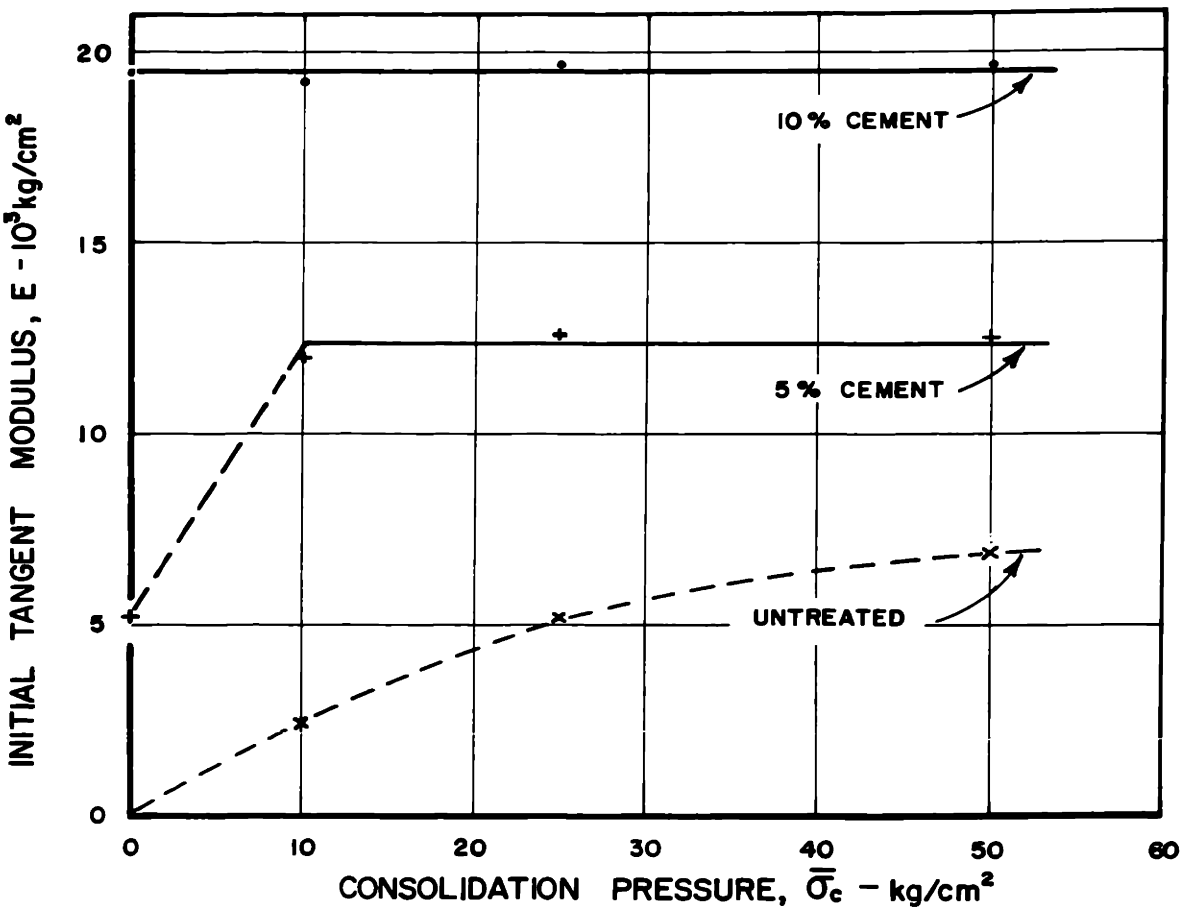

Fig. 9-3. INFLUENCE OF CEMENT CONTENT ON THE INITIAL TANGENT MODULUS OF MEDIUM OTTAWA SAND AS A FUNCTION OF CONSOLIDATION PRESSURE.

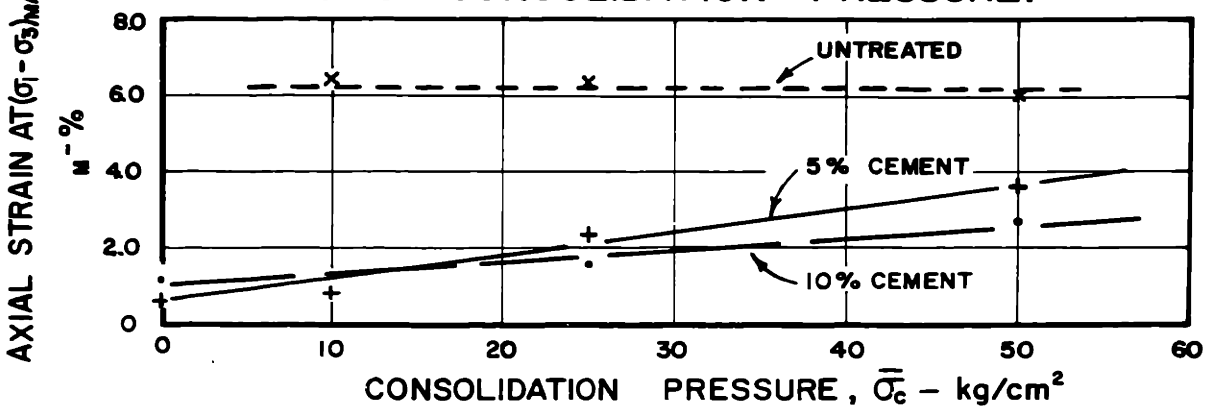

Fig. 9-4. INFLUENCE OF CEMENT CONTENT ON THE AXIAL STRAIN AT $(\sigma_1 - \sigma_3)$ MAXIMUM OF MEDIUM OTTAWA SAND AS A FUNCTION OF CONSOLIDATION PRESSURE

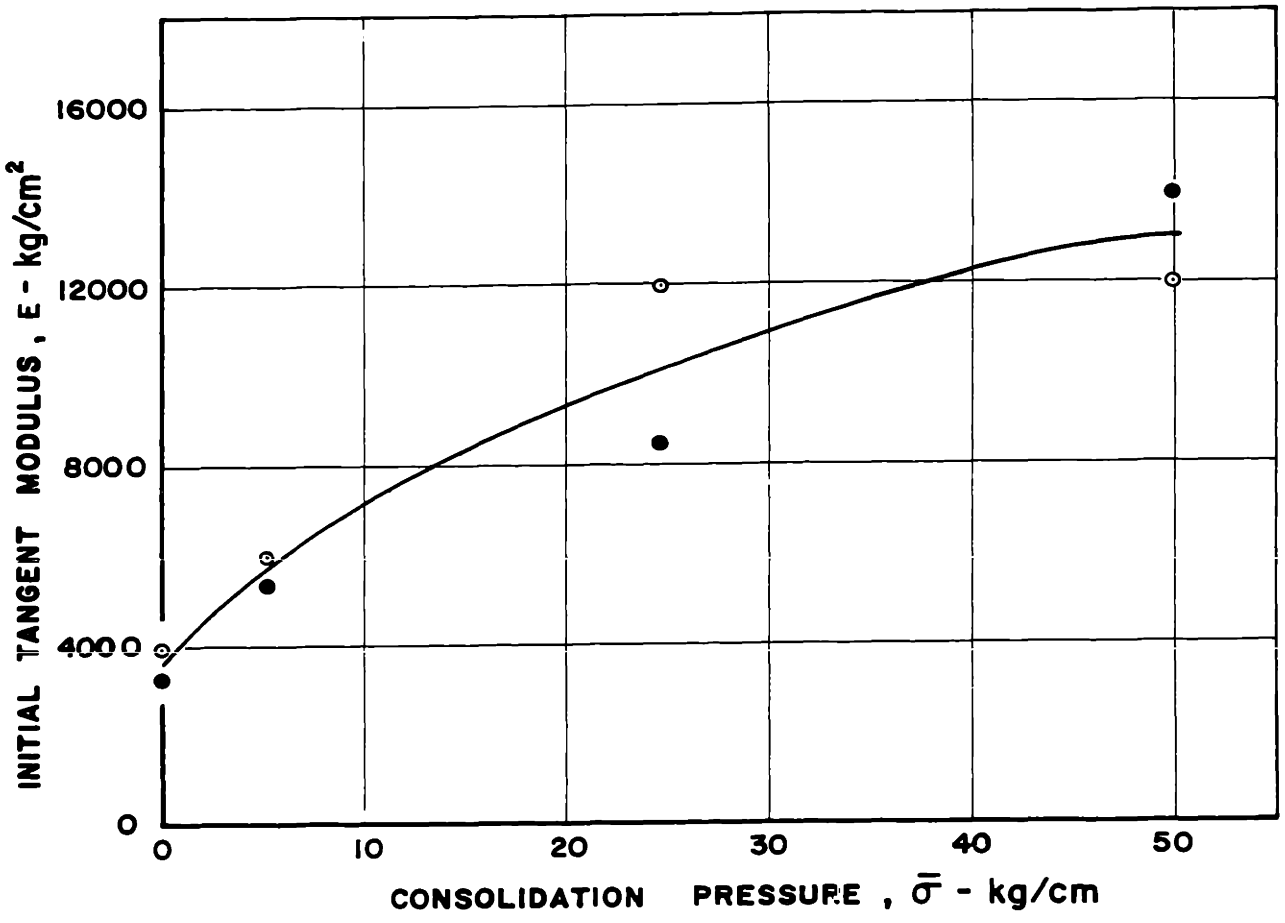

Fig. 9-5. INFLUENCE OF DRAINAGE CONDITIONS ON THE INITIAL TANGENT MODULUS OF VBC + 5% LIME CURED FOR ONE YEAR

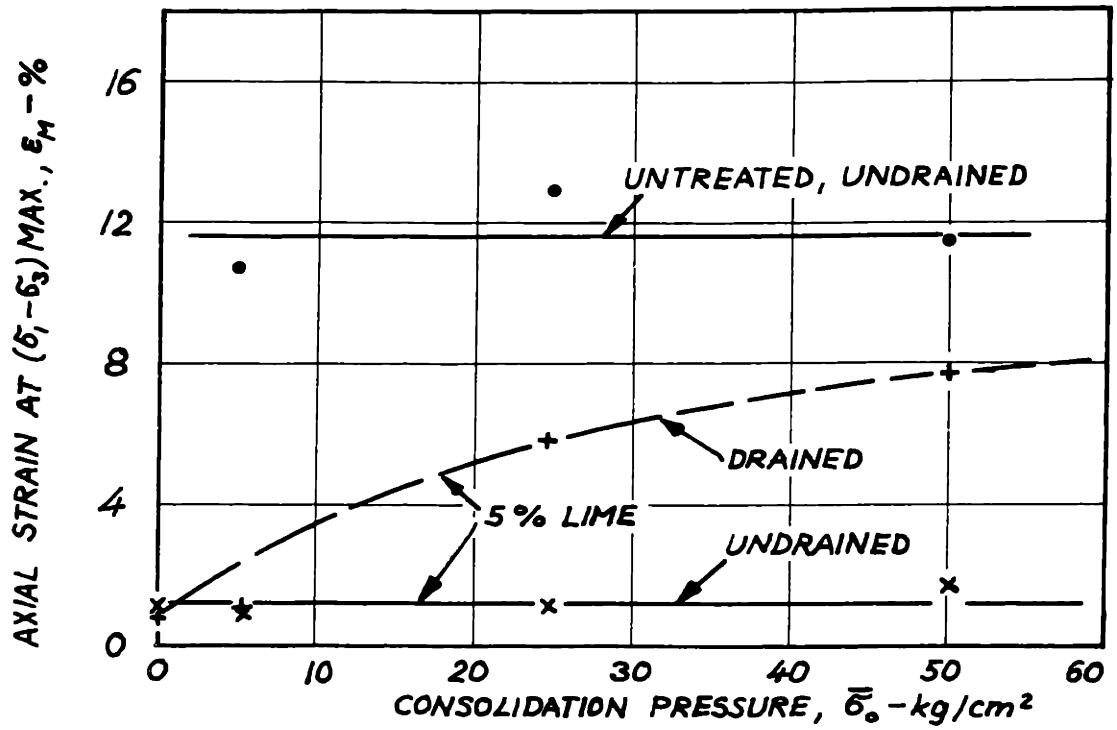

FIG. 9-6. AXIAL STRAIN REQUIRED TO REACH $(\sigma_1-\sigma_3)$ MAX. AS A FUNCTION OF CONSOLIDATION PRESSURE FOR UNTREATED VBC AND VBC + 5 % LIME.

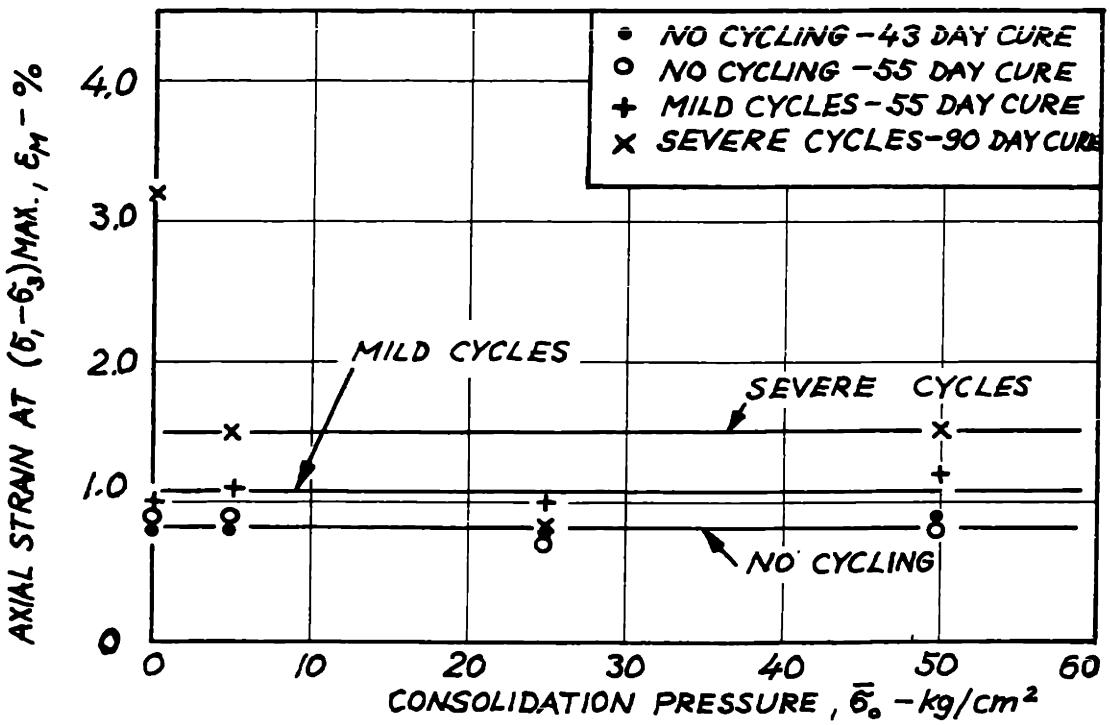

FIG. 9-7. INFLUENCE OF CYCLES OF WET-DRY ON THE AXIAL STRAIN REQUIRED TO REACH $(\sigma_1-\sigma_3)$ MAX. FOR VBC + 10 % CEMENT.

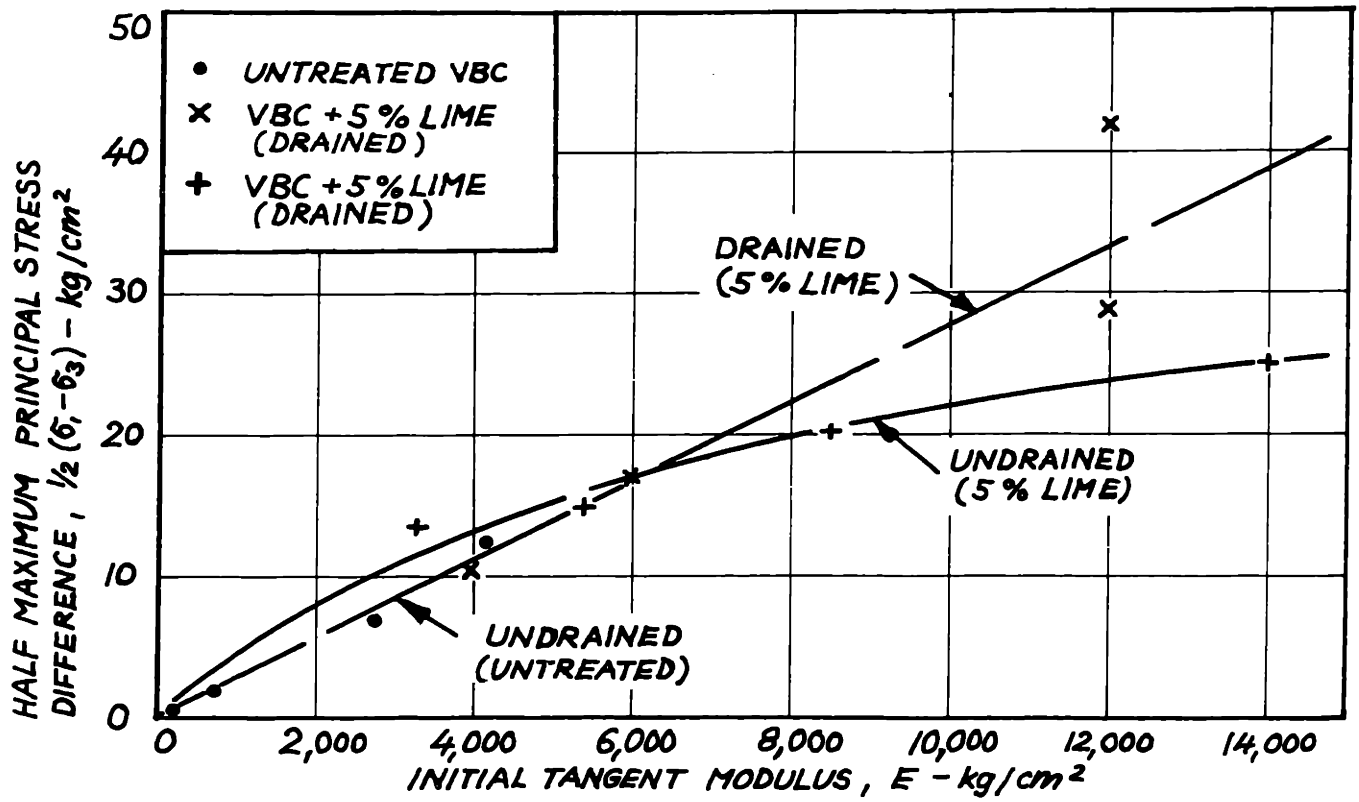

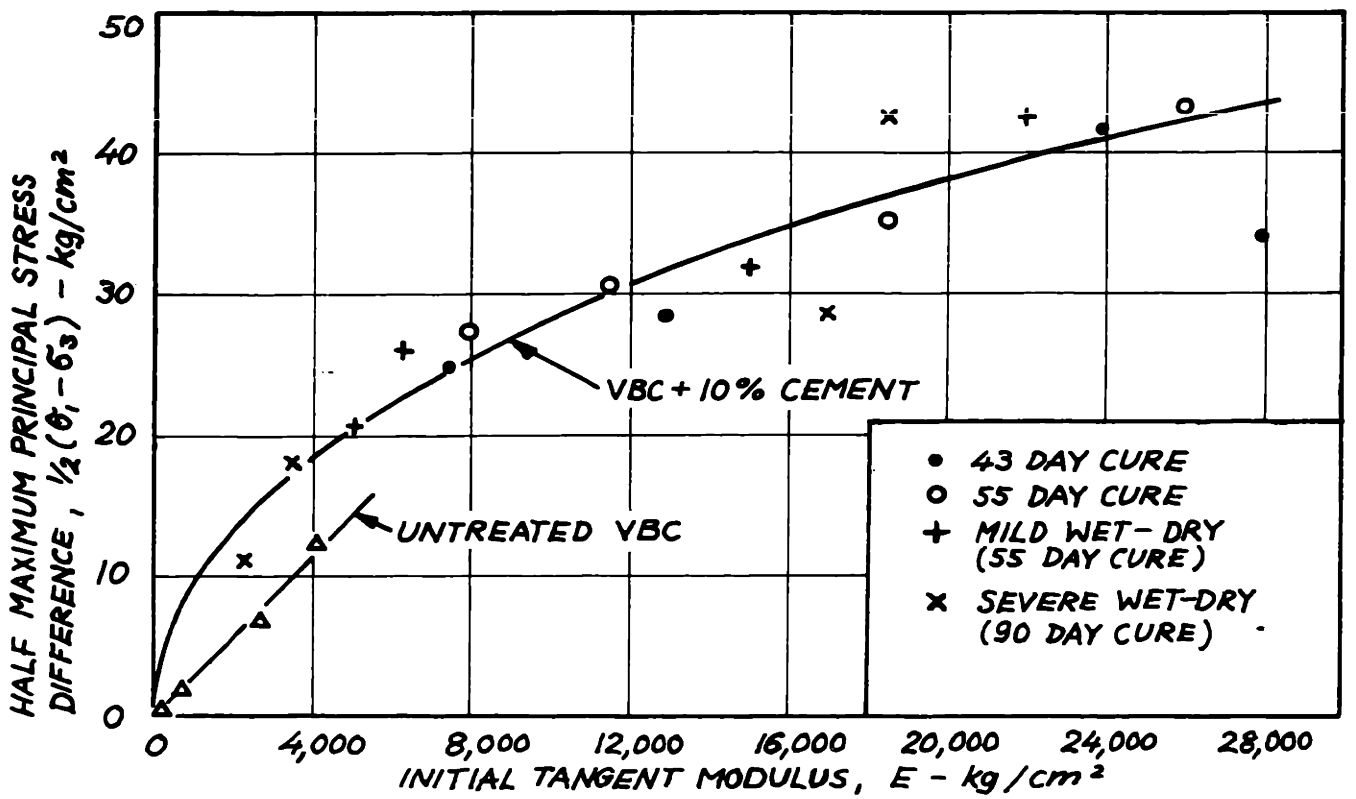

FIG. 9-8. *RELATION BETWEEN INITIAL TANGENT MODULUS AND MAXIMUM STRESS DIFFERENCE FOR VBC SYSTEMS.*

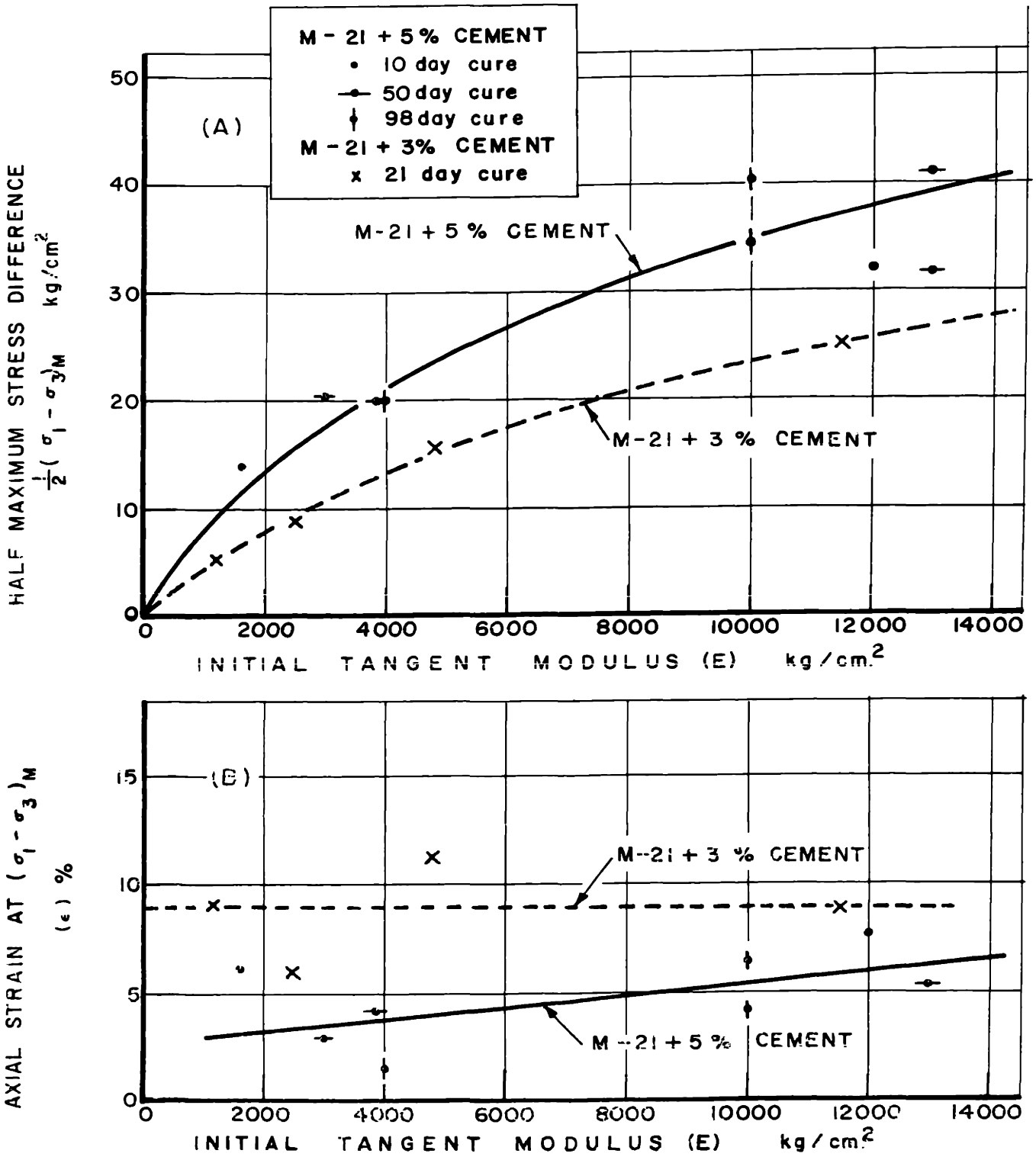

FIGURE 9-9. INFLUENCE OF CEMENT CONTENT ON STRESS-STRAIN RELATIONS OF M-21

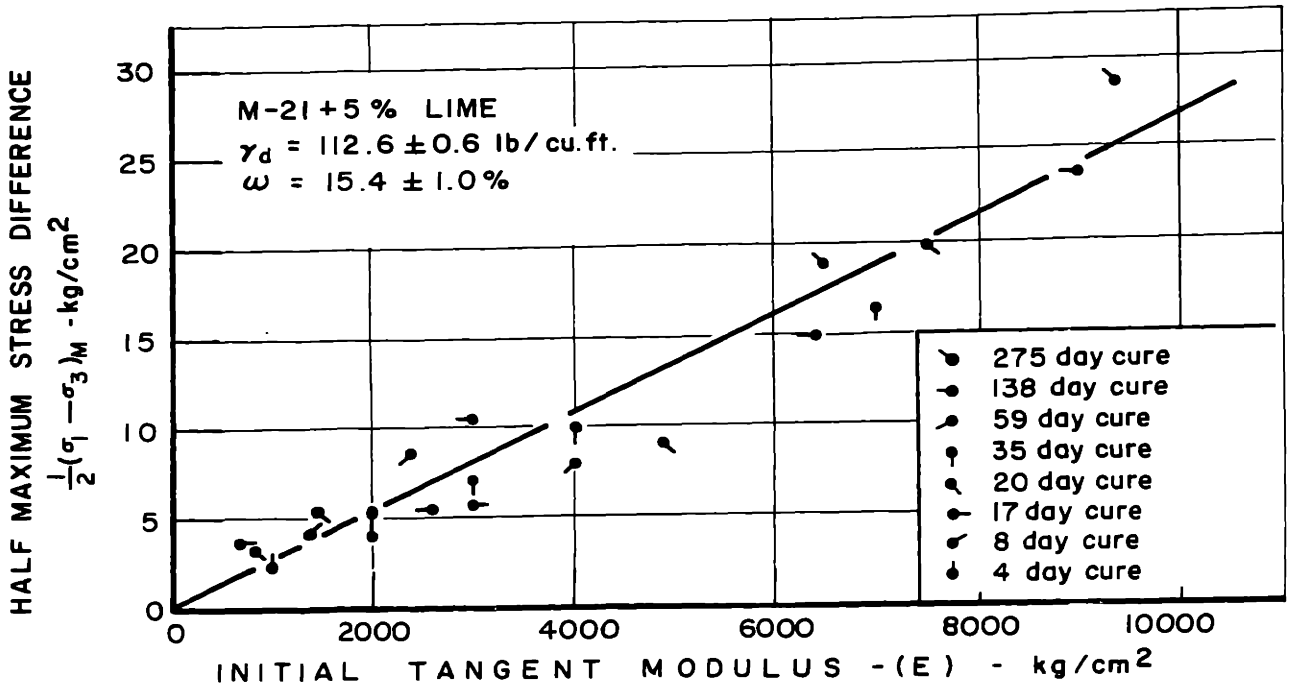

FIGURE 9-10a. RELATION BETWEEN INITIAL TANGENT MODULUS AND SHEAR STRENGTH FOR M-21+5 % LIME

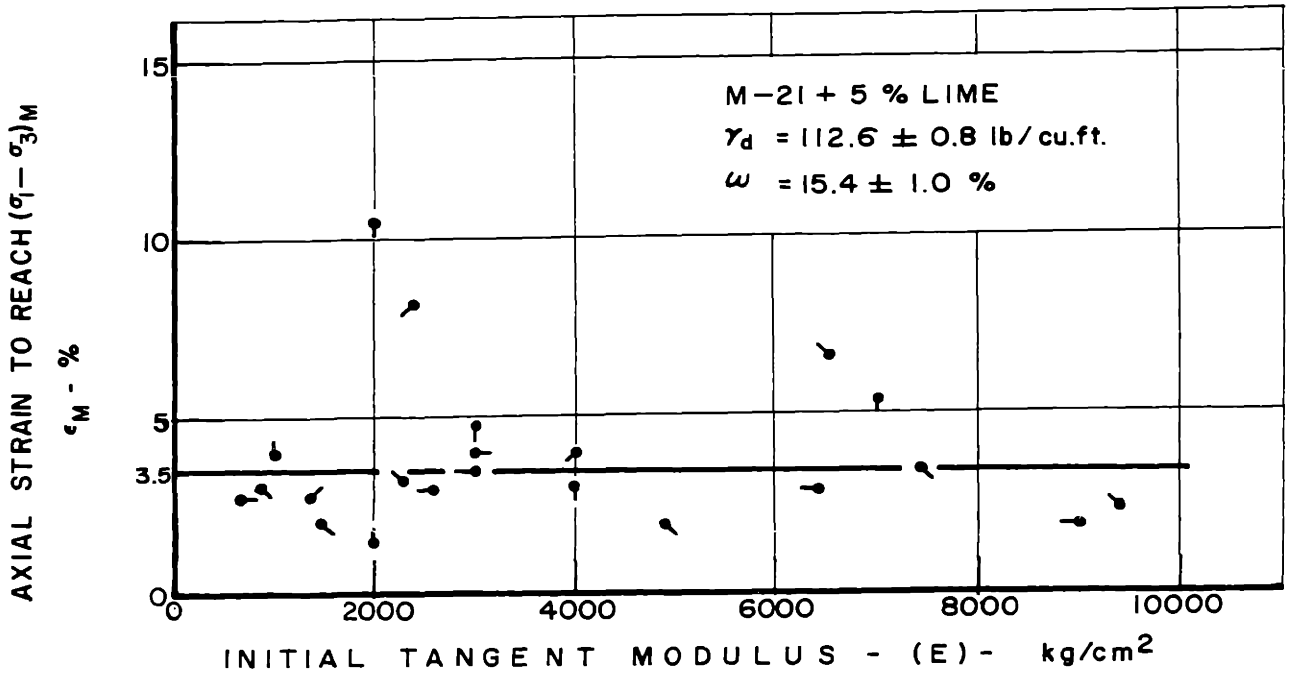

FIGURE 9-10b. EFFECT OF INITIAL TANGENT MODULUS ON THE STRAIN REQUIRED TO REACH THE MAXIMUM SHEAR STRENGTH OF M-21 + 5% LIME

Chapter 10

SUMMARY AND CONCLUSIONS

10.1 Objective of The Thesis

In dealing with naturally and artificially cemented soils the engineer should have a fundamental understanding of the behavior of cementation in such materials. This knowledge would help him rationally evaluate and apply the results of laboratory tests to field conditions. The primary goal of this thesis was therefore to determine the influence of artificial cementation on the stress-strain and strength behavior of soils in the laboratory and to develop a mechanistic picture which would help in the prediction of field performance.

Three soils were used in this investigation, a sand (uniform Ottawa sand), a clayey silt (Massachusetts Clayey Silt or M-21), and a highly plastic clay (Vicksburg Buckshot Clay or VBC). The two cementing materials (stabilizers) used with these soils were hydrated lime (reagent grade) and portland cement (type I). The stress-strain and strength behaviors of the untreated and the cemented soils were determined in triaxial compression over a wide range of consolidation pressures (0 to over 50 kg/cm^2). Both drained tests with volume change measurements and undrained tests with pore pressure measurements were used.

10.2 Shearing Resistance of Artificially Cemented Soils in Terms of Effective Stresses

Chapter 5 covered the influence of artificial cementation on the shearing resistance of soils in terms of effective stresses. It was shown that:

1. At any given axial strain the shearing resistance of an untreated or a cemented soil can be considered to be made up of two components: a cohesive resistance which is independent of the normal effective stress, and a frictional resistance which is directly proportional to the normal effective stress.
2. The maximum cohesive resistance of an untreated soil is negligible compared to that of a cemented soil.
3. Cementation can substantially increase the maximum frictional resistance of a fine-grained soil probably by the formation of large strongly cemented aggregates of soil particles. In sands, cementation only slightly increased the maximum frictional resistance provided the density of the sand excluding cement is kept constant.
4. The maximum cohesive resistance of cemented soils occurs at lower axial strains than the Mohr-Coulomb effective stress envelope and then

decreases rapidly on further straining due to a breakdown of the cementation. At very large strains (ultimate conditions) the cementation between aggregates is completely destroyed in the shear zone and the cohesive resistance is zero.

5. The frictional resistance of cemented soils increases with increasing axial strain and only reaches a maximum at very large strains (ultimate conditions) when the cohesive resistance is completely destroyed. The Mohr-Coulomb effective stress envelope occurs at lower strains than those required to mobilize the maximum frictional resistance.
6. The Mohr-Coulomb effective stress envelope for cemented soils represents conditions when the sum of the shearing resistance due to friction and the shearing resistance due to cohesion is a maximum.
7. For cemented fine-grained soils the Mohr-Coulomb envelope in terms of effective stresses is essentially independent of drainage conditions. This is not the case for untreated and cemented sands.
8. Provided premature fracture does not occur, the Mohr-Coulomb effective stress envelope of cemented fine-grained soils can be represented by the equation:

$$\tau_{ff} = \bar{c} + \bar{\sigma}_{ff} \tan \bar{\phi}$$

where $\bar{c}$ = the effective cohesion intercept and is a function of:
- (a) soil type
- (b) type and amount of cementing material
- (c) molding conditions
- (d) curing history which includes the time of humid cure and amount of weathering

$\bar{\phi}$ = the effective angle of internal friction and is a function of:
- (a) soil type
- (b) type and amount of cementing material

9. Both the effective cohesion intercept and effective angle of internal friction of the Mohr-Coulomb envelope of a fine-grained soil can be substantially increased by artificial cementation.

10. The effective cohesion intercept of a cemented fine-grained soil increases at a decreasing rate with increasing curing time. Increasing the amount of cementing material increases the magnitude of the cohesion intercept. Volume changes which may occur during curing or weathering (cycles of wet-dry) can damage the cementation and thus reduce the magnitude of the cohesion intercept.

11. For a given fine-grained soil the effect angle of internal friction, $\bar{\phi}$, increases by increasing

the amount of cementing material added to the soil probably due to the formation of strongly cemented soil aggregates. The more clay in the soil the larger the increase in $\bar{\phi}$. $\bar{\phi}$ is essentially independent of the strength of the cementing material (curing time) and it is not influenced by weathering (cycles of wet-dry) provided premature fracture does not occur.

12. The Mohr effective stress envelope for both untreated and cemented sands is appreciably curved at low consolidation pressures but the curvature tends to disappear at very high pressures. Cementation causes the Mohr envelope in terms of effective stresses to exhibit an effective cohesion intercept which increases with increasing cement content and probably also with increasing curing time. The effective angle of internal friction is not appreciably influenced by cementation and is mainly a function of the density of the sand excluding cement because the cementation cannot produce strongly cemented aggregates of large sand size grains which can withstand breakage during shear.

13. Premature fracture due to the existence of shrinkage cracks which develop during curing and

weathering exhibits itself at low consolidation pressures by a decrease in the effective cohesion intercept and an increase in the effective angle of internal friction. The cracks close at high consolidation pressures and then they cause a decrease in the effective cohesion intercept without altering the effective angle of internal friction.

14. At ultimate conditions (large strains) the shearing resistance of a cemented fine-grained soil is solely frictional and can be represented by the equation:

$$\tau_{ult} = \bar{\sigma}_{ult} \tan \bar{\phi}_{ult}$$

where τ_{ult} = the ultimate shearing resistance on the failure plane assumed to be oriented at $45^{o} + \bar{\phi}_{ult}/2$ to the major principal plane.

$\bar{\sigma}_{ult}$ = the ultimate effective normal stress acting on the same plane as τ_{ult}

$\bar{\phi}$ = the ultimate angle of shearing resistance at ultimate conditions and is the maximum angle of internal friction of the system. It is independent of molding and curing conditions. It is a function of the type of soil as well as the type and amount of cementing material. Artificial cementation may considerably increase $\bar{\phi}_{ult}$ of a soil.

10.3 Pore Pressure Response in Stabilized Soils

Chapter 6 covered the influence of cementation on the pore pressure response of soils prior to shear

(Skempton B factor). It was shown that:

1. The pore pressure response of both untreated and cemented soils decreases with increasing consolidation pressure even when they are completely saturated because of the decrease in the compressibility of the soil skeleton with increasing consolidation pressure.
2. At a given consolidation pressure the pore pressure response decreases with increasing cementation and increasing curing time because of the influence of the amount and the strength of the cement on the rigidity of the soil skeleton.
3. From the pore pressure response and initial tangent modulus, E, of the stress-strain curve it is possible to determine Poisson's ratio assuming the theory of elasticity is applicable. The values of Poisson's ratio ranged from 0.25 to 0.45 using this method but it is believed that they are on the high side due to experimental errors in determining E.

10.4 Effective Stress-Volume Change Behavior During Shear

Chapter 7 covered the influence of artificial cementation on the volume change behavior during drained shear and the effective stress (pore pressure) behavior during undrained. It was shown that:

1. Cementation does not alter the general characteristics of the effective stress-volume change behavior of compacted soils.
2. In undrained shear at low consolidation pressures compacted untreated and compacted cemented fine-grained soils behave like overconsolidated clays, i.e., there is an initial tendency for the soil to decrease in volume (a pore pressure decrease) followed by a large tendency for the soil to dilate (pore pressure decrease) as the maximum principal stress is reached. The tendency for dilation reaches a maximum as ultimate conditions are reached. At high consolidation pressures the behavior is typical of normally consolidated remolded soils. The volume tends to decrease (the pore pressure increases) at a decreasing rate with increasing axial strain and approaches a constant value as ultimate conditions are reached (at large strains).
3. In undrained shear the excess pore pressures of cemented and untreated compacted fine-grained soils, at tangency and at maximum principal stress difference increase linearly with increasing consolidation pressure. At a given consolidation pressure a cemented soil may have a higher excess pore pressure than the same soil uncemented.

4. For a given cemented fine-grained soil, the strength of the cementation (curing time) has no effect on the excess pore pressures developed during undrained shear.
5. The $\bar{A}$ factors of cemented and untreated compacted fine-grained soils increase rapidly with increasing consolidation pressure at low consolidation pressures but tend to a constant value at high consolidation pressures which is typical of normally consolidated clays.
6. Cementation reduces the $\bar{A}$ factors of a fine-grained soil because cementation only slightly influences the excess pore pressures developed during shear but considerably increases the shearing resistance, $(\sigma_1 - \sigma_3)$. Similarly increasing the curing time causes the $\bar{A}$ factors to decrease.
7. In the case of dense sands cementation alters the volume change behavior at low strains in drained shear but has no appreciable effect on the maximum dilation. It is the relative density of the sand excluding cement which primarily controls the volume change behavior.
8. Cementation has no effect on the volume change tendency of a sand during undrained shear (the pore pressure behavior) provided the density of the sand excluding the cement is kept constant.

10.5 Shear Strength of Stabilized Soils

The influence of artificial cementation on the maximum shear strength of soils, i.e., $(\sigma_1 - \sigma_3)$ maximum was covered in Chapter 8. It was shown that:

1. Artificial cementation increases the shear strength of soils due to an increase in $\bar{c}$ and usually $\bar{\phi}$.
2. As with untreated soils drainage conditions during shear have a major influence on the shear strength of a cemented soil.

   For cemented fine-grained soils the undrained shear strength is higher than the drained shear strength at low consolidation pressures and vice versa.

   For cemented dense sands the undrained strength is higher than the drained strength at all consolidation pressures provided the volume is kept constant during undrained shear.
3. The shear strength of stabilized soils increases with increasing consolidation pressure.
4. The undrained strength of cemented fine-grained soils at high consolidation pressures increases with increasing curing time in the same way as the effective cohesion intercept increases with increasing curing time since the effective angle of

the internal friction and excess pore pressure are independent of curing time.

5. The unconfined shear strength of a stabilized soil which is at zero consolidation pressure due to soaking is less than the undrained shear strength of a corresponding saturated sample at the same consolidation pressure because the degree of saturation of the unconfined sample is less than 100% and therefore it develops smaller negative excess pore pressures during shear than the saturated sample.

10.6 Stress-Strain Behavior of Stabilized Soils

The influence of artificial cementation on the initial tangent modulus of soils and on the axial strain required to reach $(\sigma_1 - \sigma_3)$ maximum was covered in Chapter 9. It was shown that:

1. The initial tangent modulus of untreated sands increases with increasing consolidation pressure but that of cemented sands is essentially independent of consolidation pressure because shearing resistance of cemented sands at these relatively low stress levels is primarily due to the cementation which is cohesive in nature.

2. Artificial cementation reduces the axial strain required to reach $(\sigma_1 - \sigma_3)$ maximum of sands.
3. The initial tangent modulus of untreated and cemented fine-grained soils increases with increasing consolidation pressure. At a given consolidation pressure cementation increases the initial tangent modulus.
4. The initial tangent modulus of a cemented fine-grained soil increases with increasing curing time because the cohesive resistance of the soil increases.
5. Cycles of weathering (wet-dry) may cause the initial tangent modulus of a stabilized soil to decrease if cycling damages the cementation causing a decrease in the cohesive resistance.
6. Artificial cementation causes a decrease in the axial strain required to reach $(\sigma_1 - \sigma_3)$ maximum of a fine-grained soil. In undrained shear ϵ_M is independent of consolidation pressure and curing time provided premature fracture does not occur. In drained shear ϵ_M increases with increasing consolidation pressure.
7. The relation between E and $\frac{1}{2}(\sigma_1 - \sigma_3)$ maximum for a given cemented soil is independent of curing time and weathering but it is dependent on the

drainage conditions during shear. The relation is not necessarily linear.

10.7 Practical Implication of The Investigation

It has been shown that for a fine-grained soil the addition of a stabilizer is beneficial in increasing its frictional and cohesive resistance. The increase in cohesive resistance may be partially destroyed due to weathering but the increase in frictional resistance is apparently unaffected so that even though severe cracking may occur due to weathering a stabilized fine-grained soil will be considerably stronger than the untreated soil in most field applications because of its higher frictional resistance. In the case of granular soils the increase in strength is solely due to the increase in cohesion so that if cracking occurs the stabilizer will have little or no beneficial effect.

The initial tangent modulus of a soil can be substantially increased by stabilization but then the soil can no longer take large deformations. This poses severe limitations on the potential uses of stabilized soils when large deformations are expected. The stress-strain modulus in practice may therefore be considerably less than the initial tangent modulus.

As with untreated soils, the strength of stabilized soils is dependent on the magnitudes of the pore pressures

which develop during shear. For saturated conditions the pore pressures developed during shear can be extremely large and then the strengths will depend on the amount of drainage (dissipation of pore pressures). At low confining pressures the drained strength of a stabilized soil is smaller than the undrained strength whereas at high confining pressure the reverse is true. When a stabilized soil is used above the water table it will not be completely saturated in which case the pore pressures developed during undrained shear will be relatively small and then drainage conditions will have only a small effect on the strength; however, the effective consolidation pressure of the stabilized soil may be considerably larger than the overburden pressure because of negative pore pressures which probably exist in partially saturated stabilized soils.

LIST OF REFERENCES

Alperstein, Robert (1964), "A Swell Test for Expansive Soils," S.M. Thesis, Department of Civil Engineering, M.I.T. (Unpublished).

Andreson, A., Bjerrum L., DiBiago, E., Kjaernski, B. (1957), "Triaxial Equipment Developed at the Norwegian Geotechnical Institute," Norwegian Geotechnical Institute, Publication No. 21, Oslo.

Bishop, Alan W., and Henkel, D. J. (1962), The Measurements of Soil Properties in the Triaxial Test, 2nd Edition, Edward Arnold (London).

Coulomb, C. A. (1776), "Essai sur une Application Des Régles des Maximis et Minimis à quelques problems de Statique Relatifs a L'Architecture," pp. 343-82, Memoires de Mathématique et de Physique, Presentes à L'Academie Royale Des Sciences, Paris, Vol. 7, 1776.

Hall, E. G., and Gordon, B. B. (1963), "Triaxial Tests with Large-Scale High Pressure Equipment," ASTM Special Technical Publication No. 361.

Hirschfeld, R. C., and Poulos, S. J. (1963), "High Pressure Triaxial Tests on a Compacted Sand and an Undisturbed Silt," ASTM Special Technical Publication No. 361.

Hvörslev, M. J. (1937), "Uber die Festigkeitseigenschaften Gestorter Bindiger Boden," Ingeniørvidenskabelige Skrifter, A, No. 45, Copenhagen.

Hvörslev, M. J. (1960), "Physical Components of the Shear Strength of Saturated Clays," Amer. Soc. of Civil Engr. Research Conference on Shear Strength of Cohesive Soils, Colorado.

Jürgenson, Leo (1934), "The Shearing Resistance of Soils," Journal of The Boston Soc. of Civil Engr. Discussion by A. Casagrande.

Kim, J. H. (1964), "Effect of Weathering Cycles on Triaxial Strength of Stabilized Soils," S.M. Thesis, Department of Civil Engineering, M.I.T. (Unpublished).

Ladd, C. C. (1964), "Stress-Strain Modulus of Clay in Undrained Shear," Journal of the Soil Mechanics and Foundation Division, ASCE, Vol. 90, No. SM5, Proc. Paper 4039.

Lambe, T. William (1951), Soil Testing for Engineers, John WileY and Sons, Inc., New York.

Lambe, T. William (1960), "A Mechanistic Picture of Shear Strength of Clays," Amer. Soc. of Civil Engr. Research Conference on Shear Strength of Cohesive Soils, Colorado.

McClintock, F. A., and Walsh, J. (1962), "Friction on Griffith Cracks in Rocks under Pressure," 4th Nat. Cong. Applied Mechanics.

M.I.T. (1963), "Triaxial Equipment and Computer Program for Measuring the Strength Behavior of Stabilized Soils," Soil Stabilization Phase Report No. 2, Department of Civil Engineering Research Report R63-45, Cambridge, Mass.

Rowe, P. W. (1962), "The Stress-Dilatancy Relation for Static Equilibrium of an Assembly of Particles in Contact," Proc. Royal Soc., Series A, London, Vol. 269, No. 1339.

Serani-Mertelli, M. (1961), "An Investigation of Retarders for Soil-Cement Stabilization," S.M. Thesis, Department of Civil Engineering, M.I.T. (Unpublished).

Seed, H. B., Mitchell, J. K., and Chan, C. K. (1960), "The Strength of Compacted Cohesive Soils," Amer. Soc. of Civil Engr., Research Conference on Shear Strength of Cohesive Soils, Boulder, Colorado.

Skempton, A. W. (1954), "Pore-Pressure Coefficients A and B," Geotechnique, 4:4:148.

Taylor, D. W. (1948), Fundamentals of Soil Mechanics, John Wiley and Sons, Inc., New York.

Terzaghi, K. (1923), Die Berechnug der Durchlässigkeitsziffer des Tones aus dem Verlauf der Hydrodynamischen Spannungser-scheinungen, Sitz. Akad. Wissen. Wien Math-naturwKl Abt. IIa, 132, 105-124.

Vesić, A. B., and Barksdale, R. D. (1963), "On Shear Strength of Sands at Very High Pressures," Preprint of Paper Prepared for the Symposium on Laboratory Shear Testing of Soils, Ottawa, Canada.

BIOGRAPHICAL SKETCH OF THE AUTHOR

The author of this thesis, Anwar Ernest Zaki Wissa, was born in Alexandria, Egypt, on March 21, 1935. He attended school at Victoria College, Alexandria, from 1942 to 1952 during which time he received the Oxford and Cambridge General School Certificate.

In 1952 the author was accepted at Pembroke College, Oxford University, where he received in 1957 Second Class Honors in Engineering Sciences and was awarded a Master of Arts in 1962.

Following graduation from Oxford the author worked for a year as a junior engineer in the soils and structures departments of Richard Costain, Ltd., London.

The author entered graduate school at M.I.T. in the fall of 1958 and received his Master of Science in Civil Engineering in 1961.

While in graduate school the author worked as a Research Assistant in the Soil Mechanics Division (1959-1962).

In 1962 he was promoted to Instructor of Civil Engineering at M.I.T. and taught courses in Soil Mechanics, Experimental Soil Mechanics, and Soil Mechanics for Highways.

During his stay at M.I.T. the author acted as a consultant on a number of jobs involving soil stabilization.

He is a member of the American Society of Civil Engineers, the International Society of Soil Mechanics and Foundation Engineering, Chi Epsilon, and Sigma Xi.

The author has prepared a paper entitled "The Effective Stress-Strength Behavior of Stabilized Soils," which was co-authored with Charles C. Ladd and T. William Lambe and will be published in the Proceedings of the Sixth International Conference on Soil Mechanics and Foundation Engineering.

APPENDIX A

DESCRIPTION OF TESTING EQUIPMENT*

The general layouts of the low pressure and high pressure triaxial systems used in this investigation are given in Figs. A-1 and A-2 respectively. Step-by-step operational procedures are given by M.I.T. (1963).

1. Triaxial Cells

   a. Low pressure cells (Fig. A-1)

      These cells are essentially as described in pp. 33 to 39 of Bishop and Henkel (1962) and are designed for a maximum cell pressure of 160 psi and 1.405 in. dia. (10 cm^2) samples. The main modification is an extra port in the lower platen of the triaxial cell; with two connections to the sample base it is then possible to flush out any air entrapped in the pore pressure lines. One of these connections provides drainage during consolidation under a back pressure, while the other is used for measuring the pore pressures during undrained shear (Fig. A-1). All connections in the cell base are equipped with no volume change Klinger valves. The sample is sealed from the

*See Table A-1 for names of suppliers of equipment and components.

surrounding water in the triaxial cell by enclosing it in two thin rubber prophylactics with silicon grease between them. The membranes are sealed to the cell base and top loading cap by means of neoprene O-rings. The top loading cap has a 3/4-in. long collar which is guided by the loading ram thus preventing it from tilting during shear.

b. High pressure cells (Figs. A-2 and A-3)

This cell is also for 1.405-in. dia. samples but can be used for cell pressures up to 1000 psi. The main differences between this cell and the low pressure cell are:

(1) The removable cell cylinder is made of steel instead of lucite.

(2) The loading ram is made of high grade, high tensile steel and is 1 in. in diameter instead of the 0.5-in. diameter used with the low pressure cell. The ram runs in a honed bronze bushing with 0.0003-in. clearance but in addition an O-ring seal is used between the ram and the bushing to prevent excessive leakage at high cell pressures.

(3) The Klinger valves are replaced by stainless steel ball valves with teflon seatings. These valves are also no volume change and have a maximum working pressure of 3000 psi.

(4) The samples are enclosed in 0.01-in. thick isoprene rubber membranes, rather than two 0.002-in. thick rubber prophylactics, to reduce membrane leakage. The guided top loading cap is made of stainless steel. To prevent damage to the rubber membranes at high confining pressures, a rubber sleeve 0.1-cm thick and 1.5-cm long is placed around the top joint between the sample and loading cap. A similar sleeve surrounds the bottom of the sample, the porous stone, and the top of the cell base pedestal.

2. Constant Pressure Supplies

a. Low pressures (Fig. A-1)

For pressures up to 160 psi self-compensating mercury controls* are used. The main advantages of this apparatus are:

(1) It is entirely free from hunting and can maintain a constant pressure (within 0.1 psi) for months without adjustment since it can compensate for about 150 cc of flow before refilling is required.

*See Bishop and Henkel (1962, pp. 45 to 52 for the principle and practical details of this equipment.

(2) It directly applies a water pressure. The water in it will not become saturated with air from the atmosphere since it is a closed system in which only the mercury is in direct contact with the atmosphere. The mercury control apparatus is used for applying the back pressure to both the low and high pressure tests. It reduces the back pressure required to saturate the samples since the deaired water in the system will dissolve the air in the sample without becoming saturated with air from the atmosphere.

The mercury control apparatus is also used for applying the cell pressure to the low pressure triaxial cells.

b. High pressures (Fig. A-2)

For pressures much above 160 psi a mercury control is not readily adaptable, and therefore pressures up to 1000 psi are obtained from nitrogen tanks and controlled by means of pressure regulators. The pressure is measured on an 8-in. Bourdon-tube type of test gauge which has a range of 0 to 1000 psi and can be read to the closest 1 psi. This system is not entirely free from hunting but at cell pressures above 600 psi the fluctuation is less than 1% and therefore usually of no major concern.

The nitrogen pressure cannot be applied directly to the cell chamber because the rubber membranes in which the samples are enclosed are about ten thousand times more permeable to gases than to water. To overcome this problem the nitrogen pressure is converted to a water pressure by means of a nitrogen-water interchange.

The cell chamber is connected to the water side of the interchange by 50 ft of copper tubing followed by 10 ft of high pressure rubber hose. The water between the cell and the water-nitrogen interface is sufficient to prevent diffusion of nitrogen into the sample for at least four or five days. The main disadvantage of this system is that it is necessary to replace the water in it prior to each test with freshly deaired water; however, this takes only about 10 minutes which is not too serious.

3. Pore Pressure Measuring Equipment

a. For small excess pore pressures (Fig. A-1)

Manually-operated mercury null systems* are used to measure the pore pressures during

*Both the Imperial College "glass tube" unit and the NGI "lucite" unit were used. For details see Bishop and Henkel (1962), pp. 52-60, and Andreson et al. (1957), respectively.

undrained shear in samples consolidated in the low pressure triaxial cells. These systems can measure pore pressures up to 160 psi and have an overall flexibility (i.e., volume change of the pore pressure measuring system) of about 6×10^{-6} in.^{3} per psi when properly deaired. Provided the compressibility of the soil skeleton is greater than 10^{-3} cm^2/kg the flexibility of the measuring equipment reduces the pore pressures during undrained shear by less than 2%* which is within the accuracy of the rest of the equipment.

b. For large excess pore pressures (Fig. A-2)

With the high pressure triaxial cells the pore pressures during undrained shear of samples consolidated to pressures up to 60 kg/cm^2 may reach values well above the maximum pressure which can be measured with the mercury null systems. Further, at high consolidation pressures the compressibility of the soil skeleton is a magnitude of more or less than 10^{-3} cm^2/kg and therefore the flexibility of the mercury null systems would substantially reduce the excess pore pressures during undrained shear. This would not alter the effective stress-strength

*This calculation is based on a triaxial sample which is 80 cc in volume and has a porosity of 0.30.

envelope, since the actual pore pressures are still being measured, as long as the rate of shearing is slow enough for the fluid pressures in the soil pores and in the measuring equipment to equalize. However the magnitude of the excess pore pressures will always be numerically smaller due to the flexibility of the equipment and therefore the measured shear strengths will be higher than the truly undrained shear strengths if positive excess pore pressures exist at failure. Similarly the measured pore pressure responses* will always be too low.

To reduce the flexibility of the pore pressure measuring devices and to measure excess pore pressures up to 1000 psi the mercury null systems have been replaced by electrical transducers on the high pressure triaxial cells. The transducers, which were manufactured by the Dynamic Instrument Company, employ unbonded strain wires attached to a diaphragm. The transducers are excited at six volts and the output can be measured with a millivoltmeter.** For this apparatus differential

*The pore pressure response is identical to Skempton's (1954) pore pressure coefficient B (also called B factor and B Parameter).

**Car batteries were used initially but their output voltages fluctuated considerably. They have now been replaced by a voltage regulator which keeps the voltage constant within ±5 mV.

pressure transducers are used to measure the difference between the cell pressure and the pore pressure, and since the cell pressures are known (measured on a Bourdon-tube gauge) the pore pressures can be calculated. The differential pressure transducers range in sensitivities from 500 psi differential full output to 1000 psi differential full output. The outputs of these transducers are plotted on an X-Y recorder, which is adjusted to give 1 in. = 50 psi differential.

Each transducer has two ports. The high pressure port, which is on the uninsulated side of the diaphragm, is connected to the nitrogen side of the cell pressure. A calcium chloride trap is used in this line to prevent water vapor from the cell pressure system condensing on the uninsulated side of the transducer. This trap is not fully effective, which sometimes causes the zero output of the transducer to shift. The low pressure port connects the insulated side of the diaphragm to the no volume change valve of one of the pore pressure ports in the cell base. The full range displacement of the diaphragm of these transducers is about 350×10^{-6} in., which represents flexibilities of 14×10^{-8} and 7×10^{-8} in. per psi

differential for the 1000-psi and 500-psi transducers respectively. The pore pressure lines between the sample and the transducer contains about 0.5 cu in. of water. Since these lines are extremely rigid the flexibility of the system between the sample and the transducer is primarily due to the compressibility of the water, i.e., 170×10^{-8} in.^{3} per psi. In other words when a transducer is used to measure pore pressures most of the flexibility in the measuring system is due to the compressibility of water. The overall flexibility of these measuring systems is about 1.8×10^{-6} in.^{3} per psi, which causes less than 5% reduction in the pore pressures when the compressibility of the soil skeleton is greater than 10^{-4} cm^2/kg. This accuracy is acceptable since most of the soil-stabilizer systems presently being investigated do not have such a rigid soil skeleton.

It is useful to note that the reduction in pore pressures can be made considerably smaller by decreasing the volume of water in the system which in turn will decrease its flexibility, e.g., if the volume of water in the system is reduced

to 0.1 cu in., the overall flexibility of the system is reduced to about 42×10^{-8} in.^{3} per psi which causes a pore pressure drop of a little over 1% when the rigidity of the soil skeleton is 10^{-4} cm^2/kg.

A recent improvement in the high pore pressure measuring equipment has been to replace the differential pressure transducers by absolute measuring transducers (Dynisco PTA 25) with a 1000-psi pressure range. This was done because the diaphragms of the differential pressure transducers had started to leak and cause the nitrogen from the cell pressure side to penetrate into the pore pressure lines. In addition the X-Y recorder has been replaced by a digital millivoltmeter which has a much higher sensitivity and can easily read 0.5 psi.

4. Volume Change Measuring Apparatus

The apparatus used for measuring volume changes during drained shear consists of the paraffin type as described by Bishop and Henkel (1962), pp. 207-208. This apparatus enables the volume changes to be measured under a back pressure of up to 160 psi. Five cubic centimeter

burettes are used enabling changes in volume of about 0.01 cc to be measured.*

5. Compression Test Machines

The compression test machines are strain controlled by a synchronous motor and gear box. The gear box has six 5-1 reductions and additional change wheels giving a total of thirty different rates of feed ranging from 0.3 to 0.000024 in./min. The capacity of the machines is 5 tons. The axial load is measured on a proving ring. For low pressure tests a number of proving rings having capacities of 300 to 1000 lb are used and sensitivies ranging from 0.125 to 0.725 lb/div. For high pressure tests proving rings with 3000-lb capacity and a sensitivity of about 2 lb/div. are used.

*In one test a higher accuracy was required and therefore a fine horizontal capillary tube with a mercury index was used as described by Alperstein (1964).

Table A-1

LIST OF SUPPLIERS OF EQUIPMENT

Low Pressure Triaxial Cells (0 to 160 psi)	Clockhouse Engineering, Ltd. Wykeham Farrance Engineering, Ltd.
High Pressure Triaxial Cells	Wykeham Farrance Engineering, Ltd.
Self-Compensating Mercury Controls (0 to 160 psi)	Wykeham Farrance Engineering, Ltd.
Compression Test Machines	Wykeham Farrance Engineering, Ltd. (Models 57 and 56)
High Pressure Test Gauges (0 to 1000 psi)	U. S. Gauge (Series 1400
High Pressure Nitrogen Tank Regulators	Air Reduction Co., Inc. (Style 1143
Proving Rings	A. S. Geonor Wykeham Farrance Engineering, Ltd.
Mercury Null Indicators	A. S. Geonor Wykeham Farrance Engineering, Ltd.
No Volume Change Valves (high pressure)	Hydromatics, Inc. (Series 715)
Differential Pressure Transducers	Dinisco Co. (Model PT 35)
Absolute Pressure Transducers	Dinisco Co. (Model PT 25)
X-Y Recorder	F. L. Mosely Co. (Model 4-S)
Differential (Digital) Voltmeter	Keithley Instruments, Inc. (Model 660)
Voltage Supply	Electronic Measurements Co. of Red Bank (Model TRO 18-1)
Volume Change Apparatus	M.I.T. Wykeham Farrance Engineering, Ltd.

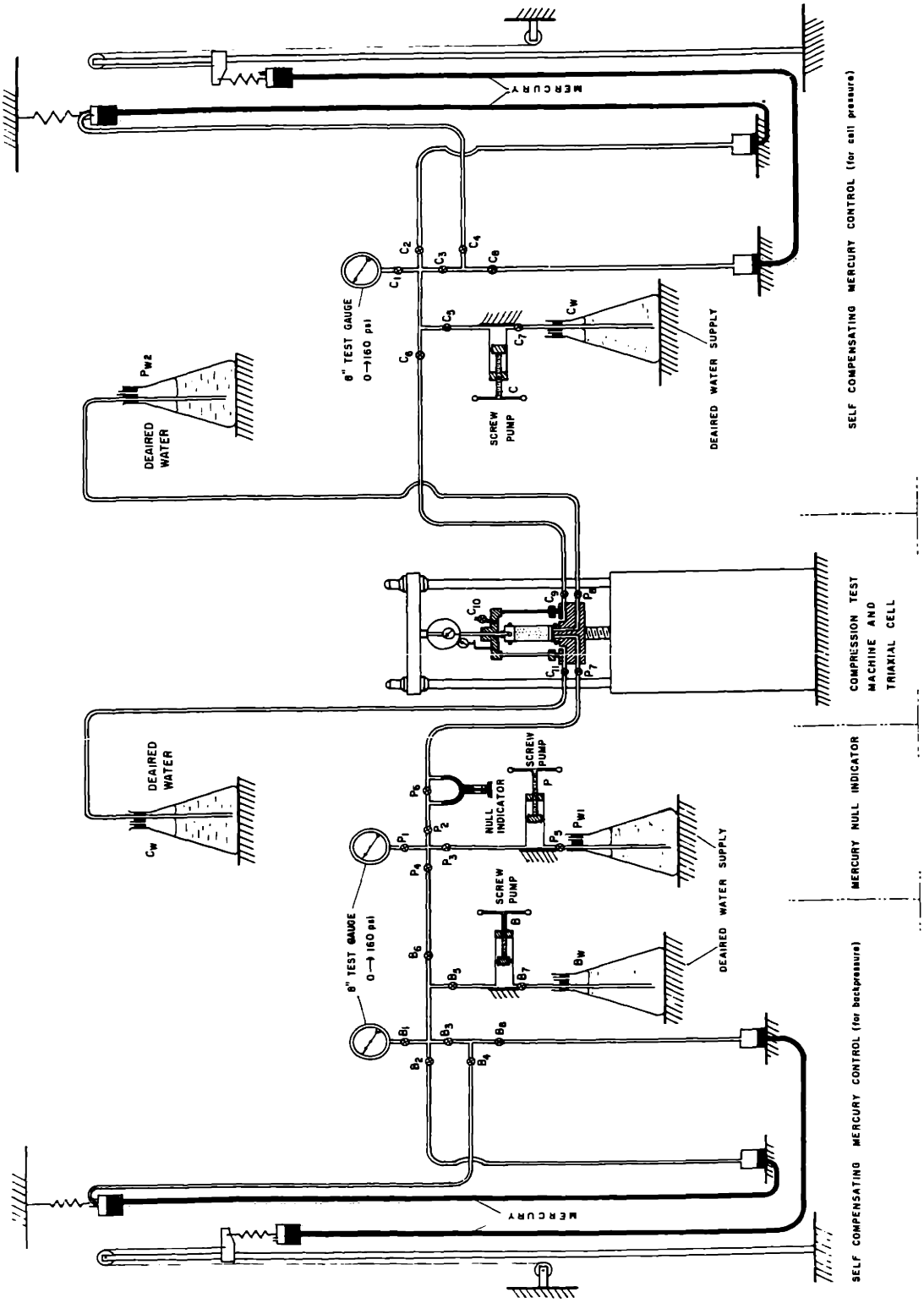

FIG. A-1 SCHEMATIC OF LOW PRESSURE TRIAXIAL SET UP

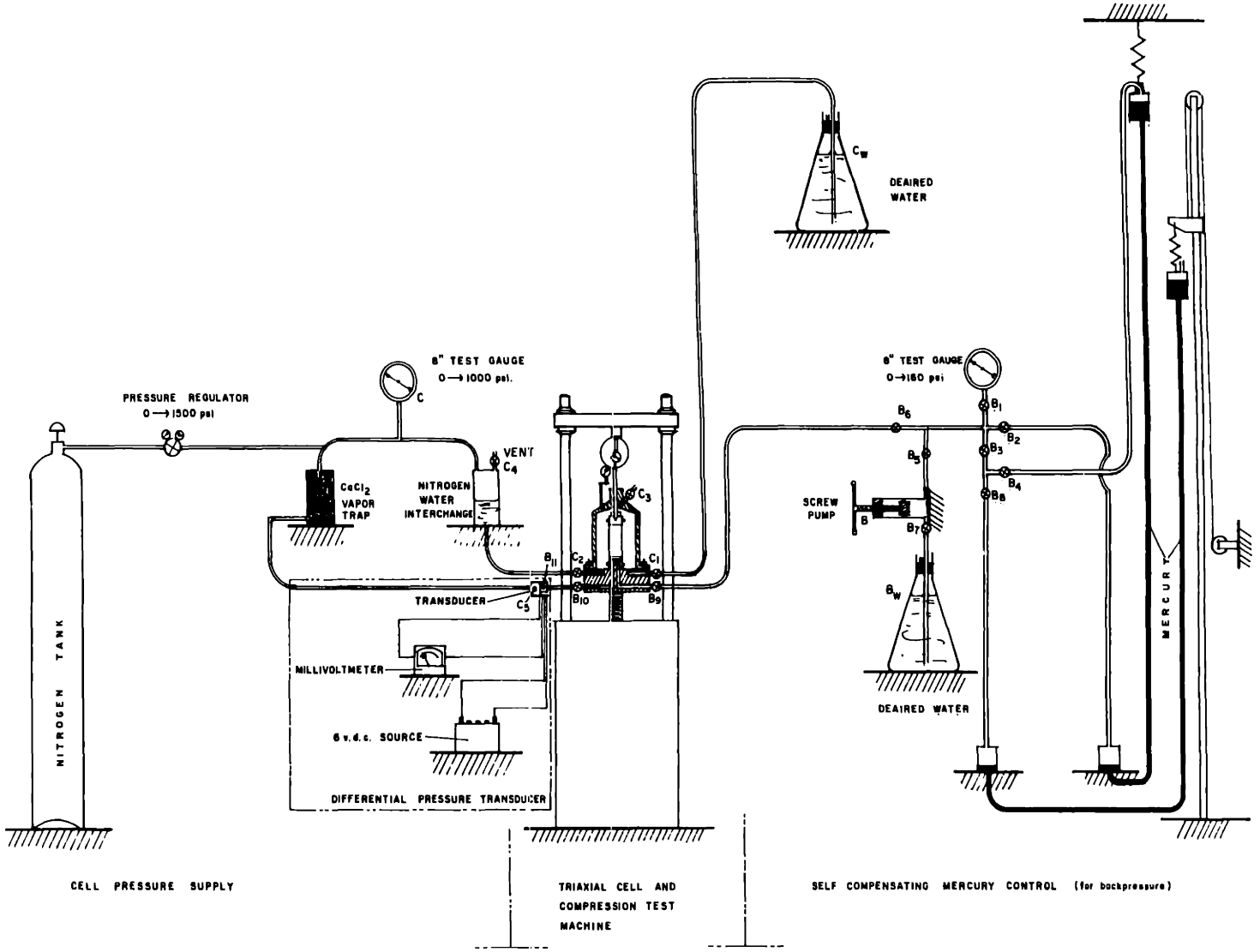

FIG. A-2 SCHEMATIC OF HIGH PRESSURE TRIAXIAL SET UP

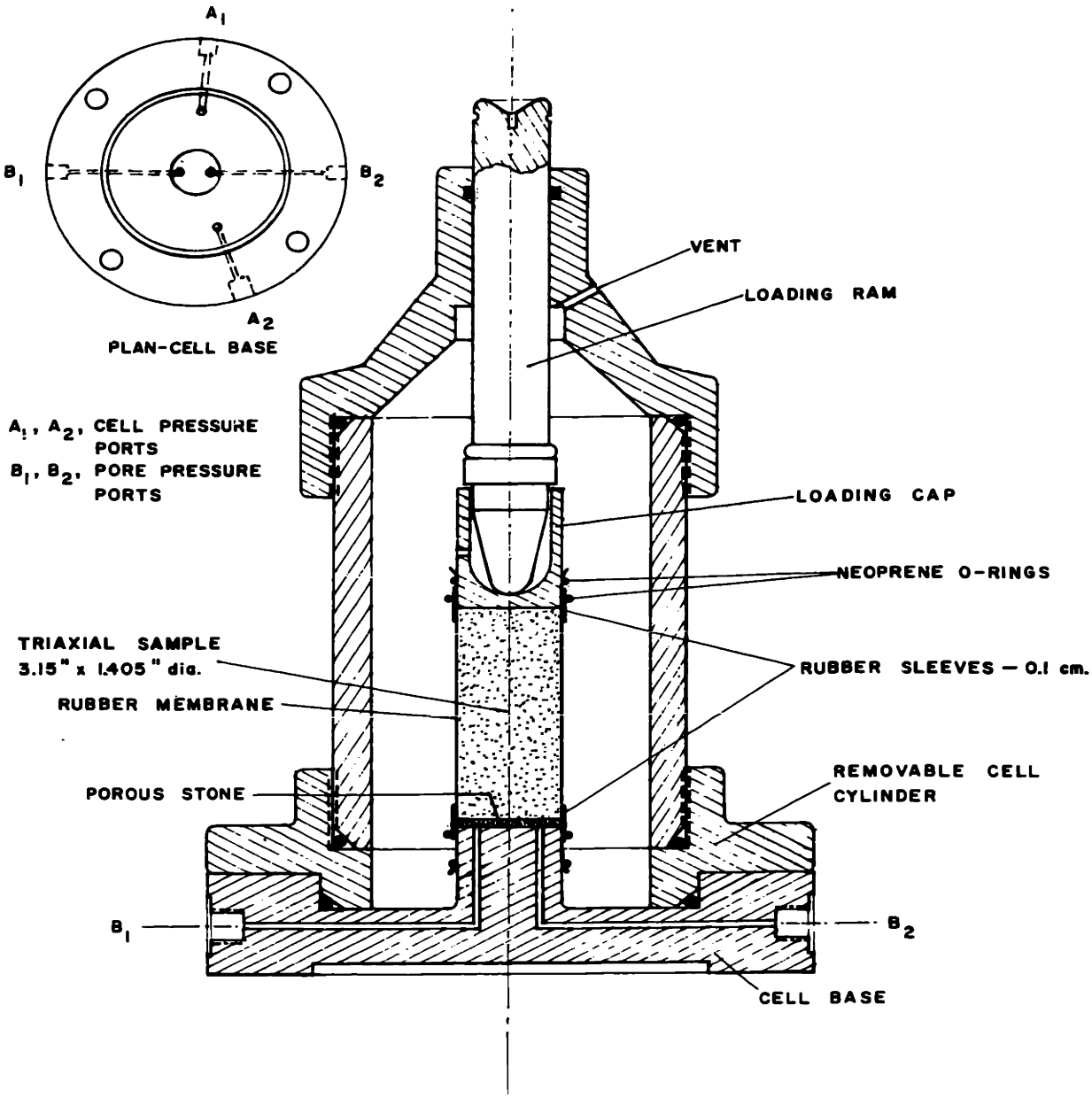

FIG. A-3 DETAILS OF THE HIGH PRESSURE TRIAXIAL CELL

APPENDIX B

STRESS-STRAIN RESULTS

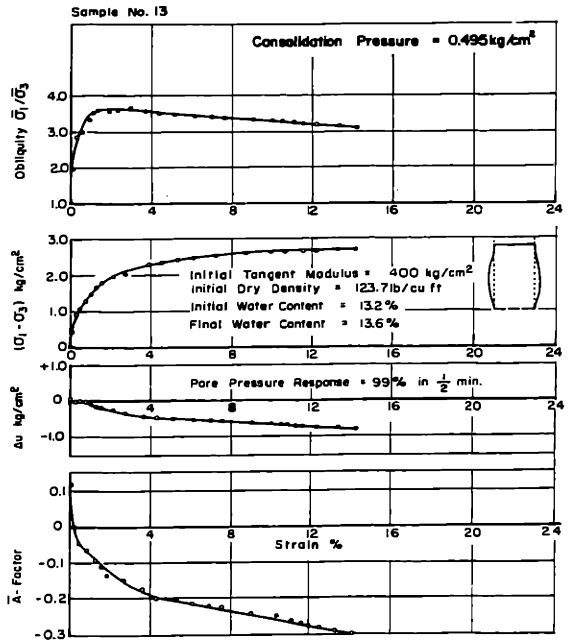

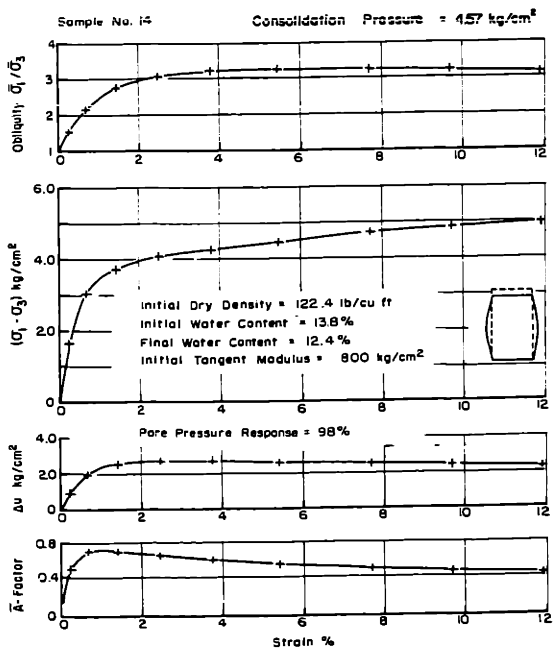

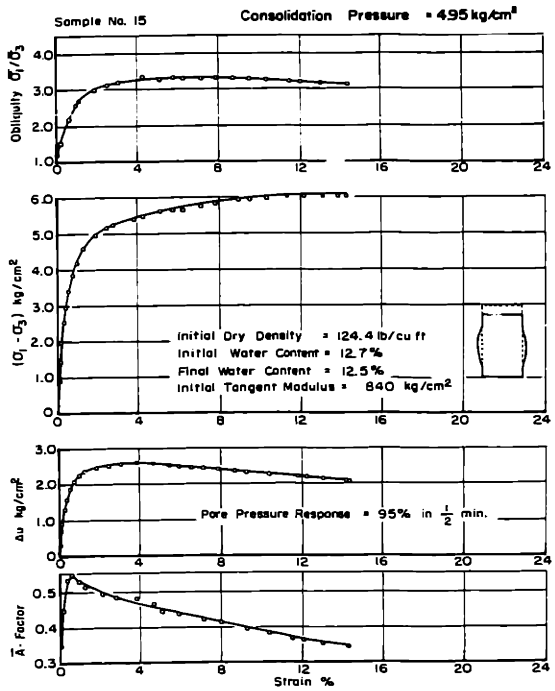

FIG. M - 1 STRESS - STRAIN BEHAVIOR OF UNTREATED M - 21 IN UNDRAINED SHEAR
(Low Consolidation Pressures)

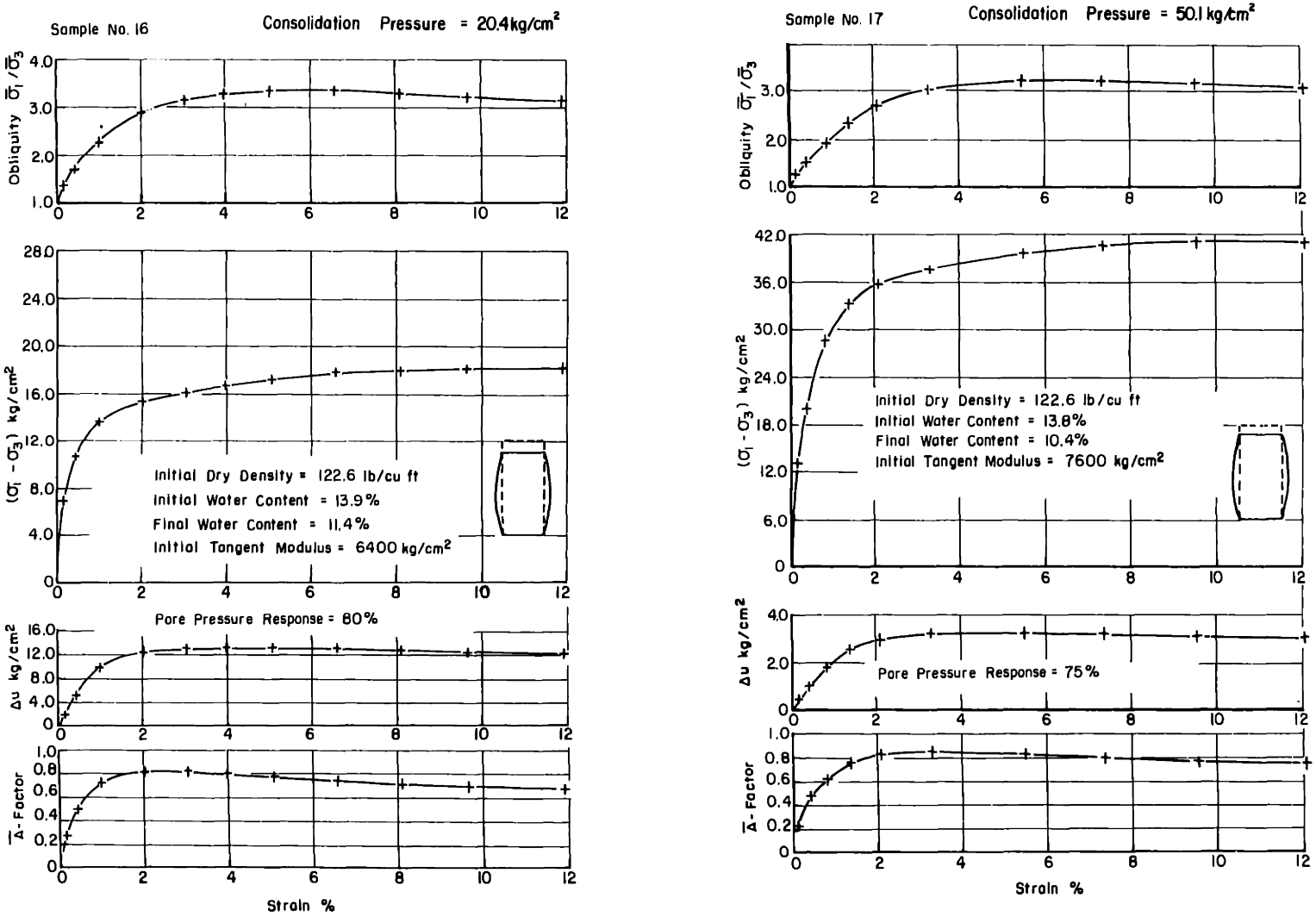

FIG. M - 2 STRESS - STRAIN BEHAVIOR OF UNTREATED M - 21 IN UNDRAINED SHEAR (High Consolidation Pressures)

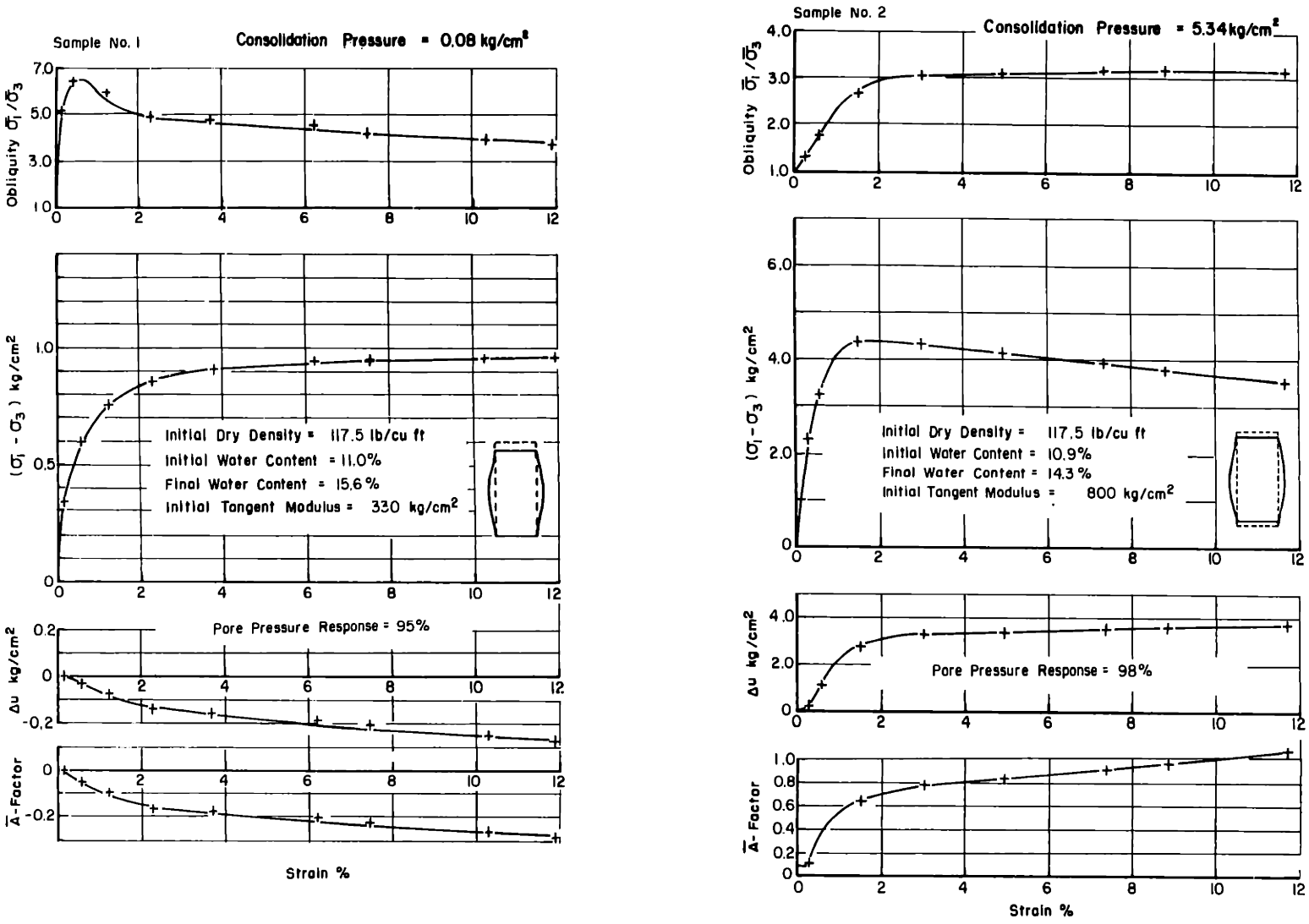

FIG. M-3 STRESS - STRAIN BEHAVIOR OF UNTREATED M-21 IN UNDRAINED SHEAR (DRY OF OPTIMUM)

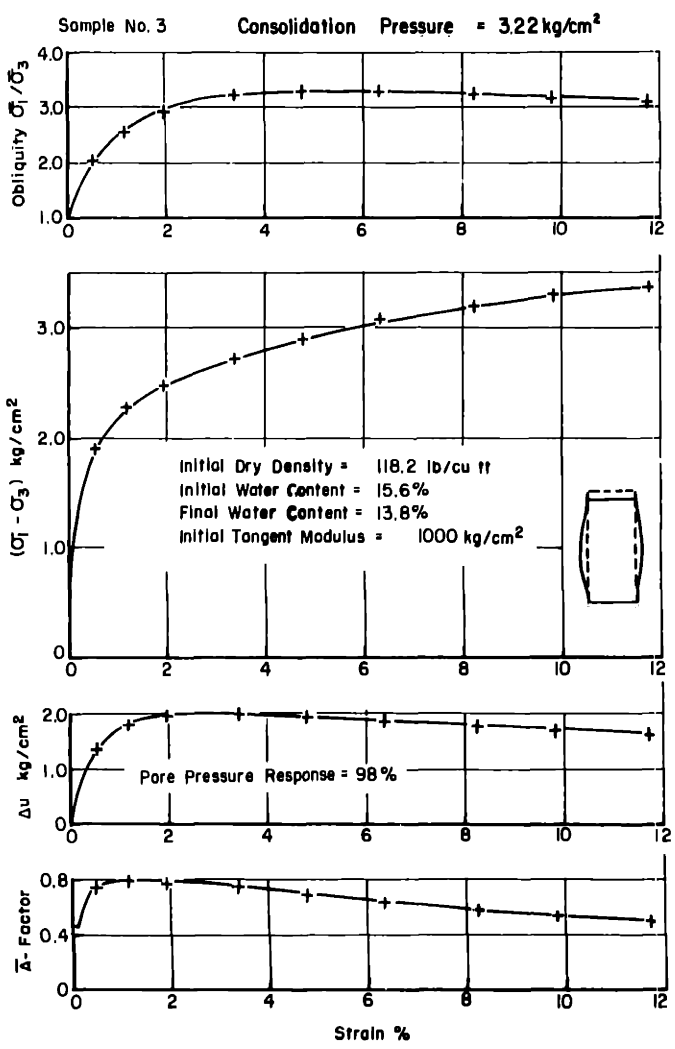

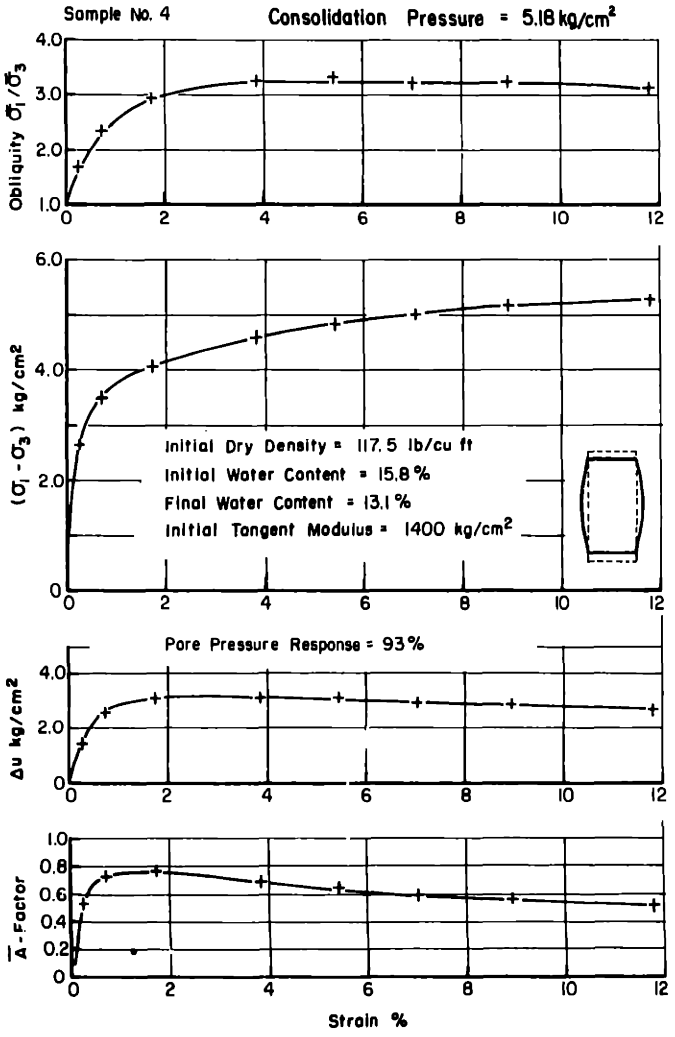

FIG. M - 4 STRESS - STRAIN BEHAVIOR OF UNTREATED M - 21 IN UNDRAINED SHEAR. (WET OF OPTIMUM)

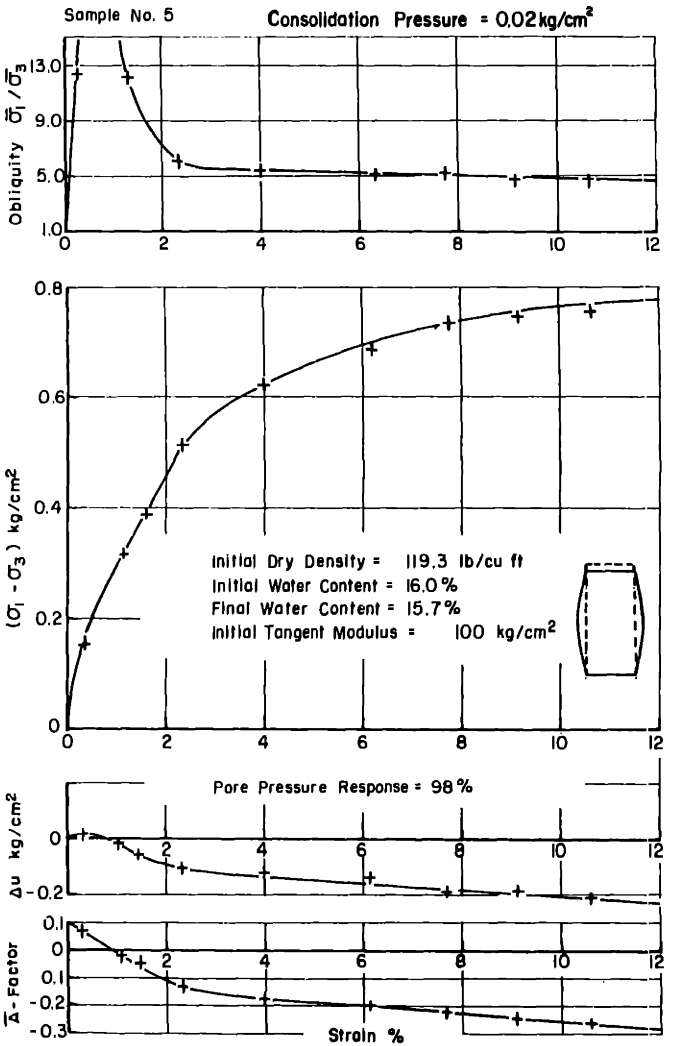

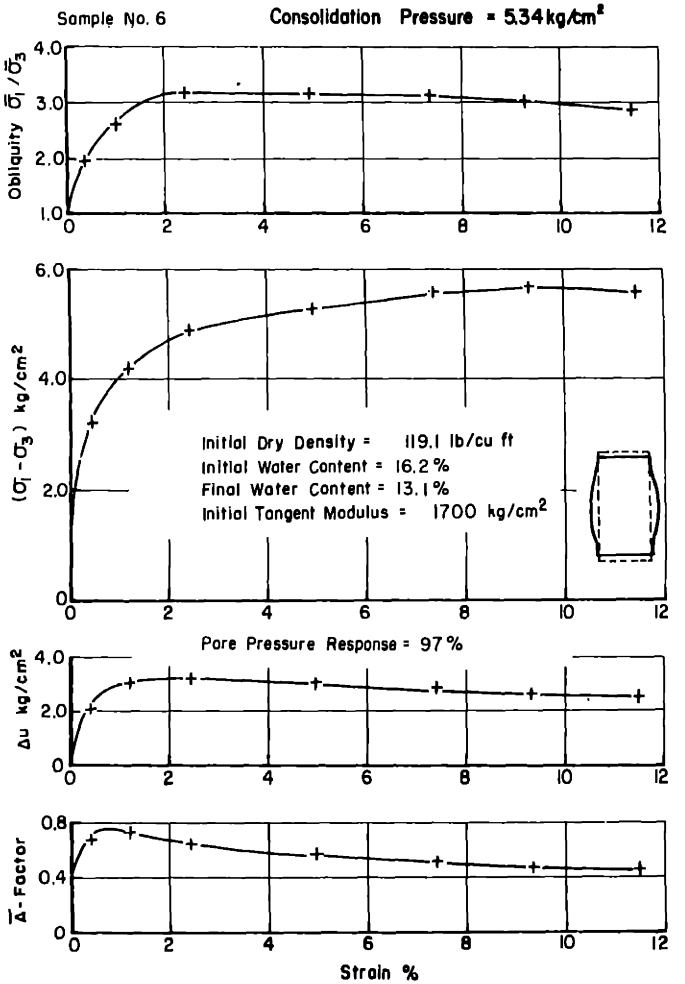

FIG. M-5 STRESS - STRAIN BEHAVIOR OF UNTREATED M-21 IN UNDRAINED SHEAR (800 psi COMPACTIVE EFFORT)

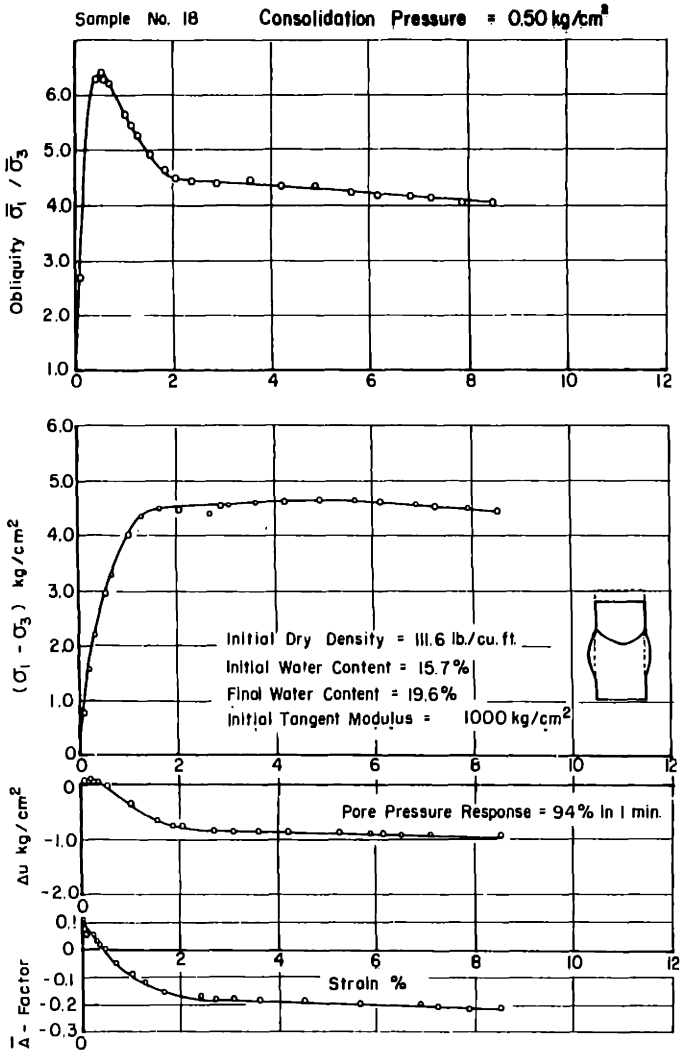

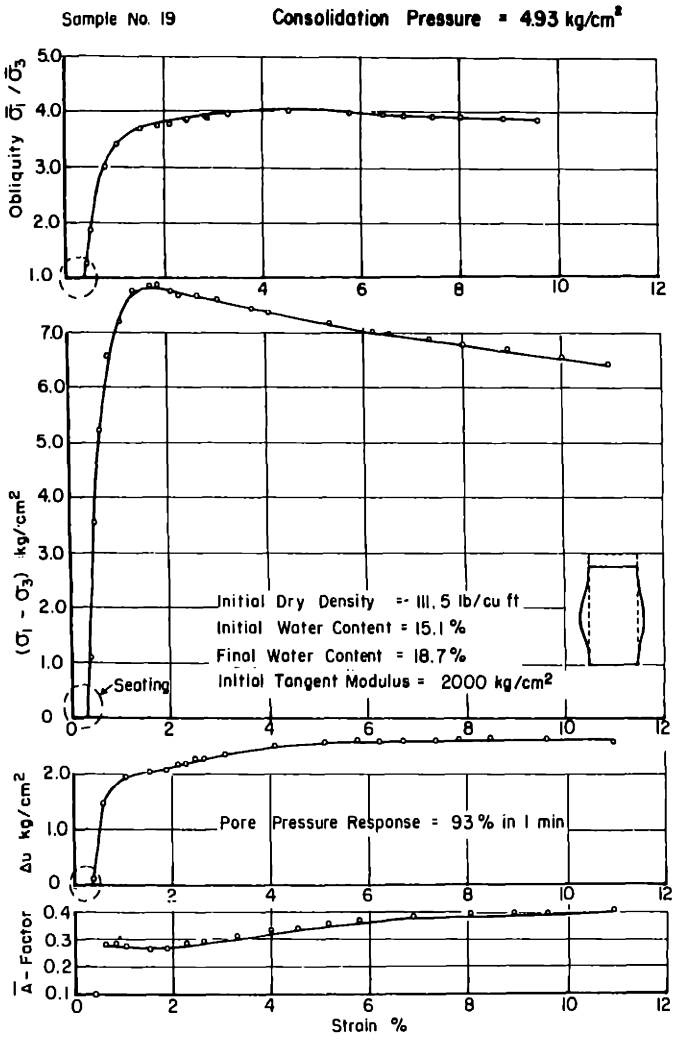

FIG. ML - 1 STRESS - STRAIN BEHAVIOR OF M - 21 + 5% LIME IN UNDRAINED SHEAR. CURING TIME 4 DAYS.

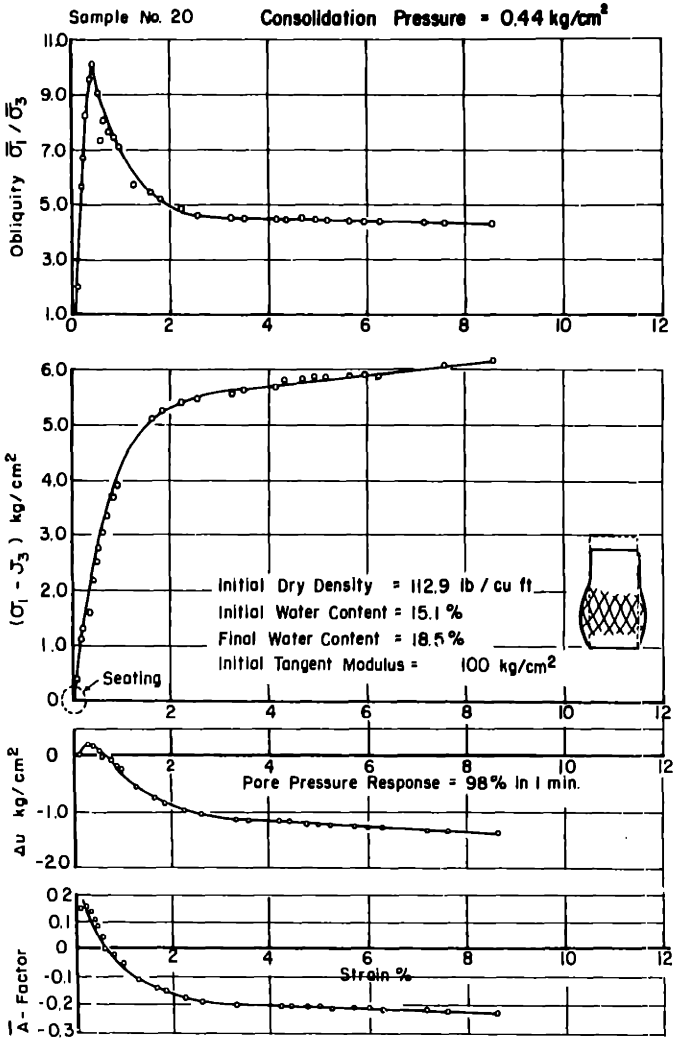

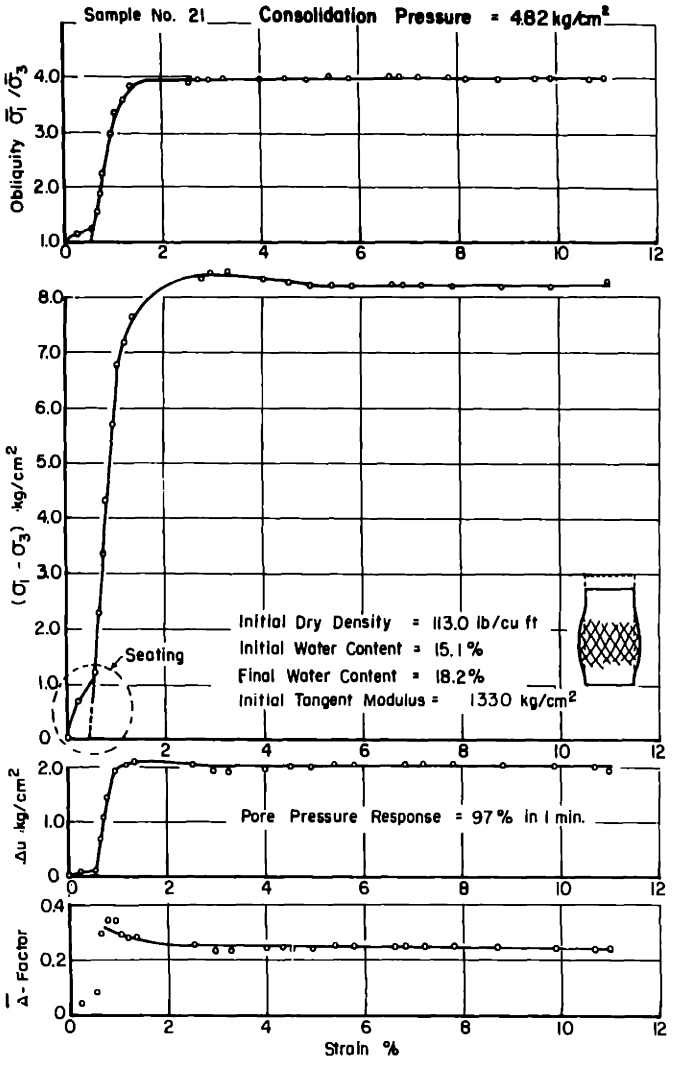

FIG. ML - 2 STRESS - STRAIN BEHAVIOR OF M - 21 + 5% LIME IN UNDRAINED SHEAR CURING TIME 8 DAYS.

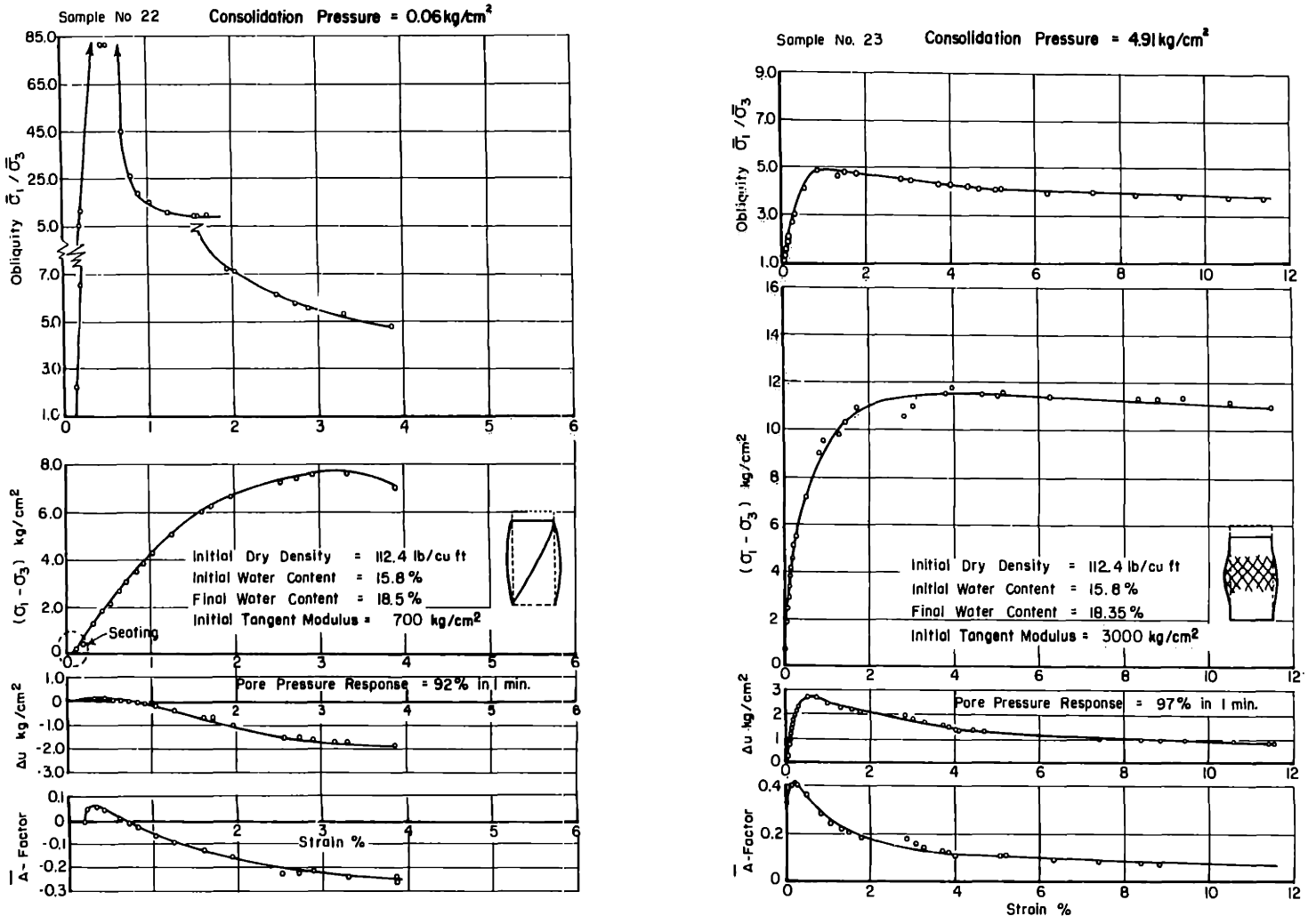

FIG. ML-3 STRESS - STRAIN BEHAVIOR OF M-21 + 5% LIME IN UNDRAINED SHEAR. CURING TIME 17 DAYS.

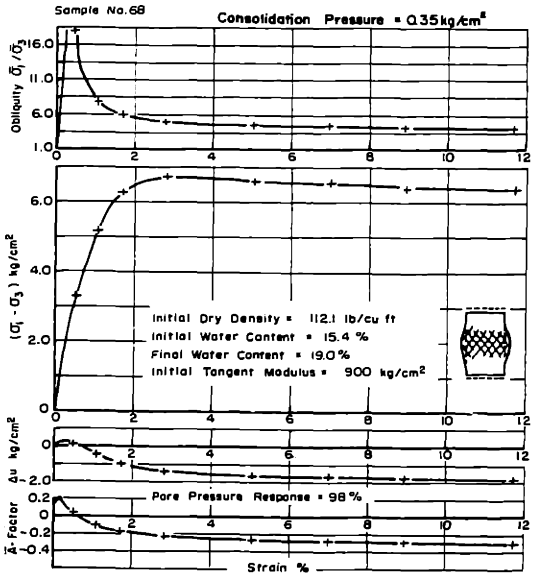

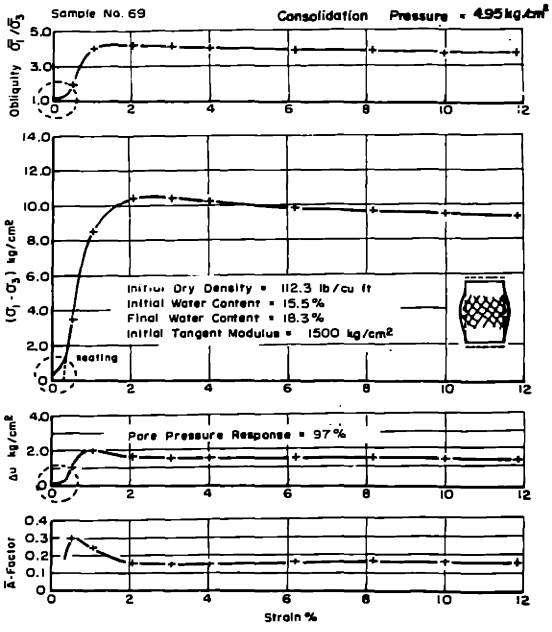

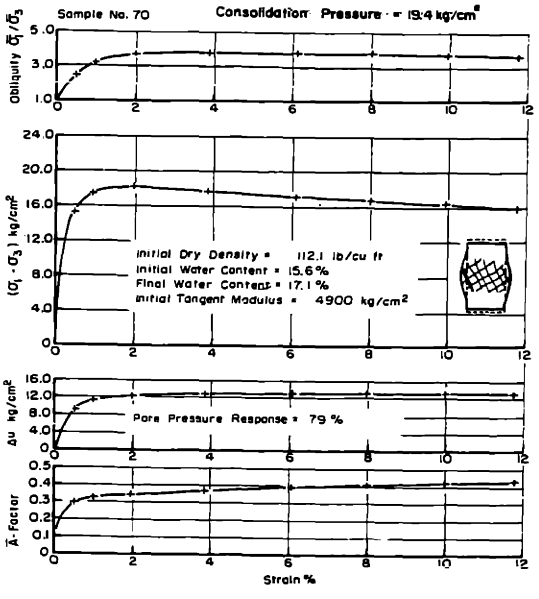

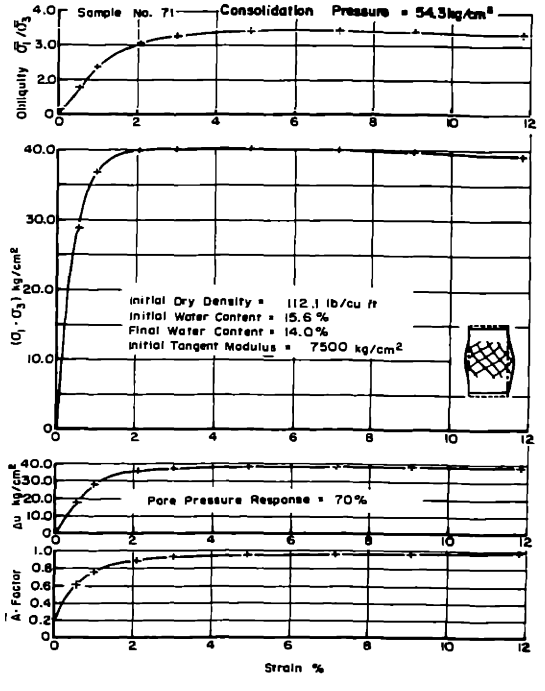

FIG. ML - 4 STRESS - STRAIN BEHAVIOR OF M - 21 + 5% LIME IN UNDRAINED SHEAR. CURING TIME 20 DAYS.

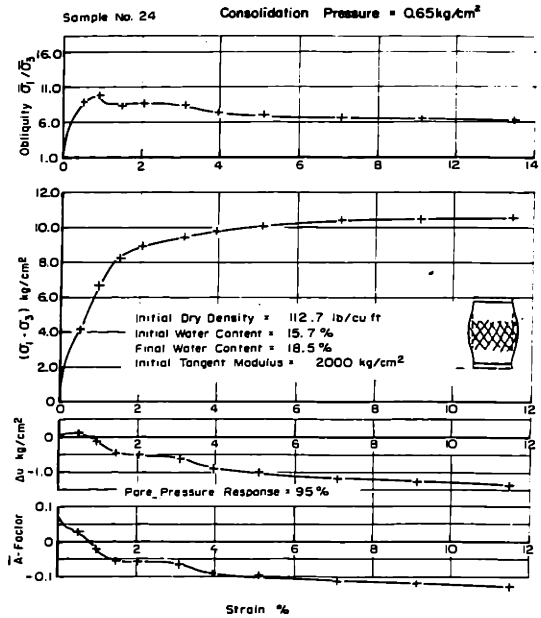

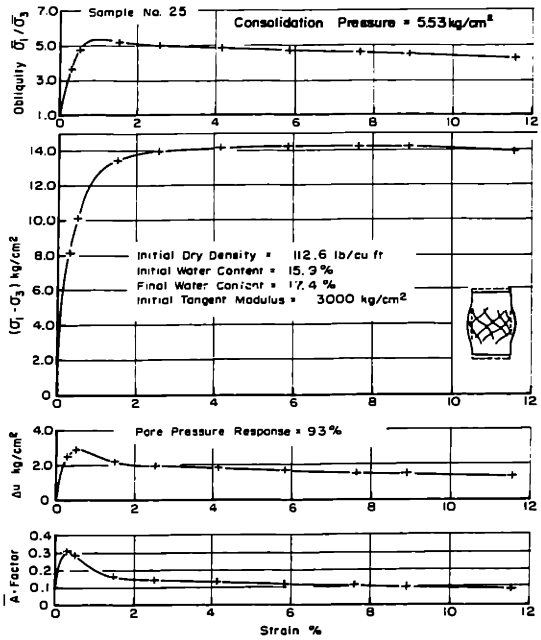

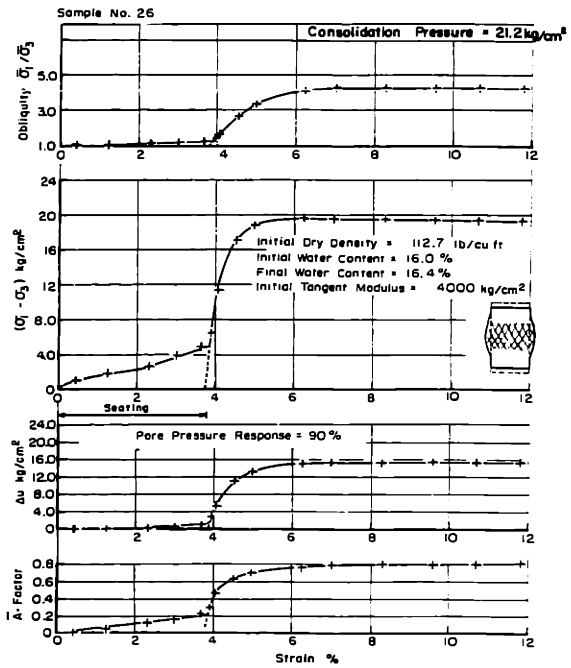

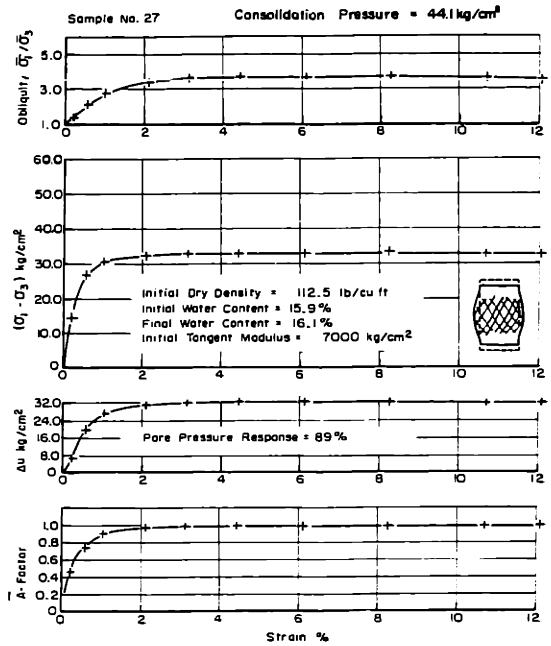

FIG. ML - 5 STRESS - STRAIN BEHAVIOR OF M - 21 + 5% LIME IN UNDRAINED SHEAR. CURING TIME 35 DAYS.

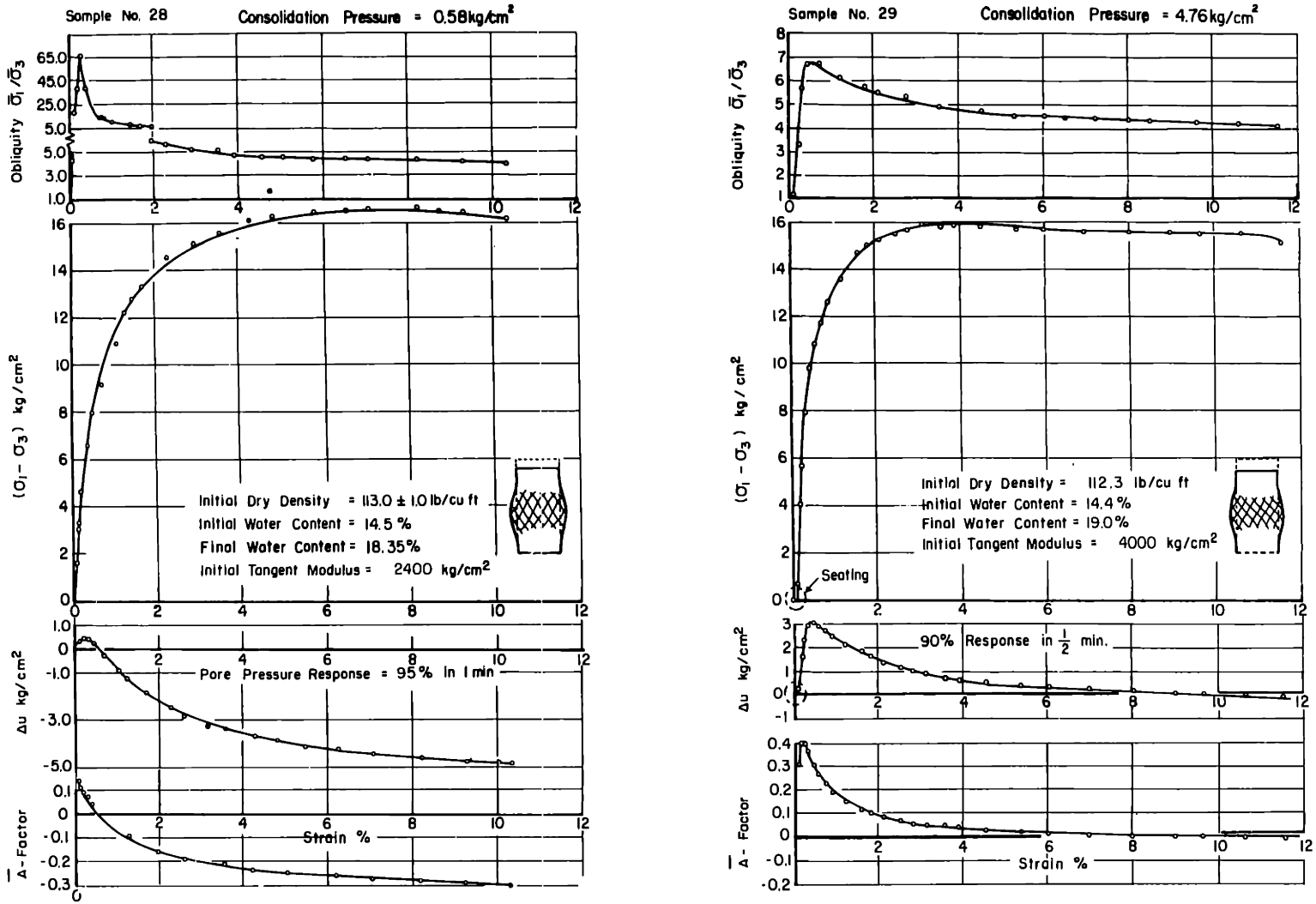

FIG. ML - 6 STRESS - STRAIN BEHAVIOR OF M - 21 + 5% LIME IN UNDRAINED SHEAR. CURING TIME 59 DAYS.

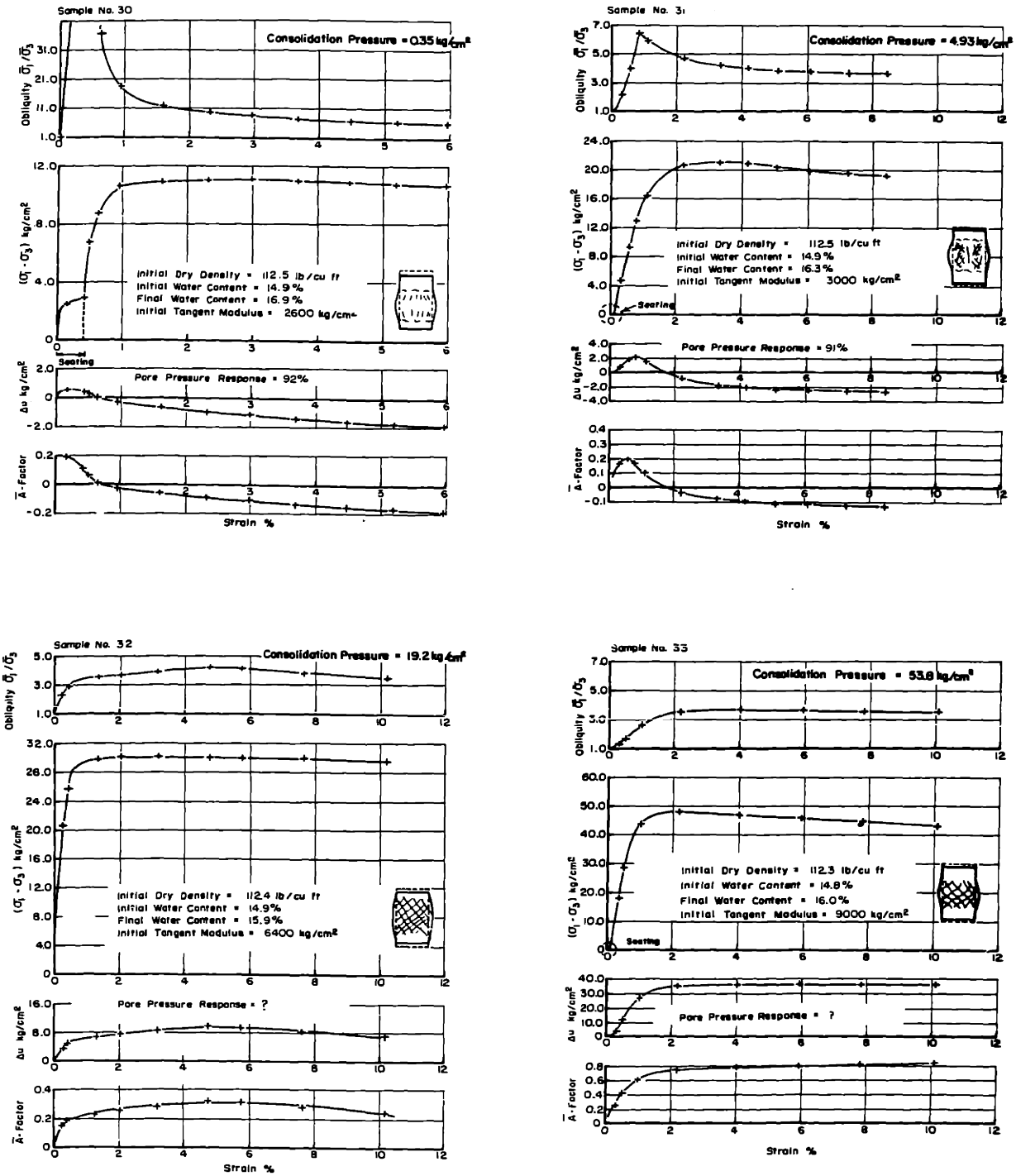

FIG. ML - 7 STRESS - STRAIN BEHAVIOR OF M - 21 + 5% LIME IN UNDRAINED SHEAR. CURING TIME 138 DAYS.

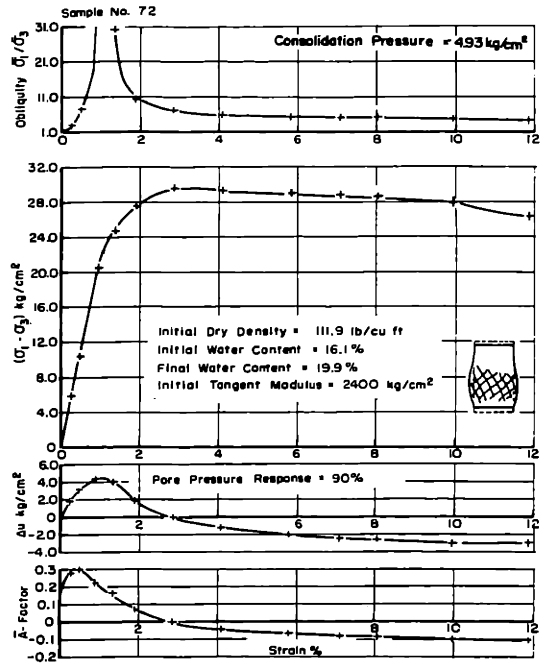

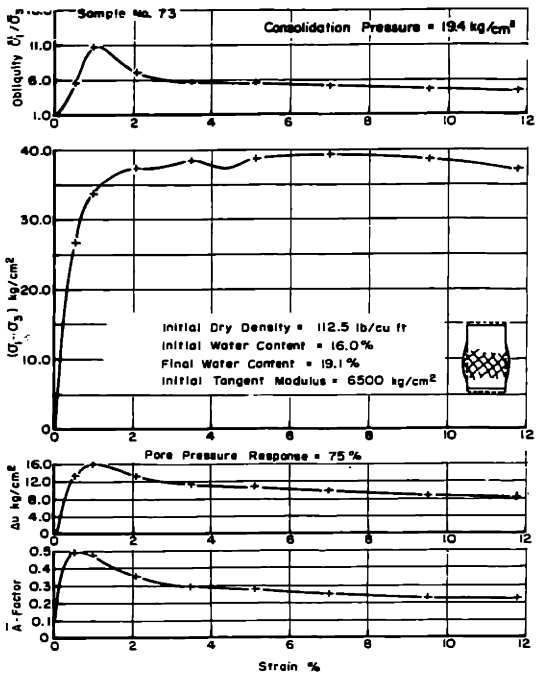

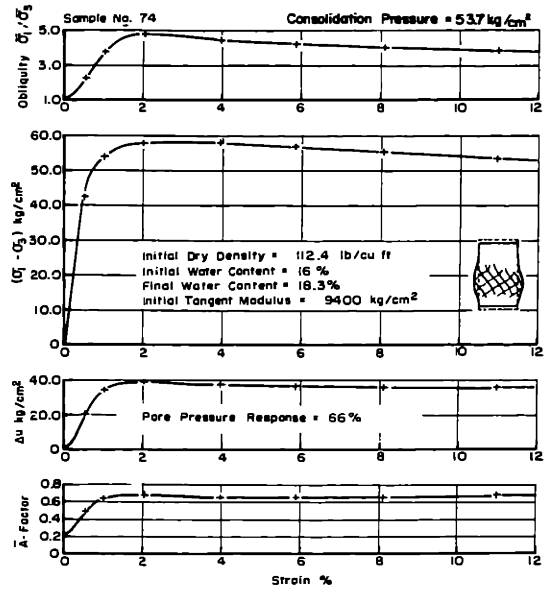

FIG. ML-8 STRESS - STRAIN BEHAVIOR OF M-21•5% LIME IN UNDRAINED SHEAR. CURING TIME 275 DAYS

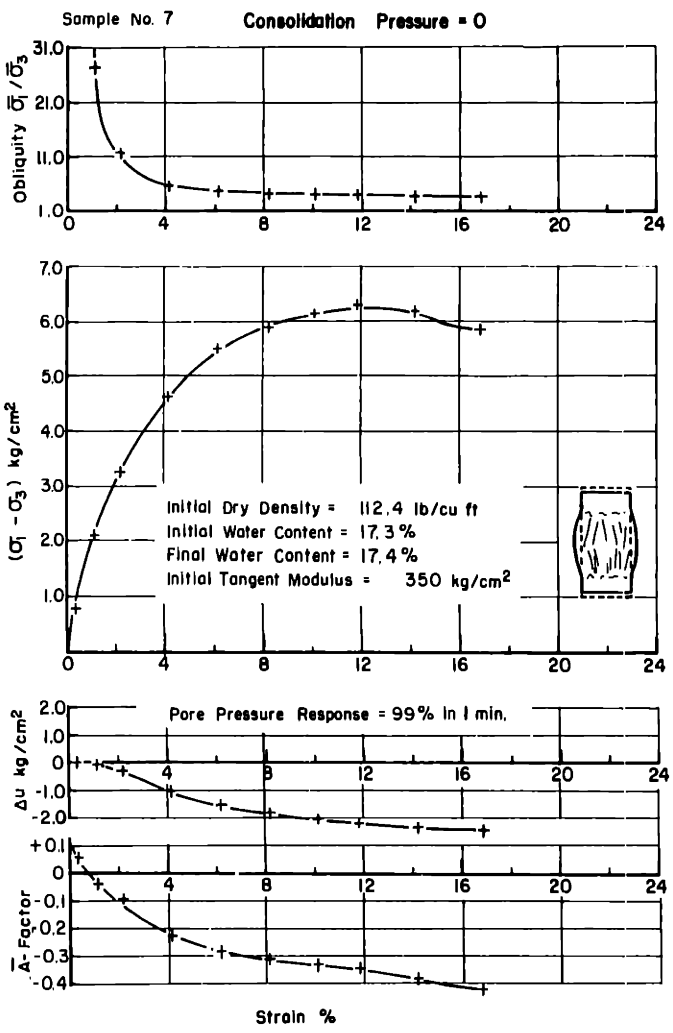

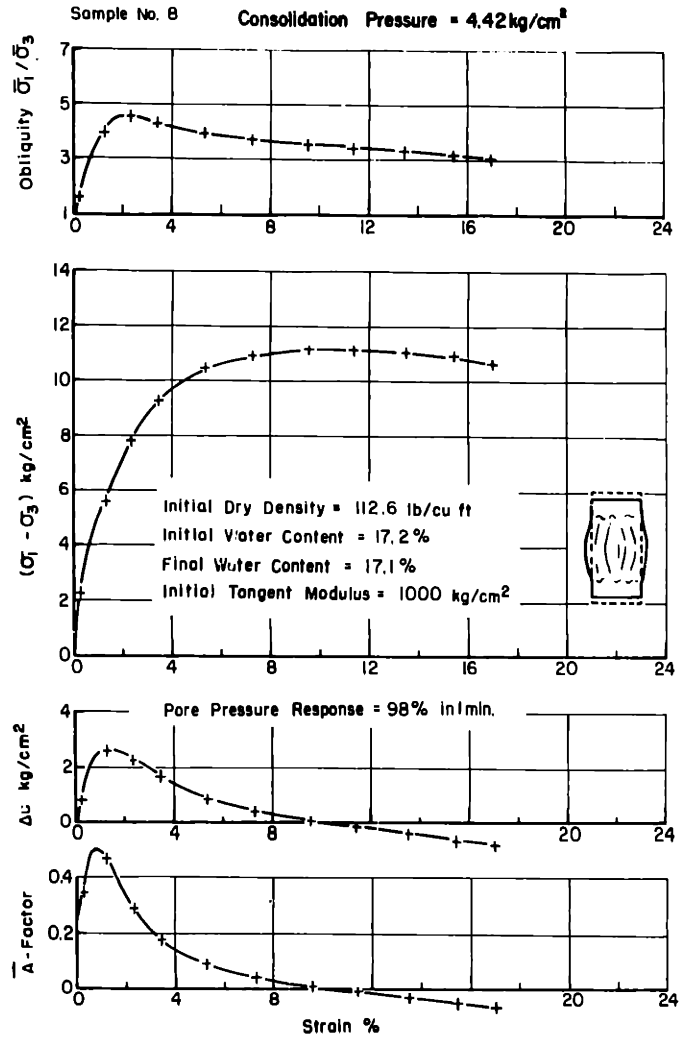

FIG. ML-9 STRESS - STRAIN BEHAVIOR OF M-21 + 5% LIME IN UNDRAINED SHEAR (WET OF OPTIMUM)

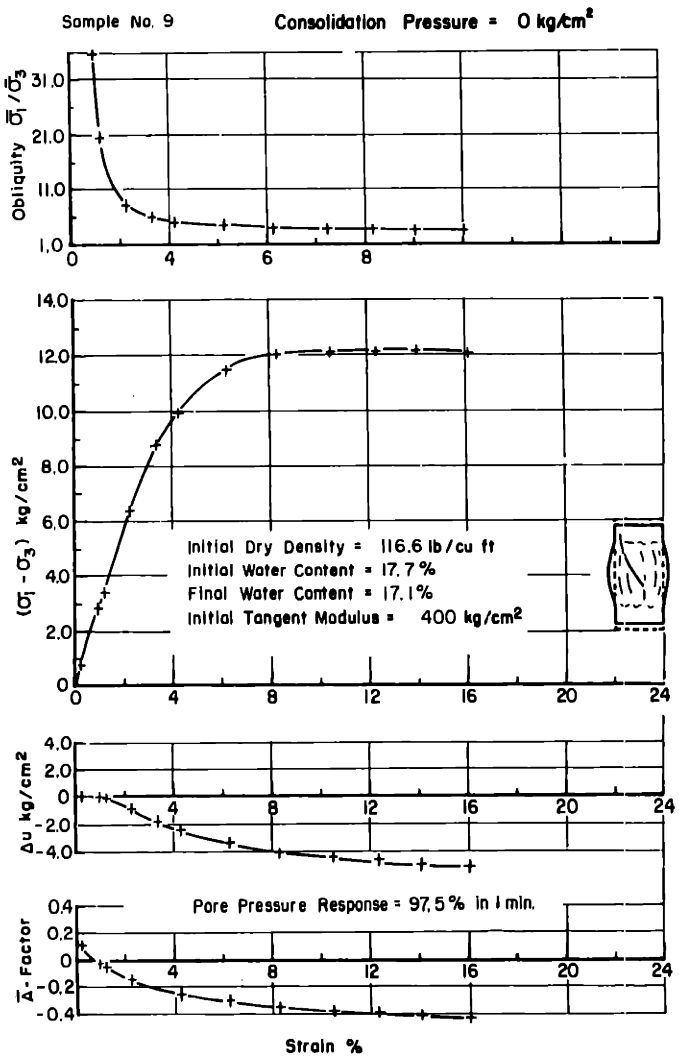

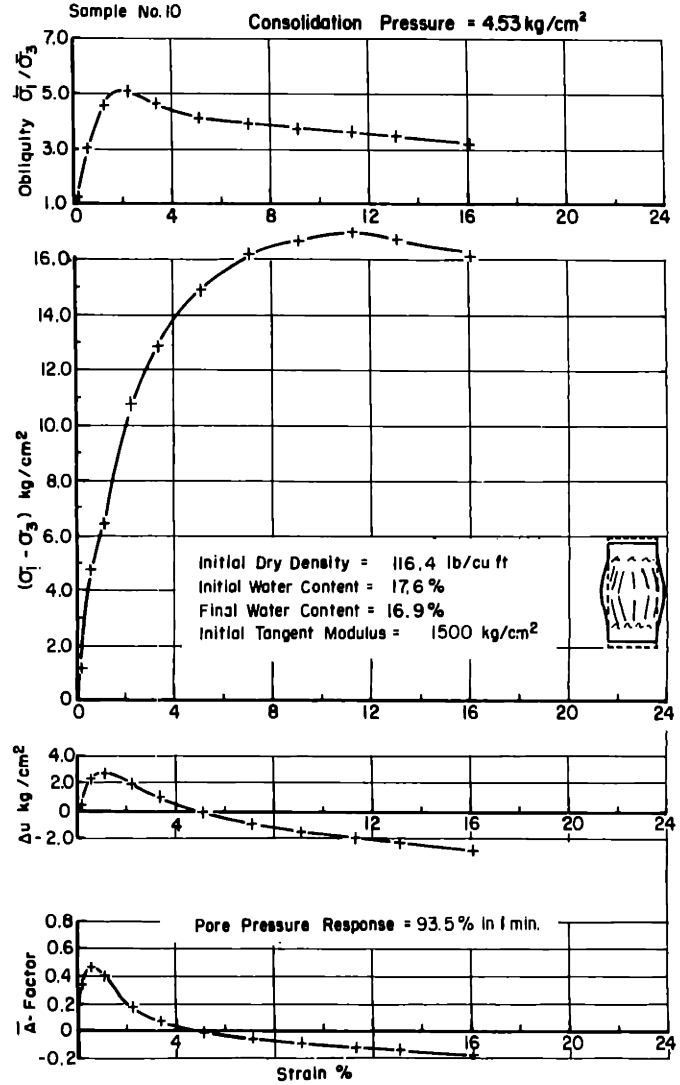

FIG. ML-10 STRESS - STRAIN BEHAVIOR OF M - 21 + 5% LIME IN UNDRAINED SHEAR (800 psi COMPACTIVE EFFORT)

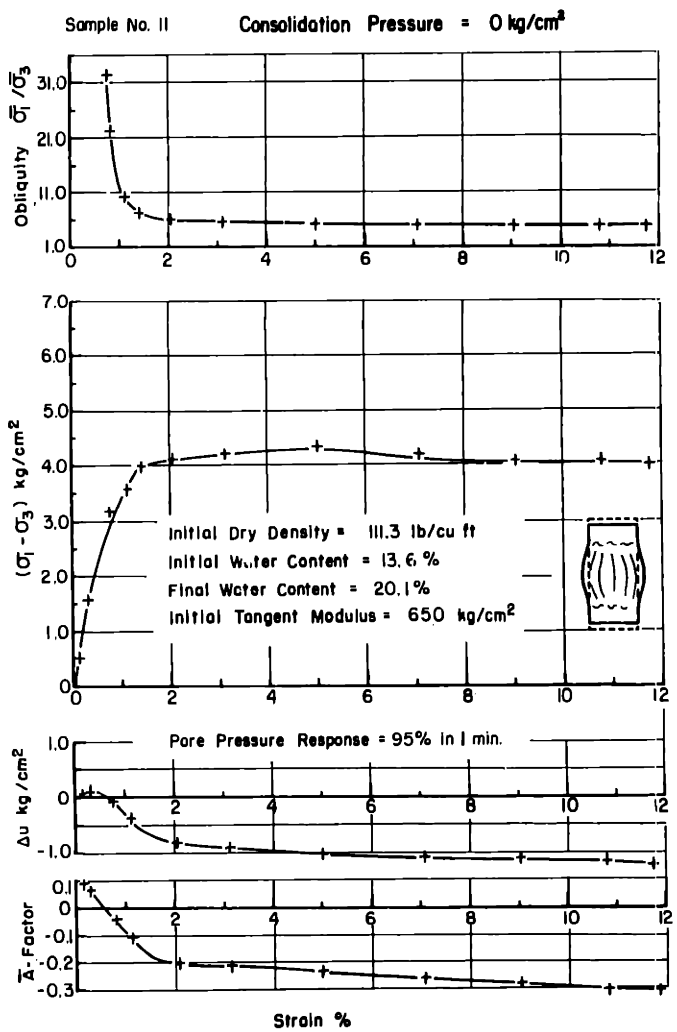

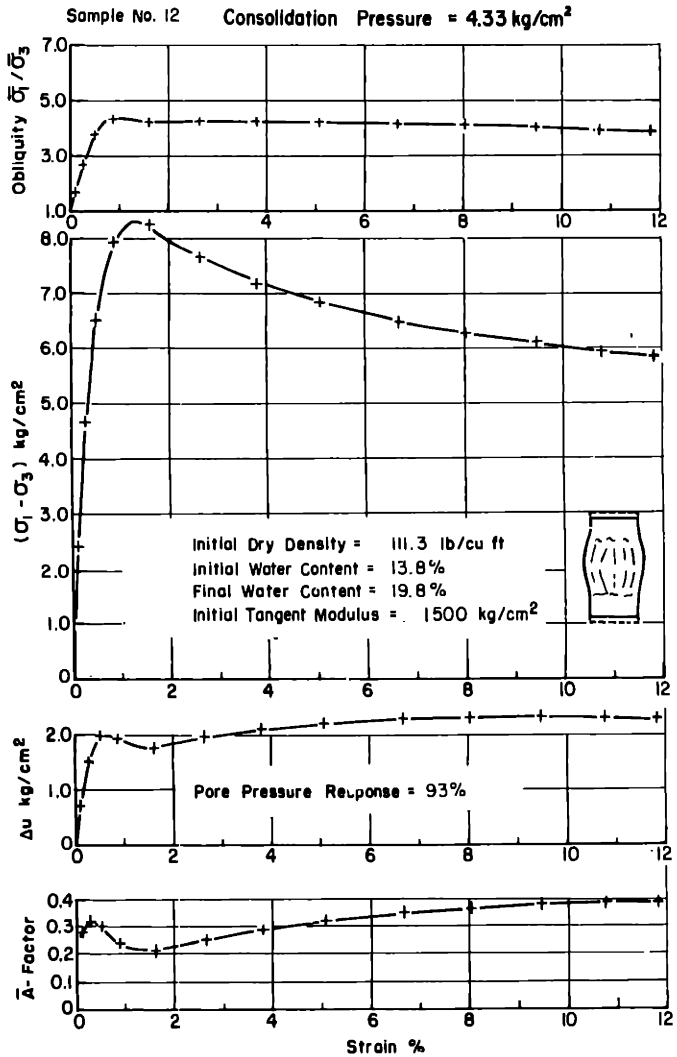

FIG. ML-11 STRESS - STRAIN BEHAVIOR OF M - 21 + 5% LIME IN UNDRAINED SHEAR (DRY OF OPTIMUM)

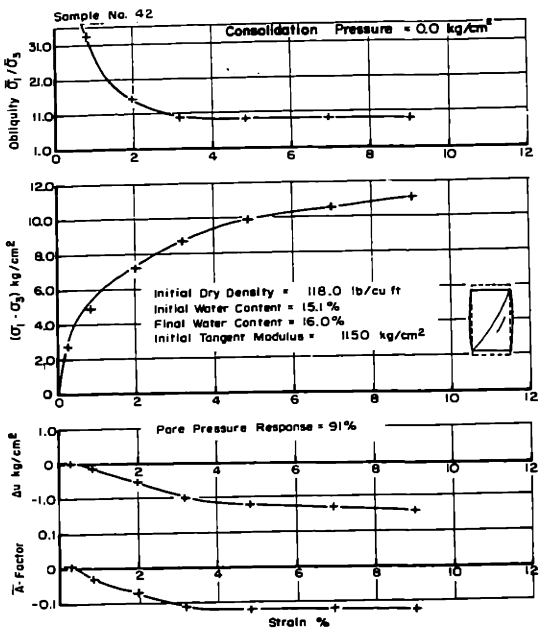

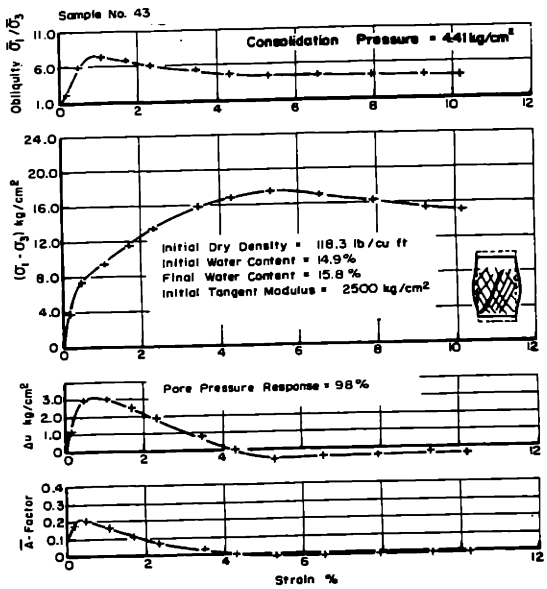

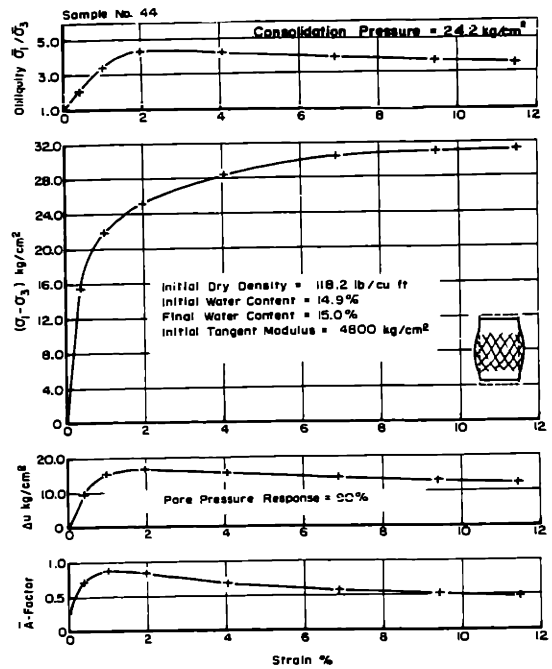

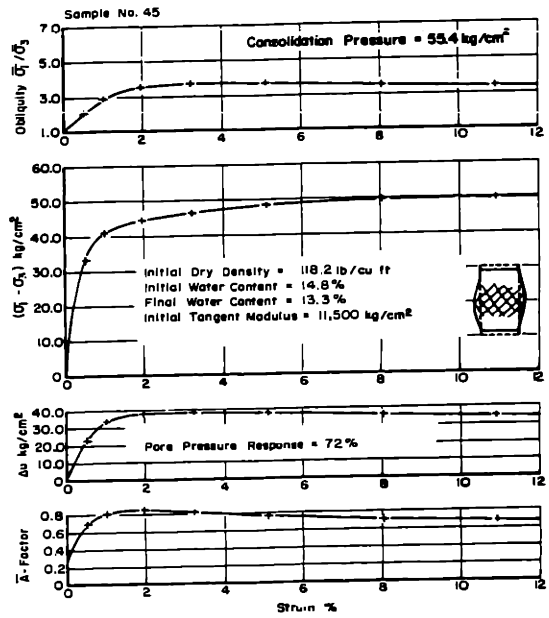

FIG. MC - 1 STRESS - STRAIN BEHAVIOR OF M - 21 + 3% CEMENT. CURING TIME 21 DAYS

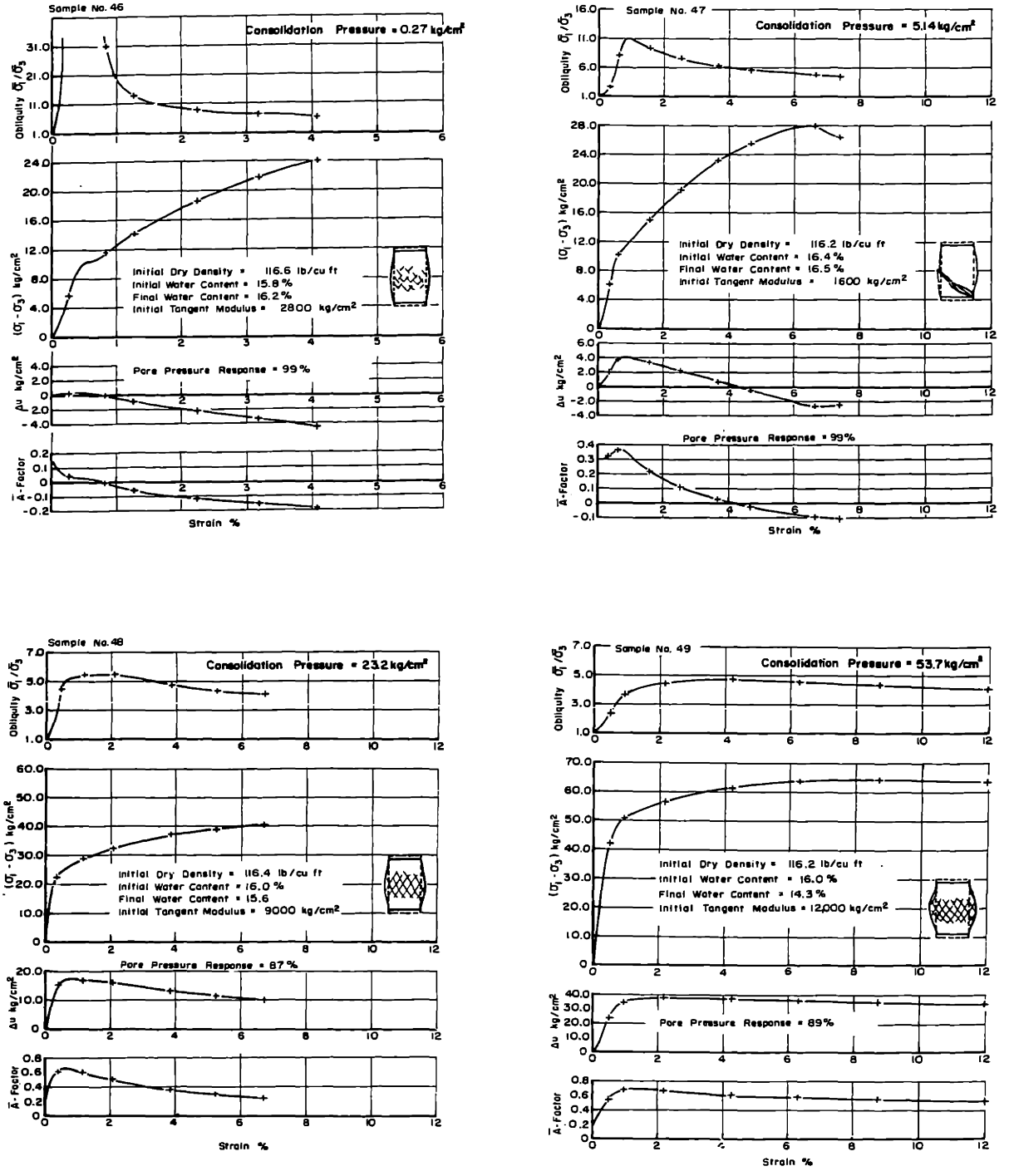

FIG. MC - 2 STRESS - STRAIN BEHAVIOR OF M - 21 + 5% CEMENT. CURING TIME 10 DAYS

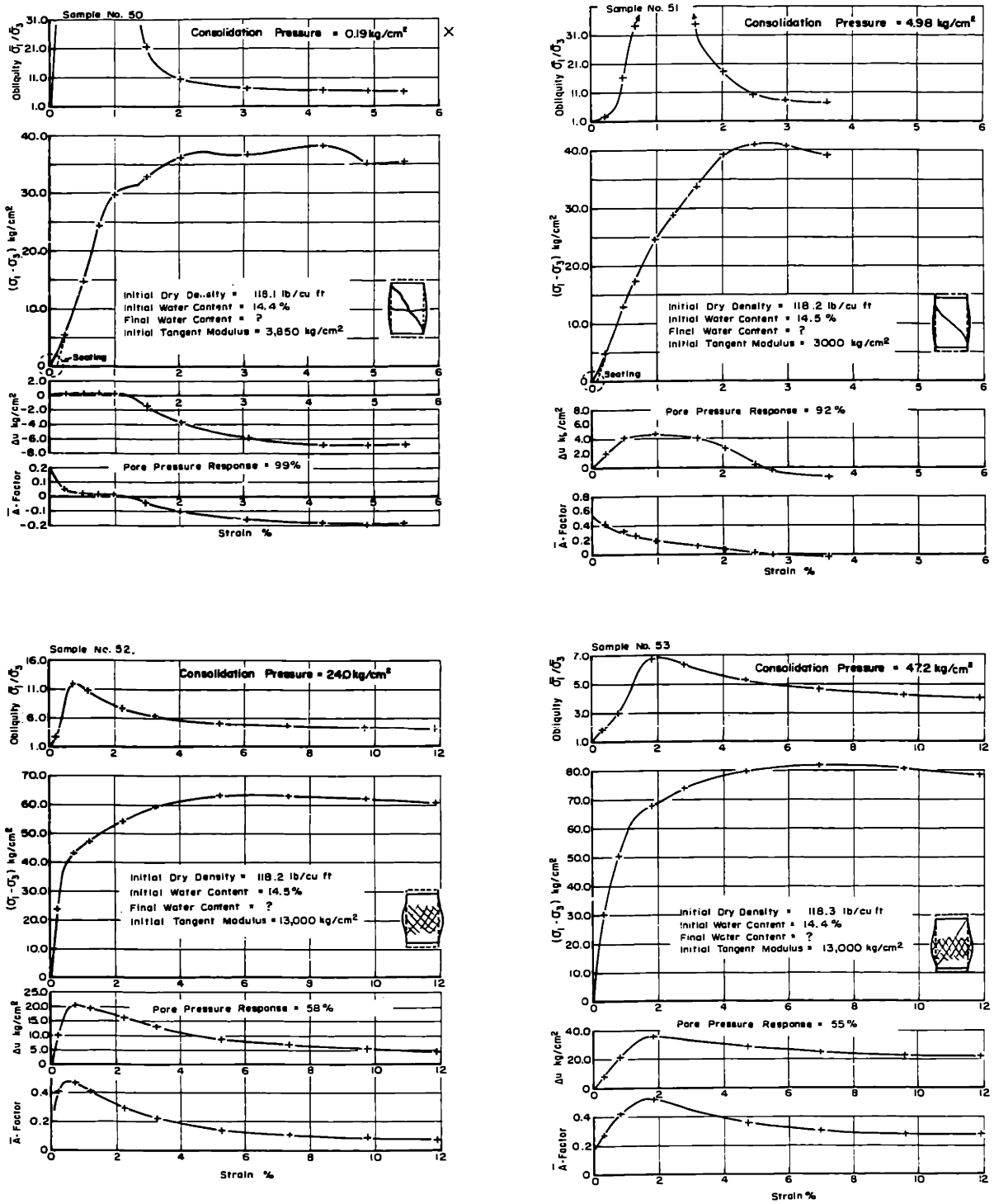

FIG. MC-3 STRESS - STRAIN BEHAVIOR OF M-21 + 5% CEMENT. CURING TIME 50 DAYS.

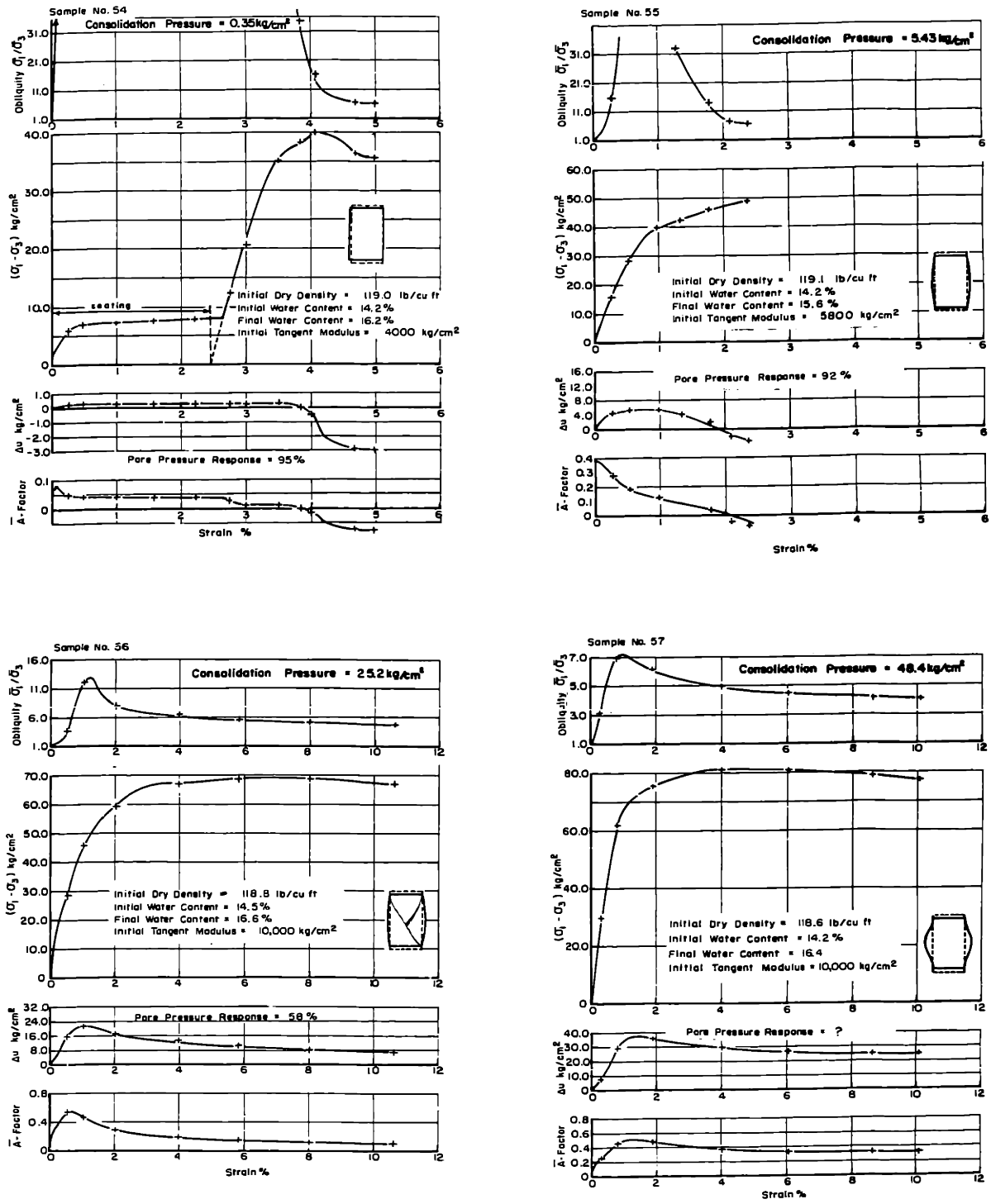

FIG. MC - 4 STRESS - STRAIN BEHAVIOR OF M - 21 + 5% CEMENT. CURING TIME 98 DAYS.

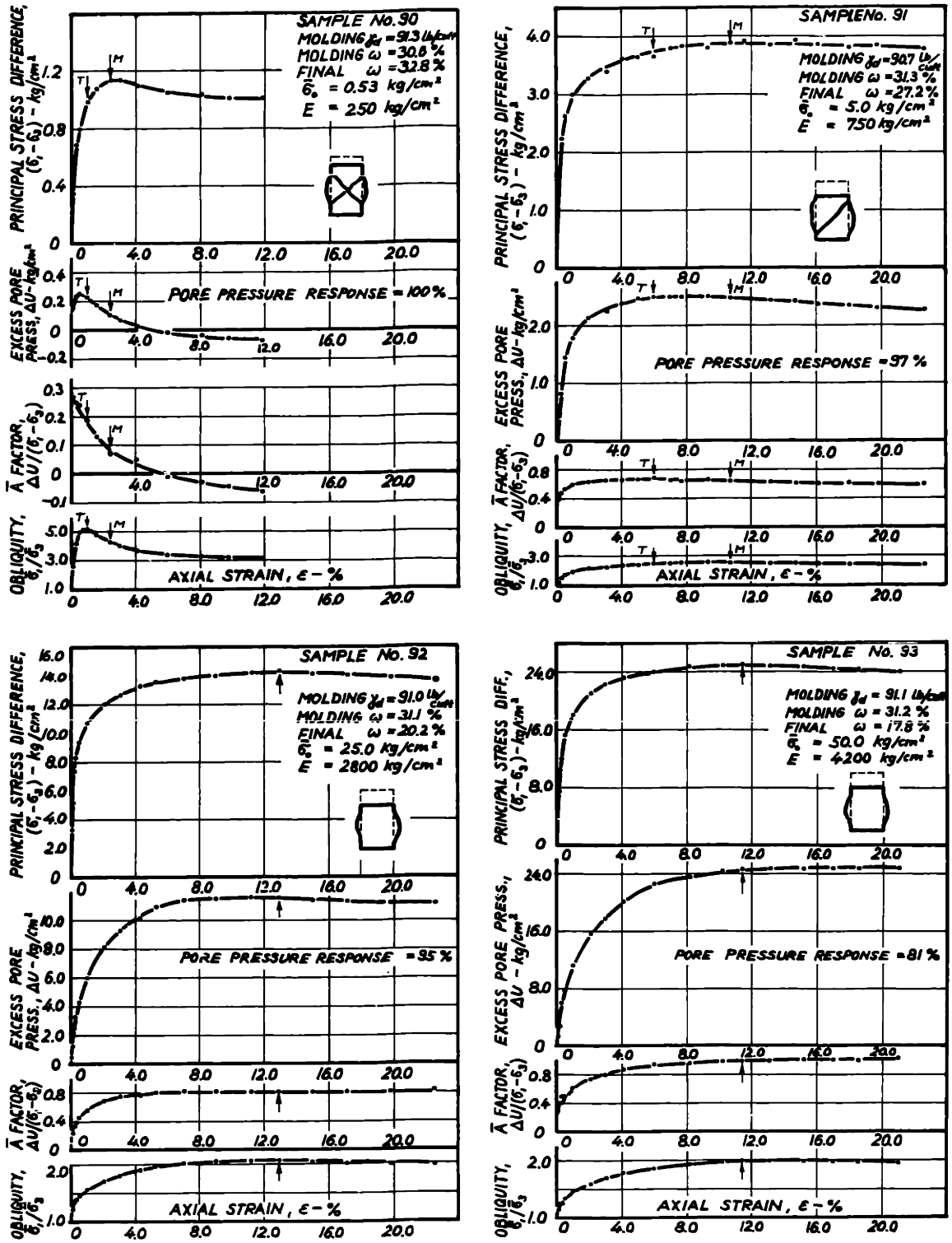

FIG. V-1 STRESS-STRAIN BEHAVIOR OF UNTREATED VICKSBURG BUCKSHOT CLAY IN UNDRAINED SHEAR.

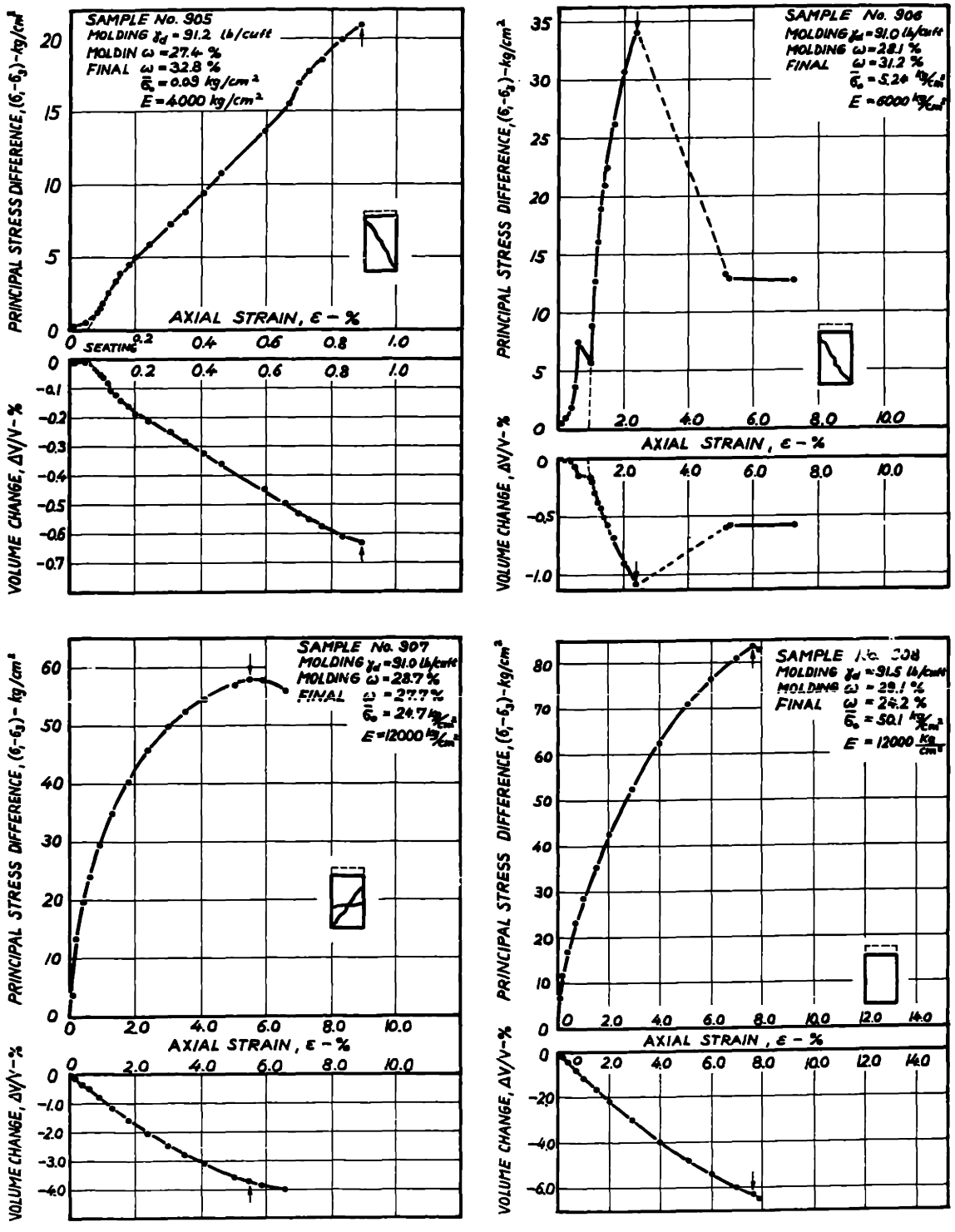

FIG. V-2 STRESS-STRAIN BEHAVIOR IN DRAINED SHEAR OF VICKSBURG BUCKSHOT CLAY STABILIZED WITH 5% LIME AND CURED 1 YEAR.

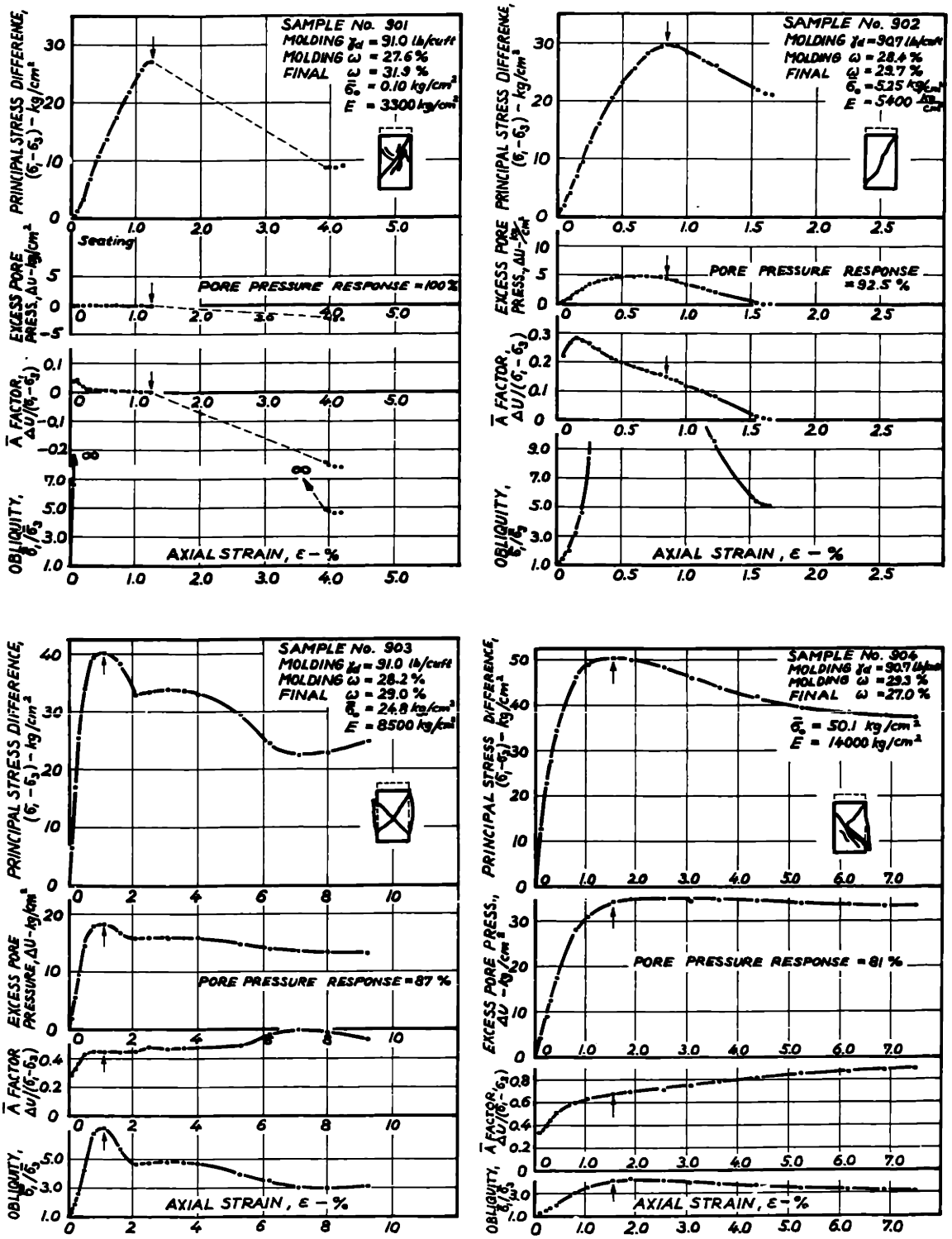

FIG. V-3 STRESS-STRAIN BEHAVIOR IN UNDRAINED SHEAR OF VICKSBURG BUCKSHOT CLAY STABILIZED WITH 5% LIME AND CURED FOR 1 YEAR.

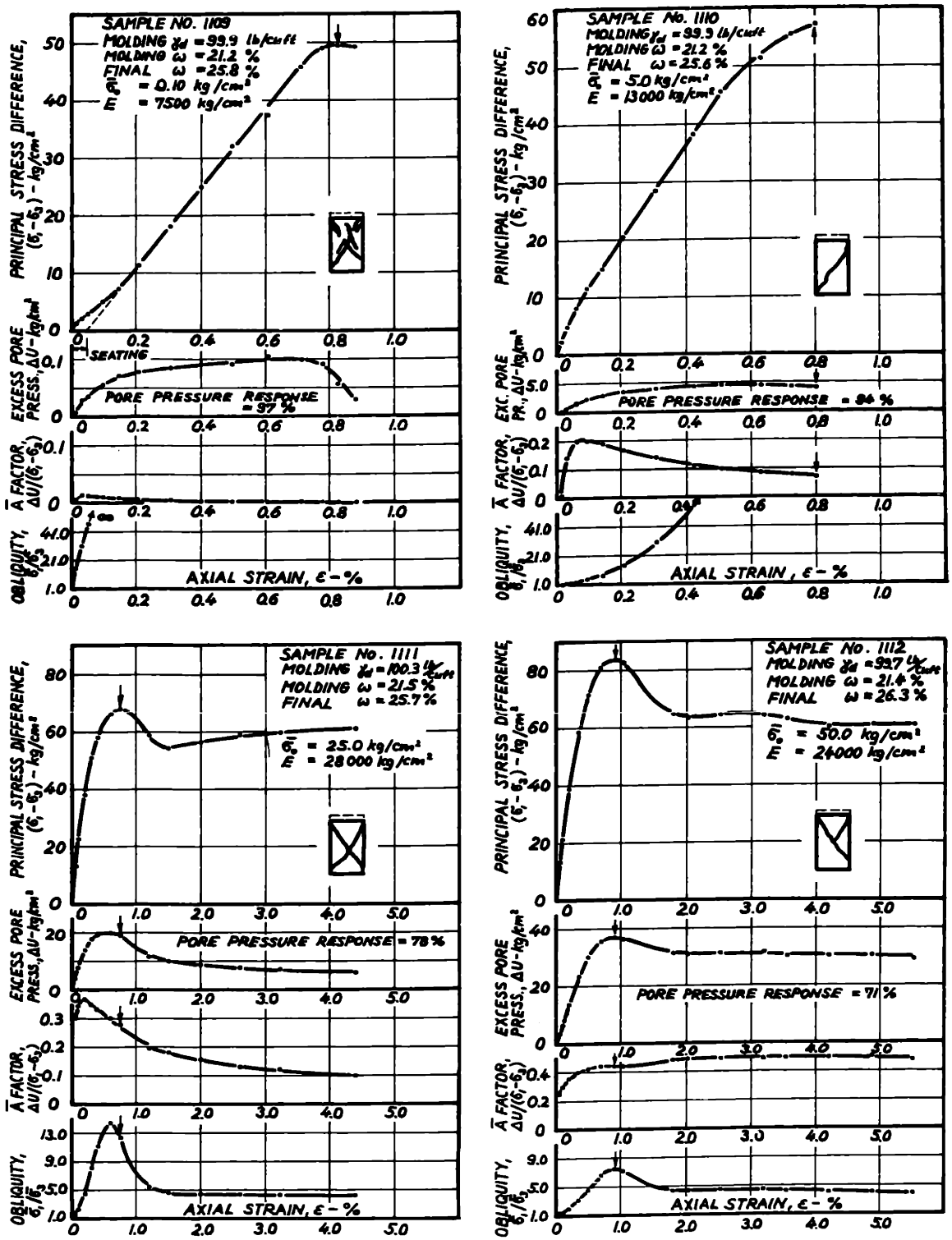

FIG. V-4 STRESS-STRAIN BEHAVIOR IN UNDRAINED SHEAR OF VICKSBURG BUCKSHOT CLAY STABILIZED WITH 10% CEMENT + 0.5 N. NaOH AND CURED FOR 43 DAYS.

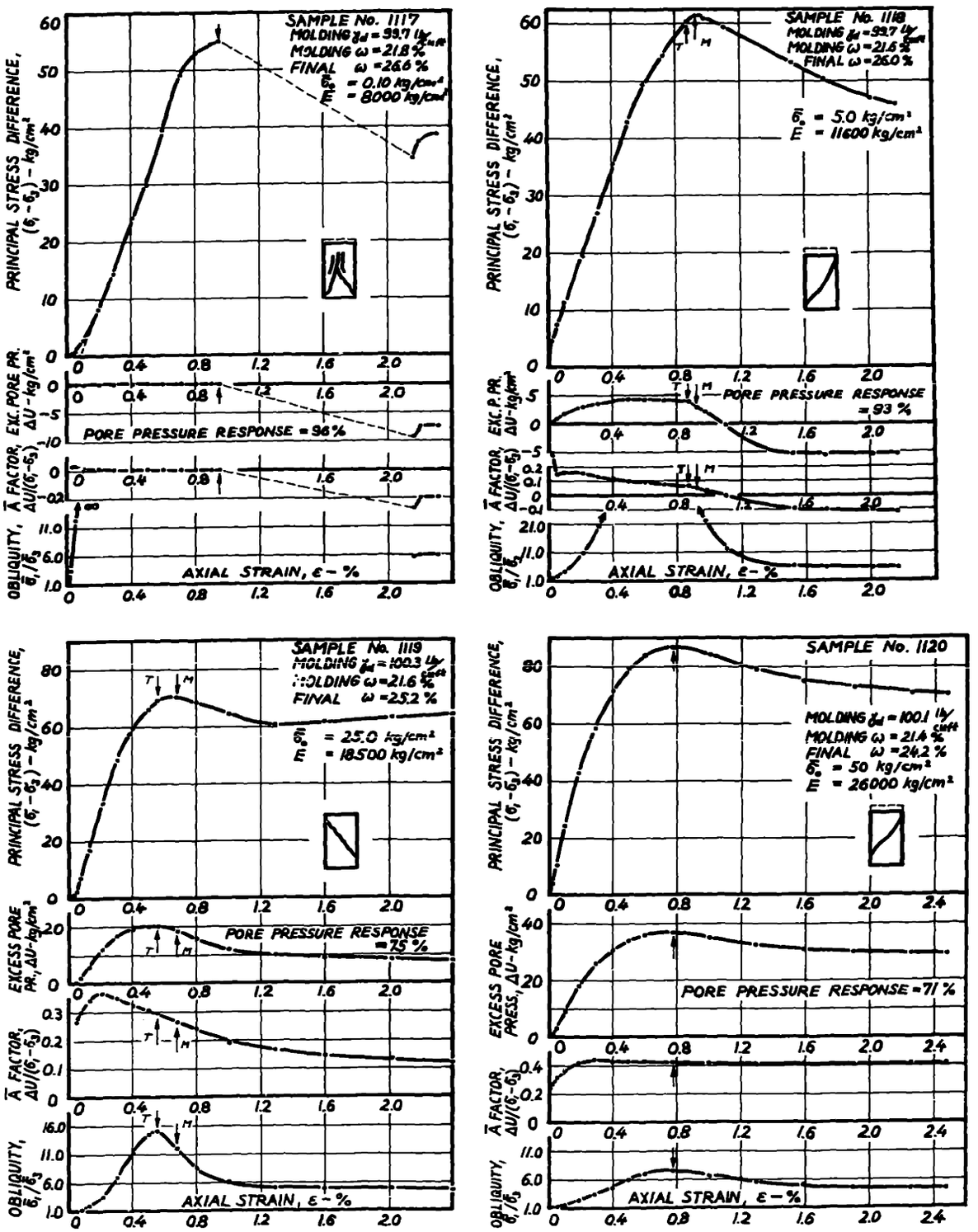

FIG. V-5 STRESS-STRAIN BEHAVIOR IN UNDRAINED SHEAR OF VICKSBURG BUCKSHOT CLAY STABILIZED WITH 10 % CEMENT + 0.5 N. NaOH AND CURED FOR 55 DAYS.

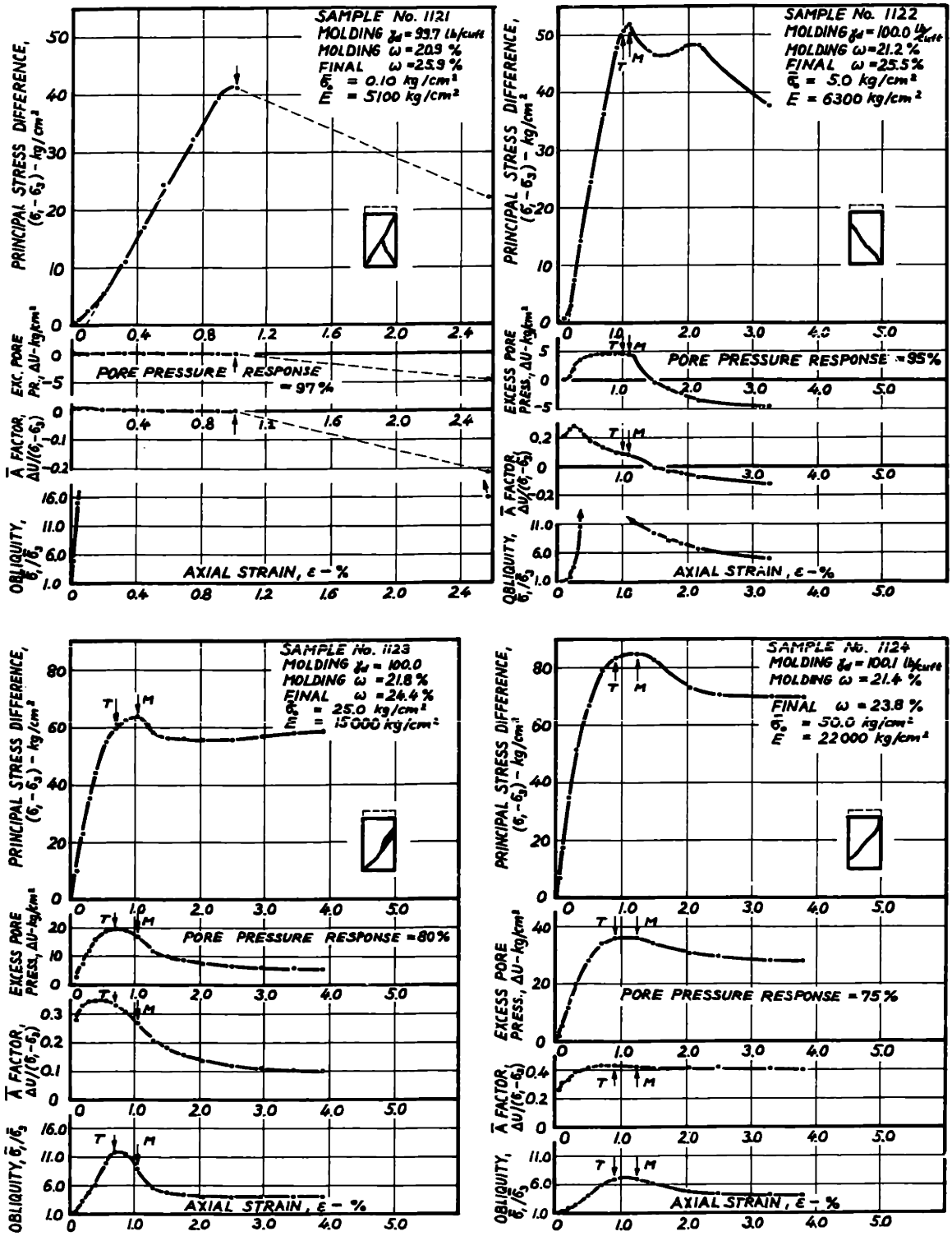

FIG. V-6 STRESS-STRAIN BEHAVIOR IN UNDRAINED SHEAR OF VICKSBURG BUCKSHOT CLAY STABILIZED WITH 10% CEMENT + 0.5 N. NaOH AND CURED FOR 55 DAYS INCLUDING TWO CYCLES OF MILD WET-DRY.

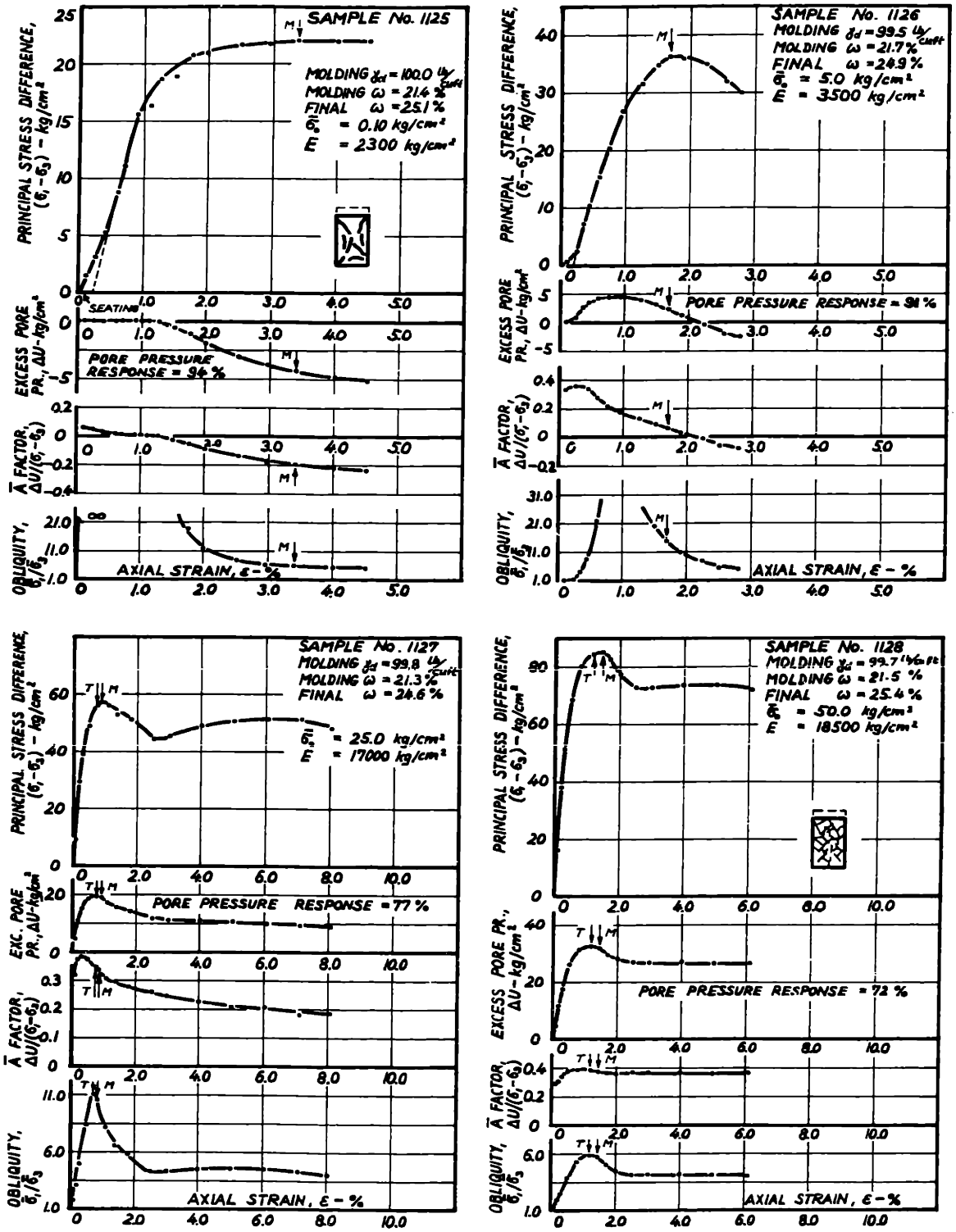

FIG. V-7 STRESS-STRAIN BEHAVIOR IN UNDRAINED SHEAR OF VICKSBURG BUCKSHOT CLAY STABILIZED WITH 10% CEMENT + 0.5 N.NaOH AND CURED FOR 90 DAYS INCLUDING TWO CYCLES OF SEVERE WET-DRY.

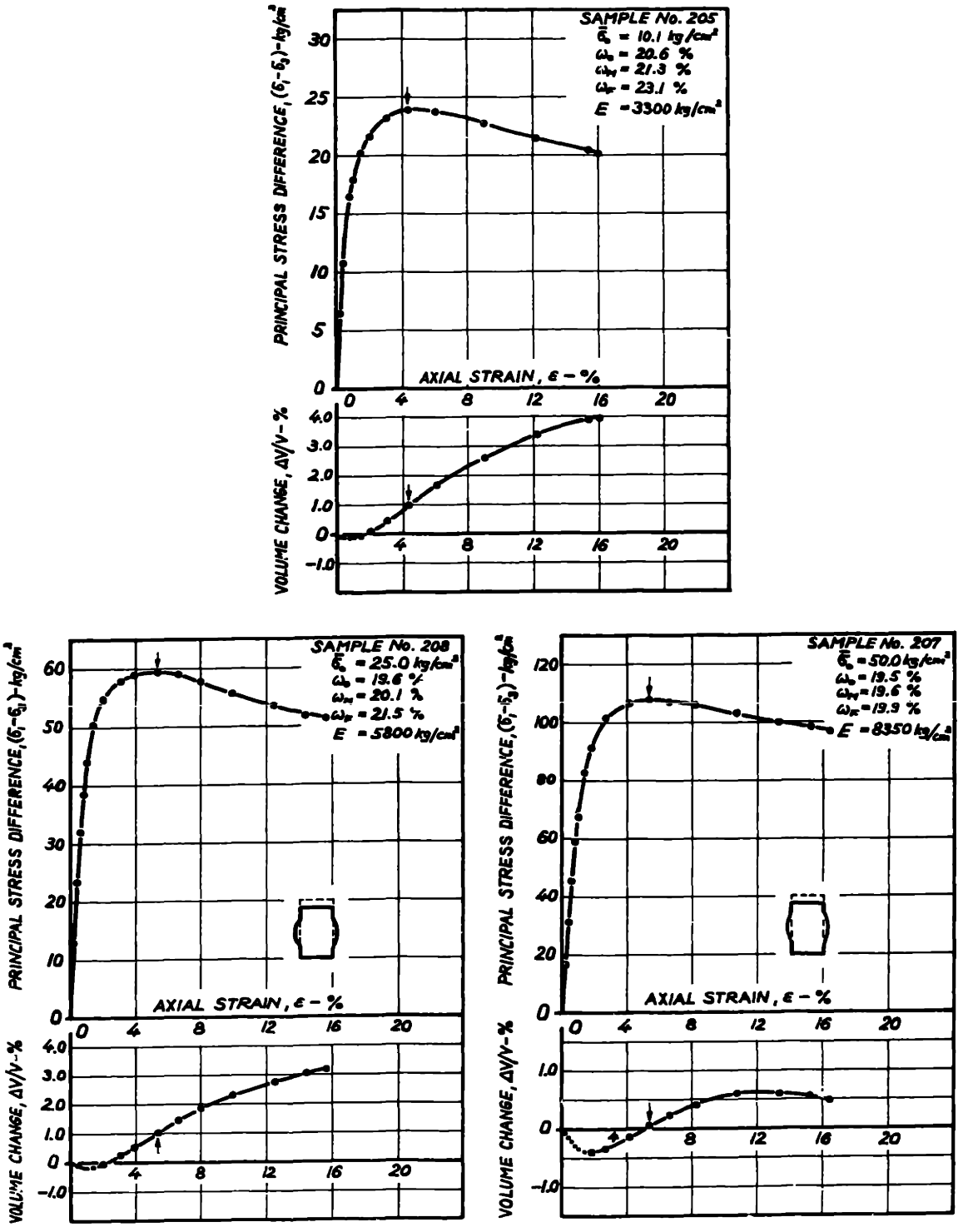

FIG. SC-1 STRESS-STRAIN BEHAVIOR IN DRAINED SHEAR OF UNTREATED COARSE OTTAWA SAND AT A RELATIVE DENSITY OF 42%.

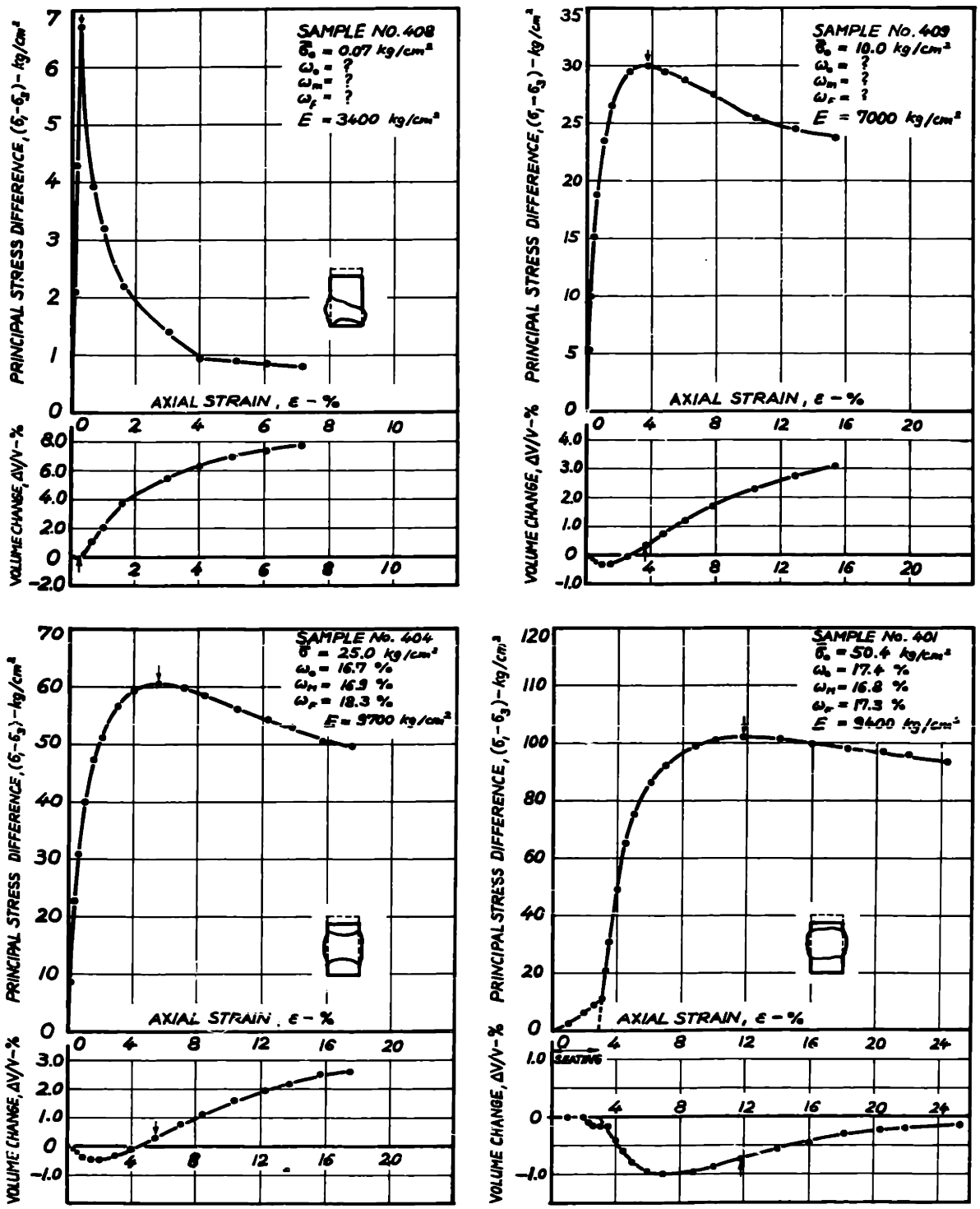

FIG. SC-2 STRESS-STRAIN BEHAVIOR IN DRAINED SHEAR OF COARSE OTTAWA SAND STABILIZED WITH 5% CEMENT (RELATIVE DENSITY OF SAND EXCLUDING CEMENT = 42 %).

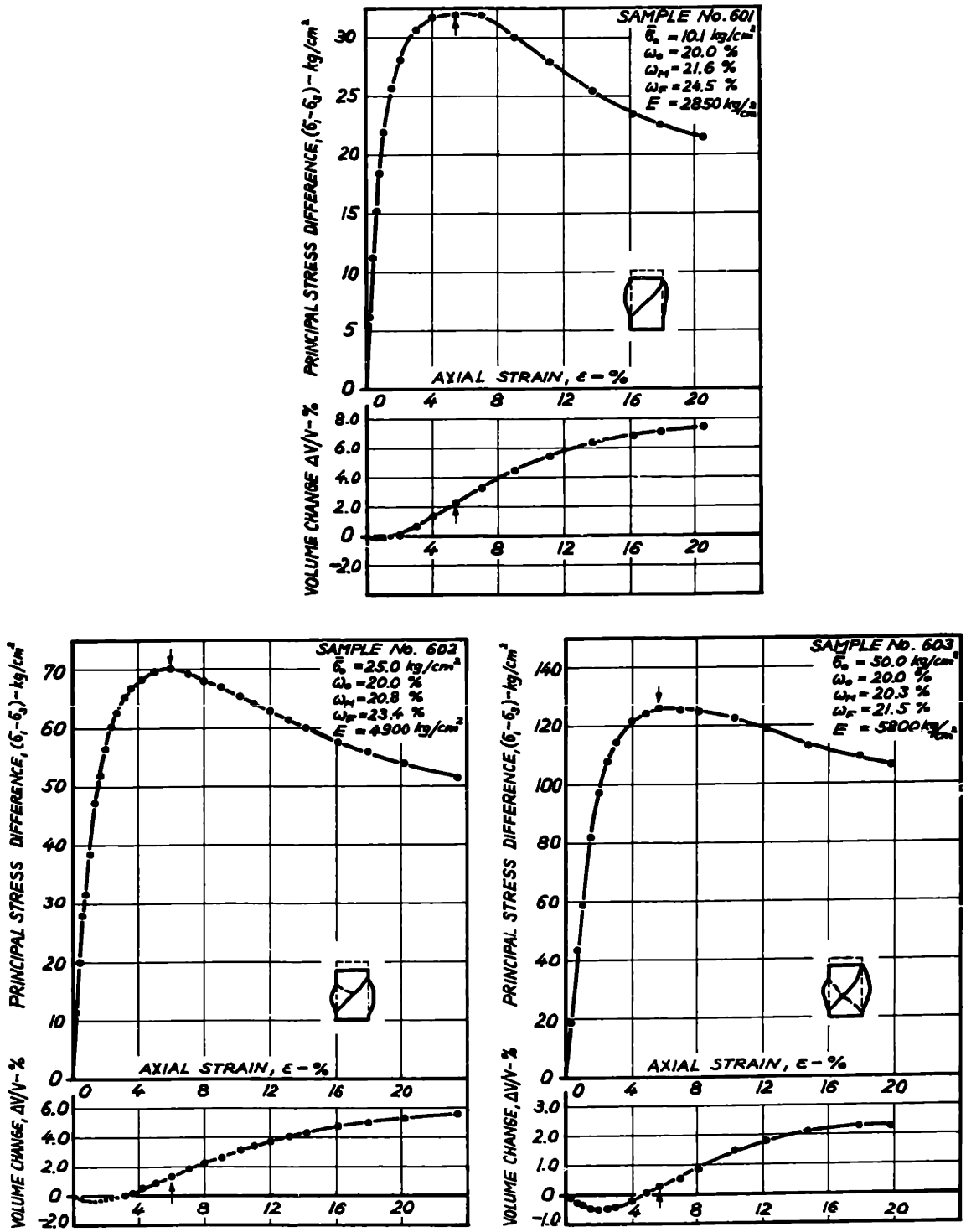

FIG. SM-1 STRESS-STRAIN BEHAVIOR IN DRAINED SHEAR OF UNTREATED MEDIUM OTTAWA SAND AT A RELATIVE DENSITY OF 75 %.

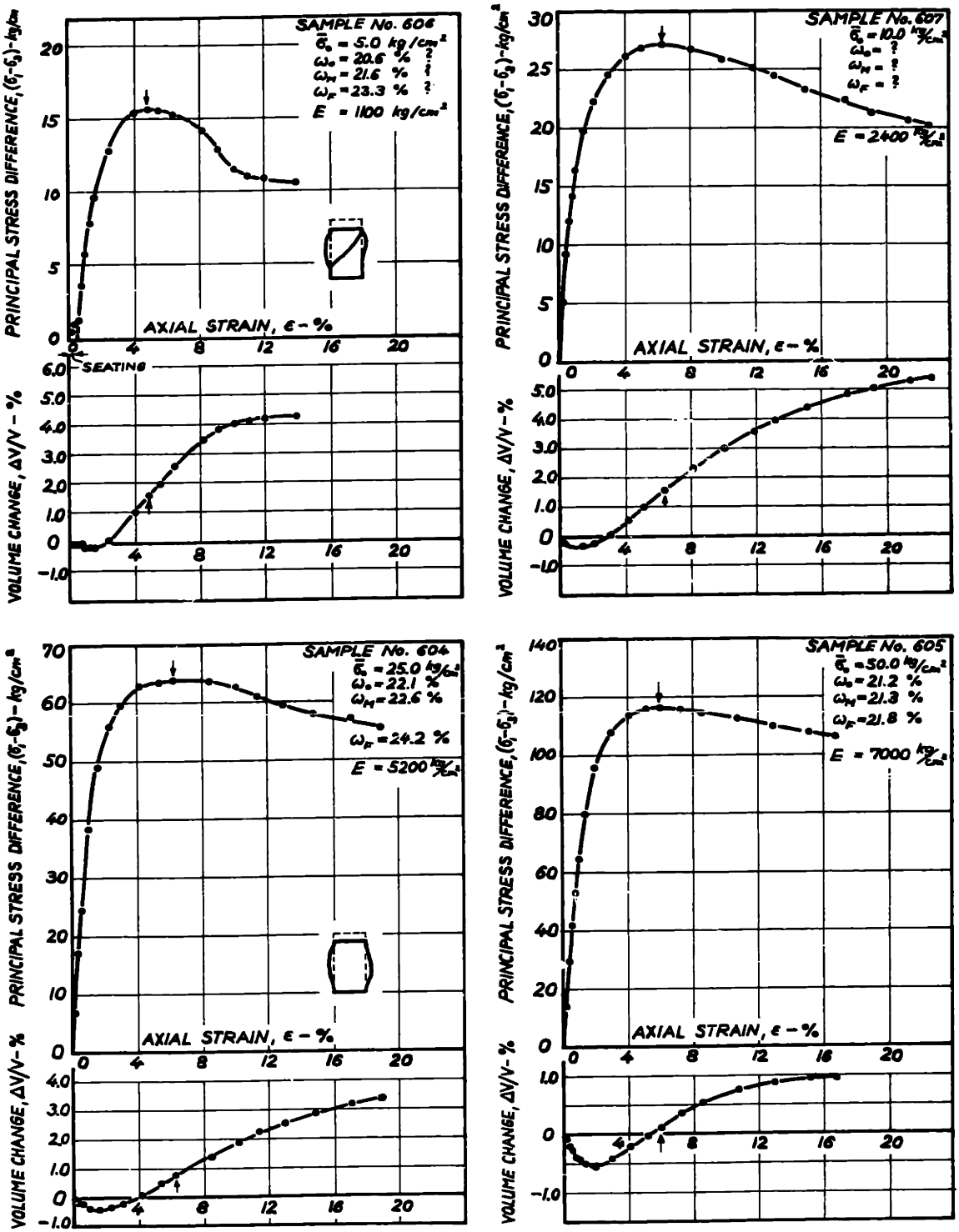

FIG. SM-2 STRESS-STRAIN BEHAVIOR IN DRAINED SHEAR OF UNTREATED MEDIUM OTTAWA SAND AT A RELATIVE DENSITY OF 62%.

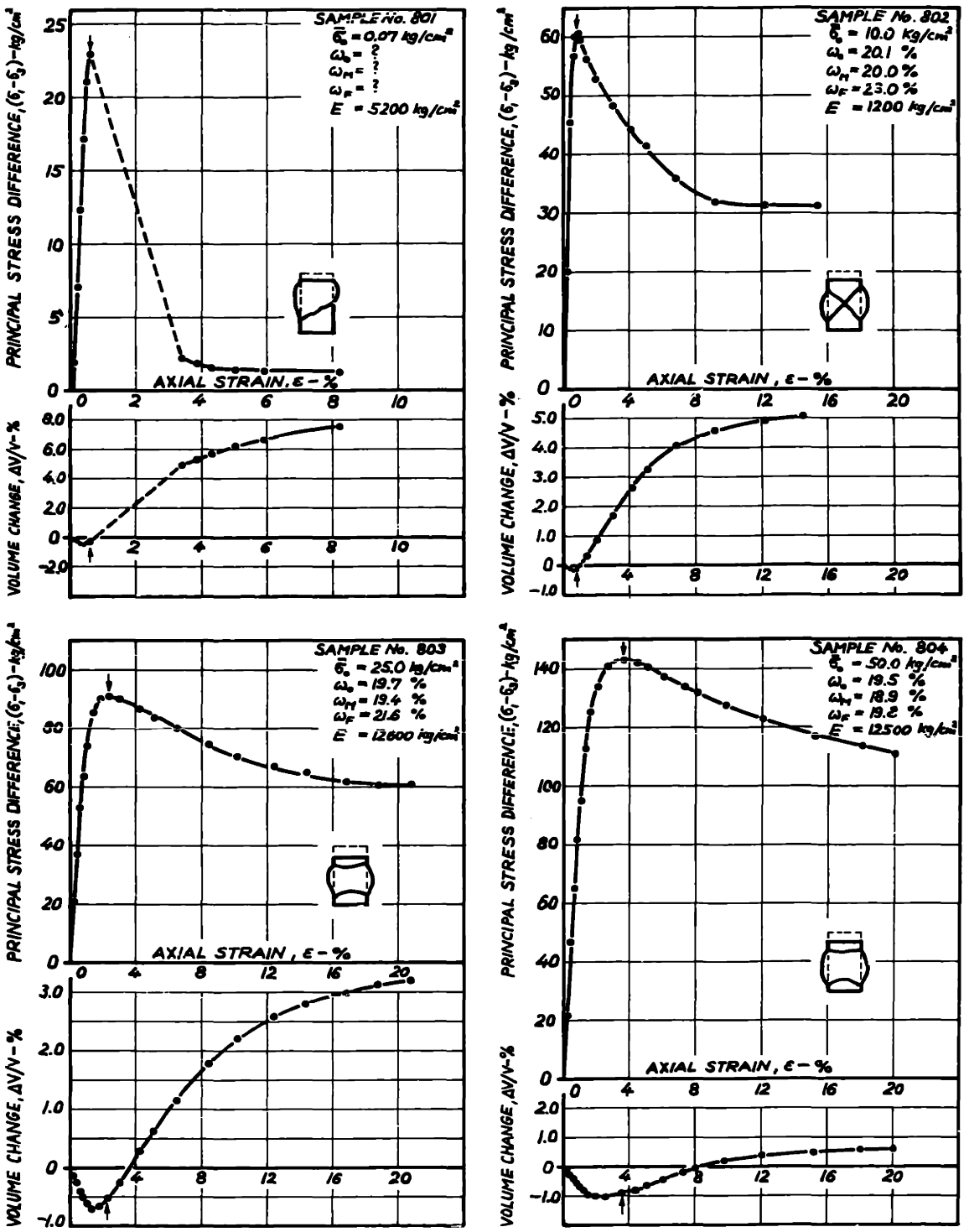

FIG. SM-3 STRESS-STRAIN BEHAVIOR IN DRAINED SHEAR OF MEDIUM OTTAWA SAND STABILIZED WITH 5% CEMENT. CURING TIME 32-33 DAYS. (RELATIVE DENSITY OF SAND EXCLUDING CEMENT = 63 %).

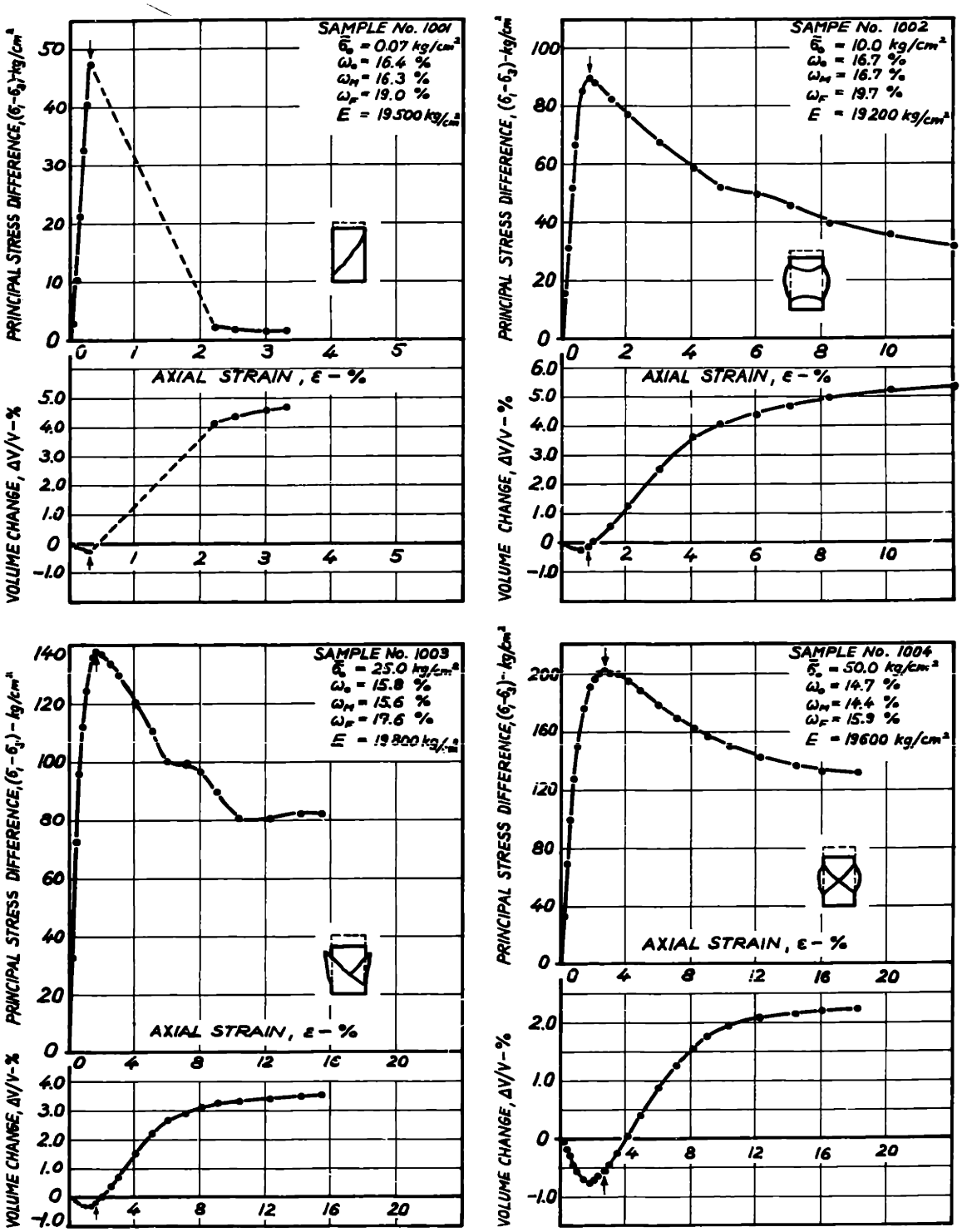

FIG. SM-4 STRESS-STRAIN BEHAVIOR IN DRAINED SHEAR OF MEDIUM OTTAWA SAND STABILIZED WITH 10% CEMENT. CURING TIME 21-22 DAYS. (RELATIVE DENSITY OF SAND EXCLUDING CEMENT = 64 %).

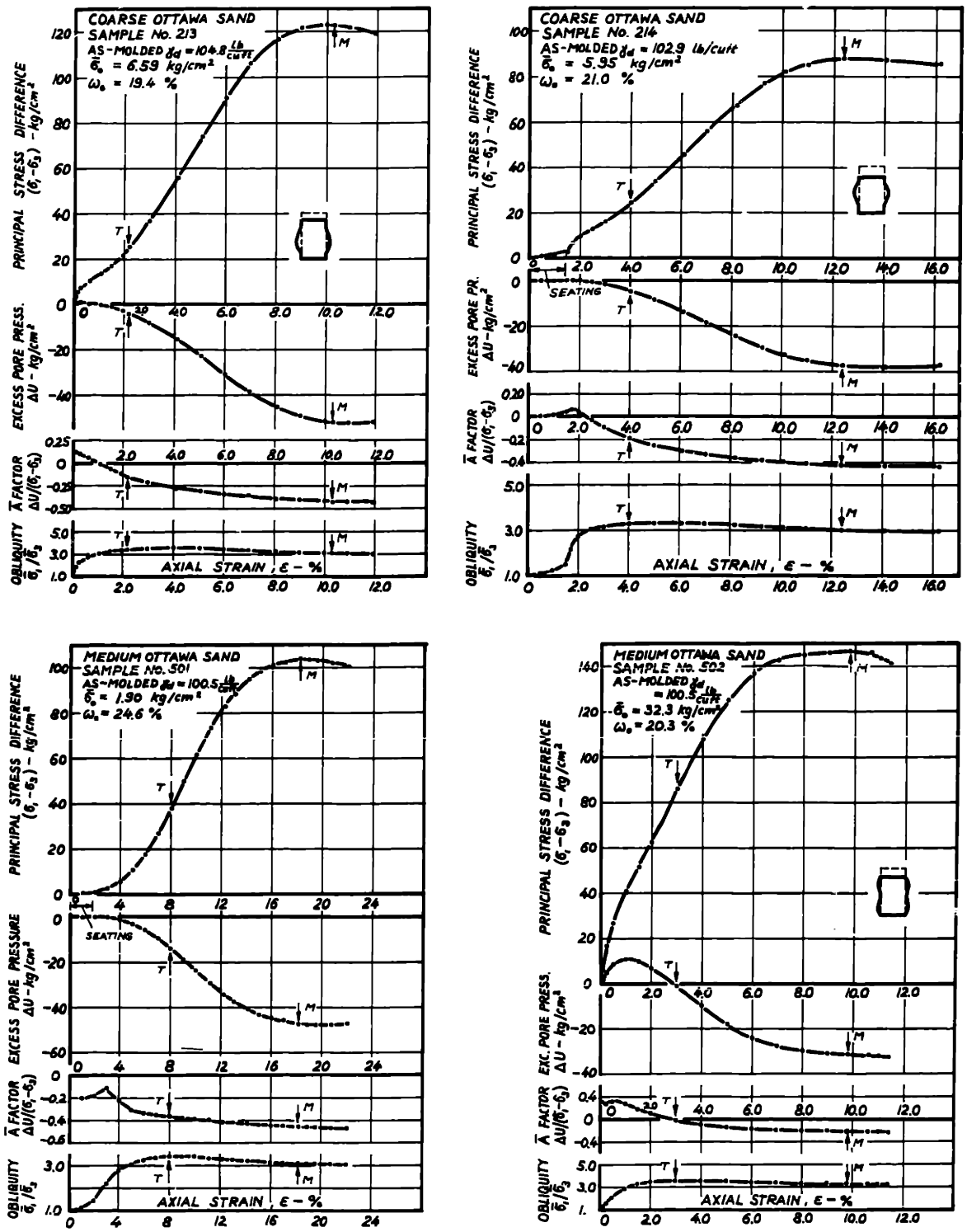

FIG.S-I STRESS-STRAIN BEHAVIOR OF UNTREATED OTTAWA SAND IN UNDRAINED SHEAR.

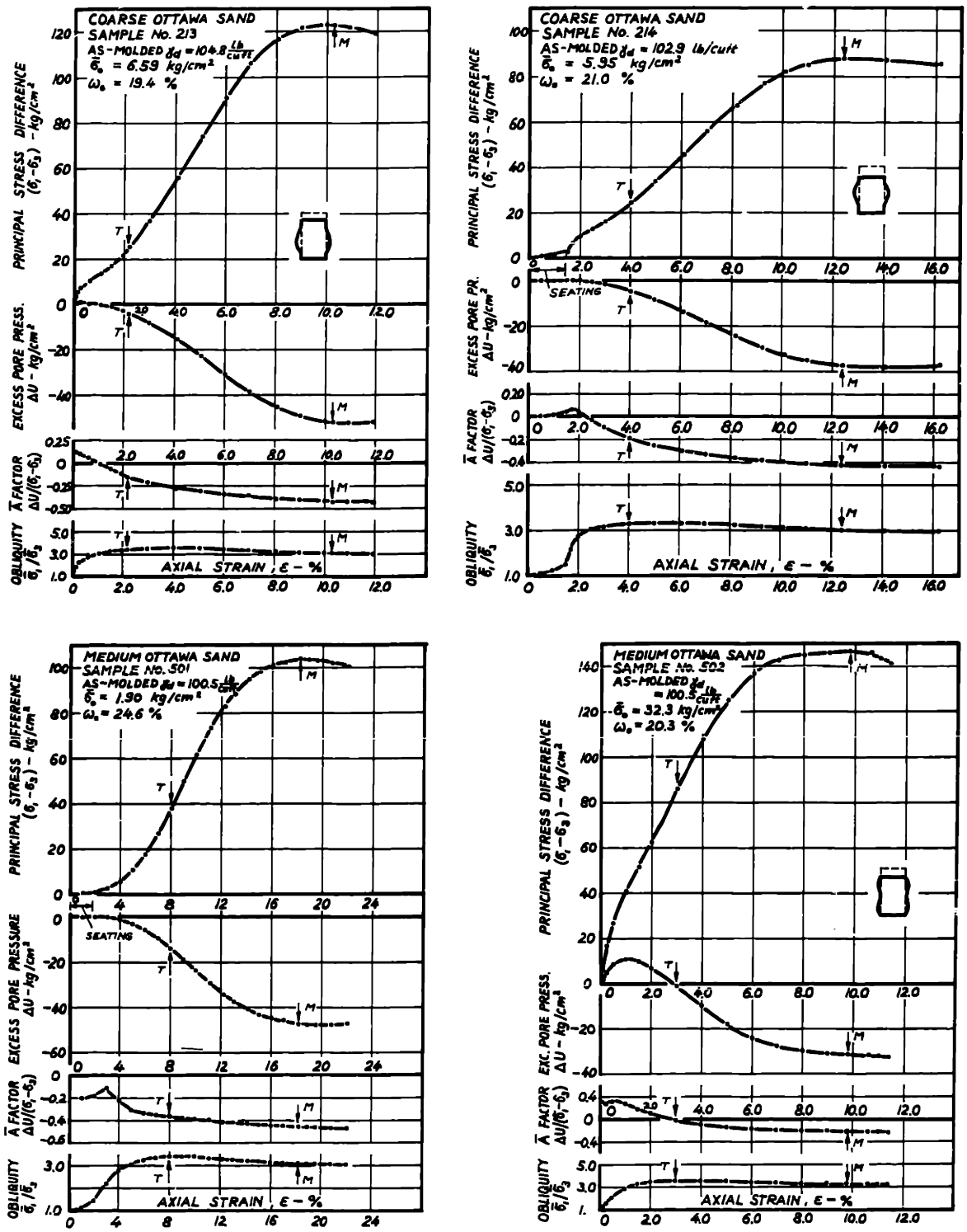

FIG.S-I STRESS-STRAIN BEHAVIOR OF UNTREATED OTTAWA SAND IN UNDRAINED SHEAR.